



Norwegian University of
Science and Technology

The New Ulriken Tunnel

TBM Performance Prediction in Hard Rock

Joakim Braa

Roy-Remy Magnus Jensen

Hopland

Master of Science in Civil and Environmental Engineering

Submission date: June 2017

Supervisor: Amund Bruland, IBM

Co-supervisor: Pål Drevland Jakobsen, IBM

Norwegian University of Science and Technology
Department of Civil and Environmental Engineering



| | |
|--|--|
| Report Title: The New Ulriken Tunnel: TBM Performance Prediction in Hard Rock | Date: 09.06.2017 Number of pages (incl. appendices): 187 |
| | Master Thesis <input type="checkbox"/> X Project Work <input type="checkbox"/> |
| Name: Joakim Braa and Roy-Remy Hopland | |
| Professor in charge/supervisor: Amund Bruland | |
| Other external professional contacts/supervisors: Pål Drevland Jakobsen (NTNU) Leon Eide (Bane NOR) Tobias Andersson (JVSS) | |

Abstract:

This thesis is written in relation with the New Ulriken Tunnel, and the main objective is to study and compare seven different prediction models for TBM. A field study was conducted over a period of eight weeks to gather machine and geological data. The study consisted of detailed mapping of the rock, various tests with the machine, and drilling of core samples. A 700-meter section of the tunnel was investigated, from TM 3775 – TM 4475. Results for the model predictions are compared towards each other as well as the achieved net penetration rate at the New Ulriken Tunnel. This comparison give a deeper understanding of the models and how they behave with different input values.

The study of the different models show that cutter thrust, rock mass fracturing, and *UCS* are the machine and geological parameters most affecting the net penetration rate.

The results from this thesis show that TBM prediction models are a good tool for project management. Predictions are relevant both for the early stages as well as during the construction of a project. However, more than one prediction model should be calculated to ensure a reliable result.

Keywords:

| |
|-------------------------|
| 1. TBM tunneling |
| 2. Prediction models |
| 3. Net penetration rate |
| 4. Hard rock |


Roy-Remy Hopland


Joakim Braa

Preface

This report is our master's thesis in Construction Engineering at the Department of Civil and Environmental Engineering (IBM) at the Norwegian University of Science and Technology (NTNU). The purpose of the report is to study and compare different prediction models for TBM performance in hard rock. The thesis is a cooperation between NTNU, Bane NOR and Joint Venture Skanska Strabag (JVSS). Project data is collected from the New Ulriken Tunnel project in Arna, Norway.

The results presented are a product of our own work, as we have gathered, processed and calculated the data obtained. Findings and remarks in this thesis are presented from our own point of view, and do not reflect neither the client's, nor the contractor's perspective. During our stay at Ulriken JVSS covered our living expenses, while Bane NOR granted us scholarships when the collaboration was completed. Despite these gestures, we want to ensure the reader that we did not feel obligated to put forth the interests of neither of the two parties.

During our work with the master's thesis, we have gotten invaluable help from multiple people whom we would like to show our appreciation. Especially, we would like to express our gratitude to our supervisors at NTNU, Professor Amund Bruland and Associate Professor Pål Drevland Jakobsen. Their expertise and enthusiasm within the field of TBM tunneling has been of great help and a huge inspiration.

Javier Macias, former PhD student at NTNU and now scientist at SINTEF deserves a special thanks. He is behind the latest update of the NTNU prediction model, and his knowledge has been invaluable. He has been available for questions and discussions, purely based on his passion for the field of TBM.

We would also like to thank all the involving parties at the project in Arna for an interesting stay. The expertise and interest for TBM tunneling of the people at the project has given us valuable knowledge to use in the thesis and further in our careers. Especially our external contacts Leon Eide (Bane NOR) and Tobias Andersson (JVSS) contributed with their field experience and welcoming personalities.

The personnel at NTNU/SINTEFs engineer geological laboratory deserves a recognition for their time and effort.

Finally, we would like to thank each other for a great collaboration and productive master's thesis period. Both of us got to use our individual strengths, and we consider ourselves equal in the contribution of the final result that is the master's thesis. We hope that this study will be of value for both the New Ulriken Tunnel project, IBM at NTNU and the field of TBM tunneling.

Trondheim, 09.06.2017



Roy-Remy Hopland



Joakim Braa

Summary

A new railway tunnel through the mountain of Ulriken is constructed from Arna to Bergen, Norway. The tunnel project is named the New Ulriken Tunnel, and is constructed with a combination of drill and blast and Tunnel Boring Machine (TBM). This is the first time a TBM is used to construct a railway tunnel in Norway.

Consequently, this thesis is written in relation with the New Ulriken Tunnel with the main objective to study and compare different prediction models for TBM. Seven models were chosen, and will be presented and calculated individually. The different models are:

- The NTNU-model
- A model by Farrokh et al. (2012) presented in the journal *Tunnelling and Underground Space Technology*
- A model by Hassanpour et al. (2011) presented in the journal *Tunnelling and Underground Space Technology*
- The Gehring model
- The Apline model (modified Gehring)
- The Q_{TBM} -model
- The CSM- and MCSM-model (Modified CSM)

At last, the different results are compared towards each other as well as the achieved net penetration rate at the New Ulriken Tunnel. This comparison will give a deeper understanding of the models and how they behave with different input values.

The models require multiple input parameters, consisting of both machine and geological data. Thus, gathering field data at the New Ulriken Tunnel project has been a priority in this thesis. Over a period of eight weeks detailed mapping of the rock, various tests with the machine, and drilling of core samples were conducted. A 700-meter section of the tunnel was investigated, from TM 3775 – TM 4475. In addition, TBM machine data was collected through an automatic logging system. This software logs every 10th second, providing a vast amount of data. After the collection of necessary data was completed, the in-situ samples were taken back to the laboratory and tested. The combination of the data was later put together and calculations of the different models were carried out.

Several spreadsheets are created in Microsoft Excel, creating a large amount of graphs and tables. The different spreadsheets display calculations and results for the geological investigation, TBM performance data, penetration- and *RPM* tests, chip analysis, and model performance predictions. The organization and calculations of this data in Excel have been a time-consuming activity. All results presented in this thesis are an outcome of this work.

All the used methodologies contain possible sources of error. Therefore, a thorough review of methodologies, calculations and results has been completed.

When all the needed parameters are established the prediction models can be calculated. The predicted net penetration rates from each model are compared to what has been achieved at the selected tunnel segment at the New Ulriken Tunnel. The results indicate that the model by Hassanpour et al. and the Alpine model show the most promising

predictions. These models estimate net penetration rates very close to what has been achieved at the New Ulriken Tunnel. However, if a conservative result is more sought after, the Gehring model calculates the best values.

The study of the different models shows that cutter thrust, rock mass fracturing, and *UCS* are the machine and geological parameters most affecting the net penetration rate. It is therefore important that the models include these parameters to better reflect real situations.

Cutter ring life has been calculated using the NTNU-model. The estimations show good correlation with the actual cutter consumption while using achieved net penetration rates from the New Ulriken Tunnel.

The results in this thesis show that TBM prediction models are a good tool for project management. Predictions are relevant both for the early stages as well as during the construction of a project. However, more than one prediction model should be calculated to ensure a reliable result.

Sammendrag

En ny jernbanetunnel gjennom fjellet Ulriken bygges fra Arna til Bergen, Norge. Tunnelprosjektet Nye Ulriken Tunnel blir bygget med en kombinasjon av konvensjonell drivemetode og tunnelboremaskin (TBM). Dette er første gang en TBM brukes til å drive en jernbanetunnel i Norge.

Denne masteroppgaven er skrevet i tilknytning til Nye Ulriken Tunnel, og hovedmålet er å studere og sammenligne ulike prognosemodeller for TBM. Syv modeller ble valgt, og vil bli presentert og estimert individuelt. De ulike modellene er som følger:

- NTNU-modellen
- En modell presentert av Farrokhi et al. i tidsskriftet *Tunnelling and Underground Space Technology*
- En modell presentert av Hassanpour et al. i tidsskriftet *Tunnelling and Underground Space Technology*
- Gehring-modellen
- Alpine-modellen (modifisert Gehring)
- Q_{TBM} -modellen
- CSM- og MCSM-modellen (modifisert CSM)

Tilslutt ble de ulike resultatene sammenlignet opp mot hverandre og den oppnådde framdriften ved Nye Ulriken Tunnel. Sammenligningen vil sørge for en bedre forståelse av modellene, og hvordan de opererer med forskjellige inngangsverdier.

Modellene krever mange forskjellige inngangsparametere som består av både maskin- og geologiske data. Dermed ble innsamling av feltdata fra tunnelprosjektet en prioritert i denne oppgaven. Over en periode på åtte uker ble det utført detaljert kartlegging av fjellet, ulike tester med tunnelboremaskinen og boring av kjerneprøver. En seksjon på 700 meter ble undersøkt, fra TM 3775 – TM 4475. Loggføring av maskindata skjer automatisk, og ble innsamlet ved hjelp av et dataprogram. Programvaren logger verdier hvert tiende sekund, noe som sørger for en enorm datamengde. Etter at innsamlingen av nødvendig data var fullført, ble in situ prøvene sendt til laboratoriet for testing. Kombinasjonen av data ble senere satt sammen og de ulike prognosemodellene ble beregnet.

Flere regneark ble laget i Microsoft Excel, hvor det ble utarbeidet store mengder grafer og tabeller. De ulike regnearkene viser kalkulasjoner og resultater fra den geologiske kartleggingen, data for TBM ytelse, penetrasjons- og RPM-tester, chip analyse og framdriftskalkulasjoner med de ulike modellene. Arbeidene i Excel, med organisering og utregninger, har vært en tidkrevende aktivitet. Alle resultatene som er presentert i oppgaven kommer fra dette arbeidet.

Alle benyttede metoder kan inneholde mulige feilkilder. På bakgrunn av dette har det blitt foretatt en grundig gjennomgang av metodikk, kalkulasjoner og resultater.

Når alle de nødvendige parameterne var tilgjengelig, ble de ulike modellene beregnet. Den estimerte framdriften fra hver modell ble deretter sammenlignet med oppnådd framdrift ved prosjektet Nye Ulriken Tunnel. Resultatene indikerer at det er modellen presentert av Hassanpour et al. og Alpine-modellen som viser de mest lovende prediksjonene. Disse modellene estimerer framdriftsprognoser som er veldig nære det som er oppnådd ved

tunnelprosjektet i Ulriken. Hvis et konservativt resultat er mer ønsket, er det derimot Gehring-modellen som gir de beste resultatene.

Studien av de ulike modellene viser at matekraft per kutter, fjellets oppsprekkingsgrad og trykkstyrken til en bergart er de viktigste parameterne som i størst grad påvirker framdriften. Det er derfor viktig at en modell inneholder alle disse for å bedre beskrive faktiske situasjoner.

Kutterlevetiden ble beregnet med NTNU-modellen. Utrekningene korrelerer godt med faktisk kutterforbruk når faktiske framdriftsrater fra Nye Ulriken Tunnelen benyttes i modellen.

Resultatene i denne oppgaven viser at prognosemodeller for TBM er et godt hjelpemiddel å benytte i styringen av et prosjekt. Anslagene er relevante både i tidligfase og utføringsfasen av et prosjekt. Likevel anbefales det å bruke mer enn én modell i beregningsarbeidet for å sikre et mer troverdig resultat.

Table of contents

| | |
|--|-------------|
| PREFACE | I |
| SUMMARY | II |
| SAMMENDRAG | IV |
| TABLE OF CONTENTS | VI |
| DEFINITIONS AND ABBREVIATIONS | VIII |
| 1 INTRODUCTION | 1 |
| 1.1 BACKGROUND..... | 1 |
| 1.2 OBJECTIVE OF THE THESIS | 1 |
| 1.3 SCOPE AND LIMITATIONS | 2 |
| 1.4 OUTLINE | 3 |
| 2 THEORY AND RELATED INFORMATION | 5 |
| 2.1 HARD ROCK TUNNEL BORING | 5 |
| 2.2 TUNNEL BORING MACHINES | 6 |
| 2.3 ROCK SUPPORT FOR TBMS | 8 |
| 2.4 COMPARISON BETWEEN TBM AND DRILL AND BLAST TUNNELING | 9 |
| 2.5 THE NEW ULRIKEN TUNNEL | 11 |
| 3 PREDICTION MODELS FOR HARD ROCK | 18 |
| 3.1 NTNU-MODEL | 18 |
| 3.2 MODEL PRESENTED BY EBRAHIM FARROKH ET AL..... | 32 |
| 3.3 MODEL PRESENTED BY HASSANPOUR ET AL. | 34 |
| 3.4 GEHRING AND ALPINE MODEL | 35 |
| 3.5 Q_{TBM} -MODEL | 38 |
| 3.6 CSM- AND MCSM-MODEL | 40 |
| 4 METHODOLOGY | 43 |
| 4.1 LITERATURE STUDIES | 43 |
| 4.2 FIELD WORK..... | 43 |
| 4.3 LABORATORY TESTING | 53 |
| 4.4 DATA ANALYSIS | 62 |
| 5 RESULTS | 64 |
| 5.1 GEOLOGICAL INVESTIGATION AND MAPPING..... | 64 |
| 5.2 TBM PERFORMANCE DATA | 68 |
| 5.3 PENETRATION TESTS | 73 |
| 5.4 <i>RPM</i> TESTS | 75 |
| 5.5 CHIP ANALYSES | 81 |
| 5.6 CUTTER CONSUMPTION | 93 |
| 5.7 LABORATORY RESULTS | 97 |
| 5.8 PENETRATION ESTIMATIONS WITH THE DIFFERENT PREDICTION MODELS | 98 |
| 5.9 CUTTER LIFE ESTIMATIONS | 124 |
| 6 DISCUSSION AND COMPARISON | 126 |
| 6.1 COMPARISONS OF MODELS TOWARDS ACTUAL PERFORMANCE DATA | 126 |
| 6.2 STUDY AND DISCUSSION OF MODEL BEHAVIOR | 139 |
| 6.3 FINAL RESULT OF PREDICTION MODELS COMPARED TO ACHIEVED NPR | 150 |
| 6.4 POSSIBLE SOURCES OF ERROR | 153 |

| | | |
|----------|---------------------------------|------------|
| 7 | CONCLUSIVE REMARKS | 155 |
| 8 | FURTHER WORK..... | 156 |
| | REFERENCES..... | 157 |
| | APPENDICES | 159 |

Definitions and abbreviations

| | |
|-------------|--|
| <i>AVS</i> | Abrasion Value Cutter Steel |
| <i>BTS</i> | Brazilian Tensile Strength |
| <i>CLI</i> | Cutter Life Index |
| D&B | Drill and blast |
| Dip | Orientation of the planes of weakness |
| <i>DRI</i> | Drilling Rate Index |
| F_n | Thrust per cutter (kN) |
| Fractures | All continuous and non-continuous fractures representing weak areas of rock influencing performance |
| I_{50} | Point Load Index |
| IBM | Institutt for bygg- og miljøteknikk ved NTNU (Department of Civil and Environmental Engineering at NTNU) |
| IRIS.tunnel | TBM data logging software |
| JVSS | Joint Venture Skanska Strabag |
| <i>LBC</i> | <i>LCPC</i> breakability coefficient |
| NPR | Net penetration rate (m/h) |
| NTNU | Norges Teknisk-Naturvitenskapelige Universitet (Norwegian University of Science and Technology) |
| PR | Penetration rate (mm/rev) |
| ROP | Rate of penetration (m/h) |
| <i>RPM</i> | Cutterhead velocity in revolutions per minute |
| <i>RQD</i> | Rock Quality Designation (%) |
| S_{20} | Brittleness Value |
| SINTEF | Stiftelsen for industirell og teknisk forskning |
| <i>SJ</i> | Sievers' J-value |
| Strike | Orientation of the planes of weakness |
| TBM | Tunnel Boring Machine |
| TM | Tunnel meter |
| <i>UCS</i> | Uniaxial Compression Strength |

1 Introduction

This chapter introduces the master's thesis with a description of background and purpose, putting it in context with history of the field and earlier work. In addition, a description of scope, limitations and outline of the thesis is provided to give the reader a sense of what can be expected in the thesis.

1.1 Background

The increasing demands on safety, available space and lifetime perspectives of civil and mining infrastructures have led to a worldwide growth of placing infrastructures underground. This leads to a demand for better rock excavation methods and development within the field of underground construction. (Macias, 2016)

Tunnel Boring Machines, or TBMs, are an excavation method that is widely used in the tunneling industry today. The method is developed and applied to a broad range of project types. The constant development of the TBM technology has made this tunneling method applicable to a wide range of rock mass conditions, including hard rock. (Macias, 2016)

Major investments and a high geological risk come with using TBMs to excavate rock. Predictions of performance and cutter consumption are therefore important to control risk and avoid delays and budget overruns in a project. Therefore, TBM prediction models are important in order to help managing a project for both the contractor and the owner. With the help of these models, one can predict different variables, such as penetration in meters per hour. Over the years several TBM prediction models have been developed, with different input and output values. Some of these models are based on empirical data while others are numerical models. (Macias, 2016)

One of the most recognized prediction models in the world for TBM performance is, according to Hassanpour et al. (2011), the NTNU-model. The first version of the model was published in 1976 and has been revised and updated several times ever since. The latest version was published in 2016 in the doctoral thesis by Javier Macias. The model is based on empirical data from 40 tunnel jobs with more than 300 km of documented tunnel. (Macias, 2016)

Throughout the hydropower development in 1970s and 1980s in Norway, the TBM-method was a preferred way to excavate the mountain. During these times, Norway was a front nation on using TBM technology, however in the mid-1990s the use of TBMs stopped (Bruland, 2000a). The TBM-method was not utilized again until the construction of the Nedre Røssåga hydropower project, which was completed in 2015. Today, two major railway projects are being constructed; the New Ulriken Tunnel and Follobanen. Therefore, the need for knowledge concerning TBM performance is increasing again in Norway.

1.2 Objective of the thesis

The main objective of this master's thesis is to study and compare a number of existing prediction models for TBM. Comparison between the models and towards actual performance data will show the accuracy of each model. Further, it will provide a deeper understanding of the models, and how they behave with different input values.

As the prediction models are based on different geological and machine parameters, several secondary objectives are established to accomplish the main objective. These are as follow:

- Perform detailed geological back-mapping of the tunnel, measuring average spacing and angle of fractures
- Gather actual TBM performance data, including average cutter thrust, net penetration rate and cutterhead velocity
- Collect core samples to be tested in the laboratory
- Log cutter consumption, giving number of changes, reason for change and average cutter life data
- Complete laboratory tests to acquire all parameters needed for calculation of the prediction models

The selection of featured prediction models will be calculated using geological and TBM data from a selected tunnel section at the project New Ulriken Tunnel in Bergen, Norway.

An underlying goal is that the results will be of value for the New Ulriken Tunnel project as well as IBM at NTNU. This provides new empirical data for future improvements of NTNU's existing prediction model. To secure this, a number of additional investigations are performed. These are not directly supporting the main objective of the thesis; however, it provides important supplementary information about the geology and machine interaction. This extra field work includes:

- Performing *RPM* and penetration tests with the TBM
- Complete chip analysis in combination with the *RPM* and penetration tests
- Sieve testing of the TBM muck

1.3 Scope and limitations

In this master's thesis, several prediction models for TBM are calculated based on data from the New Ulriken Tunnel. The list includes a broad variation of models, which addresses different parameters to calculate the net penetration rate. Recognized and updated models published in renowned institutions and journals were chosen. Comparing the results towards actual net penetration rates will enable a comparison to spot which conditions differently affect the models. The following prediction models for TBM net penetration rate are calculated in this thesis:

- The NTNU-model (2016)
- A model by Farrokhi et al. (2012) presented in the journal *Tunnelling and Underground Space Technology*
- A model by Hassanpour et al. (2011) presented in the journal *Tunnelling and Underground Space Technology*
- The Gehring model
- The Apline model (modified Gehring)
- The Q_{TBM} -model
- The CSM- and MCSM-model (Modified CSM)

A large part of the work entailed gathering field data at the New Ulriken Tunnel project in Norway. Detailed mapping of the rock, various tests with the machine, and drilling of core

samples were conducted over a period of eight weeks. In addition, TBM machine data was gathered through an automatic logging system, providing a vast amount of data. After this was completed, the in-situ samples were taken back to the laboratory and tested. The combination of the data was later put together and calculations of the different models were carried out.

The main limitations in this thesis are:

- Cutter wear calculations are only performed using the NTNU-model. The cutter wear estimations were solely included to provide a wider overview of the project. Calculations for this parameter with other models were not done in this thesis, as it was not a main focus of the study
- Analysis of utilization, weekly advance rate and specific cost estimates has not been done in this thesis. Some of the models give estimates of several factors, while others just calculate penetration rates. The only comparable factor that could be calculated from all the chosen models was the net penetration rate
- The tunnel section length is a limiting factor due to the available time on the project site. It was decided early on, together with internal and external supervisors, that the thesis would only include a short and specific part of the tunnel. 700 meters of the tunnel was examined, from TM 3775 to TM 4475. This gives a limited number of tests on the TBM and rock samples

1.4 Outline

The thesis consists of eight chapters. A short presentation of each chapter is given below:

- **Chapter 1: Introduction**
 - Presents background, objective, scope and limitations of the master's thesis
- **Chapter 2: Theory and related information**
 - Theory about hard rock tunnel boring and TBMs
 - Information about the project
- **Chapter 3: Prediction models for hard rock**
 - Presentation of different prediction models for hard rock
- **Chapter 4: Methodology**
 - Detailed description of all methodologies used in this thesis
- **Chapter 5: Results**
 - Results from the field work is given
 - Calculations, results and evaluation of the different prediction models
- **Chapter 6: Discussion and comparison**
 - The models are compared and the results are discussed
- **Chapter 7: Conclusive remarks**

- Conclusive remarks are given to sum up the thesis
- **Chapter 8: Further work**
 - Recommendations for further work

2 Theory and related information

This chapter provides fundamental theory and related information regarding TBM tunneling in hard rock. The chapter offers a brief description of the different types of machinery used as well as advantages and disadvantages of choosing TBM. In addition, information about the project this thesis is written in relation to will be provided. The majority of the work presented in this chapter has been carried out by the authors of this thesis in a previous report at NTNU in fall 2016. (Braa and Hopland, 2016)

2.1 Hard rock tunnel boring

2.1.1 Introduction

Tunnel boring is a common method for building in hard rock today. The machines used are called Tunnel Boring Machines or TBMs, and are used for full face excavation of a tunnel. The front end of the machine is called the cutterhead and is embedded with disc cutters. Excavation of the rock is achieved when the cutterhead is rotated and pressed against the rock with great force. (Macias, 2016)

2.1.2 Rock fragmentation process

The rock fragmentation process is initiated when the cutterhead is rotated and force is applied against the tunnel face. The disc cutters on the cutterhead will inflict the rock with cracks that propagate radially from where the cutter ring tip meets the rock surface. This will break the rock, and fragments called chips will detach from the rock surface along the inflicted cracks between the cutter kerfs. See Figure 2.1 for visualization. (Macias, 2016)

The excavation process causing the penetration of the rock is a combination of the chip breaking process, and crushing of the rock surface. As the contact zone between the cutter tip and the rock surface is applied with a high thrust force, high stress is generated in the contact area. Thus, the rock will be crushed to powder. (Macias, 2016)

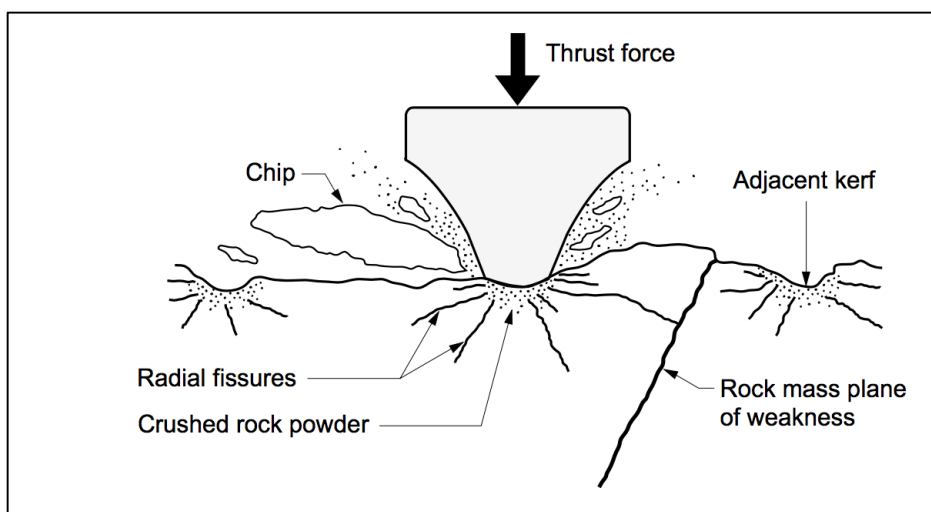


Figure 2.1 Chip formation from a disc cutter (Bruland, 2000d)

2.2 Tunnel boring machines

TBMs exist in different designs and the machines specifications are classified as different types in regard to the appropriate rock conditions. Open-type, single-shield and double-shield TBMs are the most used nowadays for tunneling in rock. Each of these will be explained below. (Bilgin et al., 2013)

2.2.1 Open-type TBMs

Open-type TBMs are used where the rock conditions are competent, when there are few geological discontinuities and when there is a low amount of water ingress. This type is also referred to as gripper or main beam-type TBM. Open-type TBMs operates by fracturing the rock using disk cutters pressed against the tunnel face with hydraulic thrust cylinders. This process causes chips of the rock to break away from the tunnel face. The excavated rock is then collected through the cutterhead and transported out of the tunnel or to the back-up area by a conveyor belt. (Bilgin et al., 2013)

The excavation of the rock is performed in a repeated cycle. The rotation of the cutterhead is engaged after the gripper system has locked the machine in place by pushing against the tunnel sidewalls. The advance of the TBM is made possible by the thrust cylinders extending and pushing the cutterhead against the tunnel face. After the thrust cylinders have reached their extending limit, the boring process is stopped and one boring stroke is completed. The machine is then moved forward and stabilized by a support system during the move. When the machine is moved forward retracting the thrust cylinders, a new cycle can begin. (Bilgin et al., 2013)

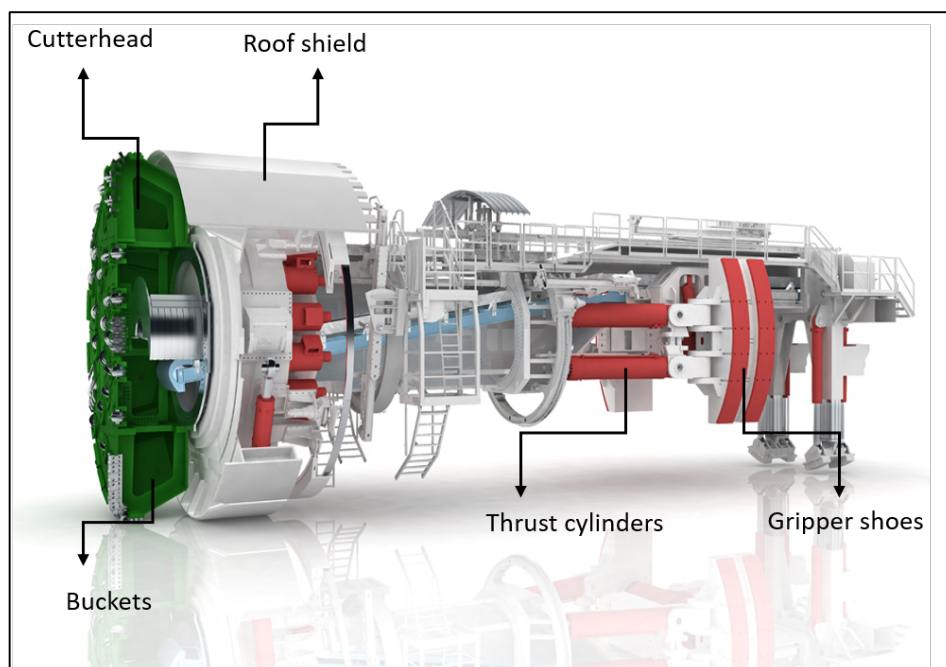


Figure 2.2 Open-Type TBM (Herrenknecht, 2016b)

2.2.2 Single-Shield TBMs

Single-Shield TBMs are used when there are frequent geological discontinuities present in hard rocks. With ground conditions like these the personnel and machine are in danger from falling rock. To protect against the unsafe conditions, the TBM is equipped with a shield somewhat smaller than the tunnel diameter. This shield covers the machine's body and keeps the personnel safe. (Bilgin et al., 2013)

Single-Shield TBMs use the same principle as open-type TBMs, it operates by fracturing the rock using free rolling disk cutters pressed against the tunnel face with hydraulic thrust cylinders. This process cause chips of the rock to break away from the tunnel face. The rock is collected in muck buckets placed behind each cutter and is carried behind the cutterhead. The material can then be transported out of the tunnel or to the back-up area by a conveyor belt. The advance of the TBM is created by a ring of hydraulic cylinders making a forward thrust through shoes that push against the tunnel lining. When using single-shield TBMs the only tunnel support that can be used are segment lining. The installation of the tunnel support and the boring are performed as sequential operations. (Bilgin et al., 2013)

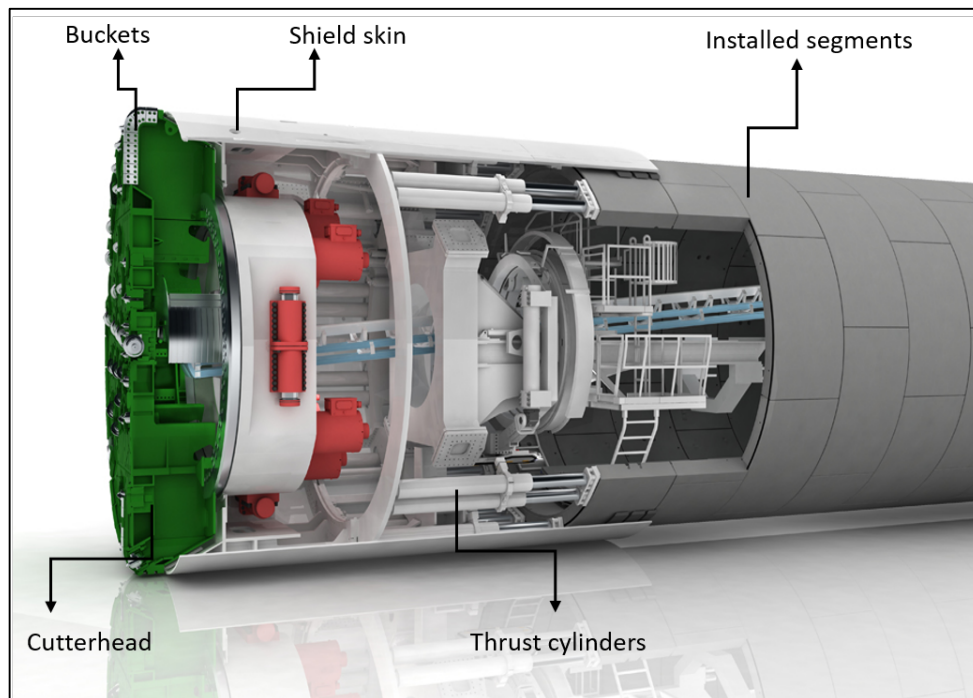


Figure 2.3 Single-Shield TBM (Herrenknecht, 2016c)

2.2.3 Double-Shield TBMs

Double-Shield TBMs are used where geological faults and shear zones are present in hard rock conditions. These machines are built up by a rotating cutterhead, a sliding telescopic shield placed within a larger outer shield, a gripper shield and a tail shield. Double-Shield TBMs can operate in a normal double-shield mode and in a single-shield mode depending on the ground conditions. When operating the machine in normal double-shield mode the rock is chipped out by the rotating cutterhead. The advance of the TBM is made possible by thrust cylinders moving the cutterhead forward through gripper shoes pushing against the tunnel walls. To protect the machine against the surrounding ground, the telescopic shield is extended as the machine advances. Double-Shield TBMs have good machine utilization time when used in normal mode. Under normal conditions, the time between the

boring strokes are just a few minutes. Sometimes the TBM needs to be operated in a single-shield mode when the ground conditions are too weak to handle the gripper shoes pressure. The thrust moving the TBM forward with auxiliary thrust cylinders is transferred to the tunnel lining when operating in single-shield mode. (Bilgin et al., 2013)

When using a double-shield TBM all types of tunnel support can be used. The most common is segment lining. Precast segments can be installed simultaneously as the machine is boring when it is operated in normal mode. When operating in single-shield mode the installation of the tunnel support and the boring is performed as sequential operations. (Bilgin et al., 2013)

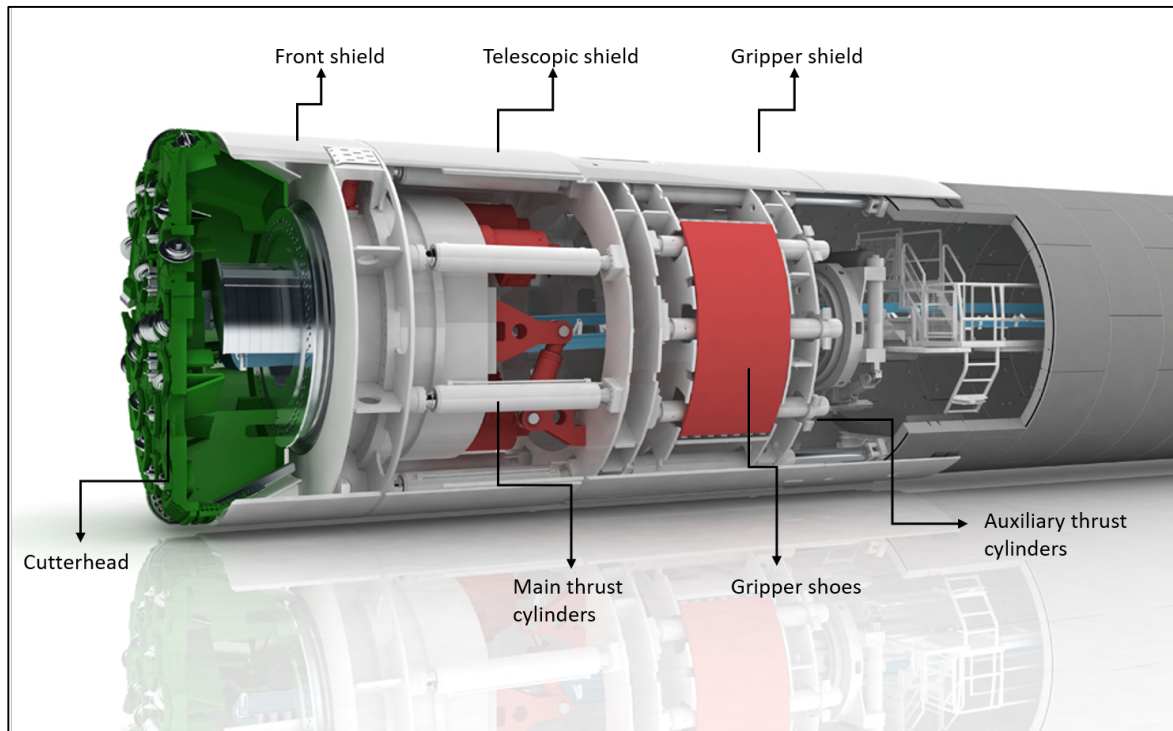


Figure 2.4 Double-Shield TBM (Herrenknecht, 2016a)

2.3 Rock Support for TBMs

Tunnels that are built in hard rock using TBMs generally require less rock support compared to a tunnel built with drill and blast. Different types of rock support are put in place at different parts of the TBM. It is normal to divide the parts in three areas:

- The area right behind the cutterhead
- The area further back on the TBM
- The back-up area

Different rock support methods for each type of hard rock TBMs will be presented below.

Open-Type TBMs

When using an open-type TBM there is no closed shield present, thus the performance of the TBM is dependent on the time it takes to install rock support. Rock support used in the area right behind the cutterhead are rock anchors and bolts, spilling bolts, shotcrete, steel arches, liner plates, reinforcing mesh, probe drilling, and pre-grouting. In the area further back on the TBM, rock support used are rock anchors and bolts, shotcrete, steel arches,

reinforcing mesh, and grouting. Further, rock support used in the back-up area are rock anchors and bolts, shotcrete, reinforcing mesh, and grouting. The extent of rock support depends on the quality of the rock in the tunnel. (Jakobsen et al., 2015)

Single-Shield and Double-Shield TBMs

When using these types of TBMs, there are limited access to the tunnel walls. The shield is used as support during the boring and then segment lining is mounted for permanent rock support. When the ground conditions are less good, spilling bolts, probe drilling, and pre-grouting can also be used. This support is put in place in the area right behind the cutterhead and the area on the back of the TBM. (Jakobsen et al., 2015)

2.4 Comparison between TBM and drill and blast tunneling

The two main choices to choose from when excavating a tunnel in hard rock conditions are the drill and blast method and the TBM method. Choosing the wrong method in these conditions can have huge consequences and an entire overview of the parameters present is necessary. There are several parameters determining which excavating method to select, according to Macias and Bruland (2014). The following parameters need to be taken into consideration:

- *Project design considerations.* The geometry of the excavation, the curve radius, slope, and the length of the tunnel
- *Final purpose considerations.* This reflects upon the final use of the tunnel in terms of the excavation geometry and the final quality required
- *Start-up time.* The time it takes to get a project up and running
- *Health, safety and working environment.* The methods differ in execution and give different aspects regarding this parameter
- *Advance rate.* This parameter is important and directly linked to the total construction time and cost
- *Flexibility.* How flexible the methods are in regard to changing ground conditions and layout profile
- *Risk.* The limited knowledge of existing ground conditions is a risk when tunneling. The methods handle this differently
- *Ground stability.* Rock support is a high cost in tunnel excavation. The two methods give different stability situations when excavating
- *Operation and construction crew.* How much skillset that is needed from the crew
- *Costs.* In this parameter, the construction time and cost is examined for the two methods
- *Overbreak and tunnel profile quality.* This parameter considers the amount of geological overbreak the methods produce
- *Environmental disturbance.* Describes the quantity of environmental disturbances, noise and vibrations the excavation adds to the surrounding areas
- *Temporally access and implantation layout.* The access and the available area at project region itself

The process of choosing the right method when excavating in hard rock is complex as it is difficult to have good overview in the early stages of a project. The list presented above helps to get an impression of the parameters that need to be evaluated before deciding the excavation method.

To sum up this section, a list of pros and cons for TBM compared to the drill and blast method is introduced according to Macias and Bruland (2014), Jakobsen et al. (2015).

Advantages using TBM:

- The TBM method provides more ground stability in normal conditions by boring a circular profile. The excavation also causes less damage to the rock mass and the required rock support is significantly reduced compared to the drill and blast method
- The use of TBM is favorable in water tunnels since the head loss, due to wall friction, is much lower than when the drill and blast method is used
- When using the TBM method all risk of handling and storing of explosives are avoided. Also, the rock support is installed from protected areas compared to the drill and blast method where some of the work area is unsupported
- Normally the TBM method achieve much higher advance rates than the drill and blast method
- For long tunnels the use of TBM is more favorable than drill and blast
- The TBM method is more environmentally suited. The surrounding areas gets less environmental disturbances, noise and vibrations
- When using TBM the workers get a better working environment without gas emissions from blasting and the use of machines
- Several work operations can go on simultaneously

Disadvantages using TBM:

- The TBM method has limitations regarding excavation geometry, curve radius and slope. The excavation geometry cannot be changed when the cross section area is defined
- The circular excavation is less convenient for some purposes. E.g. road tunnels, rock caverns, etc.
- Due to longer delivery time and assembly of the equipment, the start-up time is much longer for TBM than drill and blast
- The TBM excavation is much more sensitive for changing rock mass conditions; the advance rate can change rapidly
- During the planning stage an extensive geological investigation, mapping and testing is required for the TBM method compared to the drill and blast method
- The TBM method requires important funding early in a project, which leads to negative cash flow
- The TBM method has high demand for mobilization and infrastructure. This requires more electric power than the drill and blast method

2.5 The New Ulriken Tunnel

The existing Ulriken tunnel between Arna and Bergen is one of the most congested single-track railway tunnels in Europe. The capacity is insufficient; thus a new tunnel is now being constructed to create double-tracks. This will improve the situation for goods and passenger services by increasing the speed and enhance the traffic management flexibility. (BaneNOR, 2016b)



Figure 2.5 The existing Ulriken tunnel and the New Ulriken Tunnel shown with a white and red line respectively (BaneNOR, 2016b)

The existing Ulriken tunnel was completed in 1964 and is one of longest railway tunnels in Norway. Construction of this tunnel was highly beneficial for the society, shortening the railway by 16 kilometers and the travel time by 40 minutes. The existing tunnel is 7670 meter and was excavated using the drill and blast method. (BaneNOR, 2015)

The new tunnel will be built with a combination of drill and blast (D&B) and Tunnel Boring Machine (TBM). The D&B method is used for the first 765 meters as this part of the tunnel has a larger and varying cross section size. D&B is also used for two diagonal tunnels between the old and the new tunnel, as well as 16 smaller cross-passages. The remaining 7 kilometers of the tunnel are constructed using a TBM. This is the first time a TBM is used to build a railway tunnel in Norway. (BaneNOR, 2016b)

The project schedule is described below, as presented by BaneNOR (2016b):

- November 2014- October 2015: Blasting of the first part of the main tunnel and diagonal tunnels
- January 2016: TBM start-up
- Autumn 2017: Break through at Fløen
- Blasting of the 16 cross-passages will be performed when boring with the TBM is completed
- 2020: New Ulriken Tunnel will open for traffic
- 2020-2021: Renovation of the old tunnel
- 2017-2021: Technical railway work and installation of the signaling system
- The double-track will open after completion of all the other project operations

2.5.1 The TBM

In this project an open-type TBM is chosen. As mentioned earlier, these open type TBMs are used where the rock conditions are competent, when there are few geological discontinuities and when there is a low amount of water ingress. (Bilgin et al., 2013). In Ulriken, the rock conditions are expected to be hard and stable with a low degree of fracturing. Hence, this open-type machine is well suited. When such rock conditions are present, the need for rock support is less. The support methods used are bolts, steel arches and shotcrete, and are applied as the tunnel progresses. (BaneNOR, 2016a)

The TBM is built by Herrenknecht and has been given the name “Ulrikke”. See Table 2.1 for more specifications about the machine, and Appendix A for a machine drawing. Figure 2.7 presents a drawing of the cutterhead, showing the different type of cutters on the cutterhead.

Table 2.1 TBM specifications (BaneNOR, 2016a)

| | |
|----------------------------|--|
| TBM manufacturer | Herrenknecht |
| Publicly known as | Ulrikke |
| Cutterhead diameter | 9.33 m |
| Face area | 68 m ² |
| Length | 155 m, including 130 m back-up |
| Total weight | 1800 tons |
| Number of cutters | 62 |
| Cutter diameter | 19”, 483 mm |
| Machine power | 5250 kW, where 4200 kW are on the cutterhead |
| Thrust | 27500 kN |



Figure 2.6 The TBM for the New Ulriken Tunnel (Photo: Øystein Grue)

2.5.2 Geology at Ulriken

When building a tunnel with TBM, comprehensive pre-investigations are needed to have an overview over the geological situation. TBMs are sensitive to changing geological conditions, and the advance rate can be highly affected by this.

Seven rock mass samples were collected from different locations in the existing Ulriken tunnel during the pre-investigations for the New Ulriken Tunnel. Laboratory tests were conducted by SINTEF to establish the rock mass drillability and abrasive properties of the samples. Six of the samples were collected at niches in the existing tunnel and one sample was collected at the tunnel entrance in Fløen. (SINTEF, 2013)

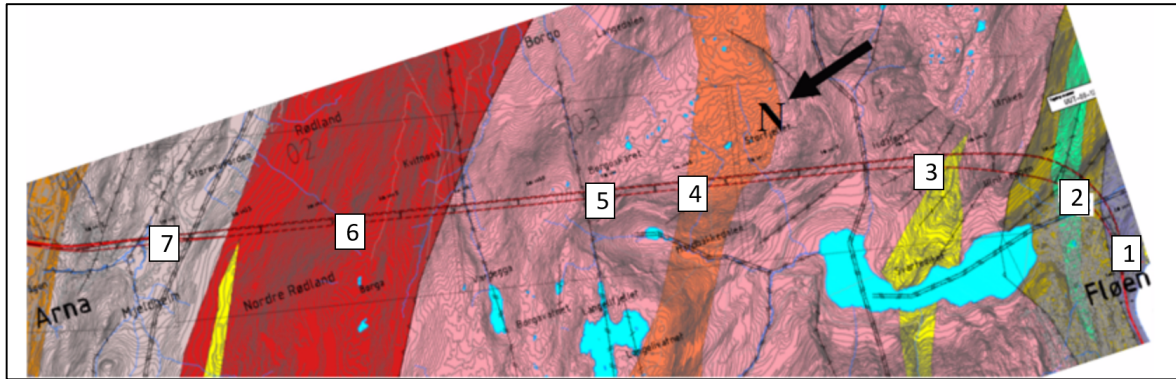


Figure 2.8 Locations for collected rock samples (Norconsult, 2013b)

Table 2.2 Test results for rock samples given by SINTEF (2013) and information obtained from geological profile made by Norconsult (2013a)

| Sample No. | 1 | 2 | 3 | 4 | 5 | 6 | 7 |
|---------------------------------------|----------------------------|----------------------------|----------------------------|----------------------|-----------------------|-------------------------|-----------------------|
| Sample ID | B-TBM 1 | B-TBM 2 | B-TBM 3 | B-TBM 4 | B-TBM 5 | B-TBM 6 | B-TBM 7 |
| Chainage | 469.805 | 469.170 | 468.195 | 466.610 | 465.930 | 464.080 | 463.010 |
| Rock type | Mylonite gneiss | Greenstone | Granitic gneiss | Gneiss | Granitic gneiss | Granitic gneiss | Anorthosite |
| Brittleness Value (S_{20}) | 34.9 | 40.1 | 44.3 | 40.5 | 40.2 | 51.0 | 54.7 |
| | Very low | Low | Medium | Low | Low | High | High |
| Siewers' J-Value (SJ) | 3.0 | 2.8 | 3.0 | 23.4 | 4.0 | 12.8 | 5.8 |
| | Very high surface hardness | Very high surface hardness | Very high surface hardness | Low surface hardness | High surface hardness | Medium surface hardness | High surface hardness |
| Abrasion Value (AV) | 5.0 | 13.0 | 12.0 | 8.0 | 14.5 | 1.5 | 2.0 |
| | Low | Medium | Medium | Low | Medium | Very low | Very low |
| Abrasion Value Cutter Steel (AVS) | 14.0 | 13.5 | 23.5 | 22.5 | 14.5 | 3.5 | 5.5 |
| | Medium | Medium | Medium | Medium | Medium | Very low | Low |
| Drilling Rate Index™ (DRI^{TM}) | 29 | 34 | 38 | 45 | 36 | 52 | 52 |
| | Very low | Low | Low | Medium | Low | Medium | Medium |
| Bit Wear Index™ (BWI^{TM}) | 51 | 54 | 46 | 36 | 52 | 20 | 22 |
| | High | High | High | Medium | High | Very low | Low |
| Cutter Life Index™ (CLI^{TM}) | 7.6 | 7.5 | 6.3 | 14.0 | 7.5 | 22.8 | 14.1 |
| | Low | Low | Low | Medium | Low | High | Medium |
| Quartz content (DTA) weight % | 13 | 25 | 21 | 12 | 19 | 2 | 2 |
| Cerchar Abrasivity Index (CAI) | 4.4 | 3.9 | 4.1 | 5.4 | 4.9 | 4.7 | 3.3 |
| | High abrasiveness | High abrasiveness | High abrasiveness | High abrasiveness | High abrasiveness | High abrasiveness | High abrasiveness |

| Fracturing class (St) | I- to I | I to II | I- to I | I- to I | I- | 0-I to I- | 0-I to I- |
|-----------------------|---------|---------|---------|---------|----|-----------|-----------|
| Fracturing sets | 3-4 | 3 | 1-2 | 2+ | 1+ | 1-2 | 1+ |

The geology in the Bergen-area consists of several rock complexes with various metamorphic sedimentary and igneous rocks, referred to as the Bergen-arches. (Norconsult, 2013b)

Area nearest Fløyen

The area nearest Fløyen consists of mylonite gneiss, amphibolite, greenschist and amphibole-garnet schist. This area has a very low-to-low Drilling Rate Index™ and the Cutter Life Index™ is expected to be low. (Norconsult, 2013b)

Central area of Ulriken

The central area of Ulriken consists of different types of gneisses and an area with quartzite. This area has a low to medium Drilling Rate Index™ and the Cutter Life Index™ is expected to be from low to medium. (Norconsult, 2013b)

Area nearest Arna

The area nearest Arna consist of granitic gneiss, anorthosite, meta-gabbro and charnockite/granulite. This area has a medium Drilling Rate Index™ and the Cutter Life Index™ is expected to be from medium to high. (Norconsult, 2013b)

Foliation and fracturing of the rock mass

The rock mass nearest Bergen has a foliation with strike direction NW-SE while the area closer to Arna has a strike direction NNW-SSE. The foliation has a varying dip towards NE. In the existing Ulriken tunnel the dominating strike direction seems to be the direction of the foliation. (Norconsult, 2013b)

97 registrations have been made to map the fracture directions. The mapping was performed outside the tunnel at Arna and Fløyen as well as inside the existing tunnel. This investigation gave 4-5 occurring fracture directions. (Norconsult, 2013b)

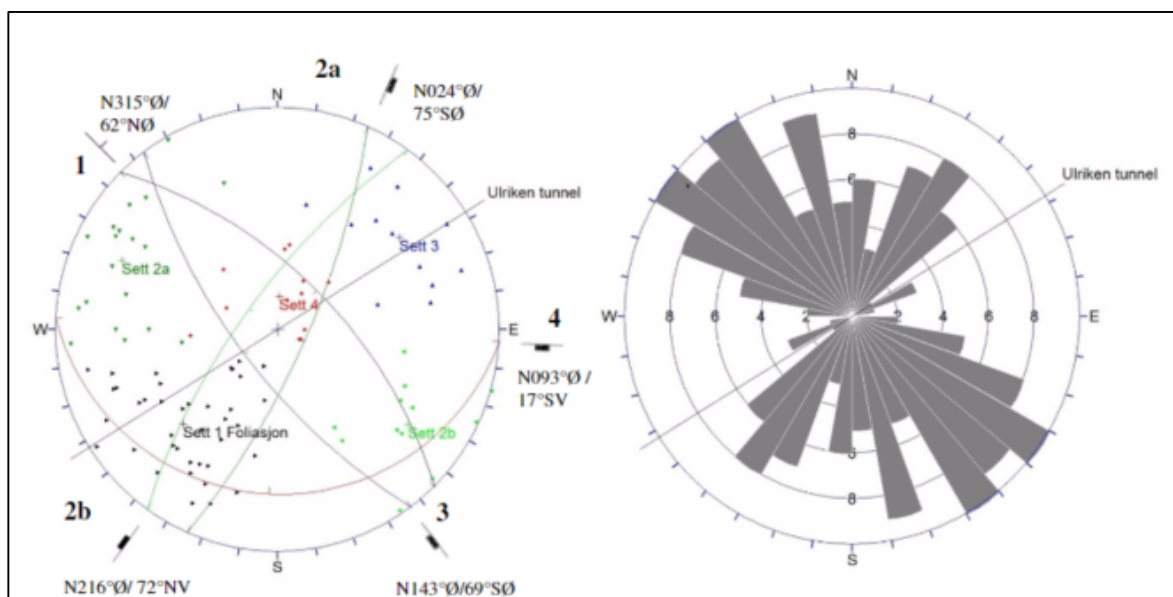


Figure 2.9 Mapped fracture directions for the different fracture sets (Norconsult, 2013b)

Fracture set 1 lays parallel to the foliation direction of the rock mass. This set is most noticeable and goes through all of the Ulriken Mountain. The strike direction varies between W-E to NW-SE and the dip is between 20-30° up to 80-90°. (Norconsult, 2013b)

Fracture set 2a and 2b are perpendicular to the foliation direction and have a strike direction NE-SW. These sets have a high variation for the dip direction going from 55-90° towards SE to 45-90° towards NW. (Norconsult, 2013b)

Fracture set 3 has the same strike direction as the foliation direction SE-NW. The dip direction goes the opposite way and varies between 50-85° towards SW. The fractures lay perpendicular to the foliation. (Norconsult, 2013b)

Fracture set 4 has the same strike and dip direction as set 3, strike direction SE-NW and dip direction SW. The dip lies more flat in this set, varying between 10-40°. This fracture set is mostly found in the area near Fløyen. (Norconsult, 2013b)

The occurrence of the different sets varies across the length of the tunnel. 2-3 fracture sets being present at the same time is a normal observation. The fracture distance is also highly varying between the different rock masses and in different parts of a specific rock mass. Characteristic fracture distances mapped are between 0.2-0.6 meters in the area nearest Fløyen and between 0.6-2.0 meters for the rest of the rock masses. (Norconsult, 2013b)

2.5.3 Geology at TM 3775 – TM 4475

The geology at the selected tunnel section between TM 3775 – TM 4475 consists mainly of migmatite and gneiss. Migmatite is found between TM 3775 – TM 4075 and gneiss between TM 4075 – TM 4475. The migmatite is banded and biotite rich with pegmatite and quartz rich intrusions. There are also mixtures and hints of banded augen gneiss, granitic gneiss, and feldspar in the migmatite section. The gneiss section consists of augen gneiss that is both banded and not banded, with a biotite rich matrix. There are hints of feldspar, mica, and glimmer in the gneiss area.

2.5.4 IRIS.tunnel-software

Mechanical tunneling is an operation that requires a constant overview and control of the information and data streams; this to operate the TBM effectively and securely. The TBM excavating the New Ulriken Tunnel uses 197 sensors to measure different functions, from total advance force to gripper cylinder pressure. All essential functions are controlled electrohydraulically, making it possible to measure. The sensors record and create datasets every 10th second. This generates a vast amount of data not only essential for the operation, but can additionally be useful to analyze performance at a later time. (ITC-Engineering, 2016)

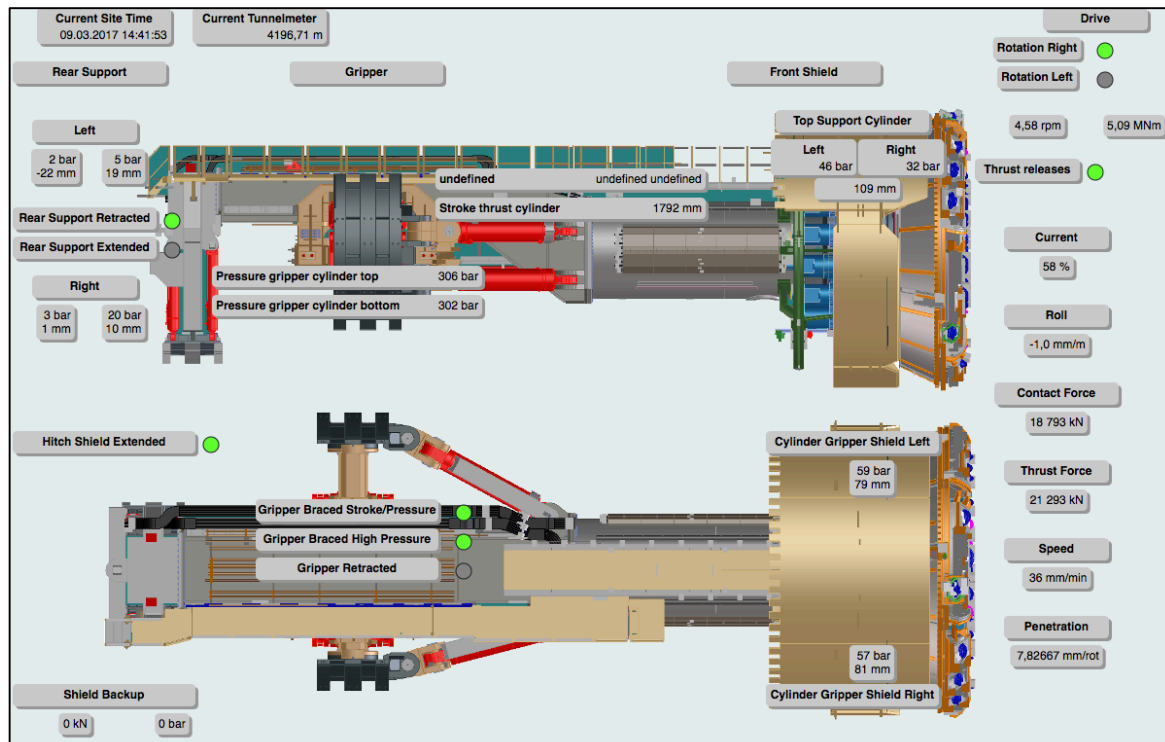


Figure 2.10 Screenshot of the IRIS.tunnel sensor board while boring. (ITC-Engineering, 2017)

3 Prediction models for hard rock

It exists numerous prediction models for TBM tunneling. In addition to the NTNU-model, this thesis also analyses a number of other more or less known models. All prediction models used in this thesis will be presented in this chapter. The majority of the work presented in this chapter has been carried out by the authors of this thesis in a previous report at NTNU in fall 2016. (Braa and Hopland, 2016)

3.1 NTNU-model

The model was first presented in 1976, but has been updated multiple times since then. The latest update was made in 2016, and was revised by Javier Macias. The model is empirical, and today's version is based on data from more than 300 km of tunnel from 40 different tunnel jobs (Macias, 2016). According to Hassanpour et al. (2011) the NTNU-model is, together with the CSM-model, the most recognized TBM performance prediction and prognosis model in the world.

Amund Brulands version of the NTNU-model from 2000 is presented first, before the updates made by Javier Macias in 2016 is given in chapter 3.1.5. The latest version of the model by Macias will be used in this thesis.

To estimate time consumption and cost for tunnel boring, the NTNU model consists of four different interdependent parts. According to Bruland (2000a), these are as follows:

- Net penetration rate in mm/rev and m/h
- Cutter life in h/cutter
- Gross advance rate expressed by time consumption as h/km
- Excavation costs in NOK/m

To achieve the output parameters listed above, the factors influencing the penetration rate and cutter wear is, as stated by Bruland (2000a):

- Input machine data:
 - Cutter parameters
 - TBM diameter
 - Average cutter thrust
 - Cutterhead *RPM*
- Input geology:
 - Rock mass fracturing
 - *DRI*
 - *CLI*
 - Porosity
 - Rock quartz content

3.1.1 Net penetration rate

The net penetration rate is defined as “meters tunnel bored per hour while the cutterhead rotates with thrust against the face” (Bruland, 2000b, p. 14). This model bases its predictions on a penetration curve. This curve is derived from various TBM tunnel projects where penetration tests have been performed. (Bruland, 2000a)

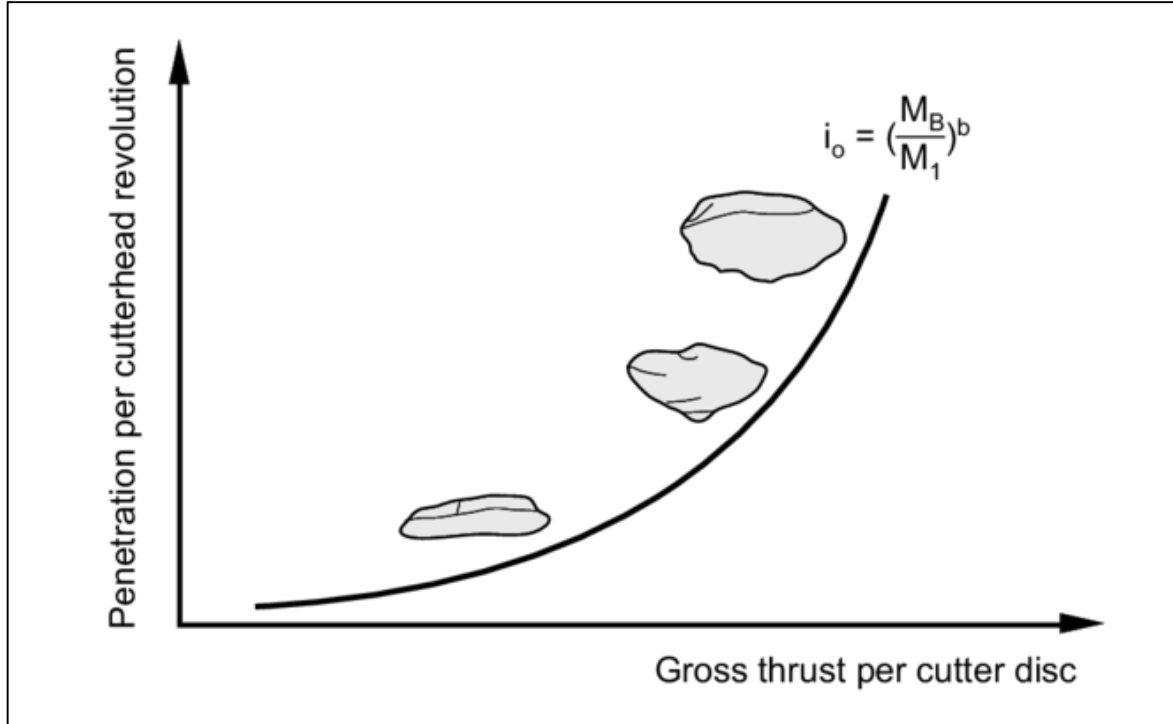


Figure 3.1 General progress of a penetration test curve (Bruland, 2000a)

As shown in Figure 3.1, the formula for the basic penetration rate is given by Bruland (2000b):

$$i_0 = \left(\frac{M_{ekv}}{M_1} \right)^b \quad (3.1)$$

| | |
|-----------|---|
| i_0 | basic penetration rate (mm/rev) |
| M_{ekv} | equivalent cutter thrust (kN/c) |
| M_1 | critical cutter thrust in kN/c (necessary thrust to achieve 1 mm/rev) |
| b | penetration coefficient |

The main parameters in this penetration curve are, from Bruland (2000b):

- M_1 – The critical or necessary thrust to achieve a penetration of 1 mm per cutterhead revolution
- b – The penetration coefficient or penetration exponent. Describes the effect of a change in the applied cutter thrust.

Parameters

The parameters needed to predict the penetration are divided into geological and machine parameters. (Bruland, 2000a)

Table 3.1 Net penetration rate parameters (Bruland, 2000a)

| Rock Mass Parameters | Machine Parameters |
|---|-------------------------------|
| - Fracturing; frequency and orientation | - Gross average cutter thrust |
| - Drilling Rate Index, <i>DRI</i> | - Average cutter spacing |
| - Porosity | - Cutter diameter |

Of the three rock mass parameters, the *DRI* expresses the drillability of intact rock. The *DRI* is composed by the Sievers' J-value and the S_{20} . The Sievers' J-value expresses the surface hardness, while the S_{20} expresses the rock brittleness. (Bruland, 2000a)

The k_s factor expresses the rock mass fracturing. This geological factor is identified to have the largest influence on the net penetration rate in hard rock conditions. It consists of two parts. The first is the rock mass degree of fracturing, or in other words the average spacing between planes of weakness. The second is the angle between the tunnel axis and the planes of weakness. (Bruland, 2000a)

The degree of fracturing is set by the distance between the fractures and the type of fracture. Fractures are divided into two groups, fissures and joints. They have little or no shear strength along the planes of weakness. The distance between the fractures also plays an important role. The smaller the distance between these fractures, the more the penetration rate of the TBM is affected (Bruland, 2000b). The different types of fractures are:

- **Joints (Sp):** These types are continuous joints, which mean that they can be followed all around the tunnel profile. They can either be filled with clay or other weak materials, or they can simply be open joints. (Bruland, 2000b)
- **Fissures (St):** Fissures include non-continuous joints, which mean that they can only be followed partly around the tunnel profile, filled joints with low shear strength and bedding plane fissures. (Bruland, 2000b)
- **Homogenous Rock Mass (Class 0):** A massive rock with no joints or fissures present. Some rock masses where the joints are filled and have high shear strengths could come close to this classification. (Bruland, 2000b)

To make the classification easier when mapping in the tunnel, the rock mass is divided into different classes as shown in Table 3.2.

Table 3.2 Fracture classes and the different distance between the planes of weakness (Bruland, 2000b)

| Fracture Class (Joints = Sp / Fissures = St) | Distance between planes of weakness [cm] | |
|---|--|-----|
| | 0 | - |
| 0-I | 160 | - |
| I- | 80 | 160 |
| I | 40 | 80 |
| II | 20 | 40 |
| III | 10 | 20 |
| IV | 5 | 10 |

The k_s value is dependent on the angle between the tunnel axis and the planes of weakness. This angle, α , is calculated using the following equation presented by Bruland (2000b):

$$\alpha = \arcsin(\sin \alpha_f \cdot \sin(\alpha_t - \alpha_s)) \quad (3.2)$$

- α_s strike angle (°)
- α_f dip angle (°)
- α_t tunnel direction (°)

In Figure 3.3 the fracturing factor is shown as a function of fissure or joint class and angle between the tunnel axis and the planes of weakness, is shown. This is used to calculate the fracturing factor, k_s . The curves indicate that the optimal angle for highest fracture is about 60° between the tunnel axis and the planes of weakness. With a very low spacing between the weakness zones, the optimal angle is 90°. (Bruland, 2000d)

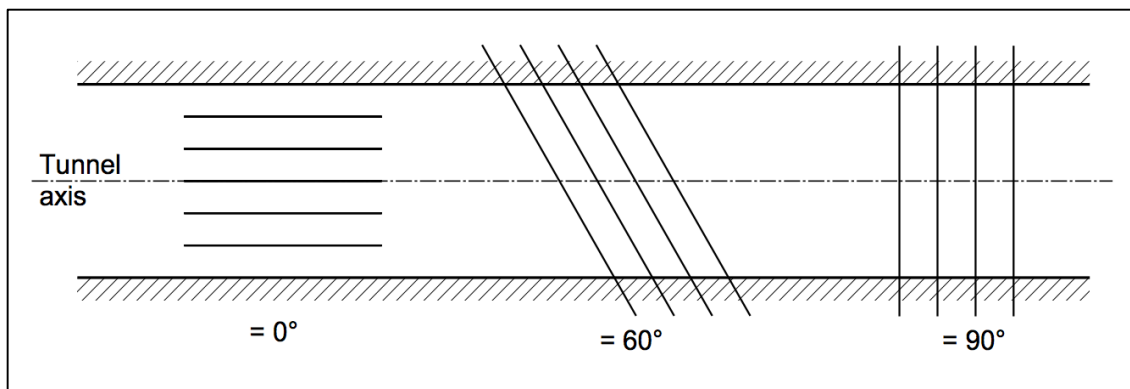


Figure 3.2 Influence of systematically occurring fissures or joints at various angles to the tunnel axis (Bruland, 2000d)

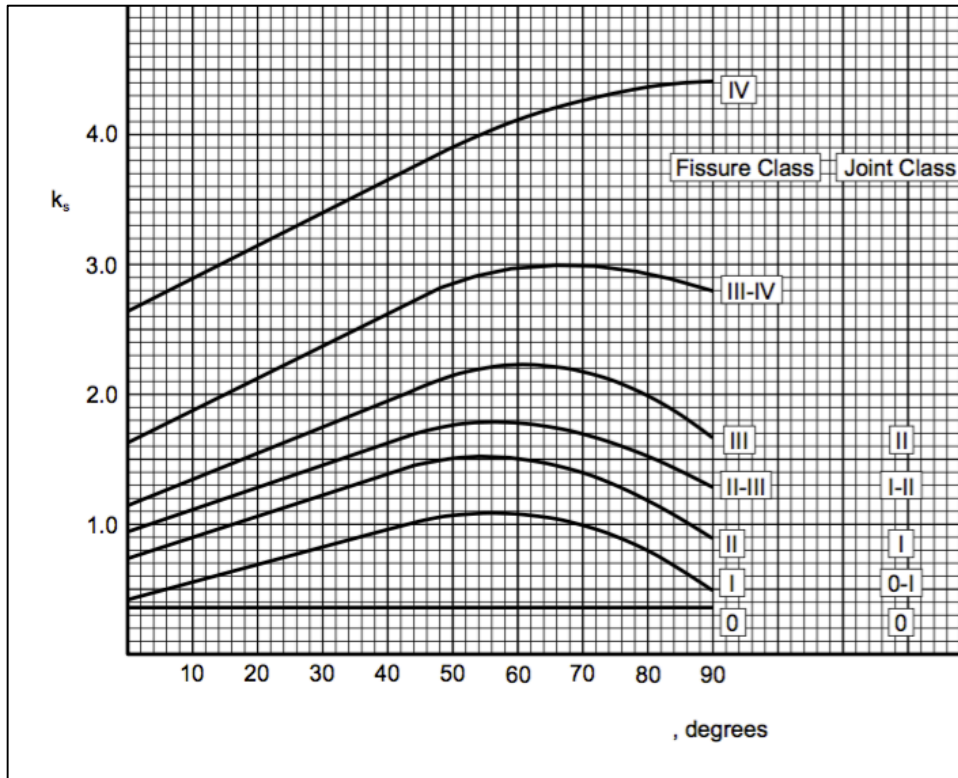


Figure 3.3 Fracturing factor (Bruland, 2000b)

In a tunnel, you usually have more than one set of weakness planes. When this occurs the total fracturing factor is defined as follows, according to Bruland (2000b):

$$k_{s-tot} = \sum_{i=1}^n k_{si} - (n - 1) \cdot 0.36 \quad (3.3)$$

k_{s-tot} total fracturing factor
 k_{si} fracturing factor for set no. i
 n number of fracturing sets

While mapping the tunnel, it usually gets divided into different sections. Further, an average k_s value is found by a weighted total average calculated from the different k_{si} values. Bruland (2000c) presents the following equation:

$$k_{s-avg} = \frac{\sum_{i=1}^n l_i}{\sum_{i=1}^n \frac{l_i}{k_{si}}} \quad (3.4)$$

k_{s-avg} average fracturing factor for tunnel
 k_{si} fracturing factor for set no. i
 l_i length of set no. i
 n number of fracturing sets

The porosity in hard rocks is typically less than 2 % (volumetric). However, this can in some cases be higher. The pores work as crack initiators and amplify the propagation of cracks in the rock. The effect the porosity has on the *DRI* is less than the actual effect on

the penetration rate; therefore, a correction factor is added to the model to compensate. (Bruland, 2000a)

Of the machine parameters needed to calculate the net penetration rate, the average cutter load is the most influential. The higher load or thrust used, the more efficiently the energy from the cutterhead is transferred to the rock mass. This assures a deeper penetration of the cutter ring edge into the rock surface. For this parameter, the NTNU model divides the total cutterhead thrust by the number of cutters on the cutterhead. This is called the gross average cutter thrust. To make sure that the cutterhead thrust relates to the average thrust cylinder pressure and not only to the maximum values, the cutter thrust is averaged over time. Also, for this model there are not made any correction for friction. (Bruland, 2000a)

The cutter diameter, the cutter ring quality and the rock mass fracturing are all important to how much cutter thrust should be applied (Bruland, 2000b). The relation between the cutter diameter and the maximum recommended thrust is shown below.

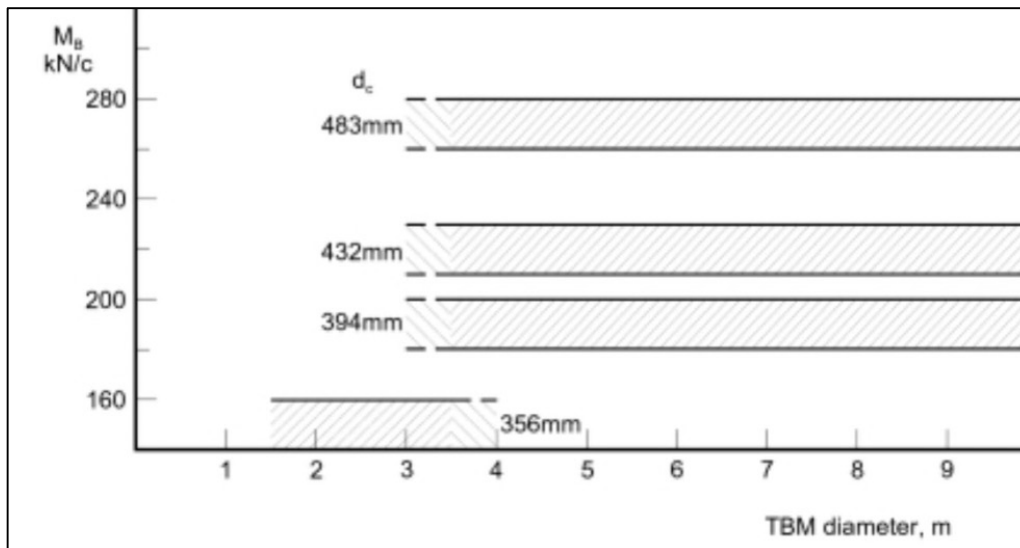


Figure 3.4 Recommended maximum gross average thrust per disc (Bruland, 2000b)

The correction factor for cutter diameter, in addition to the applicable cutter thrust, determine the contact area under the cutter ring edge. This has a direct influence on the cutter ring indentation for a given cutter load. (Bruland, 2000a)

The third and last machine parameter the model includes, is the average spacing of the cutters on the cutterhead. To calculate the average spacing, the cutterhead radius is divided by the number of cutters on the TBM. The model has some limitations regarding this parameter. There are some cutterheads that operate with more than one cutter per track in the outer gauge tracks. This can only be used if the cutterhead does not have double-tracking cutters that exceeds 10% of the total number of cutters. (Bruland, 2000a)

The NTNU-model assumes that the cutterhead's *RPM* has approximately the same value as the rolling velocity of the outer gauge cutter (Bruland, 2000a). This might not always be accurate, but according to Bruland (2000a) there was not enough field data to incorporate the cutterhead *RPM* as a separate parameter in the model as of that time.

The basic net penetration rate I_0 from Bruland (2000b):

$$I_0 = i_0 \cdot RPM \cdot \left(\frac{60}{1000} \right) \quad (m/h) \quad (3.5)$$

3.1.2 Cutter wear

The NTNU-model bases the calculations regarding cutter life on the fact that the wear of the cutter rings is mainly abrasive. It is assumed that the TBM is operated at a trust level resulting in a wear as such. (Bruland, 2000b)

Cutter wear and cutter life are important factors to pay attention to as cutter inspections and cutter changes are time-consuming activities. During these activities, the boring is stopped. This leads to a decrease in the advance rate, as a high degree of cutter wear cause longer downtimes of the machine. (Bruland, 2000a)

Parameters affecting cutter life in the NTNU-model according to Bruland (2000a) are displayed in Table 3.3.

Table 3.3 Rock and machine parameters affecting cutter life (Bruland, 2000a)

| Rock Mass Parameters | Machine Parameters |
|---------------------------------|---------------------------------------|
| - Cutter Life Index, <i>CLI</i> | - Number of cutters on the cutterhead |
| - Rock quartz content | - Cutter diameter |
| | - TBM diameter |
| | - Cutterhead <i>RPM</i> |

The *CLI* value is a rock parameter describing the abrasion properties of crushed rock powder and the rock surface hardness at the tunnel face. These properties will highly affect the wear of the cutters and the *CLI* will express the cutter ring life in hours. Abrasion Value Cutter Steel, *AVS*, and the Sievers' J-value, *SJ*, is used to calculate the *CLI*. *AVS* is the abrasion value of crushed rock powder and indicate how fast the cutter ring will abrade due to crushed rock and rock chips. *SJ* is the abrasion caused by the rock surface hardness and expresses the wear pattern on the cutter ring. (Bruland, 2000a)

The database forming the basis for the NTNU-model shows a deviation for the experienced cutter life in different rock types with the same quartz content. Therefore, a correction factor for quartz content in the rock mass is incorporated into the model. (Bruland, 2000a)

These machine parameters will effect cutter life, as described by Bruland (2000a):

- Increased cutter diameter gives a higher cutter life due to more steel to abrade on the cutter ring
- The number of cutters on the cutterhead will affect the penetration
- The TBM diameter will affect the cutter life; an increased diameter gives a higher cutter life
- The cutter ring life is inversely proportional to the cutterhead *RPM*

All these parameters have correction factors in the NTNU-model to assess their importance for cutter life.

Cutter wear can happen due to abrasive wear, destructive wear, damaged hub or other reasons. Abrasive wear should be the main cause for cutter ring wear. Other reasons for cutter change like blocked cutters and ring chipping of the cutter rings should be kept to a minimum. According to Bruland (2000b, p. 27), these changes “*should be less than 10-20 % of the total changed cutters*”.

Destructive wear happens in mainly two ways for steel ring cutters as stated by Bruland (2000c):

- Chipping along the cutter edge. This happens due to too high steel hardness relative to the cutter thrust and/or the rock strength
- Mushrooming of the cutter edge. This happens due to too low steel hardness relative to the cutter thrust and/or the rock strength

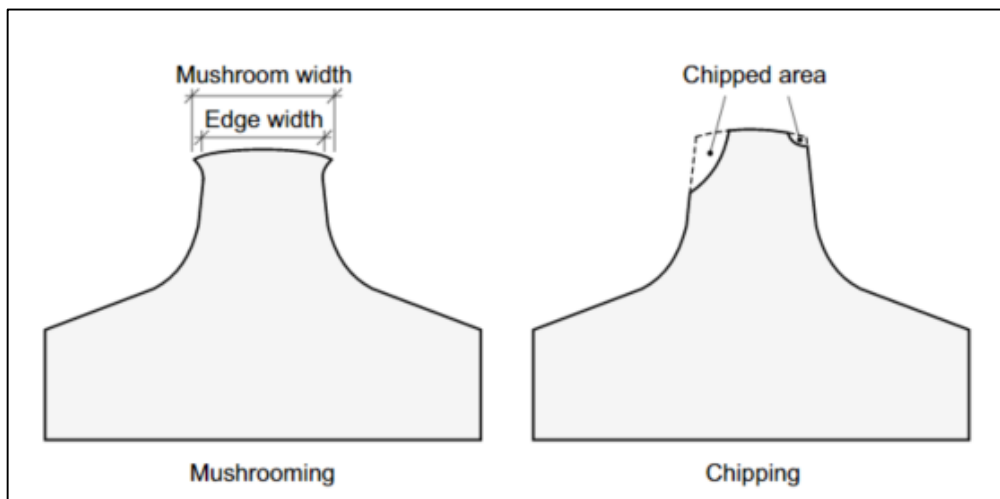


Figure 3.5 Destructive wear of cutter rings (Bruland, 2000c)

A high degree of chipping of the cutter rings can cause other problems like bevel edge wear, disc loosening and frozen bearings. Fractured rock mass and marked single joints cause more chipping of the cutter rings as these conditions will expose the cutter edge for large momentary loads. (Bruland, 2000d)

The cutter consumption in a project should be recorded in order to have a concrete overview of the cutter wear and see if any adjustments should be made. According to

Bruland (2000c), the cutter change log, inspections log and cutter repair log should provide enough data to calculate:

- Instantaneous and average cutter wear for the cutterhead
- Cutter consumption for each cutter position
- Reason for change
- Type and extent of the wear of each ring
- Consumption of spare parts

Each cutter should be given a unique identity to be able to trace all necessary data for the calculations mentioned above.

3.1.3 Cutter ring life

The average cutter ring life in the NTNU-model is given by the following equations, from Bruland (2000b):

$$H_h = (H_0 \cdot k_D \cdot k_Q \cdot k_{RPM} \cdot k_N) / N_{TBM} \quad (3.6)$$

$$H_m = H_h \cdot I_n \quad (3.7)$$

$$H_f = H_h \cdot I_n \cdot \pi \cdot d_{TBM}^2 / 4 \quad (3.8)$$

| | |
|-----------|--|
| H_h | average cutter ring life in hours (h/c) |
| H_0 | basic average cutter ring life |
| k_D | correction factor for TBM diameter |
| k_Q | correction for quartz content |
| k_{RPM} | correction for cutterhead <i>RPM</i> |
| k_N | correction for number of cutters |
| N_{TBM} | actual number of cutters |
| H_m | average cutter ring life in meters (m/c) |
| I_n | net penetration rate (m/h) |
| H_f | average cutter ring life solid cubic meters (sm ³ /c) |
| d_{TBM} | TBM diameter |

A brief description of the different parameters used in the equations for cutter ring life is shown in the list below, as said by Bruland (2000b):

- The cutter ring life is given in boring hours and is proportional to the Cutter Life Index *CLI*
- The correction factor for TBM diameter is used with increasing TBM diameter. This is due to a higher average cutter life when the ratio of the center and gauge cutters decrease with an increasing diameter
- The correction factor for quartz content account for the varying cutter ring life when quartz and other hard and abrasive minerals are present in the rock mass
- The correction factor for cutterhead *RPM* is used to correct the cutter ring life with varying cutterhead *RPMs*
- The correction factor for number of cutters is used if the actual number of cutters differs the model

3.1.4 Advance rate

Advance rate is given in meter per day, per week or similar. The net penetration rate given in m/h and machine utilization in percentage, is used to estimate the advance rate. It also uses the number of working hours for various operations during the period. (Bruland, 2000a)

Parameters

By using the net penetration rate and the cutter life in the calculations of the advance rate, geological and machine parameters are indirectly included. It is difficult to say how much the different parameters have an effect on the advance rate, since the background data are combined values. (Bruland, 2000a)

The machine utilization is according to Bruland (2000b) given by:

$$u = \frac{100 \cdot T_b}{T_b + T_t + T_c + T_{tbm} + T_{bak} + T_a} \quad (\%) \quad (3.9)$$

| | |
|-----------|-------------------------------|
| T_b | boring |
| T_t | regripping |
| T_v | cutter change and inspection |
| T_{tbm} | repair and service of the TBM |
| T_{bak} | repair and solve the backup |
| T_a | miscellaneous |

The weekly advance rate I_u is according to Bruland (2000b) given by:

$$I_u = u \cdot T_e \cdot \frac{I_m}{100} \quad (3.10)$$

| | |
|-------|--|
| I_u | weekly advance rate (m/week) |
| u | machine utilization |
| T_e | effective working hours per week |
| I_m | average net penetration rate over the tunnel |

3.1.5 NTNU-model updated as of 2016

In December 2016, an updated NTNU-model was published as part of the doctoral thesis of Javier Macias. This update incorporates data and experience from several ongoing and recently completed TBM projects. The model is also revised regarding developments in TBM technology. (Macias, 2016)

An overview over the topics revised or extended in the updated model is presented below, from Macias (2016):

- General machine specifications; the standard number of cutters, cutter diameter, installed cutterhead power, recommended applied gross cutter thrust and cutterhead velocity (revised)
- The category intervals for *DRI* and *CLI* (revised)
- Fracture classes (revised)
- Graphs used to calculate the rock mass fracturing factor, k_s (revised)
- The *DRI* correction factor (revised)
- The penetration coefficient (b) and basic penetration (i_0) (revised)
- Influence of cutterhead velocity on TBM penetration (extension)
- Correction factor for cutterhead velocity (extension)
- Cutter life model (revised)
- Time consumption factor linked to the influence of tunnel length on operational activities (extension)

Some of the topics mentioned above are further presented in the following subchapters.

Fracture classes and rock mass fracturing factor

In the updated model, all continuous and non-continuous fractures representing weak areas of rock influencing performance, are incorporated in the term “fractures”. The previous model version divided the fractures into two groups, fissures and joints. Also, the different classes describing the degree of fracturing in a rock mass are revised (Macias, 2016). The updated model’s classifications of fracture classes will be used in this thesis.

Table 3.4 Updated fracture classes with distance between the planes of weakness (Macias, 2016)

| Fissure class (St) (Bruland, 2000b) | Fracture class (Sf) | Average spacing between fractures a_f (cm) | Range class (cm) | Degree of fracturing |
|--|---------------------|--|------------------|----------------------|
| 0 | 0 | ∞ | 480 – ∞ | Non-fractured |
| 0 | 1 | 320 | 240 – 480 | Extremely low |
| 0 - I | 2 | 160 | 120 – 240 | Very low |
| I - | 3 | 80 | 60 – 120 | Low |
| I | 4 | 40 | 30 – 60 | Medium |
| II | 5 | 20 | 15 – 30 | High |
| III | 6 | 10 | 7.5 – 15 | Very high |
| IV | 7 | 5 | 4 – 7.5 | Extremely high |

The graphs used to find the k_s -value describing the rock mass fracturing are also revised. In addition, a detailed graph for calculating low values of the fracturing factor are added. These graphs are displayed in Figure 3.6 and Figure 3.7.

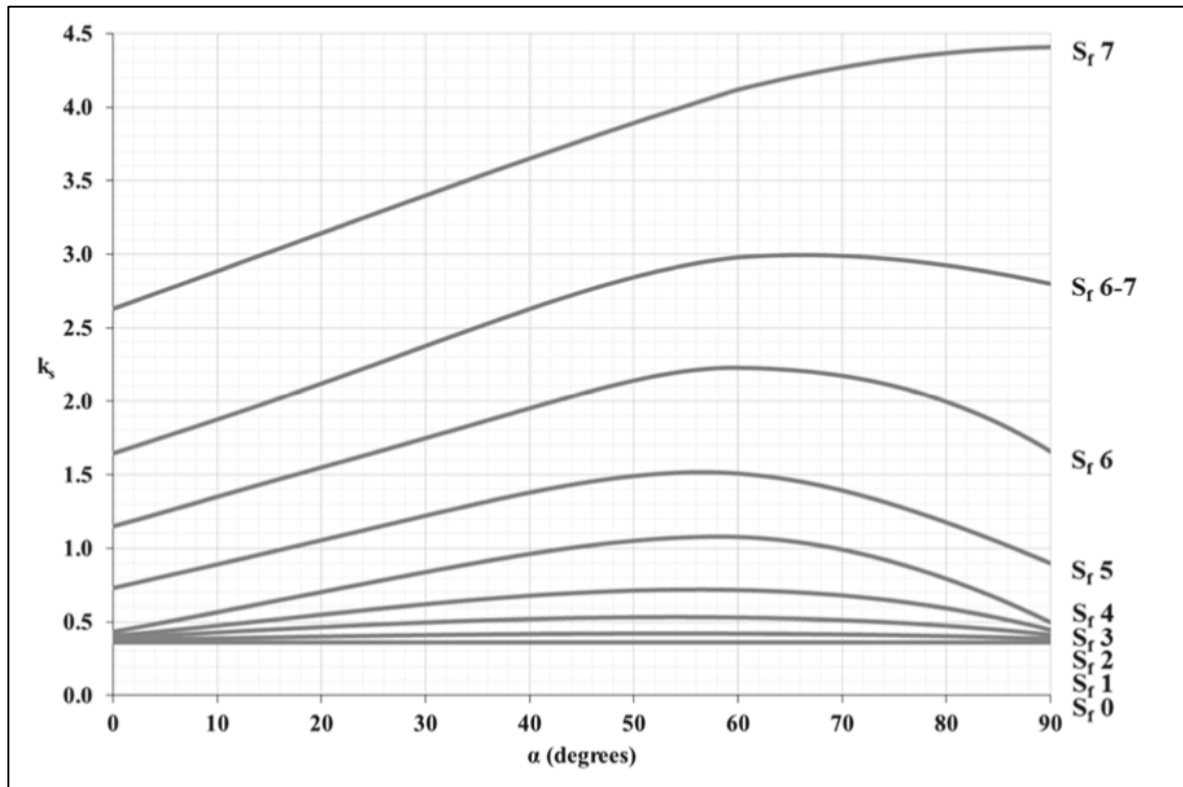


Figure 3.6 Rock mass fracturing factor (k_s) as a function of the angle between the tunnel axis and the fractures (Macias, 2016)

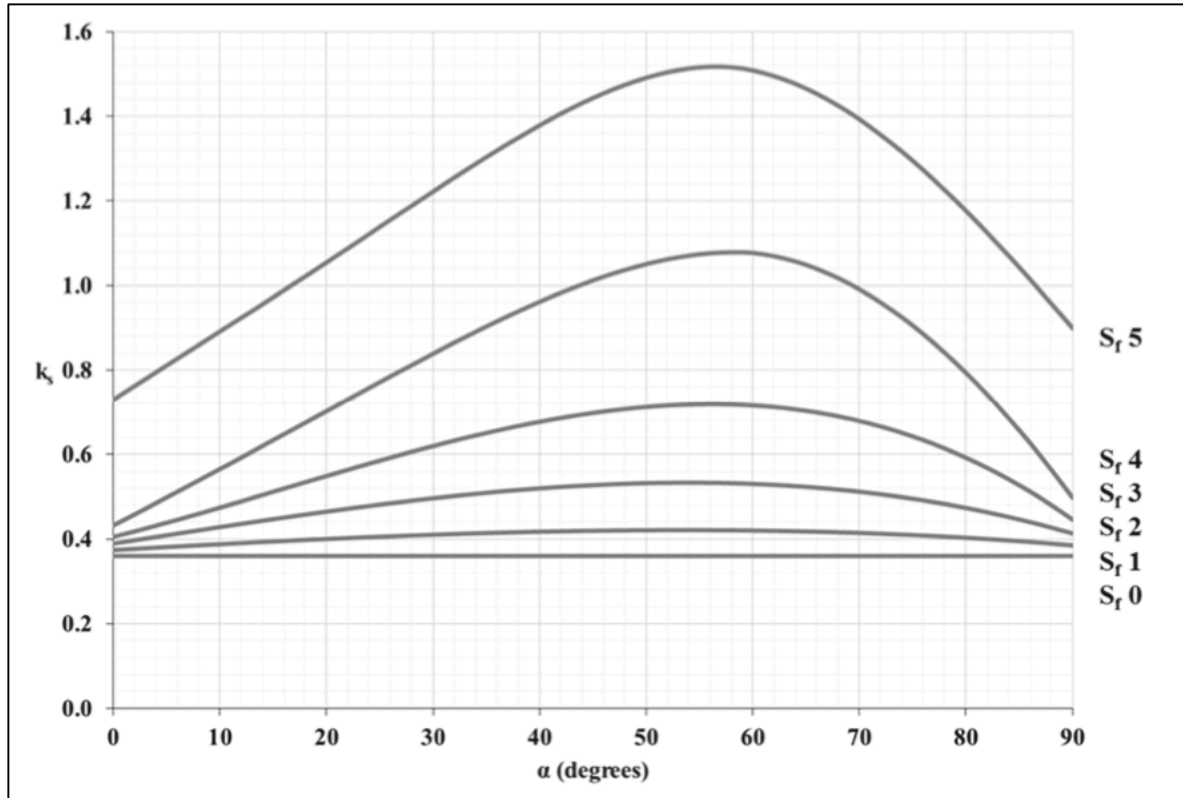


Figure 3.7 Detailed graph for calculating low values of the fracturing factor (k_s) (Macias, 2016)

Influence of cutterhead velocity on net penetration rate

A new test method called *RPM* test was introduced in the thesis of Macias (2016) to assess the influence of cutterhead velocity on net penetration rate. The results from this show that a reduction of the *RPM* can improve boring efficiency and reduce excavation costs. To account for this in the model, a correction factor for cutterhead velocity (k_{RPM}) is added to the basic net penetration rate formula. (Macias, 2016)

$$I_0 = i_0 \cdot RPM \cdot \left(\frac{60}{1000} \right) \cdot k_{RPM} \quad (3.11)$$

Cutter life model

The cutter life model is revised in the updated NTNU-model. This is based on sections from several projects providing detailed information about geology, rock mass, drillability testing and instantaneous cutter life. (Macias, 2016)

The recommended cutterhead *RPM* has been updated. This leads to an updated correction factor for cutterhead *RPM*. (Macias, 2016)

The correction factor for quartz content is revised to account for the content of abrasive minerals, including quartz, garnet, epidote, pyrite and olivine. (Macias, 2016)

A new correction factor for the influence of cutter thrust on cutter life has been added to the cutter life model. This correction factor is used when the rock mass has extremely or very abrasive properties, with a corresponding *CLI*-value of 4.5-6.0. (Macias, 2016)

The average cutter ring life equation is now presented as follows:

$$H_h = (H_0 \cdot k_D \cdot k_Q \cdot k_{RPM} \cdot k_N \cdot k_T) / N_{TBM} \quad (3.12)$$

| | |
|-----------|---|
| H_h | average cutter ring life in hours (h/c) |
| H_0 | basic average cutter ring life |
| k_D | correction factor for TBM diameter |
| k_Q | correction for quartz content |
| k_{RPM} | correction for cutterhead <i>RPM</i> |
| k_N | correction for number of cutters |
| N_{TBM} | actual number of cutters |
| k_T | cutter thrust factor |

Length factor advance rate

The tunnel length is of importance for the time used on tunneling activities. Problems related to muck transport, ventilation, electricity and water supply systems are more likely the longer the tunnel is. Waiting times for transport will also increase. Therefore, a length factor is added to the calculation of the machine utilization.

The machine utilization is now, according to Macias (2016), given by:

$$u = \frac{100 \cdot T_b}{T_b + T_r + T_c + T_{tbm} + T_{back} + T_m + T_l} \quad (\%) \quad (3.13)$$

| | |
|------------|---|
| T_b | boring |
| T_r | regripping |
| T_c | cutter replacement and inspection |
| T_{tbm} | repair and service of the TBM |
| T_{back} | repair and service of the backup system |
| T_m | miscellaneous |
| T_l | tunnel length |

3.2 Model presented by Ebrahim Farrokh et al.

An article published by Ebrahim Farrok, Jamal Rostami and Chris Laughton in *Tunnelling and Underground Space Technology* in 2012, proposes a new prediction model for TBM performance. They have generated a new model based on analysis of data from a database containing more than 300 TBM projects. This database is used to generate new formulas for prediction of the penetration rate. The obtained results were compared with the actual field performance data for each project to be able to ensure the predictive capabilities of the newly presented formulas. (Farrokh et al., 2012)

Table 3.5 A description of the TBM penetration rates. (Farrokh et al., 2012)

| Description | Typical unit |
|--|--------------|
| PR = Penetration rate | m/h |
| PRev = Penetration rate per revolution | mm/rev |

The article demonstrates two different formulas calculating the penetration rate. The first, explained by equation (3.14) and (3.15), is found with regression analyses with *PRev* as the objective parameter. From this, the *PR* is found by multiplying *PRev* with the TBMs *RPM*. The regression to obtain equation (3.14) has a coefficient of determination, R^2 , of 63%. This means that 63% of the variance in *PRev* is predictable from the variables. (Farrokh et al., 2012)

$$PRev = e^{(0.41+0.404 \cdot D - 0.027 \cdot D^2 + 0.0691 \cdot RT_c - 0.00431 \cdot UCS + 0.0902 \cdot RQD_c + 0.000893 \cdot F_n)} \quad (3.14)$$

| | |
|---------|---|
| D | tunnel diameter (m) |
| RT_c | rock type numerical code (Table 3.6) |
| UCS | Uniaxial Compressive Strength (MPa) |
| RQD_c | RQD numerical code (Table 3.7) |
| F_n | disc cutter normal force (kN) |

$$PR = \frac{PRev \cdot RPM \cdot 60}{1000} \quad (3.15)$$

The second formula, presented here as equation (3.16), provides the penetration rate directly. Here Farrokh et al. (2012) used log transformation of most of the model parameters to obtain the equation. The coefficient of determination for this is slightly less than for equation (3.14), with an R^2 of 58%. The regression equation is, from Farrokh et al. (2012):

$$PR = \frac{F_n^{0.186} \cdot RQD_c^{0.133} \cdot RT_c^{0.183} \cdot RPM^{0.363} \cdot D^{5.47} \cdot e^{(0.046 \cdot D^2)}}{5.64 \cdot UCS^{0.248} \cdot e^{(1.58 \cdot D)}} \quad (3.16)$$

| | |
|---------|---|
| D | tunnel diameter (m) |
| RT_c | rock type numerical code (Table 3.6) |
| UCS | Uniaxial Compressive Strength (MPa) |
| RQD_c | RQD numerical code (Table 3.7) |
| F_n | disc cutter normal force (kN) |
| RPM | revolution per minute (rev/min) |

Farrokh et al. (2012) has put up a numerical code system for determining rock type and RQD . Values for RT_c and RQD_c to be used in the equations can be found in Table 3.6 and Table 3.7 respectively.

Table 3.6 Rock type categorization used in article (Farrokh et al., 2012)

| Rock Type | Code | RTc |
|---|------|-----|
| Claystone, mudstone, marl, slate, phyllite, argillite | C | 5 |
| Sandstone, siltstone, conglomerate, quartzite | S | 3 |
| Limestone, chalk, dolomite, marble | L | 3 |
| Karstic Limestone | K | 3 |
| Metamorphic rocks such as gneiss and schist | M | 2 |
| Coarse igneous such as granite and diorite | G | 1 |
| Fine volcanic such as basalt, tuff and andesite | V | 2 |

Table 3.7 RQD_c classification (Farrokh et al., 2012)

| CFF | Code | Description | Corresponding RQD range |
|-------------------------|------|------------------|---------------------------|
| Less than 8 fractures/m | 1 | Low frequency | 90-100 |
| 8-12 fractures/m | 2 | Medium frequency | 60-90 |
| 12-16 fractures/m | 3 | High frequency | <60 |

3.3 Model presented by Hassanpour et al.

Hassanpour, Rostami and Zhao published an article in the journal *Tunnelling and Underground Space Technology* in 2011. Here they explain a new performance prediction model for TBM in hard rock. The work was published as Hassanpour et al. (2011) wished to develop a more accurate prediction model for different geological conditions. In the development of this new model, they collected data from four different projects; three long water conveyance tunnels and one tailrace tunnels, all with different rock mass conditions. The tunnels are fairly recently constructed.

Developing the equations for the new prediction model, Hassanpour et al. (2011) have used both single and multi-variable regression analyzes. This is to study the correlation between the TBM performance parameters and the rock properties. On this basis, empirical equations have been developed that determine the penetration rate. (Hassanpour et al., 2011)

Field Penetration Index, or *FPI*, is a machine parameter related to geological parameters (Hassanpour et al., 2011). The equation (3.17), found with multi-variable regression analysis, is shown below.

$$FPI = e^{(0.008 \cdot UCS + 0.015 \cdot RQD + 1.384)} \quad (3.17)$$

| | |
|------------|--|
| <i>FPI</i> | field penetration index (kN/cutter/mm/rev) |
| <i>UCS</i> | intact rock strength (MPa) |
| <i>RQD</i> | rock quality designation (%) |

Rate of penetration, or *ROP*, is calculated using the equation (3.18) below.

$$ROP = \frac{0.06 \cdot F_n \cdot RPM}{FPI} \quad (m/h) \quad (3.18)$$

| | |
|------------|--|
| F_n | average disk cutter load (kN) |
| <i>RPM</i> | revolution per minute (rev/min) |
| <i>FPI</i> | field penetration index (kN/cutter/mm/rev) |

3.4 Gehring and Alpine model

The Gehring penetration prediction model was developed by Austrian Dr. Karlheinz Gehring in 1995 (Gehring, 1995). The model was originally published in Austria; thus, the information was not possible to acquire from the original source. The information about the model is obtained from the PhD-thesis of Wilfing (2016).

The model is empirical and based on analyses from different tunnel projects in the Alpine-region, based on data from TBMs with a certain machine setup; 17” cutters and 80 mm spacing. The outcome of the model is a maximum penetration for a given normal force per cutter. The formula used to calculate the penetration is given in equation (3.19).

$$p = \frac{F_N}{\sigma_u} \cdot k_i \quad (mm/rev) \quad (3.19)$$

| | |
|------------|-------------------------------------|
| p | penetration rate (mm/rev) |
| F_n | normal force per cutter (kN) |
| σ_u | Uniaxial Compressive Strength (MPa) |
| k_i | correction factors |

The different correction factors are listed below:

- k_0 : basic penetration factor
- k_1 : factor for specific failure energy
- k_2 : factor for rock mass fabric
- k_3 : factor for cutter diameters \neq 432 mm
- k_4 : factor for cutter spacing \neq 80 mm

Basic penetration factor

The basic penetration factor in the Gehring-model is set at 4.0 with a given machine setup of 17” cutters and 80 mm spacing. This was seen as sufficient for practical use.

Factor for specific failure energy

The energy needed to cause failure of a material under uniaxial compression was by Gehring pointed out to be of importance for the penetration of rocks. This is accounted for in the model by a parameter called specific failure energy w_f . The parameter w_f is given by the ratio of failure energy and Uniaxial Compressive Strength shown in equation (3.20) and the correction factor is calculated according to equation (3.21).

$$w_f = \frac{W_f}{\sigma_u} \quad (3.20)$$

| | |
|------------|-------------------------------------|
| w_f | specific failure energy |
| W_f | failure energy (Nm) |
| σ_u | Uniaxial Compressive Strength (MPa) |

$$k_1 = 0.475 \cdot w_f^{-0.56} \quad (3.21)$$

k_1 factor for specific failure energy
 w_f specific failure energy

Factor for rock mass fabric

This correction factor is given by spacing and orientation of foliation, joints and other planes of weaknesses. Only the spacing and orientation of the major plane of weakness is used to find the correction factor. Other fracture sets present in the rock mass are not considered. For the spacing, only values ≤ 50 cm are expected to affect the penetration rate. The orientation is given by the smallest angle between the tunnel axis and the plane of weakness shown in equation (3.22).

$$\alpha = \sin^{-1}(\sin \alpha_f \cdot \sin(\alpha_t - \alpha_s)) \quad (^\circ) \quad (3.22)$$

α smallest angle between tunnel axis and discontinuity ($^\circ$)
 α_f dip angle discontinuity ($^\circ$)
 α_s strike angle discontinuity ($^\circ$)
 α_t tunnel direction ($^\circ$)

Once the orientation is calculated and the spacing of the discontinuity is known, the correction factor can be decided from Table 3.8.

Table 3.8 Correction factor k_2 (Wilfing, 2016)

| Spacing of discontinuity | Correction factor k_2 at $\alpha=$ | | | |
|--------------------------|--------------------------------------|------------|------------|------------|
| | 0° | 30° | 60° | 90° |
| > 50 cm | 1.0 | 1.0 | 1.0 | 1.0 |
| 10-50 cm | 1.2 | 1.3 | 1.6 | 1.3 |
| 5-10 cm | 1.4 | 1.8 | 2.3 | 1.6 |
| < 5 cm | 1.7 | 2.3 | 3.0 | 2.0 |

Factor for cutter diameters $\neq 432$ mm

The cutter diameter and penetration rate has a linear relation and the correction factor for cutter diameter can be calculated from equation (3.23).

$$k_3 = \frac{430}{d_c} \quad (3.23)$$

k_4 factor for cutter diameters $\neq 432$ mm
 d_c cutter diameter (mm)

Factor for cutter spacing $\neq 80$ mm

The correction factor for cutter spacing, k_4 , is given in Figure 3.8.

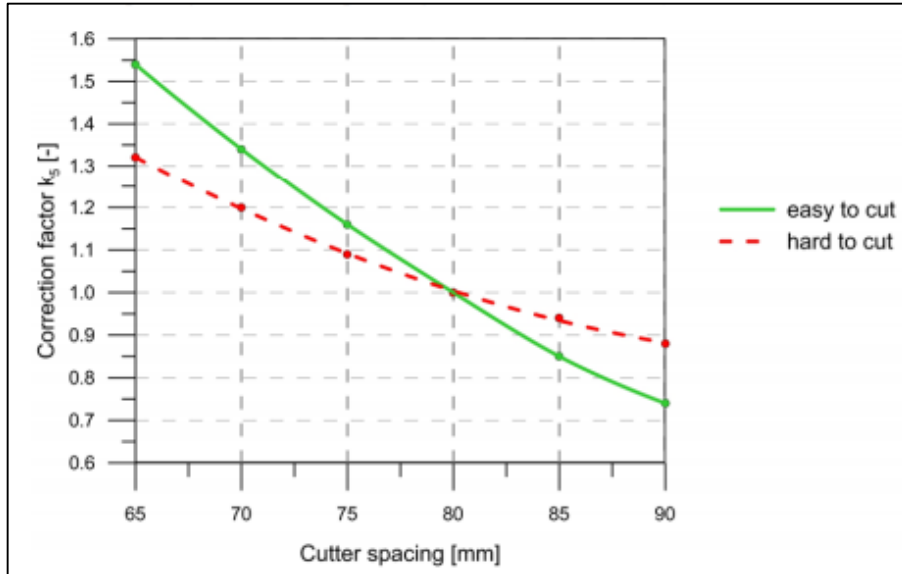


Figure 3.8 Diagram to correct for cutter spacing (Wilfing, 2016)

3.4.1 Modified Gehring model or Alpine model

In 2016 a modified Gehring model, called the Alpine model, was published by Lisa Wilfing in her doctoral thesis. The Alpine model modifies the Gehring model to better reflect the relation between the applied force and resulting penetration. This is done by incorporating a y-intercept of Brazilian Tensile Strength or *LCPC* breakability coefficient (Wilfing, 2016). The equations for calculating the two approaches are shown in equation (3.24) and (3.25).

$$b_{BTS\ 3mm} = e^{0.08 \cdot \sigma_t + 4.1} \quad (3.24)$$

$b_{BTS\ 3mm}$ y-intercept *BTS* approach at penetration 3 mm/rev
 σ_t Brazilian Tensile Strength (MPa)

$$b_{LBC\ 3mm} = -1.3 \cdot LBC + 194.7 \quad (3.25)$$

$b_{LBC\ 3mm}$ y-intercept *LBC* approach at penetration 3 mm/rev
 LBC *LCPC* breakability coefficient (%)

The penetration rate can then be found by equation (3.26).

$$p = \frac{F_N - b_{BTS/LBC}}{\sigma_u} \cdot k_0 \cdot k_2 \cdot k_i + 3 \quad (3.26)$$

p penetration rate (mm/rev)
 F_n normal force per cutter (kN)
 σ_u Uniaxial Compressive Strength (MPa)
 $B_{BTS/LBC}$ y-intercept *BTS* or *LBC* approach
 k_0 basic penetration factor = 4.0
 k_2 correction factor for discontinuity pattern
 k_i correction factors for geotechnical or machine parameters

3.5 Q_{TBM} -model

The Q_{TBM} -model was published by Nick Barton in 2000 (Barton, 2000). The model is based on the Q-system, which is widely used in Norway for D&B tunnels. The Q-system is used to determine rock support. With some adjustments, Bartons Q_{TBM} -model incorporate the basic geological factors presented in the Q-system, and adds new parameters that affect TBM performance.

The first step in the model is to calculate the Q -value:

$$Q = \left(\frac{RQD}{J_n} \right) \cdot \left(\frac{J_r}{J_a} \right) \cdot \left(\frac{J_w}{SRF} \right) \quad (3.27)$$

| | |
|-------|------------------------------|
| RQD | rock quality designation |
| J_n | joint set number |
| J_r | joint roughness number |
| J_a | joint alternation number |
| J_w | joint water reduction factor |
| SRF | stress reduction factor |

The next step is to find a Q -value that is oriented in the tunneling direction, therefore the RQD is modified to RQD_0 . The J_r and J_a values are chosen for the joint set or discontinuity that affect the cutters most. (Barton, 2000)

$$Q_0 = \left(\frac{RQD_0}{J_n} \right) \cdot \left(\frac{J_r}{J_a} \right) \cdot \left(\frac{J_w}{SRF} \right) \quad (3.28)$$

Next up, the rock mass strength named *SIGMA* is determined. This factor is dependent on the joint inclination angle β . The parameter is depended on whether the joint inclination is unfavorable or favorable. $SIGMA_{cm}$ is given in equation (3.29), and used with an unfavorable inclination. If a favorable inclination is present, $SIGMA_{tm}$ given in equation (3.30) is applied in the calculations. (Barton, 2000)

$$SIGMA_{cm} = 5\gamma Q_c^{\frac{1}{3}}, \text{ where } Q_c = Q_0 \cdot \frac{\sigma_c}{100} \quad (3.29)$$

$SIGMA_{cm}$ rock mass strength (MPa)
 γ density (g/cm³)
 σ_c Uniaxial Compressive Strength

$$SIGMA_{tm} = 5\gamma Q_t^{\frac{1}{3}}, \text{ where } Q_t = Q_0 \cdot \frac{I_{50}}{4} \quad (3.30)$$

$SIGMA_{tm}$ rock mass strength (MPa)
 γ density (g/cm³)
 I_{50} point load index

When the general rock properties are found, the cutter force, cutter life index, and quartz content need to be obtained. As all these parameters are acquired, the value for Q_{TBM} can be calculated using equation (3.31).

$$Q_{TBM} = Q_0 \cdot \frac{SIGMA}{F^{10} / 20^9} \cdot \frac{20}{CLI} \cdot \frac{q}{20} \cdot \frac{\sigma_{\theta}}{5} \quad (3.31)$$

F cutter force (tnf)
 CLI cutter life index
 q quartz content (%)
 σ_{θ} biaxial stress on tunnel face (MPa)

Once the Q_{TBM} -value is determined, the net penetration rate can then be calculated. This formula is based on case records from 145 tunnels with a total length of 1000 km.

$$NPR \approx 5Q_{TBM}^{-1/5} \quad (3.32)$$

NPR net penetration rate (m/hr)

3.6 CSM- and MCSM-model

The Colorado School of Mines (CSM) model was first published by Levent Ozdemir in 1977 (Ozdemir, 1977). It was updated in a theoretical approach by Jamal Rostami in 1997 (Rostami, 1997). The model is semi-theoretical and is based on results from linear cutting tests which are used to measure and evaluate the cutting forces on cutters individually. The cutting forces are calculated as a function of uniaxial compressive and tensile strength of rock, and of the cutter geometry. (Yagiz et al., 2012)

The model's approach is to start from the individual cutter forces and then finding the overall thrust, torque and power required to get the maximum rate of penetration. To find the total force per cutter the equations presented as equation (3.33), (3.34) and (3.35) below, needs to be calculated. (Yagiz et al., 2012)

$$\Phi = \cos^{-1} \left(\frac{R - P}{R} \right) \quad (3.33)$$

Φ angle of contact (rad)
 R cutter radius (mm)
 P penetration rate (mm/rev)

$$P^0 = C \cdot \sqrt[3]{\frac{S \cdot \sigma_u^2 \cdot \sigma_t}{\Phi \cdot \sqrt{R \cdot T}}} \quad (3.34)$$

P^0 pressure of contact area (MPa)
 C coefficient = 2.12
 S spacing of cutters (mm)
 σ_u Uniaxial Compressive Strength (MPa)
 σ_t Brazilian Tensile Strength (MPa)
 T cutter tip width (mm)

$$F_t = \left(\frac{P^0 \cdot \Phi \cdot R \cdot T}{(1 + \Psi) \cdot 1000} \right) \quad (3.35)$$

F_t total force per cutter (kN)
 Ψ Constant, usually between 0.2 to -0.2

When the total force is calculated, the normal force and rolling force per cutter can be found by equation (3.36) and (3.37).

$$F_N = F_t \cdot \cos \left(\frac{\Phi}{2} \right) \quad (3.36)$$

F_n normal force per cutter (kN)

$$F_r = F_t \cdot \sin \left(\frac{\Phi}{2} \right) \quad (3.37)$$

F_r rolling force per cutter

The following steps of the model is to calculate the total thrust requirements, torque, rotational speed, power requirement of the head and an installed thrust and power by using an efficiency factor. The equations for finding these values are shown below.

$$Th^* = \sum_1^N F_{Ni} \approx N \cdot F_N \quad (3.38)$$

Th^* total thrust requirement (kN)
 N number of cutters

$$Tq^* = \sum_1^N F_{ri} \cdot R_i \approx 0.3 \cdot D \cdot N \cdot F_r \quad (3.39)$$

Tq^* torque (kNm)
 D TBM diameter (m)

$$RPM = \frac{V}{\pi \cdot D} \quad (3.40)$$

RPM rotational speed
 V linear velocity limit of the cutters (m/min)

$$P^* = \frac{\pi}{30} \cdot Tq^* \cdot RPM \quad (3.41)$$

P^* power requirement (kW)

When all the parameters above are calculated with a given rock type and machine setup, rate of penetration is the only variable that can be changed until one of the limits is reached. The CSM model calculates the maximum penetration per revolution that is possible to achieve with the present rock and machine parameters. (Yagiz et al., 2012)

The CSM model does not account for any discontinuities or stress conditions, only intact rock strength properties such as compressive and tensile strength. This is not adequate to describe the rock failure under cutter force. So, Saffet Yagiz presented a Modified CSM (MCSM) model in 2002 (Yagiz, 2002). The modified model incorporates intact rock brittleness (BI), distances between planes of weakness/fractures (F_s) and the angle between planes of weakness and the tunnel direction (α). (Yagiz et al., 2012)

To determine the brittleness index a punch penetration test must be performed in the laboratory. This test is not common to use in European rock laboratories, and was not possible to execute for this thesis. Instead, a conversion formula incorporating Uniaxial Compression Strength, Brazilian Tensile Strength and rock density, is used. (Yagiz, 2009) This formula is shown in equation (3.42).

$$BI_p = 0.198 \cdot \sigma_u - 2.174 \cdot \sigma_t + 0.913 \cdot \rho - 3.807 \quad (3.42)$$

| | |
|------------|-------------------------------------|
| BI_p | predicted brittleness (kN/mm) |
| ρ | density (kN/m ³) |
| σ_u | Uniaxial Compressive Strength (MPa) |
| σ_t | Brazilian Tensile Strength (MPa) |

Finally, a rate of penetration can be calculated using the MCSM model, by equation (3.43).

$$ROP = 0.272 + 0.027 \cdot BI - 0.225 \cdot F_s + 0.437 \cdot \log(\alpha) + 0.097 \cdot CSM_{ROP} \quad (3.43)$$

| | |
|-------------|---|
| ROP | rate of penetration (m/h) |
| CSM_{ROP} | CSM model result (m/h) |
| BI | brittleness index (kN/mm) |
| F_s | distance between planes of weakness () |
| α | angle between planes of weakness and the tunnel direction (°) |

4 Methodology

Chapter 4 presents the research methodology in this thesis. The chapter provides a theoretical analysis of the set of methods applied. It will give the reader an understanding of the data, information and work required to complete the study.

4.1 Literature studies

To obtain the background information presented, a comprehensive literature study was completed in September 2016. This was handed in at NTNU as a separate report. The literature was retrieved from different databases and search engines. NTNU's university library database *Oria* was the most used in the study. However, other databases like *Scopus* (*Elsevier*), *Compendex (Ei Village2)*, *Science Direct (Elsevier)*, as well as the search engine *Google Scholar* were also applied.

Different keywords were used in the databases in order to select the most relevant literature. Some of the keywords that were focused on were TBM, Tunnel Boring Machine, hard rock, model, prediction, and performance. In addition, truncations and various combined searches were used with these keywords. This was done to expand the search, and at the same time narrow down the results to contain the most relevant words and phrases.

Each source was evaluated by assessment criteria to secure the quality and credibility of the literature. The different criteria used are shown in the list below:

- Number of citations
- Is the text evaluated by professionals?
- Is the text credible?
- Is the text relevant?
- Who is the publisher?
- Accuracy. Is the source updated?

The research was completed to gain a greater insight into TBM prediction models for hard rock. The literature search finalized in September 2016 was handed in as a separate report. In addition to this, further research has been conducted while writing this thesis. The most significant sources have been Amund Brulands doctoral thesis from 2000 and Javier Macias doctoral thesis from 2016. Numerous published articles and a couple of relevant books have also been used as references in this thesis.

4.2 Field work

This chapter elaborates on the field work and data collection performed by the authors of this thesis. The data was collected during an eight-week long field study at the New Ulriken Tunnel project in Arna, in the period February 13th to April 7th. It is important to know the method of how the different data was collected in order to get an understanding of the different limitations this might cause. A 700-meter-long tunnel segment in the New Ulriken Tunnel has been examined in this thesis, from TM 3775 – TM 4475.

4.2.1 Geological back-mapping

Back-mapping is a valuable method used to understand the geology in a TBM bored tunnel. In accordance with Bruland (2000c), the mapping should consist of:

- Continuous detailed mapping of rock mass fracturing
- Continuous and detailed mapping of rock type distribution
- Rock sampling and laboratory testing of rock properties

The goal for the engineering geological back-mapping of a tunnel is to create a geological model of the tunnel. This can be used to evaluate the machine performance, cutter life, machine utilization, and other factors. (Bruland, 2000c)

When back-mapping a TBM tunnel, the engineer geological procedure consists of the following steps, presented by Macias et al. (2014):

- Determination of the rock type
- Identification of the strike and dip of Marked Single Joints
- Notes on other singular phenomena such as intrusions, mixed face, water and rock support
- Determination of the number of fracture systems and type of fracturing, either joints or fissures, for each system
- Measurement of the strike (α_s) and dip (α_f) of the fracture system(s)
- Measurement of the strike of the tunnel (α_t)

Rock samples should be collected to enable laboratory testing of drillability properties. (Macias et al., 2014)

The mapping of the tunnel should be recorded on a sheet with standardized entries, and is usually concentrated on 10 meter sections of the tunnel. The geological back-mapping represents the average of the sections measured. If necessary these sections can be subdivided, e.g. if there is a change of rock type. (Bruland, 2000c)

In addition to this, the degree of fracturing must consequently be evaluated. A scanline should be set at one of the tunnel walls to make the evaluations along this line. This scanline is preferably set in the lower part of the wall as it is easier to take a closer look at the rock mass while walking in the tunnel. In some cases, the observations in a section might not be representative for the tunnel section. Therefore, it is possible that the section volume has to be evaluated as a complete. (Bruland, 2000c)

The geological back-mapping is used to decide the type and degree of fracturing, number of fracture sets, the orientation of the sets, and identifying the rock type. This process is highly subjective and some steps are recommended to secure the quality of the back-mapping, according to Bruland (2000c):

- At least two persons should perform the back-mapping
- Use enough time and map each 10 m sections individually
- Evaluate and check the mapping of the previous 30-50 m section. This to adapt the personnel to the site geology before the mapping of a new tunnel section starts

- Once the mapping of a tunnel section is completed, a re-mapping of selected shorter sections should be carried out. The sub-sections should be 20-30 m in length at 150-200 m intervals
- When the mapping is completed, check the mapping of selected subsections against the machine performance data. This to see if the degree of fracturing corresponds with performance of the machine

Back-mapping performed at Ulriken

The engineer-geological back-mapping was performed according to the theories from the NTNU-model. The tunnel length was divided into 5 meter sections and mapped separately. The sections were mapped on sheets showed in Appendix D . To secure the quality of the process, both authors completed the mapping individually using enough time on each section. Later, the results were compared and a mean value were estimated when the mapping differed. However, it is important to mention that when different observations occurred, the most conservative values were favored. This is mostly because it is preferable that the performance prediction models give a conservative net penetration rate when calculated.

Some parts of the tunnel investigated were covered in shotcrete as the TBM moved forward. Therefore, the mapping had to be performed from the TBM, before the shotcrete was applied. This complicated the procedure, as one could only see parts of the cross section simultaneously and had to move back and forth on the machine.

Sources of error

The mapping was performed on the TBM, making it difficult to see the complete cross section of the tunnel. This made it hard to have a complete overview of the direction and total number of fractures. Due to this, some of the fractures may then not have been counted or the direction of the fracture is not completely accurate.

Further, it was not possible to follow all the steps of the quality procedure presented above. Mapping of previous sections and re-mapping of selected sections was not possible to do. Some parts of our mapped length were covered with shotcrete and the geology was not visible.

4.2.2 TBM data logging and processing

The TBMs today are equipped with data logging systems that record TBM performance data automatically. The available systems make it easier to process and log the machine parameters. According to Macias (2016), the logging systems provide information about:

- Indications of when boring is taking place. This is when the cutterhead is rotating with a thrust above a given threshold value
- The cutterheads total gross thrust, excluding some factors such as towing of the back-up
- The cutterhead velocity (*RPM*)
- The cutterhead position, chainage

The term “gross average cutter thrust” is used in the NTNU-model to describe the total thrust force applied during boring. This term considers several factors that cause loss of thrust. The gross average cutter thrust is found by dividing the total gross thrust by the

number of cutters. Experience has shown that thrust is a limiting factor when boring in hard rock under normal conditions. (Macias, 2016)

The logger systems produce an immense database where every process of the machine is recorded. This means that downtimes, moving of the cutterhead, and other special events are included in the averaging of the machine parameters. It is therefore necessary to do an initial analysis to secure correct interpretation of the data. The moving of the cutterhead forward to the tunnel face without boring taking place can create very high penetration rates that can never be achieved. This can happen if the cutterhead has been retracted from the tunnel face due to cutter changes or similar. To avoid that these values get used in the averaging of the data logging it is important to filter the cutter thrust. (Macias, 2016)

TBM data logging at Ulriken

At the New Ulriken Tunnel, the software IRIS.tunnel is used as the data logging system. For more information about the software, see chapter 2.5.4.

From the IRIS.tunnel software, raw data from 25 m sections has been downloaded to Excel spreadsheets. The software logs data every 10th second and creates a large database in Excel. To secure the data, an initial analysis of the raw data was first performed to remove downtimes and other factors that are not boring. This was done by making a scatter plot showing the tunnel length (m) versus the cutter thrust (kN/cutter) for the 25 m sections. From the scatter plot a lower limit for cutter thrust could be decided. This value was chosen as 50 kN/cutter for every 25 m section. Further, the rows in Excel was filtered by setting the cutter thrust in an ascending order. The values below the chosen limit was deleted to avoid errors in the averaging of the values. At last, average values of total advance force, cutter thrust, penetration rate, net penetration rate and cutterhead velocity were calculated. There was also calculated a standard deviation of the values to assess the credibility of the results.

Sources of error

When handling the vast amount of data these data logging sets contain, there will always be possible sources of error. While importing and handling the IRIS.tunnel files, sometimes containing thousands of values, mistakes may have occurred. Blunders can for example happen while filtering or deleting values and while using the data for calculation of average or deviation values.

4.2.3 Penetration tests

Penetration tests are done to assess the machine performance in a specific geology. It is therefore important to do a detailed geological mapping and test rock drillability in the laboratory for the actual tunnel section after the test. (Bruland, 2000c)

A penetration test is done in the following steps, according to Bruland (2000c):

- Use different thrust levels and constant *RPM* over a specified time to measure the penetration of the cutterhead
- Document the average cutterhead torque of each load level
- Take a note of cutter wear state, whether the test is performed at the start, middle or end of the stroke, cutterhead vibration level, and other relevant data

- Measure the net penetration rate, cutter thrust level and cutterhead torque of the previous and following strokes
- Collect chip samples for the penetration test, and previous and following strokes

Before starting the penetration test different thrust levels must be decided. The 100 % level given by M_{B100} is chosen as the thrust level used by the operator. At least four different thrust levels should be included in a penetration test. Five levels are recommended if cutter life, torque, etc. are to be considered (Bruland, 2000c). The thrust levels are chosen as rounded numbers and calculated as shown below:

$$\begin{aligned}M_{t1} &\approx 0.7 \cdot M_{B100} \\M_{t2} &\approx 0.8 \cdot M_{B100} \\M_{t3} &\approx 0.9 \cdot M_{B100} \\M_{t4} &\approx 1.0 \cdot M_{B100} \\M_{t5} &\approx 1.05 \cdot M_{B100}\end{aligned}$$

For each thrust level, the penetration test should be performed over a time matching about 30 revolutions of the cutterhead. The thrust for each level must be stabilized by the operator before the test begins. The penetration is given by i_t and is measured in mm over a given time. (Bruland, 2000c)

Penetration tests at Ulriken

The penetration tests performed at Ulriken were carried out at selected positions of the tunnel. The tests are dependent on the operator and were therefore performed when he saw it fit; regarding the geological situation and performance. All the penetration tests were taken at the start of the stroke. This was done as an attempt to eliminate stroke length as a possible source of error. Four different thrust levels were chosen following the NTNU methodology. A test sheet from JVSS was used to note *RPM*, thrust, net penetration rate and the precise times for each thrust level. This sheet can be seen in Appendix G . Noting exact times, as displayed on the control panels at the machine, made it easy to access the necessary data from the software IRIS.tunnel. The data for penetration rate and cutter thrust were then averaged for each of the selected thrust levels.

Chip sampling was also performed during each of the thrust levels. This was done as presented in chapter 4.2.5, by measuring the 20 biggest chips from each of the different levels. As the tests were carried out within the 700-meter tunnel segment, geological mapping data is available.

The averaged data was further used to plot graphs in Excel to evaluate the test. The values M_1 and b used in the NTNU-model was found from a plot of the penetration test in a log-log diagram.

Sources of error

During a penetration test it is important that the geology is relative homogenous over the complete test length. This is difficult to account for because the geology is continuously changing, especially for large diameter TBMs.

The recommended length for each thrust level of a penetration test is 30 revolutions on the cutterhead. The tests are as mentioned dependent on the operator. The recommended test length was followed as best as possible, but in some cases the operators were not so cooperative regarding the length of the test. Thus, some thrust levels ended prior to reaching 30 revolutions on the cutterhead.

When starting a new thrust level during the test, there will already be radial fissures created by each cutter from previous strokes and test levels. Thus, the tunnel face has already been subjected to strain. This could influence the penetration rate positively for the separate test levels. It is difficult to address the effect of these fissures, creating a possible source of error. This is again directly related to the recommended test length, trying to minimize possible errors.

Cutter wear state was not possible to comment in regard to the penetration test. There was no access to the cutters before or after the tests.

The thrust itself is another possible source of error. It is difficult to keep the thrust level constant over a longer period. This can lead to a deviation from the selected thrust level, causing a wrong result of the test.

4.2.4 RPM tests

RPM tests are performed to assess the influence of cutterhead velocity (*RPM*) on penetration rate (mm/rev) and net penetration rate (m/h) for a given machine, geology and thrust level. The *RPM* test is completed by measuring the cutterhead penetration over a given period with different cutterhead velocities under a constant cutterhead thrust.

The procedure of the *RPM* test is according to Macias (2016):

- Measure the cutterhead's penetration rate and net penetration rate at several velocities and constant thrust. The penetration rate must be averaged over the time taken for the tests
- Rock mass assessment by collecting rock samples for drillability testing and chip sample analysis
- Recording of relevant data, for instance cutter wear state, whether the test is performed at the start, middle or end of the stroke, cutterhead vibration level, etc.

It is recommended for the *RPM* test to have a minimum of four different velocity levels. The velocity levels must be decided from tunneling experience in similar conditions. It is beneficial that the range of the velocities is as large as possible. (Macias, 2016)

The duration of a test need to be long enough to achieve representative penetration values that are not influenced by previous cutterhead *RPM* levels. The recommended duration for each cutterhead velocity level is 10 minutes for larger TBMs (7 to 12 m diameter). It is important to stabilize the cutterhead velocity and thrust for each level. (Macias, 2016)

RPM testing at Ulriken

The *RPM* tests performed at Ulriken were carried out at selected positions of the tunnel. The tests are dependent on the operator and were therefore performed when he saw it fit; regarding the geological situation and performance. All the *RPM* tests were taken at the start of the stroke. This was done as an attempt to eliminate stroke length as a possible source of error. Four different *RPM* levels were chosen following the methodology from the updated NTNU-model. A test sheet from JVSS was used to note *RPM*, thrust, net penetration rate and the precise times for each *RPM* level. This sheet can be seen in Appendix G. Noting exact times, as displayed on the control panels at the machine, made it easy to access the necessary data from the software IRIS.tunnel. The data for net penetration rate, penetration rate and *RPM* were then averaged for each of the selected thrust levels.

Chip sampling was also performed during each of the *RPM* levels. This was done as presented in chapter 4.2.5, by measuring the 20 biggest chips from each of the different levels. As the tests were carried out within the 700-meter tunnel segment, geological mapping data is available.

The averaged data was further used to plot graphs in Excel to evaluate the test and see how the different *RPM* levels influence the rock breaking.

Sources of error

During a *RPM* test it is important that the geology is relative homogenous over the complete test length. This is difficult to account for because the geology is continuously changing, especially for large diameter TBMs.

The recommended length for each velocity level of a *RPM* test is 10 minutes. The tests are as mentioned dependent on the operator. The recommended length was followed as best as possible, but in some cases the operators were not so cooperative regarding the length of the test. Thus, some thrust levels ended prior to reaching 10-minute test lengths.

When starting a new *RPM* level during the test, there will already be radial fissures created by each cutter from previous strokes and test levels. Thus, the tunnel face has already been subjected to strain. This could influence the penetration rate positively for the separate test levels. It is difficult to address the effect of these fissures, creating a possible source of error. This is again directly related to the recommended test length, trying to minimize possible errors.

Cutter wear state was not possible to comment in regard to the *RPM* test. There was no access to the cutters before or after the tests.

The thrust itself is another possible source of error. It is difficult to keep the thrust level constant over a longer period. This can lead to a deviation from the selected thrust level causing a wrong result of the test.

4.2.5 Chip collection and analysis

Test procedure

Collecting chips produced by the TBM rock breaking process is important for analyzing purposes. Collecting the largest chips may provide important information of the boring process and the rock breaking mechanisms. In addition, information about material properties of the TBM muck and important drillability parameters of the intact rock can be investigated. (Bruland, 2000c)

To get a sought result, the sampling of the chips must be combined with registration of the current machine and performance data at the time the chips are collected. If the sampling is combined with a penetration or *RPM* test, the sampling could be of extra value as more data is available. Following such a sampling test, a detailed geological mapping of the tunnel section should be carried out. (Bruland, 2000c)

As mentioned, the largest chips are collected during a penetration or *RPM* test. The procedure regarding this test is described in the list below, as stated in Bruland (2000c):

- *Sample site:* The chip sample should be collected as close to the cutterhead as possible.
- *Sample time:* The penetration measurements start when the operator of the TBM has managed to stabilize the thrust level of the machine. To be sure that the chips collected are within the penetration measurement area, one should wait at least half a minute before sampling chips. As the penetration measurement stops, the sampling of chips also ceases.
- *Sample size:* A chip sample should consist of 20 large chips collected at each thrust level. This is done by collecting a large number of chips, from 25 – 30, and then sort them by size and discard the smallest by visual judgement. The smaller chips are thrown away until 20 chips are left for measurement and possible laboratory testing. The number of chips can also be decided by the time available for sampling. If so, it is important to collect the necessary amount of chips to establish a representative mean value and standard deviation of the chip size.

The face cutters normally produce the largest chips. Chips from the gauge, for example, are usually thinner and less wide, and are therefore not picked. There are also some chips that should be discarded:

- Chips that one by visual judgement can recognize originate from the center or gauge cutters.
 - Chips that look to be broken after it were loosened from the rock face and/or during transport to the sampling site.
 - If the chip can be from a marked single joint or similar.
- *Chip size:* The largest length, width and thickness is measured of each chip, regardless of where along the chip the largest size occurs. However, it is important that the measurements are taken perpendicular to each other. As all the chips are measured, the average chip size for each thrust level is calculated. When the averages are calculated, they are plotted as a function of thrust in a chart. Next, the

shape factor is found. This can be calculated either based on the shape of an individual chip or of the average dimensions of many. The shape factor is plotted into a chart to visualize if the shape is typically flat, cubic or elongated.

- *Sieve curve:* The sieve curve is found by using a sieve with square sieves to filter the TBM muck. The muck is usually collected at the conveyor transfer points, and the sample volume should be at least 20 liters. The results from the sieving are presented in a chart. See chapter 4.2.7 for the sieve sampling performed at Ulriken.
- *Rock properties:* On the largest chips, tests can be performed to find drillability, strength and wear properties. This can be *DRI*, *Mini-DRI*, *CLI*, *CAI* and Point Load Strength tests. However, the chips have been under high stress, which might influence the properties of the rock to some extent.

Chip collection at Ulriken

Collection of chips were performed in combination with penetration or *RPM* testing. Assembling the chips was done right from the conveyor belt. Collection just behind the operator booth made it possible to pick chips about 47 meters behind the cutterhead. A collection of chips was gathered in piles for each level in a test, varying from about 25-30 chips per pile. After the test ended, the 20 largest chips were kept for each level of thrust or *RPM*, depending on the type of test performed. In addition to throw away the smallest chips, the samples not having the characteristic chip shape were also discarded, regardless of size. With 80 chips collected for a test, it was more convenient to measure all the chips at the site. Thus, only the largest chips were carried out of the tunnel for potential laboratory testing.

Sources of error

As the collection was performed during boring, the belt was moving while picking the chips. Therefore, some of the largest chips might have gone past without being picked up. This was due to lack of sight or the speed of the conveyor belt making the chips hard to catch. Hence, a rather large number of chips was picked at every variation in either *RPM* or thrust, to later sort out the 20 largest for measuring and analyzes.

While measuring the chips, the TBM was normally still boring. This means a lot of noise making communication real hard. In addition, the measurements were done with a folding ruler and numbers down to millimeters might not be completely precise.

The size of each chip was measured as largest length, width and thickness, perpendicular to each other. This is not easy to do exact in the field, but was done as best as possible with the equipment and work space available.

4.2.6 Cutter consumption

Data for cutter consumption was in this thesis attained from JV Skanska Strabags' cutter change and inspection logs. The contractor has an extensive log over cutter wear since the start of the project. These logs have been reduced to only focus on the selected tunnel section for this thesis.

Cutter consumption logging at Ulriken

Every time a cutter is replaced or repositioned, it will be logged by the personnel performing the task. The reason for the change together with other information such as chainage at the time of change are noted. Later, an Excel spreadsheet is filled out, and the reason for the cutter change is logged by using a letter-code. The code is noted for the specific cutter and its position at the cutterhead. At every change, the outgoing status of the cutter will be logged. The Excel spreadsheet used can be seen in Appendix L, with an overview of changes, graphs and other relevant information. A brief review of this spreadsheet is presented in chapter 4.4.6 Cutter journal.

Table 4.1 Reasons for a cutter change and the respective codes used in the Excel spreadsheet

| Reason for change and codes |
|-----------------------------|
| Abrasive wear (W) |
| Blocked cutter (B) |
| Chipping (C) |
| Mushrooming (M) |
| Damaged hub (H) |
| Oil leakage (L) |
| Ring crack (F) |
| Other (X) |

In the cutter logs, machine hours were not logged. This information was obtained from IRIS.tunnel to later compare the cutter wear with the NTNU-model estimations. The machine hours were found in relation to the noted chainage for changes in the cutter consumption logs.

Sources of error

As the cutter consumption logging was performed by others, it is more difficult to exactly pinpoint sources of error. But a possible error is wrongful logging of cutter changes, such as marking a change of the incorrect cutter or the wrong reason for change. Further, mistakes can be made while logging chainage at the time of change.

All information is logged in an Excel spreadsheet. This is an extensive file with a lot of information. Thus, errors in such as plotting of numbers or formulas containing numbers from more than one spreadsheet tab are possible.

The sources of error for cutter consumption are mostly human errors in the form that untidy work can affect results.

4.2.7 Sieve sampling

When collecting a sample for sieve testing, the volume of the muck sample should be minimum 20 liters. To get the most representative sample, it may be collected at conveyor belt transfer points. (Bruland, 2000c)

Sieve sampling at Ulriken

One sieve sample has been collected at Ulriken. The sample was gathered in two 10 liter buckets, and was collected right from the conveyor belt, at the nearest point possible to the cutterhead. The belt was stopped, and an area of the belt was swept for all the muck to fill the 20 liters. The sample site secures a good representativeness of the muck, as the particle sizes are as intact as possible. The result of the sieve test can be seen in Appendix O .

Sources of error

Sweeping of the belt by hand may have caused some of the finer particles to be left in the conveyor belt. In addition, only a single sample might not be representative for the tunnel section selected in the thesis.

4.3 Laboratory testing

Rock samples collected in the field work are tested in the laboratory for multiple purposes. Mainly, the laboratory work consists of investigation of drillability, strength properties, and mineral composition. Drillability and strength properties have a major influence on the time consumption in mechanized boring. These are also important factors for choosing method and equipment in the first place.

In this thesis, the laboratory tests carried out are of standard and well established methodologies. The work consists of a series of tests, and some are performed solely to be able to determine indices. Table 4.2 display which tests have been used in this thesis. The tests and methods will be further described in the subchapters below.

Table 4.2 Laboratory tests carried out in this study.

| Test method | Used for: | Used in model: |
|------------------------------------|--|---|
| Density | - Density - S_{20} | - NTNU - Q_{TBM} - MCSM |
| Brittleness value, S_{20} | - Drilling Rate Index, DRI | - NTNU |
| Sievers' J-value, SJ | - Drilling Rate Index, DRI - Cutter Life Index, CLI | - NTNU - Q_{TBM} |
| Abrasion Value Steel (AVS) | - Cutter Life Index, CLI | - NTNU - Q_{TBM} |
| Point Load Strength | - Point Load Strength - Uniaxial Compressive Strength, UCS - Brazilian Tensile Strength, BTS | - Farrokh - Hassanpour - Gehring - Alpine - Q_{TBM} - MCSM |
| Differential thermal analysis, DTA | - Quartz content | - NTNU - Q_{TBM} |

4.3.1 Rock sampling

Rock samples from core drilling will be used in this thesis. These need to have a minimum diameter of 32 mm, and preferably 10 kg of core material should be collected. At Ulriken, the rock samples were gathered from the left tunnel wall, close to the tunnel floor. Each sample was drilled by a handheld machine, and six samples of approximately 52 mm were collected at every sample location. To get the most representative sample locations, a review of the geological conditions was performed. Three locations were chosen; TM 3843, TM 4091, and TM 4468. It is difficult to get a complete picture of the geological properties over the complete tunnel segment from just three samples. However, the samples should be representative for the given tunnel segment.



Figure 4.1 Core samples from TM 4091 (Photo: Roy-Remy Hopland)

4.3.2 Bulk density ρ_s

To find the bulk density of a rock mass, a glass cylinder called pycnometer is used. The procedure is to place the pycnometer on a weighing instrument and tare. Next the pycnometer is filled approximately $\frac{3}{4}$ full of fragments >16 mm. The weight of the specimen is noted as m_1 . The pycnometer with the specimen is then filled with distilled water and its surface is dried thoroughly. The weight of pycnometer filled with water and specimen is noted as m_2 . Further, the specimen and the distilled water are removed from the pycnometer. The pycnometer is washed thoroughly before it is filled with distilled water only. The weight of the pycnometer with distilled water is noted as m_3 . The bulk density is then found from equation (4.1). (SINTEF, 2011)

$$\rho_s = \frac{m_1}{m_1 + m_3 - m_2} \quad (4.1)$$

4.3.3 Brittleness value S_{20}

The brittleness test gives the rock's ability to resist crushing when exposed to repeated impacts. The test for brittleness used in the NTNU/SINTEF method was first developed in Sweden by N. von Matern and A. Hjelmér in 1943. The test has been modified several times, and for various purposes, since then. (Dahl et al., 2012)

Three extractions from one representative and homogenized sample is used in the S_{20} test. The samples are crushed in a jaw crusher and sieved, see Figure 4.2. The sample weight is picked from a 16-11.2 mm fraction and corresponds to 500 grams of density 2.65 g/cm^3 . The sample is then crushed by 20 impacts in an impact apparatus. The percentage of the material that passes the 11.2 mm sieve after the impacts give the S_{20} value of one extraction. The brittleness value is then given by a mean value of three parallel tests. (Dahl et al., 2012, Bruland, 2000e)

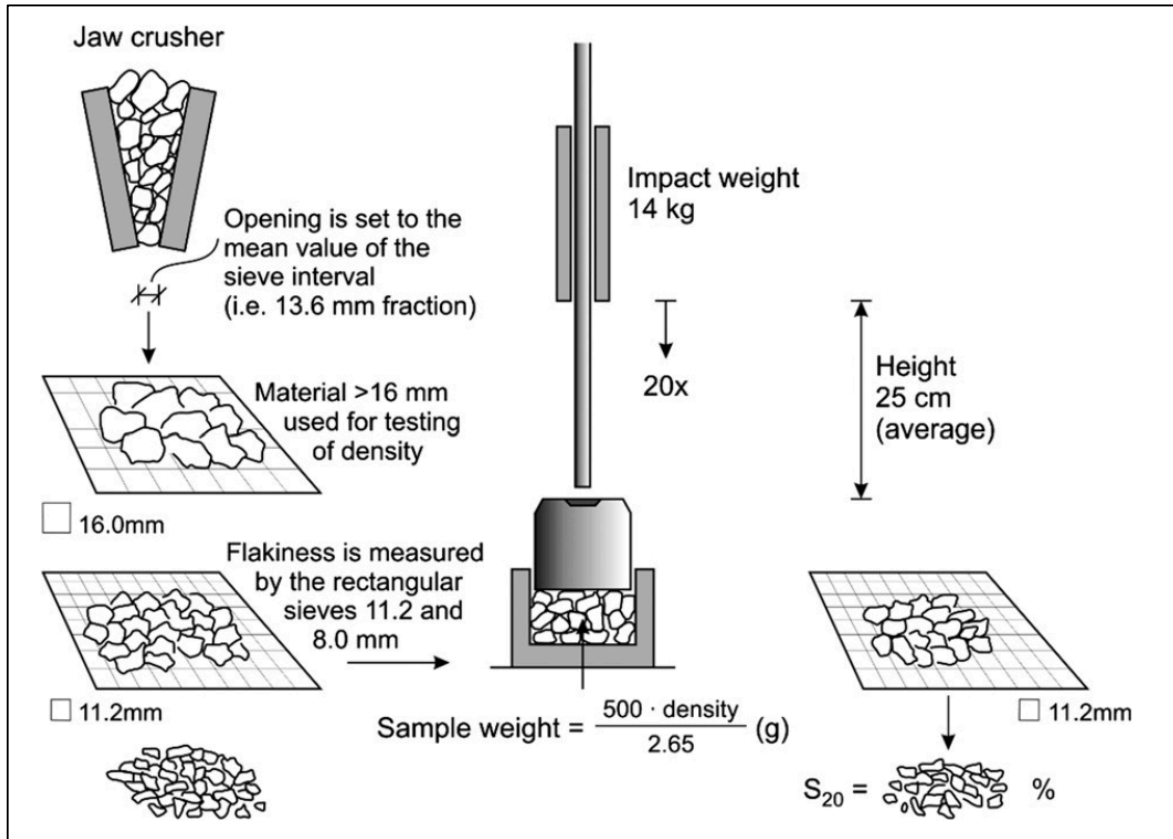


Figure 4.2 The brittleness value S_{20} test (Dahl et al., 2012)

4.3.4 Sievers' J-value

The Sievers' J-value, often simply referred to as the *SJ*-value, is found by performing a miniature drill test on a rock sample. The test was originally developed by H. Sievers in the 1950s. The *SJ*-value represents the surface hardness of the rock. The test is usually performed 4-8 times on a single sample, depending on the texture of the rock and deviation in results. Testing a sample is completed by using a 8.5 mm drill bit rotating exactly 200 revolutions, measuring the *SJ*-value as drillhole depth in 1/10 mm. From that, the surface hardness is defined as the mean value of the number of tests performed. The rock sample is usually a pre-cut surface, where it has been cut so the drilling will be performed perpendicular to the foliation in the rock. (Dahl et al., 2012)

A rock sample might have a texture that contains bands of different minerals with different hardness. As this can result in various penetration depths, it is optimal to drill in the soft and hard layers. This is done by visual interpretation in the laboratory, looking at the composition of the rock. Hence, drilling in a soft/hard combination should be avoided as best as possible. (Dahl et al., 2012) Figure 4.3 shows an illustration of the test.

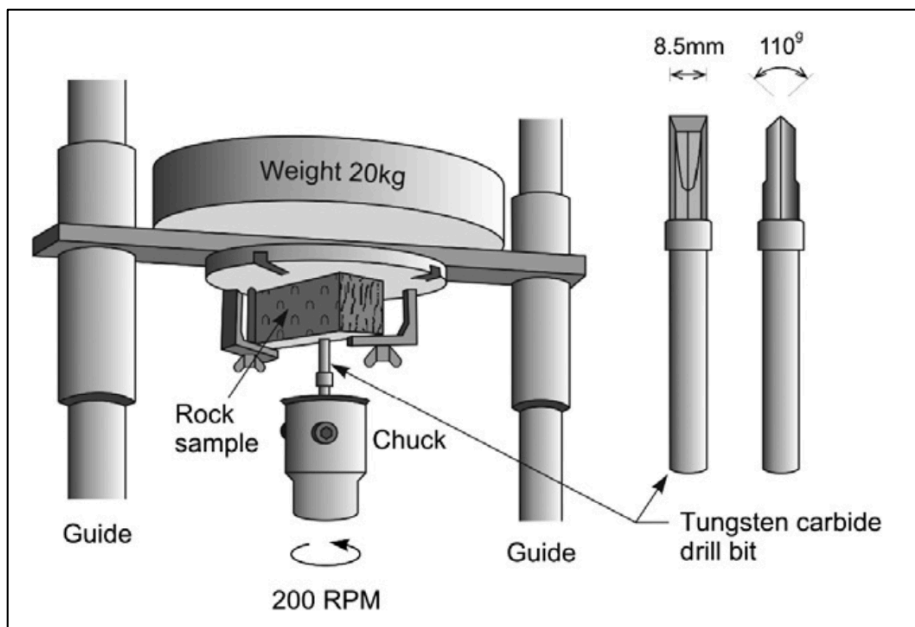


Figure 4.3 The Sievers' J-value test (Dahl et al., 2012)

4.3.5 Abrasion Value Cutter Steel (AVS)

The AVS test is based on the Abrasion Value (AV) test dating back to the beginning of the 1960s. The AV test was developed at the Department of Geology at NTH and measures the rock abrasion or ability to induce wear on a piece of tungsten carbide. The same equipment and method is used for the AVS test, but instead of using tungsten carbide the test is performed with a piece of cutter steel. (Dahl et al., 2012)

Normally, the test material for the AVS test is gathered from the extractions used to determine S_{20} . Thus, this is regarded as a representative sample for the test. Before it can be used in the AVS test, the material must be crushed down to particles < 1 mm. The AVS-value is then defined as the weight loss of the test piece in milligrams after 1 min of testing. Normally, the test is performed on 2-4 test pieces of cutter steel, and the AVS will be the mean value of these tests. As long as the test is performed correctly, variation in the results should be very low. Variations in results should not exceed 5 milligrams of weight loss. (Dahl et al., 2012) Figure 4.4 illustrates the test and adds supplementary test parameters.

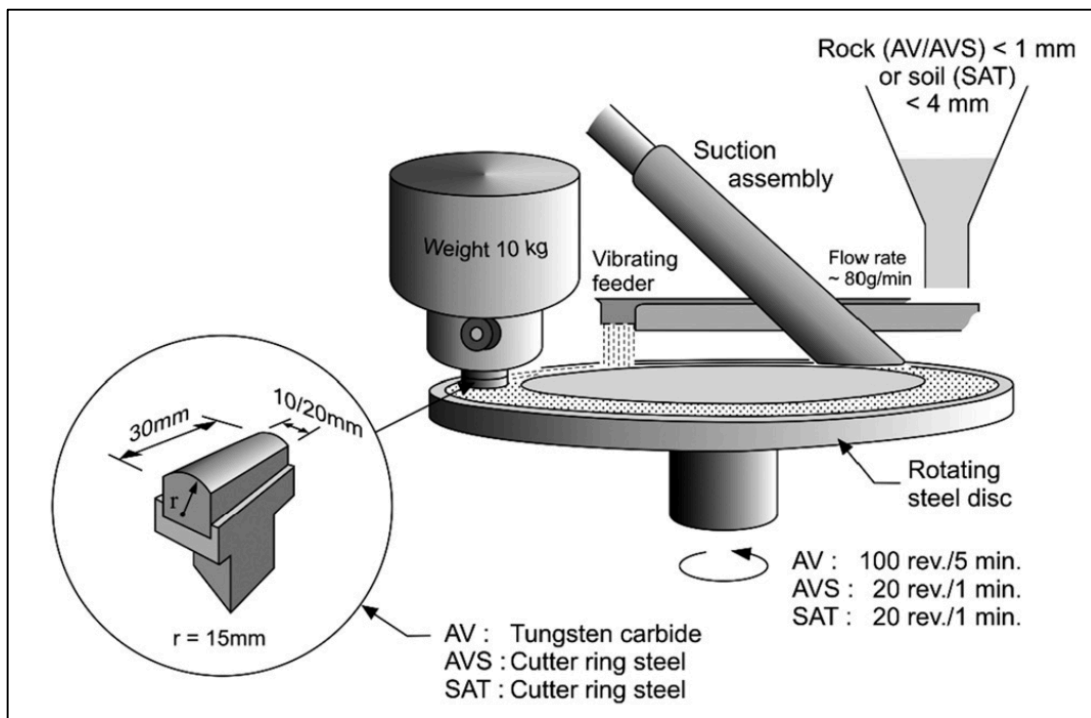


Figure 4.4 The abrasion value cutter steel test (Dahl et al., 2012)

4.3.6 Drilling Rate Index, DRI

The Drilling Rate Index is based on the Brittleness Value S_{20} and the Sievers' J-value, and is found by using the graph showed in Figure 4.5.

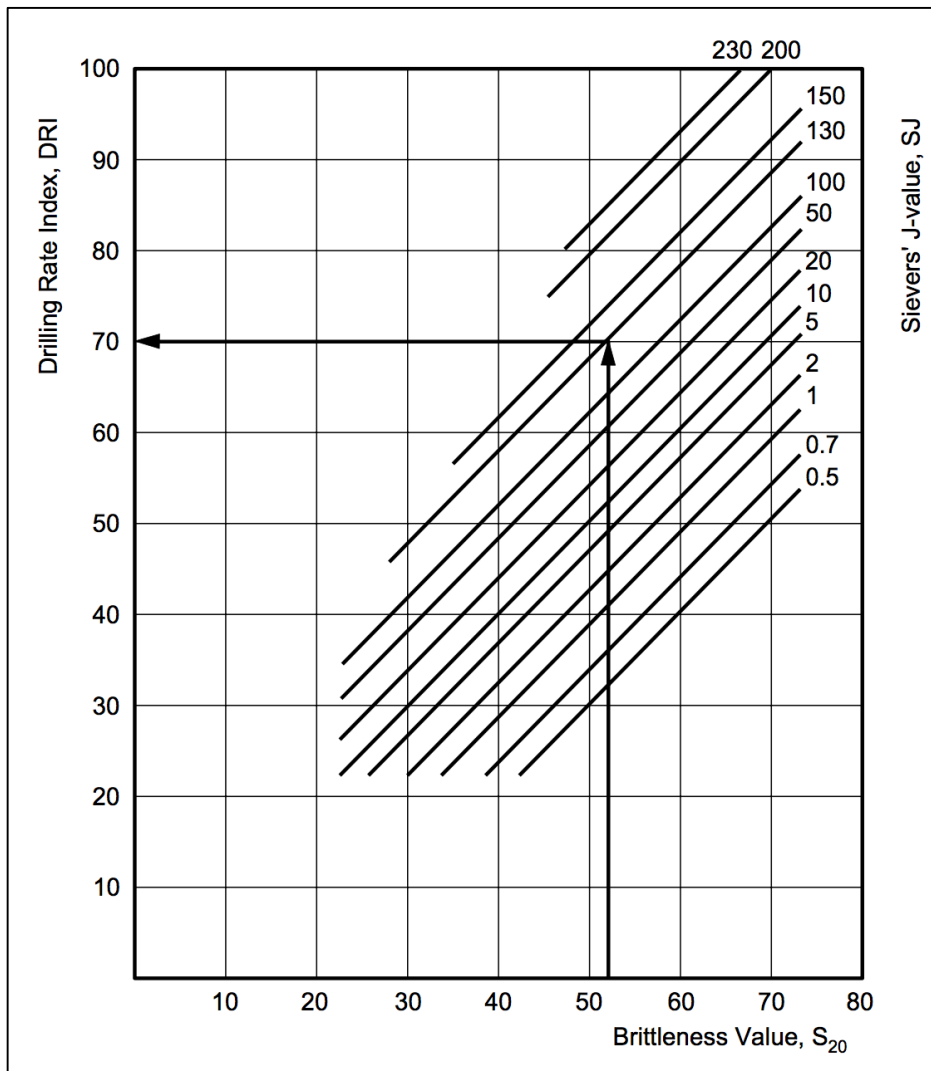


Figure 4.5 Diagram for assessment of Drilling Rate Index (DRI) (Bruland, 2000e)

4.3.7 Cutter Life Index, CLI

The life in boring hours for a TBM's cutter disc rings is expressed by the Cutter Life Index. CLI is assessed through the Sievers' J-value and the AVS. (Bruland, 2000e) The CLI value is found from the following equation:

$$CLI = 13.84 \cdot \left(\frac{SJ}{AVS} \right)^{0.3847} \quad (4.2)$$

4.3.8 Point Load Strength

The Point Load Strength test is used as an index to determine strength classification of different rock materials. In addition, it may be used to predict other strength parameters such as Brazilian Tensile Strength and Uniaxial Compressive Strength. The test performed in the laboratory measures the Point Load Strength Index ($I_{s(50)}$) and Strength Anisotropy Index ($I_{a(50)}$) of rock samples. In this thesis, the Point Load Strength Index ($I_{s(50)}$), will be the only test needed. The tests will be performed on core samples collected in the New Ulriken Tunnel, but the test may also be performed on rock specimens of different forms. (ISRM, 1985)

The point load is placed on the core sample as shown in Figure 4.6, and the point load at failure is recorded. (ISRM, 1985)

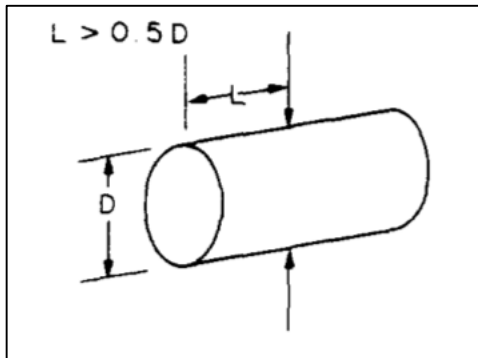


Figure 4.6 Point Load Test on core sample (ISRM, 1985)

The point load is recorded as P , and the equations needed to calculate the Point Load Strength Index, according to ISRM (1985), is shown below.

$$I_{s(50)} = F \cdot I_s \quad (4.3)$$

F is a size correction factor, and when the samples are close to $D = 50$ mm, equation (4.4) is used. D_e is the measured diameter of the core sample.

$$F = \sqrt{\frac{D_e}{50}} \quad (4.4)$$

$$I_s = \frac{P \cdot 1000}{D_e^2} \quad (4.5)$$

Preferably, at least 10 tests should be carried out per sample. When calculating the mean value of $I_{a(50)}$, the two lowest and highest values are deleted, and the mean value is calculated from the remaining data.

4.3.9 Uniaxial Compressive Strength and Brazilian Tensile Strength

In this thesis, multiple penetration prediction models will be tested, requiring several parameters. Testing for all these parameters requires not only a large amount of core samples, but also the availability of necessary equipment. Therefore, some compromises were needed. The different models require different parameters for rock strength. Thus, a decision was taken in cooperation with the supervisors and NTNU/SINTEF that the Point Load Strength test would be the strength test performed in the laboratory. Using results from this test, the Uniaxial Compressive Strength and the Brazilian Tensile Strength are calculated using conversion formulas. The formulas were given by SINTEF, and also found in ISRM (1985).

Uniaxial Compressive Strength

The correlation with Point Load Strength ($I_{s(50)}$) and Uniaxial Compressive Strength (σ_c) is expressed as shown in equation (4.6), according to Nilsen et al. (2000).

$$\sigma_c = k_{50} \cdot I_{s(50)} \quad (4.6)$$

The factor k_{50} changes with the strength of the rock. The values in Table 4.3 will be used when calculating UCS from Point Load Strength values.

Table 4.3 Uniaxial Compressive Strength in correlation from Point Load Strength (Nilsen et al., 2000)

| Uniaxial Compressive Strength σ_c [MPa] | Point Load Strength I_{s50} [MPa] | Suggested value of k_{50} |
|---|--|--------------------------------|
| 25 – 50 | 1.8 – 3.5 | 14 |
| 50 – 100 | 3.5 – 6 | 16 |
| 100 – 200 | 6 – 10 | 20 |
| > 200 | > 10 | 25 |

Brazilian Tensile Strength

The correlation with Point Load Strength ($I_{s(50)}$) and Brazilian Tensile Strength (σ_t) is expressed as shown in equation (4.7).

$$\sigma_t = 0.8 \cdot I_{s(50)} \quad (4.7)$$

Sources of error

The values for Uniaxial Compressive Strength and Brazilian Tensile Strength are only found in correlation with Point Load Strength. It is therefore important to emphasize the uncertainty in the conversion factors. It might not be as accurate as if the proper test was performed for each parameter.

4.3.10 Differential thermal analysis, DTA

The differential thermal analysis is used to determine which minerals and quantities of the minerals present in a sample. The method can give accurate results for quartz. (SINTEF, 2010)

Several minerals will change their crystal structure at given temperatures when heated or cooled. When these changes happen the mineral either absorb or release heat (endothermic or exothermic reaction). Each mineral has a characteristic reaction, making it possible to decide which minerals a sample contains. (SINTEF, 2010)

The DTA-apparatus consists of an oven where the sample material is warmed up, a control device for temperature and a data logger. The sample material must be crushed to powder before used in the test, and test time is approximately 2 hours. (SINTEF, 2010)

4.3.11 Sources of error in the laboratory

When working in the laboratory, one always try to be as accurate as possible. Nevertheless, errors can occur. Types of error in the laboratory can be instrumental, observational or environmental errors, among others. Some tests methods and results are more affected by small errors than others, but one should always be meticulous while working in a laboratory. Small errors in test results can have a huge effect on further work with the results obtained.

4.4 Data analysis

A time-consuming activity in this thesis was performing calculations and analyses in Microsoft Excel. The calculations have, to a large extent, been focused on calculating the different TBM prediction models presented in chapter 3.

4.4.1 Calculation of prediction models

The calculations of the prediction models are completed in Microsoft Excel. The tunnel section is divided in three different ways. The first one looks at an average of the complete 700-meter section. The second is divided in three parts, corresponding with geology and core sample locations. The third is divided after the fracturing factor. A separate spreadsheet is made for each of the different subdivisions.

For each model the calculations have been performed on separate spreadsheet tabs, where also the results are presented. Finally, two spreadsheet tabs are presented to show the results from the seven prediction models in graphs. These show the net penetration rate over the different subdivisions of the tunnel section.

The results of each model are then compared with each other in the spreadsheet tab “Comparison”. Charts are here displaying different ways to compare the given results. The differences of the results are given as an overview of the variation of the models. Some of them are included in this thesis while others are left in the digital appendix. All model calculations can be seen in Appendix N .

4.4.2 Chip analysis

This Excel spreadsheet is a collection of all the chip analyses performed in this thesis. The spreadsheet present chip size measurements and results for each of the chip collections carried out.

In all of the chip size measurements spreadsheet tabs; the height, width, and length of the 20 largest chips for each test level is displayed. Further, a mean size and standard deviation is calculated for each of the values of the different test levels.

With the mean size calculated for all the chips, the chipping frequency, cubic chip size, and shape factor is found. These values are displayed for each test level. The average chip size, cubic chip size, chipping frequency and chip shape are all shown in separate graphs. Complete chip analysis can be seen in Appendix K .

4.4.3 Fracture and orientation mapping

This Excel spreadsheet was originally created by Javier Macias and used in this thesis to calculate the fracturing factor for the mapped tunnel section.

The tunnel is mapped for every 5 meters and the information obtained in the mapping is presented as a row in the spreadsheet. The tunnel direction and number of joint sets are typed in the sheet. The number of sets are divided in separate spacing sets.

For the separate spacing sets, a fracture type is chosen by three alternatives; fissure, joint and mixed. Then the fracture spacing (in centimeters) is put in. The number of fractures and fracture class is then calculated for the different joint sets.

The number of fractures for each set is summed and the total fracture spacing, given in centimeters, is calculated. From this number a total fracture class is found.

When the fracture classes for each joint set are obtained, the relative angle and dip from the mapping are written in the sheet. With this information, the orientation of the weakness planes for each set is determined. The orientation is then used to calculate the k_{si} for each set. The k_{si} is a value describing the fracturing and is derived from a figure given in the NTNU-model.

With all this information, the total k_s factor is calculated. At the same time the mapped length is divided by the k_s value which is needed to calculate the average k_s .

The process described above is repeated for every of the 5 meter mapped sections and gives a complete lot of data. This is then used to calculate an average value of the k_s for the entire mapped section and smaller sections. The fracture mapping spreadsheet is displayed in Appendix E .

4.4.4 Performance data

The performance data Excel spreadsheet shows average values for total advance force, cutter thrust, penetration rate, net penetration rate and cutterhead velocity. These values are divided in 25 m sections between TM 3775 to TM 4475. Average values for the complete 700-meter tunnel section is also presented. To assess the credibility of the results, a standard deviation is given for the 25 m intervals and for the complete section. Further, the data is used to make several graphs displaying the results. Performance data is presented in Appendix H .

4.4.5 Penetration and RPM tests

The penetration and RPM tests are presented on separate Excel spreadsheets. The different spreadsheets display raw data for the complete test, raw data for each test level with average values, and results of the test on several spreadsheet tabs. The raw data is imported from the software IRIS.tunnel. This is further copied into the spreadsheet tabs for the different test levels. At last, the results are calculated and used to plot graphs displaying the outcomes of the test. Penetration tests are shown in Appendix I , while RPM tests can be seen in Appendix J .

4.4.6 Cutter journal

The cutter journal spreadsheet is made by the contractor (Joint Venture Skanska Strabag) to assess the cutter life and consumption of cutters.

Cutter consumption is presented as a monthly overview over the cutter changes. The monthly logs are then summarized to show the complete consumption.

The spreadsheet gives the total number of cutter changes done on the different cutter positions. The total number of changes are divided into different types of wear. These are abrasive wear, blocked cutter, chipping, mushrooming, damaged hub, oil leakage, ring crack, and other reasons.

From these values, an average cutter life is given in m/change, $\text{fm}^3/\text{change}$ and h/change, and further an average rolling distance in kilometers is calculated. See Appendix L .

5 Results

The results obtained in this thesis are a product of an extensive field study, laboratory testing and processing of the data attained. The field study at the New Ulriken Tunnel project in Arna took place in the time period of February 13th to April 7th. A 700-meter-long tunnel segment in the New Ulriken Tunnel was examined, from TM 3775 – TM 4475. The processed material includes data from both geological investigations and TBM performance logged at site.

5.1 Geological investigation and mapping

The geological investigation and mapping conducted for this thesis was performed over a length of 700 meters, in a part of the New Ulriken Tunnel. The selected segment of the tunnel was mapped in 5 meter sections, mainly performed at the TBM.

Table 5.1 Measurements of the chosen tunnel section

| Chainage | | TM | | Mapped length (m) |
|----------|--------|------|------|-------------------|
| 466729 | 467429 | 3775 | 4475 | 700 |

Chapter 4.2.1 offers a description on how the results were obtained. After plotting the results in Excel, the distribution of the different fracture classes shows that fracture class 4 is most represented. Results show that 55%, or 385 meter, of the chosen segment has a spacing between fractures from 30–60 centimeter. The distribution between the classes can be seen in Table 5.2 and Figure 5.1. Fracture classes 4 and 5 are the most represented, as they collectively make up 79% of the 700-meter section. Classes 4 and 5 represent a medium and high degree of fracturing respectively. In addition, 18% of the 5 meter sections fall into fracture class 3. A description of the different fracture classes can be seen in Table 3.4.

Table 5.2 Fracture class and distribution between the classes for the 700 meters included in the mapping.

| Fracture Class | | Range class (cm) | | Distribution (m) | Distribution (%) |
|----------------|-----|------------------|-----|------------------|------------------|
| 0 | 0 | 480 | | 0 | 0 % |
| 1 | 0+ | 240 | 480 | 0 | 0 % |
| 2 | 0-I | 120 | 240 | 20 | 3 % |
| 3 | I- | 60 | 120 | 125 | 18 % |
| 4 | I | 30 | 60 | 385 | 55 % |
| 5 | II | 15 | 30 | 170 | 24 % |
| 6 | III | 7.5 | 15 | 0 | 0 % |
| 7 | IV | 4 | 7.5 | 0 | 0 % |

The average k_s -value was calculated from the average spacing of fractures and the related strike and dip for each fracture set. Calculations in Excel gave an average k_s for the section at 0.97. A k_s -value of 0.97 is relatively high, and suggests a section with medium to highly fractured rock.

Table 5.3 Results from mapping of the chosen tunnel section

| Results | |
|---------------|-------|
| Average angle | 37.13 |
| Average k_s | 0.97 |

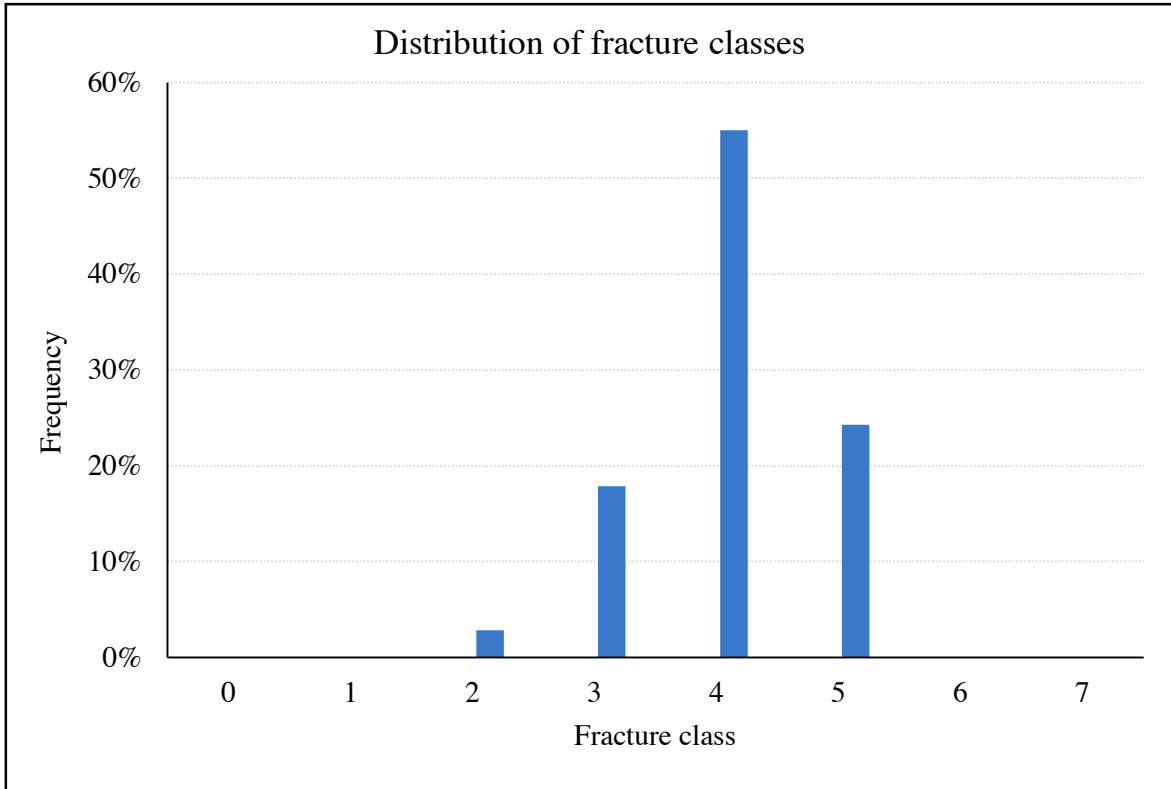


Figure 5.1 Distribution of fracture classes over the chosen tunnel section

Figure 5.2 shows the average k_s -value for 25 meter sections. The mid-part of the tunnel section has the highest average k_s -value, equal to 1.21, from TM 4075 to TM 4275.

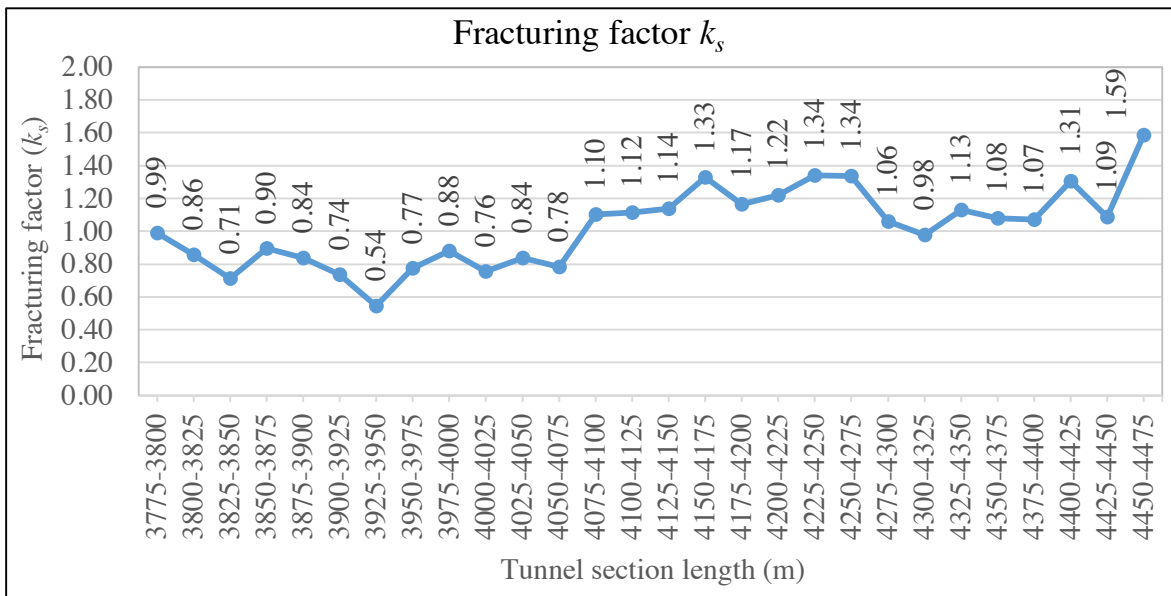


Figure 5.2 Fracturing factor k_s for 25 m sections

5.1.1 Mapping comparison to JVSS/Bane NOR

The mapping performed for this thesis is independent from JVSS and Bane NORs mapping of the rock mass. Therefore, a quick comparison between the total number of fractures counted for each 5-meter section was made. Comparison can be seen in Figure 5.3. The contractor and the owner do not map with the NTNU-model and penetration predictions in mind. Therefore, only the total number of fractures and not the k_s -value could be compared.

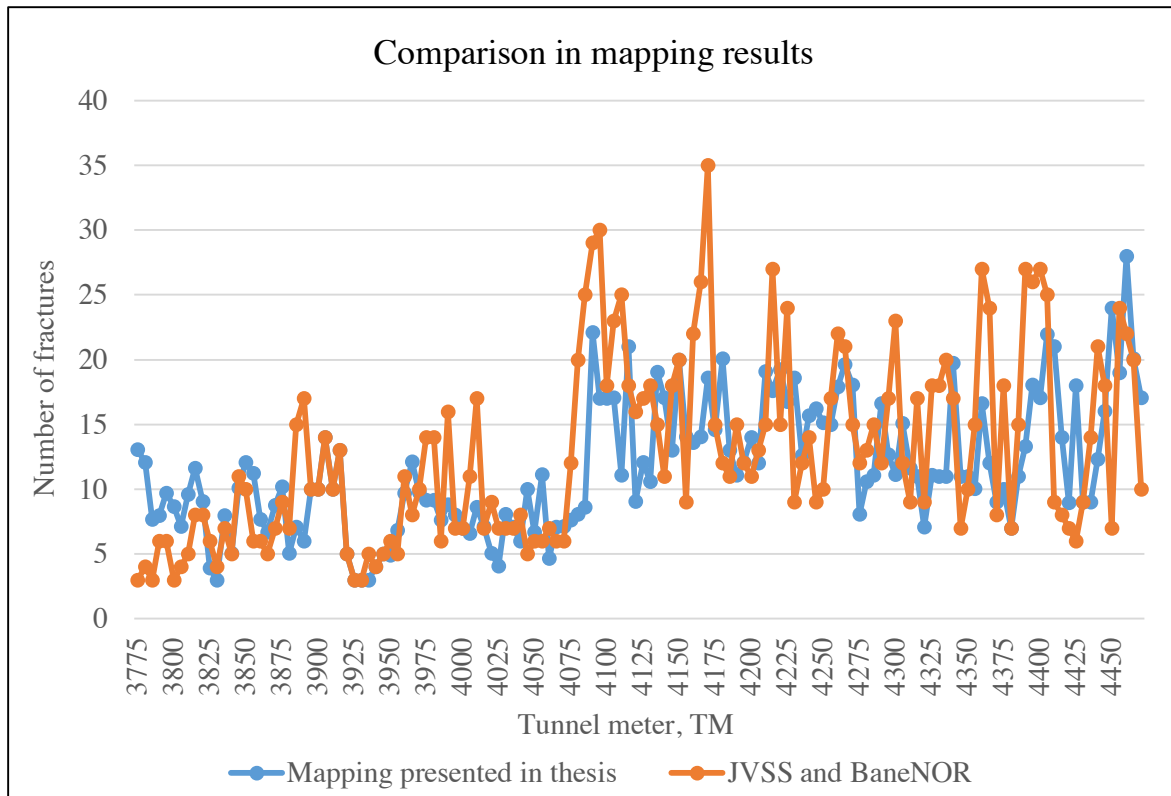


Figure 5.3 Graph showing a comparison of performed mapping between JVSS/Bane NOR and this thesis

The comparison was put together to achieve a quality control on the mapping performed for this thesis. For the total 700-meter segment, JVSS/Bane NOR have an average spacing of 39.1 cm, while the authors of this thesis found a 42.8 cm average over the same area.

5.1.2 Subdivisions of tunnel segment for model input

For calculation of the different prediction models, the tunnel segment has been divided in different subdivisions. The segment was divided into three parts; see Table 5.4 for values of the respective sectors. Description of the divisions can be found in the list below:

- The first division is an average over the complete 700-meter segment. This means that averaged values of all geological parameters were used in the calculations.
- The second was based on geology and core samples. As the first 300 meters, from TM 3775 – TM 4075, showed a geological profile consisting of migmatite, a split was made at TM 4075. From there, the mountain consisted of gneiss, and the decision to divide at TM 4250 was taken solely with the core samples in mind. As three core samples were taken at site, one sample represents each subdivision.
- The third division was done based on the k_s -values given from the NTNU-model. Two splits in the segment were made at TM 4075 and TM 4275, to best fit the k_s -value graph showed in Figure 5.2. One core sample represents each subdivision, as they fitted with the respective tunnel segmentation.

Table 5.4 Divisions of geological parameters in different sections for model calculation purposes

| Complete 700-meter segment | | | |
|--|-------------------------|-----------------------|---------------|
| Subdivisions, TM | Average angle, α | Average spacing, (cm) | Average k_s |
| 3775-4475 | 37.13 | 46.93 | 0.97 |
| Divided after geology and core samples | | | |
| Subdivisions, TM | Average angle, α | Average spacing, (cm) | Average k_s |
| 3775-4075 | 28.33 | 62.84 | 0.78 |
| 4075-4250 | 42.78 | 33.50 | 1.19 |
| 4250-4475 | 44.49 | 36.15 | 1.16 |
| Divided from k_s -values | | | |
| Subdivisions, TM | Average angle, α | Average spacing, (cm) | Average k_s |
| 3775-4075 | 28.33 | 62.84 | 0.78 |
| 4075-4275 | 43.03 | 32.79 | 1.21 |
| 4275-4475 | 44.45 | 37.19 | 1.14 |

5.2 TBM performance data

TBM performance data was downloaded as raw data from the IRIS.tunnel software. The software operates with two different thrust settings. One shows gross values including friction and other factors causing loss of thrust. The other show net values where a constant factor of 2500 kN is subtracted from the thrust, representing these factors. The gross thrust values are presented below.

The procedure of handling the raw data is given in chapter 4.2.2. The data is averaged for 25 m sections over the complete 700 meters of the chosen tunnel segment. The graphs presented below gives an overview of the used gross thrust and cutterhead velocity, and the achieved penetration and net penetration rates.

A summary of the averaged values over the complete chosen tunnel section is displayed in Table 5.5. This shows that an average net penetration rate of 2.01 m/h has been achieved over the 700-meter section.

In the NTNU-model the degree of fracturing is pointed out as the geological factor with the greatest influence on penetration rates. A higher degree of fracturing corresponds to higher penetration rates. With a higher degree of fracturing experience has shown that the thrust is reduced to avoid damage and excessive wear of cutters. This reduction in thrust will reduce the influence of the fracturing factor on penetration rates. Further, the cutterhead velocity may require lower *RPMs* when boring in highly fractured rock mass to avoid high vibration levels. (Macias, 2016)

The highest average gross advance force is 21074.78 kN for the 25-meter section between TM 3975 – TM 4000. This value corresponds to a lower fracturing factor, shown in Figure 5.2. The lowest average gross advance force is 17040.87 kN, between TM 4075 – TM 4100. A higher fracturing factor is found in this area.

The highest average penetration rate and net penetration rate are 8.34 mm/rev and 2.51 m/h respectively, between TM 4425 – TM 4450. The lowest average values are 4.70 mm/rev and 1.42 m/h, between TM 3975 – TM 4000.

The highest average cutterhead velocity is found between TM 3900 – TM 3925, and is 5.20 *RPM*. This is found in an area with a low fracturing factor. The lowest average cutterhead velocity is 4.53 *RPM*, between TM 4025 – TM 4050.

The general trend found for this tunnel section is:

- The thrust is reduced in areas with a higher fracturing factor
- The highest penetration rates and net penetration rates corresponds to sections with a higher degree of fracturing

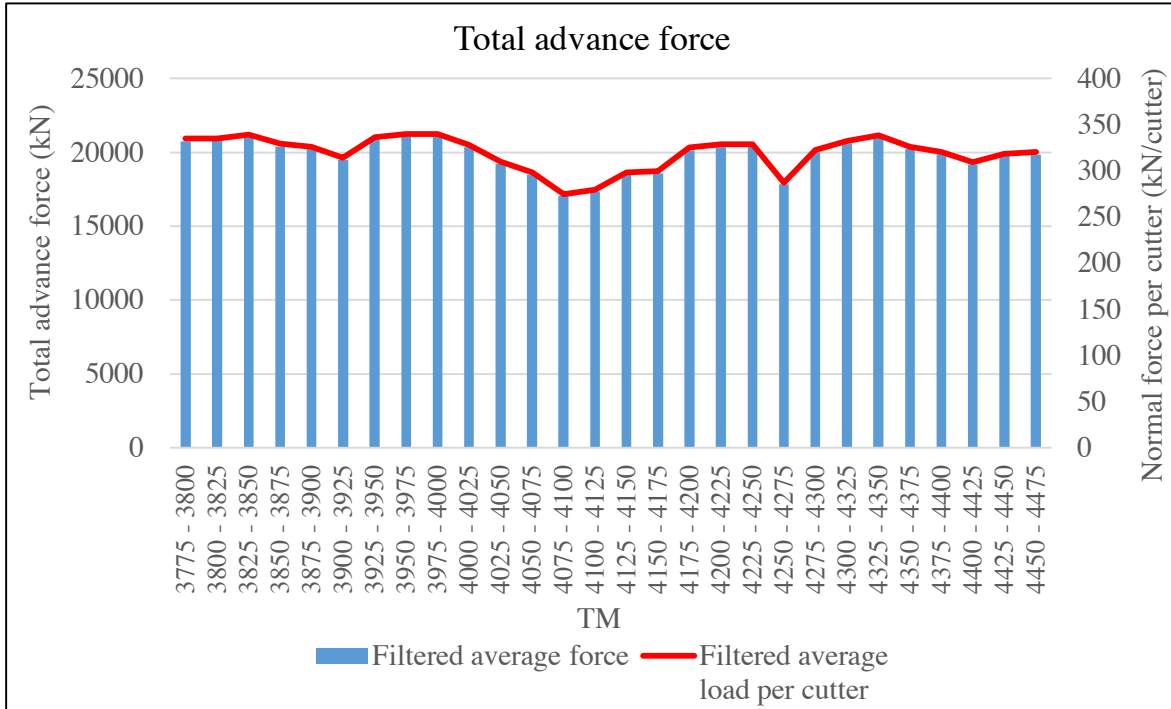


Figure 5.4 Total gross advance force for 25 m sections in kN and kN/cutter

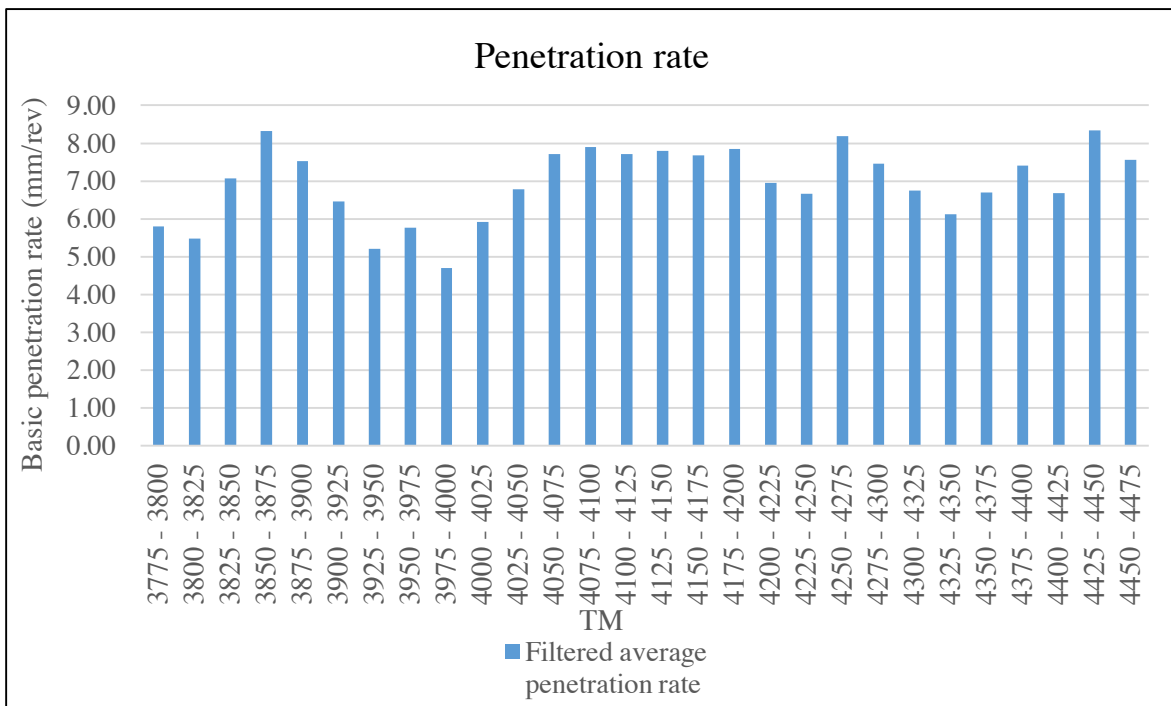


Figure 5.5 Penetration rate for 25 m sections in mm/rev

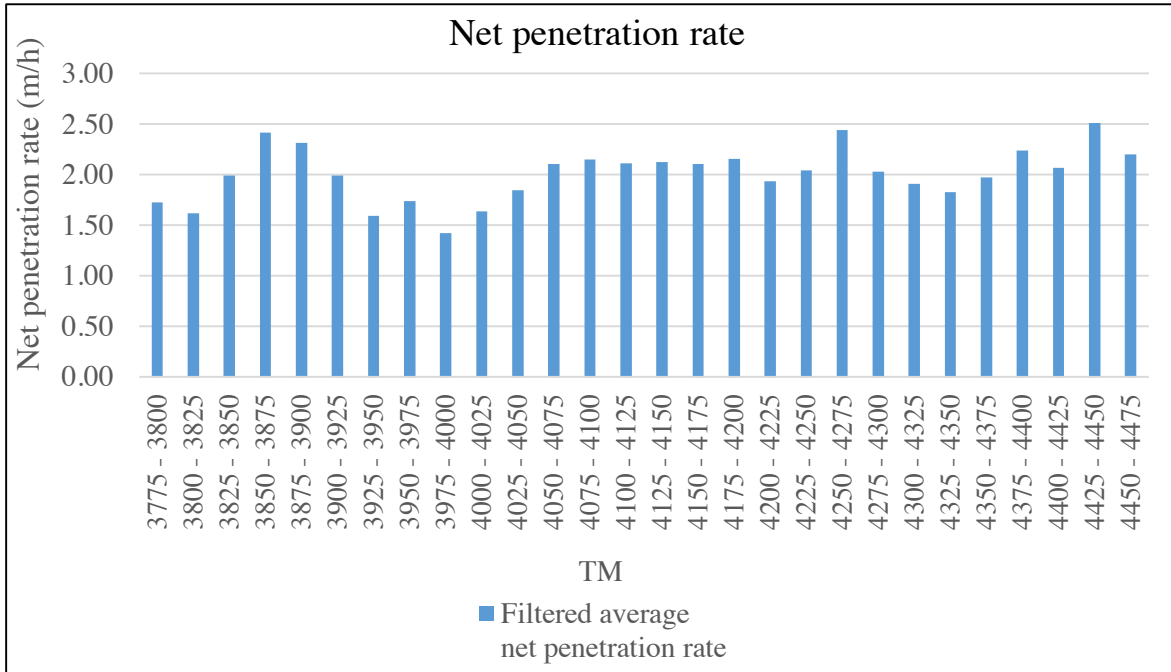


Figure 5.6 Net penetration rate for 25 m sections in m/h

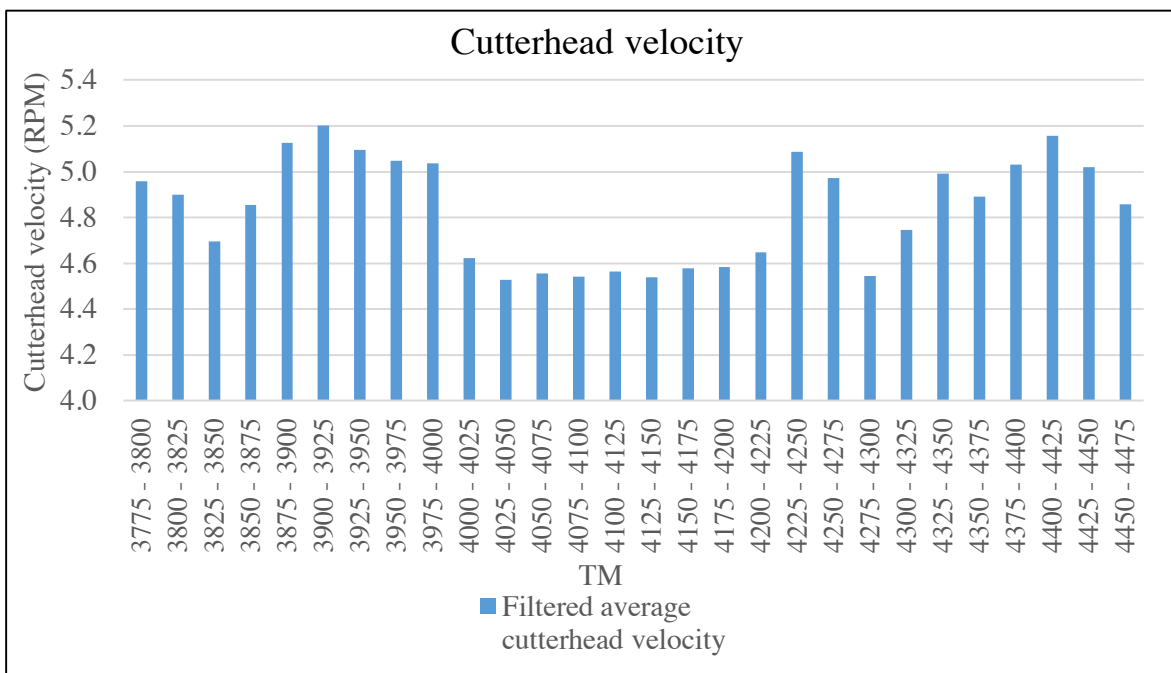


Figure 5.7 Cutterhead velocity for 25 m sections in RPM

Table 5.5 Average values for the chosen tunnel section after filtration

| | Total gross advance force (kN) | Cutter thrust (kN/cutter) | Penetration rate (mm/rev) | Net penetration rate (m/h) | Cutterhead velocity (RPM) |
|----------------------------|--------------------------------|---------------------------|---------------------------|----------------------------|---------------------------|
| Average: | 19795.93 | 319.29 | 6.95 | 2.01 | 4.83 |
| Standard deviation: | 2995.79 | 48.32 | 1.50 | 0.44 | 0.26 |
| % deviation: | 15.13 % | 15.13 % | 21.62 % | 21.69 % | 5.37 % |

5.2.1 Comparison of TBM performance data towards the rock mass fracturing

The fracturing of a rock mass is in several of the prediction models an important factor affecting the net penetration rate. A comparison of performance data towards the rock mass fracturing is shown below. This to indicate the general trends mentioned above, in the used thrust and achieved net penetration regarding the rock mass fracturing.

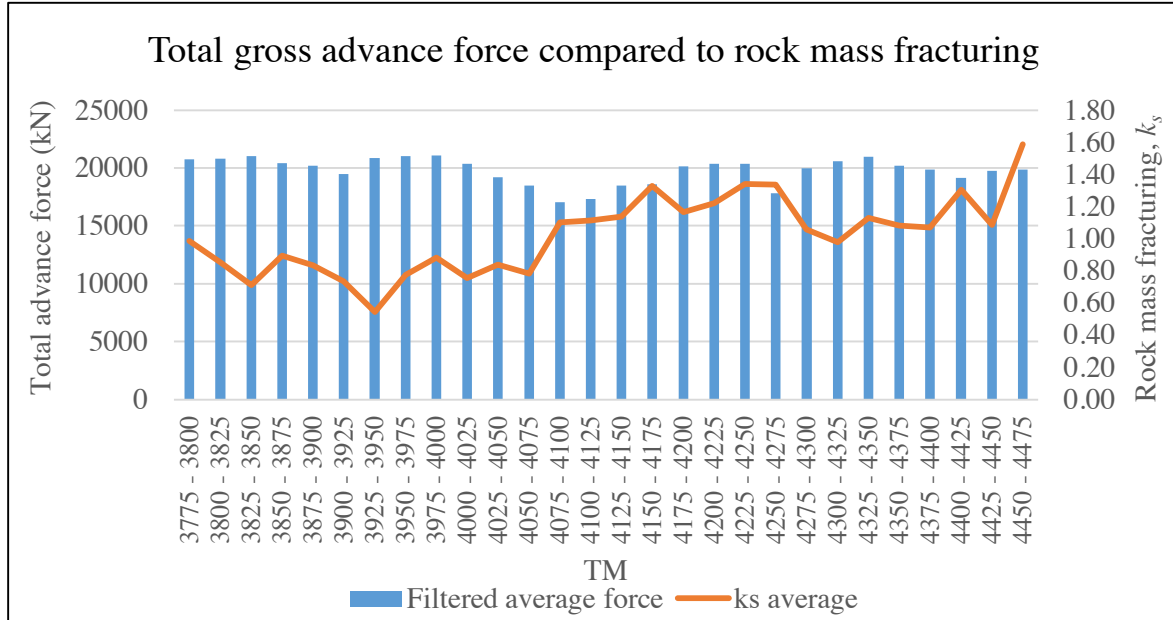


Figure 5.8 Total gross advance force compared to rock mass fracturing, k_s

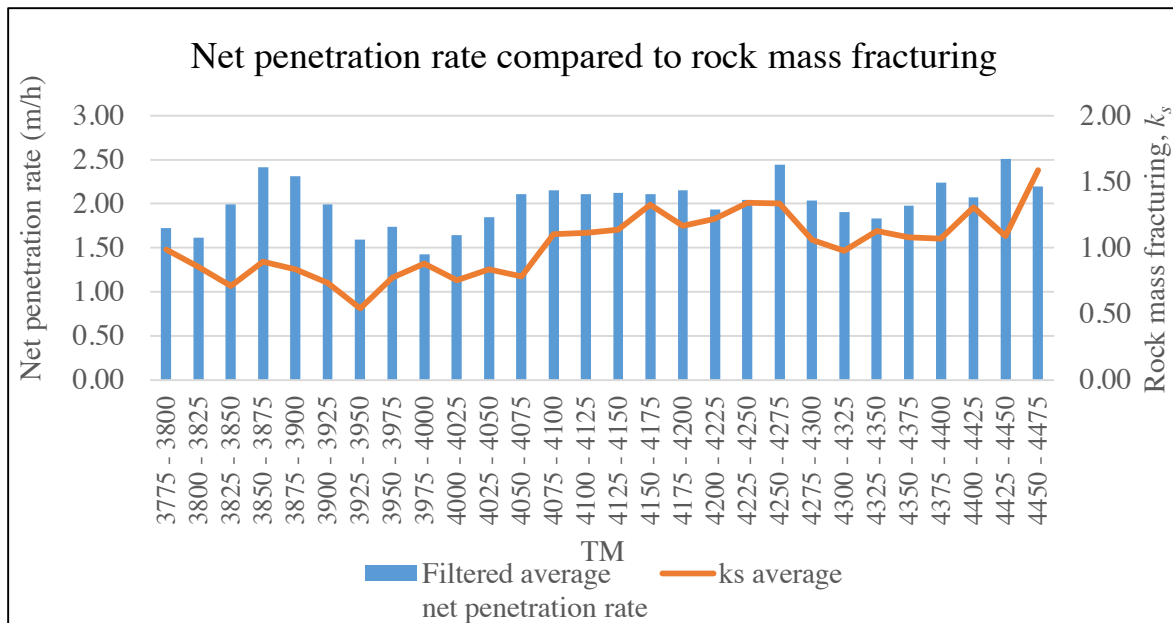


Figure 5.9 Net penetration rate compared to rock mass fracturing, k_s

5.2.2 Subdivisions of tunnel segment for model input

For calculation of the different prediction models, the tunnel segment has been divided in different subdivisions. The segment was divided into three parts; see Table 5.6 for values of the respective sectors. Description of the divisions can be found in the list below:

- The first division is an average over the complete 700-meter segment. This means that averaged values of all machine parameters were used in the calculations.
- The second was based on geology and core samples. As the first 300 meters, from TM 3775 – TM 4075, showed a geological profile consisting of migmatite, a split was made at TM 4075. From there, the mountain consisted of gneiss, and the decision to divide at TM 4250 was taken solely with the core samples in mind.
- The third division was done based on the k_s -values given from the NTNU-model. Two splits in the segment were made at TM 4075 and TM 4275, to best fit the k_s -value graph showed in Figure 5.2.

The estimations are also done with two thrust settings, one with gross thrust and one with net thrust. The net thrust is equal to the gross thrust, minus a constant friction force of 2500 kN. This means that the net cutter thrust is approximately 40 kN/cutter lower than the gross cutter thrust.

Table 5.6 Divisions of TBM performance parameters in different sections for model calculation purposes

| Complete 700-meter segment | | | | |
|--|------------------------------------|----------------------------------|-----------|------------------------------|
| Subdivisions TM | Gross cutter thrust (kN/cutter) | Net cutter thrust (kN/cutter) | NPR (m/h) | Cutterhead velocity (RPM) |
| 3775-4475 | 319.29 | 284.36 | 2.01 | 4.83 |
| Divided after geology and core samples | | | | |
| Subdivisions TM | Gross cutter thrust (kN/cutter) | Net cutter thrust (kN/cutter) | NPR (m/h) | Cutterhead velocity (RPM) |
| 3775-4075 | 327.55 | 293.79 | 1.87 | 4.89 |
| 4075-4250 | 305.02 | 268.10 | 2.09 | 4.65 |
| 4250-4475 | 319.38 | 284.45 | 2.13 | 4.91 |
| Divided from k_s -values | | | | |
| Subdivisions TM | Gross cutter thrust (kN/cutter) | Net cutter thrust (kN/cutter) | NPR (m/h) | Cutterhead velocity (RPM) |
| 3775-4075 | 327.55 | 293.79 | 1.87 | 4.89 |
| 4075-4275 | 302.81 | 266.45 | 2.13 | 4.69 |
| 4275-4475 | 323.38 | 288.15 | 2.10 | 4.90 |

5.3 Penetration tests

5.3.1 Penetration test at TM 4337.03 – TM 4337.56

This penetration test was performed with a constant *RPM* of approximately 5.0. The 100 % thrust level was taken as the thrust used by the operator, in this case about 22000 kN. The other thrust levels were chosen in collaboration with the operator to fit the geological situation. They were set at 21000 kN, 20000 kN and 19000 kN. This does not completely follow the NTNU methodology regarding the selection of thrust levels. Usually one uses a higher variation of thrust levels.

The geology in this area consisted of augen gneiss with biotite rich bands, and a mix of mica and feldspar. The related fracturing factor is found to be 1.13, with an average spacing and angel of approximately 42 cm and 65°.

A linear regression of the \log_{10} values of thrust and penetration was performed. This made it possible to calculate the parameters M_t and b used in the penetration curve of the NTNU-model. The \log_{10} values of the thrust and the penetration should fit well to a straight line. This is the case for the test performed, as shown in Figure 5.11 with a regression coefficient of 0.98. The quality of the test is therefore satisfactory.

The M_t and b values for the test is 172.46 kN/cutter and 2.73 respectively.

Table 5.7 Cutter thrust and basic penetration for the penetration test at TM 4337.03 – TM 4337.56

| Gross cutter thrust M_t [kN/cutter] | Penetration rate i_0 [mm/rev] | $\log_{10} M_t$ | $\log_{10} i_0$ |
|--|------------------------------------|-----------------|-----------------|
| 313.30 | 5.09 | 2.50 | 0.71 |
| 321.23 | 5.40 | 2.51 | 0.73 |
| 340.78 | 6.58 | 2.53 | 0.82 |
| 353.56 | 6.96 | 2.55 | 0.84 |

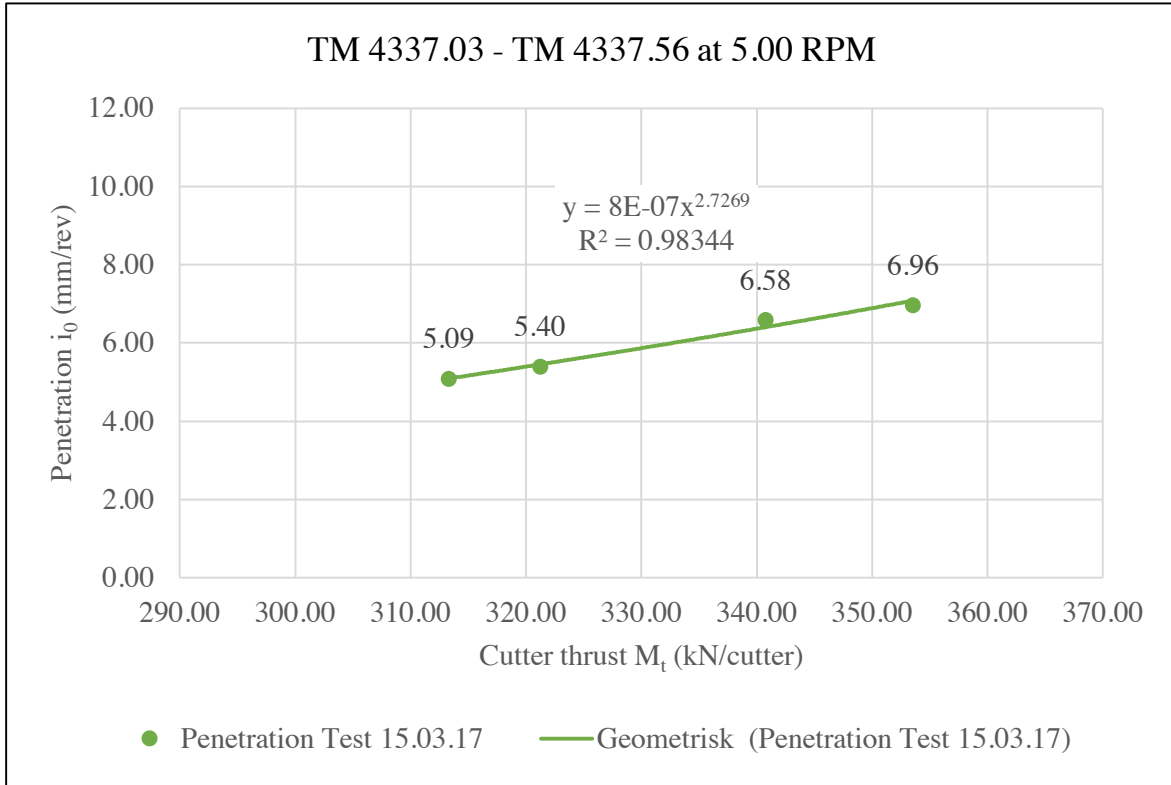


Figure 5.10 Plot of penetration curve for the penetration test at TM 4337.03 – TM 4337.56

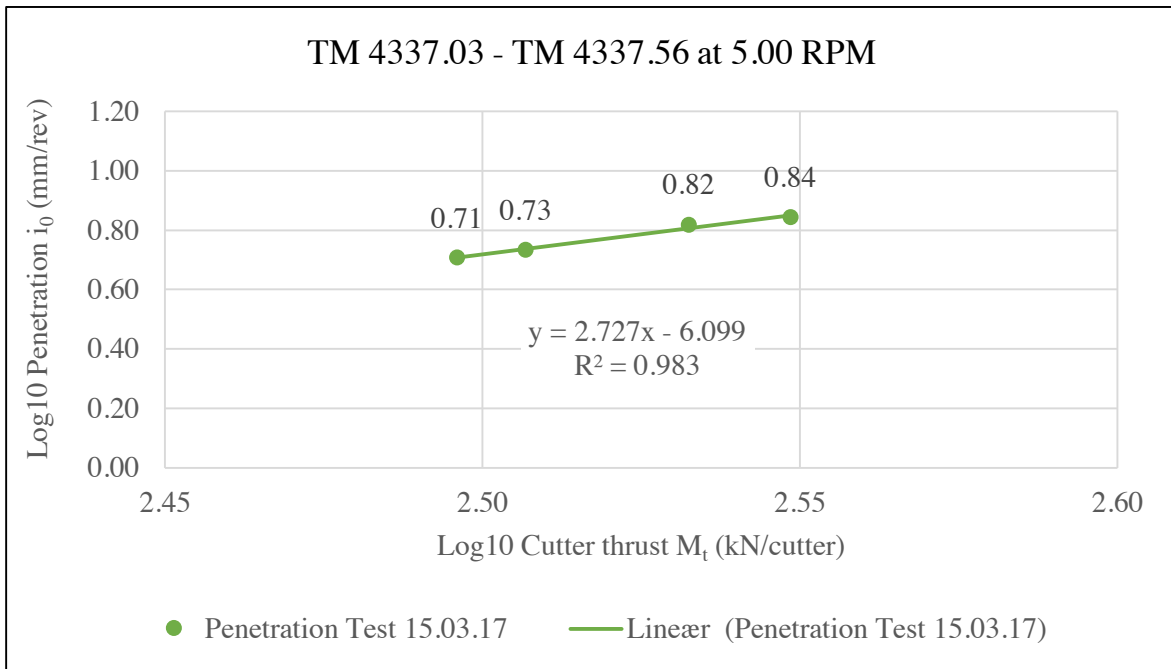


Figure 5.11 Plot of log10 values for M_t and i_0 for the penetration test at TM 4337.03 – TM 4337.56

5.4 RPM tests

A *RPM* test is most representative when performed in a competent rock mass where the geological properties are relative homogenous over the length of the test. With such properties present, the penetration rate will increase from lower *RPM*s up to a maximum penetration rate before it decreases. (Macias, 2016)

The procedure to find the optimal *RPM* is to determine the maximum net penetration value from the plot of the *RPM* test. The corresponding *RPM* and penetration rate for this value is then found. The optimal *RPM* is given by the maximum penetration rate while still maintaining an optimal net penetration rate. The optimal net penetration rate is sat to be 5% less than the maximum net penetration rate. (Macias, 2016)

An important aspect of *RPM* tests is that the rock breaking process is more efficient when the penetration rate is higher. Also, a lower *RPM* value point toward a higher cutter life, thus improving the machine utilization. (Macias, 2016)

5.4.1 *RPM* test at TM 3885.91 – TM 3886.62

This *RPM* test was completed with a constant thrust of approximately 20000 kN, equivalent to 322.58 kN/cutter. The *RPM* levels were chosen to 3.5, 4.0, 4.5, 5.0, 5.5 and 6.0. It was not performed a chip analysis in relation to this test.

The geology in this area consists of biotite rich augen gneiss. The fracturing factor is found to be 0.84, with an average spacing and angel of approximately 62 cm and 37°.

As shown in Figure 5.12, the penetration rate is on a similar level during the complete test. The representativeness of this test is uncertain. The test was performed with 6 different *RPM* levels, but the length of each level was quite short, approximately 4 minutes. This makes it highly possible that the penetration values are influenced by previous cutterhead *RPM* levels. Also, the regression coefficient for the plot of the penetration rate is very low.

The only conclusion that can be made from this test is that the net penetration rate will decide the cutterhead velocity and thrust.

Table 5.8 Data from the *RPM* test at TM 3885.91 – TM 3886.62

| Cutterhead velocity [<i>RPM</i>] | Penetration rate [mm/rev] | Net penetration rate [m/h] | Cutter thrust [kN/cutter] |
|---------------------------------------|------------------------------|-------------------------------|------------------------------|
| 3.50 | 6.28 | 1.32 | 316.09 |
| 3.98 | 6.56 | 1.57 | 324.39 |
| 4.52 | 6.11 | 1.65 | 322.59 |
| 5.04 | 6.59 | 1.99 | 329.10 |
| 5.51 | 6.06 | 2.00 | 325.13 |
| 5.99 | 6.28 | 2.26 | 327.83 |

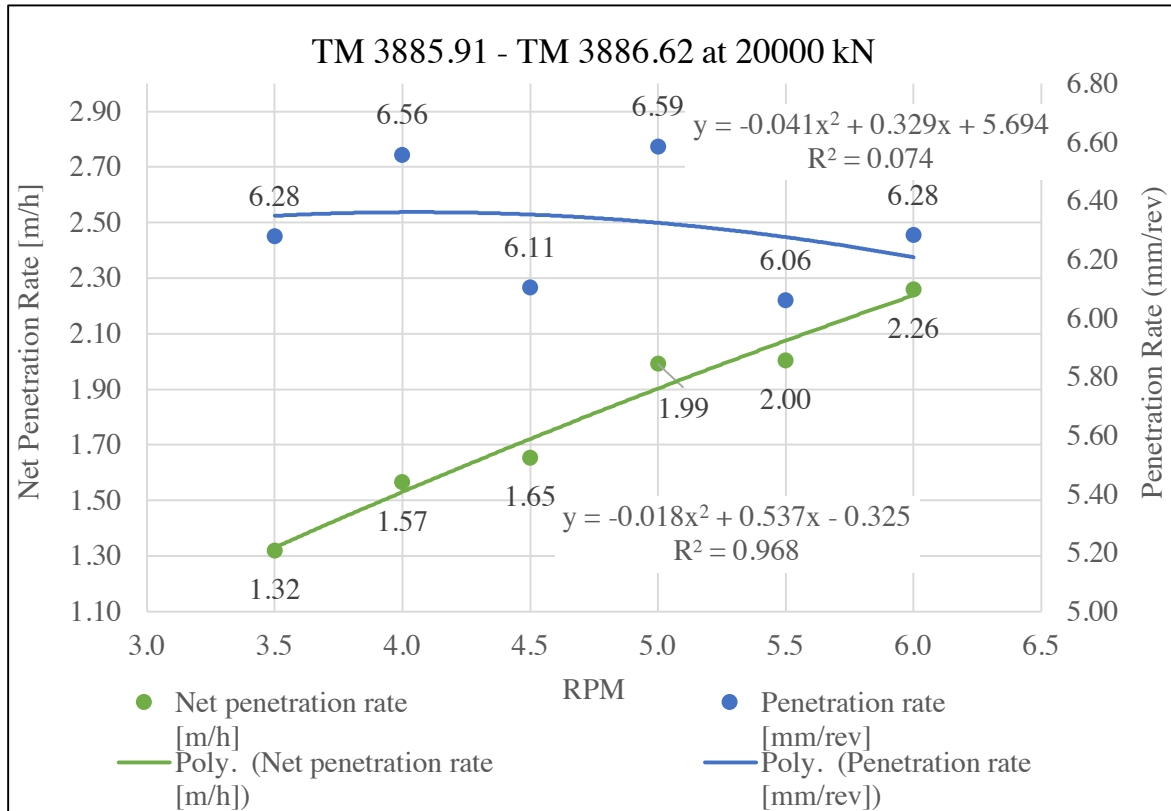


Figure 5.12 Plot of net penetration rate and penetration rate for the RPM test at TM 3885.91 – TM 3886.62

5.4.2 RPM test at TM 4029.31 – TM 4030.03

This RPM test was carried out with a constant thrust of approximately 20000 kN, equivalent to 322.58 kN/cutter. The RPM levels were chosen to 3.5, 4.5, 5.0, and 5.5.

The geology in this area consists of biotite rich migmatite, with pegmatite/quartz-rich intrusions. The fracturing factor is found to be 0.84, with an average spacing and angel of approximately 99 cm and 55°.

As can be seen in Figure 5.13, the plot of the penetration rate does not have the shape were the penetration rate are increasing up to a maximum point, before it decreases. This indicates that the rock is not competent, for such a test. Also, the first value presents a high number for penetration rate. This is probably due to the fact that the average thrust was higher for this test level, displayed in Table 5.9.

The results indicate that the optimal RPM level regarding the penetration rate, is 3.5. This result is uncertain due to the high thrust value indicated. The optimal RPM from the chip analysis presented in chapter 5.5.2, is 4.5. With a RPM of 4.5, the penetration rate is 6.00 and the net penetration rate is 1.62, taken from Figure 5.13. This net penetration rate is here 17% lower than the maximum NPR, and is therefore to low in practical use.

By using a RPM of 4.5 the rock breaking process will be more efficient and larger chips are produced. The recommendation for this situation is that the RPM and thrust level are adjusted to fill the needs of the contractor regarding time consumption.

Table 5.9 Data from the RPM test at TM 4029.31 – TM 4030.03

| Cutterhead velocity [RPM] | Penetration rate [mm/rev] | Net penetration rate [m/h] | Cutter thrust [kN/cutter] |
|---------------------------|---------------------------|----------------------------|---------------------------|
| 3.49 | 7.32 | 1.53 | 334.42 |
| 4.50 | 6.13 | 1.66 | 319.50 |
| 5.01 | 5.56 | 1.67 | 318.16 |
| 5.52 | 5.76 | 1.91 | 321.22 |

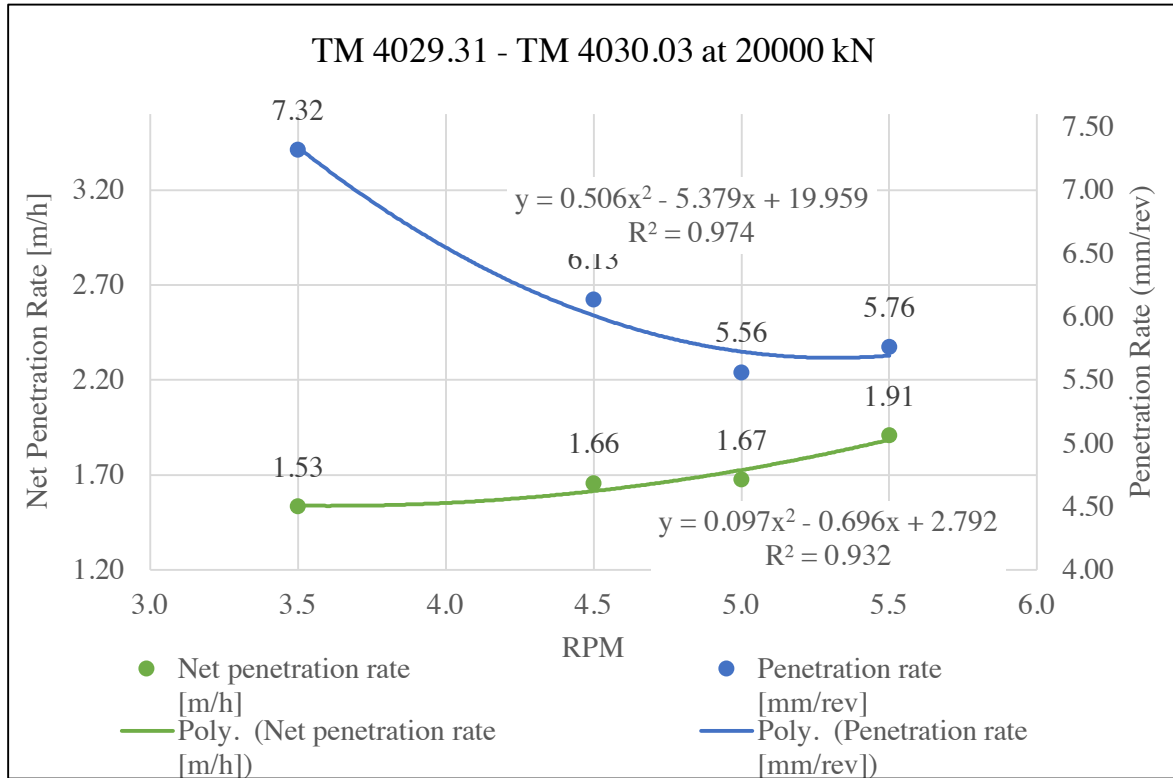


Figure 5.13 Plot of net penetration rate and penetration rate for the RPM test at TM 4029.31 – TM 4030.03

5.4.3 RPM test at TM 4106.53 – TM 4107.72

This RPM test was completed with a constant thrust of approximately 17000 kN, equivalent to 274.19 kN/cutter. The RPM levels were set to 4.0, 4.5, 5.0, and 5.5.

The geology in this area consists of biotite rich banded augen gneiss with mica layers. The fracturing factor is found to be 1.12, with an average spacing and angel of approximately 28 cm and 43°.

As can be seen in Figure 5.14, the plot of the penetration rate does not have the shape were the penetration rate are increasing up to a maximum point, before it decreases. This indicates that the rock is not competent, for such a test. Also, the low thrust level shows that this is quite soft rock. The test was first started with a thrust of 20000 kN. This gave to high penetration rates for the conveyor belt and the thrust was therefore lowered. The results indicate that the optimal RPM regarding the penetration rate is 4.0. This corresponds with the optimal RPM from the chip analysis presented in chapter 5.5.3. With

a *RPM* of 4.0, the penetration rate is 8.64 and the net penetration rate is 2.07, taken from Figure 5.14. The net penetration rate is here 18 % lower than the maximum rate, and is therefore to low in practical use.

By using a *RPM* of 4.0 the rock breaking process will be more efficient and larger chips are produced. In this situation with the soft rock it is more important to get the rock out fast. The net penetration rates are high and will help the progress better than an increment of the machine utilization.

Table 5.10 Data from the *RPM* test at TM 4106.53 – TM 4107.72

| Cutterhead velocity [RPM] | Penetration rate [mm/rev] | Net penetration rate [m/h] | Cutter thrust [kN/cutter] |
|---------------------------|---------------------------|----------------------------|---------------------------|
| 4.01 | 8.80 | 2.12 | 271.80 |
| 4.51 | 7.54 | 2.04 | 274.85 |
| 5.04 | 8.07 | 2.44 | 274.83 |
| 5.50 | 7.30 | 2.41 | 277.25 |

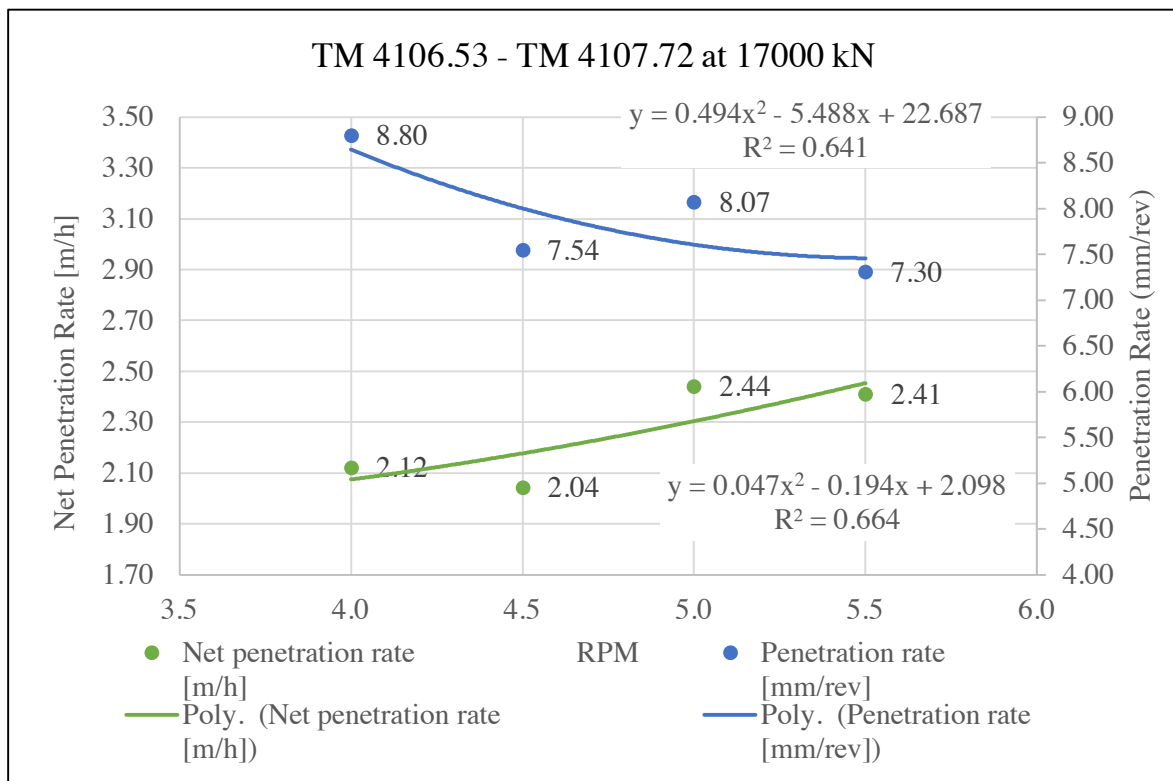


Figure 5.14 Plot of net penetration rate and penetration rate for the *RPM* test at TM 4106.53 – TM 4107.72

5.4.4 RPM test at TM 4361.59 – TM 4362.47

This *RPM* test was performed with a constant thrust of approximately 21500 kN, equivalent to 346.77 kN/cutter. The *RPM* levels were chosen to 3.5, 4.0, 4.5, and 5.0.

The geology in this area consists of augen gneiss with biotite rich bands, and a mix of mica and feldspar. The fracturing factor is found to be 1.08, with an average spacing and angle of approximately 28 cm and 45°.

In Figure 5.15 the penetration rate increases up to a maximum point before it starts to decrease. This tells that the geological properties are well suited for a *RPM* test, and the results follow in line with the theoretical aspects of such a test.

As can be seen in Table 5.12, the maximum net penetration rate is set at 2.32 m/h. The optimal net penetration rate is calculated as 5 % less than the maximum net penetration rate. This gives an optimal *RPM* for the given geology of 4.74. Which corresponds to a penetration rate and net penetration rate of 7.72 mm/rev and 2.2 m/h respectively.

Table 5.11 Data from the *RPM* test at TM 4361.59 – TM 4362.47

| Cutterhead velocity [<i>RPM</i>] | Penetration rate [mm/rev] | Net penetration rate [m/h] | Cutter thrust [kN/cutter] |
|---------------------------------------|------------------------------|-------------------------------|------------------------------|
| 3.52 | 6.86 | 1.45 | 338.57 |
| 4.02 | 7.42 | 1.79 | 343.15 |
| 4.51 | 7.65 | 2.07 | 342.82 |
| 5.01 | 7.71 | 2.32 | 345.41 |

Table 5.12 Overview of outcomes from the *RPM* test at TM 4361.59 – TM 4362.47

| | <i>RPM</i> | Penetration rate (mm/rev) | Net penetration rate (m/h) |
|---------------------------------|------------|------------------------------|-------------------------------|
| Max net penetration rate | 5.00 | 7.71 | 2.32 |
| Optimal <i>RPM</i> | 4.74 | 7.72 | 2.20 |

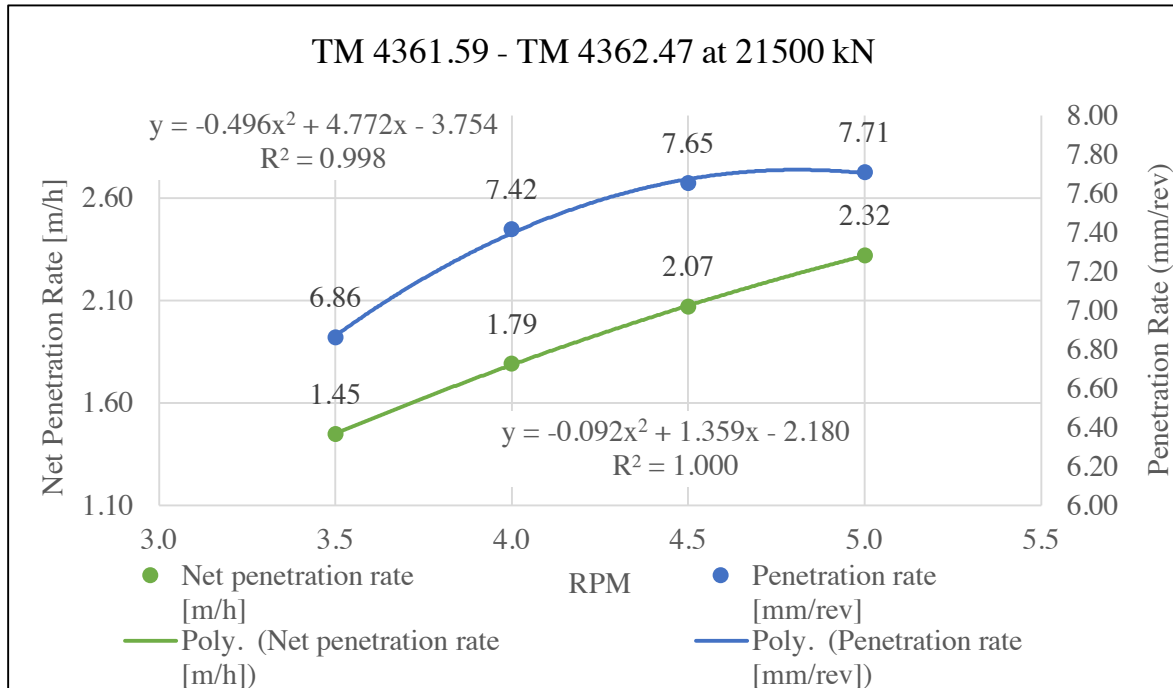


Figure 5.15 Plot of net penetration rate and penetration rate for the RPM test at TM 4361.59 – TM 4362.47

5.5 Chip analyses

5.5.1 Chip analyses of the penetration test at TM 4337.03 – TM 4337.56

This chip analysis was conducted in conjunction with the penetration test at TM 4337.03 – TM 4337.56. Chips was collected for each thrust level, and the 20 largest for the individual levels were measured. The results are shown in Table 5.13 and displays the average chip size, chipping frequency, cubic chip size and shape factor.

The chipping frequency increases with increasing thrust, shown in Figure 5.18.

The cubic ship size for the first thrust level is rather high. From level one it decreases down to 321.23 kN/cutter, before it steadily increases thereafter. According to Bruland (2000d), the cubic chip size should have a curve like the penetration test curve. Therefore, it is expected that the first value is too high and give a wrong impression of the cubic ship size for this thrust level.

The chip shape trend moves from flat and elongated at lower thrust to more elongated with higher thrust, as displayed in Figure 5.19. The general trend presented in Bruland (2000d) is that the chip shape goes from flat and elongated at low thrust levels to more elongated and more cubic at higher thrust levels. This indicate that the chip shape is in good accordance with the general trend given in the NTNU-model.

Table 5.13 Summary of chip analysis of the penetration test at TM 4337.03 – TM 4337.56

| Thrust level (kN/cutter) | Penetration i_0 (mm/rev) | Average Chip Size (mm) | | | Chipping Frequency f_{ch} (rev ⁻¹) | Cubic chip size (mm ³)/1000 | Shape factor | |
|-----------------------------|----------------------------------|---------------------------|----------|----------|--|---|-----------------|----------|
| | | h_{ch} | w_{ch} | l_{ch} | | | f_{hw} | f_{wl} |
| 313.30 | 5.09 | 32.5 | 80.6 | 179.4 | 0.157 | 469.52 | 0.40 | 0.45 |
| 321.23 | 5.40 | 30.2 | 81.8 | 156.4 | 0.179 | 386.13 | 0.37 | 0.52 |
| 340.78 | 6.58 | 31.8 | 85.7 | 172.0 | 0.207 | 468.47 | 0.37 | 0.50 |
| 353.56 | 6.96 | 29.9 | 92.1 | 174.0 | 0.233 | 478.90 | 0.32 | 0.53 |

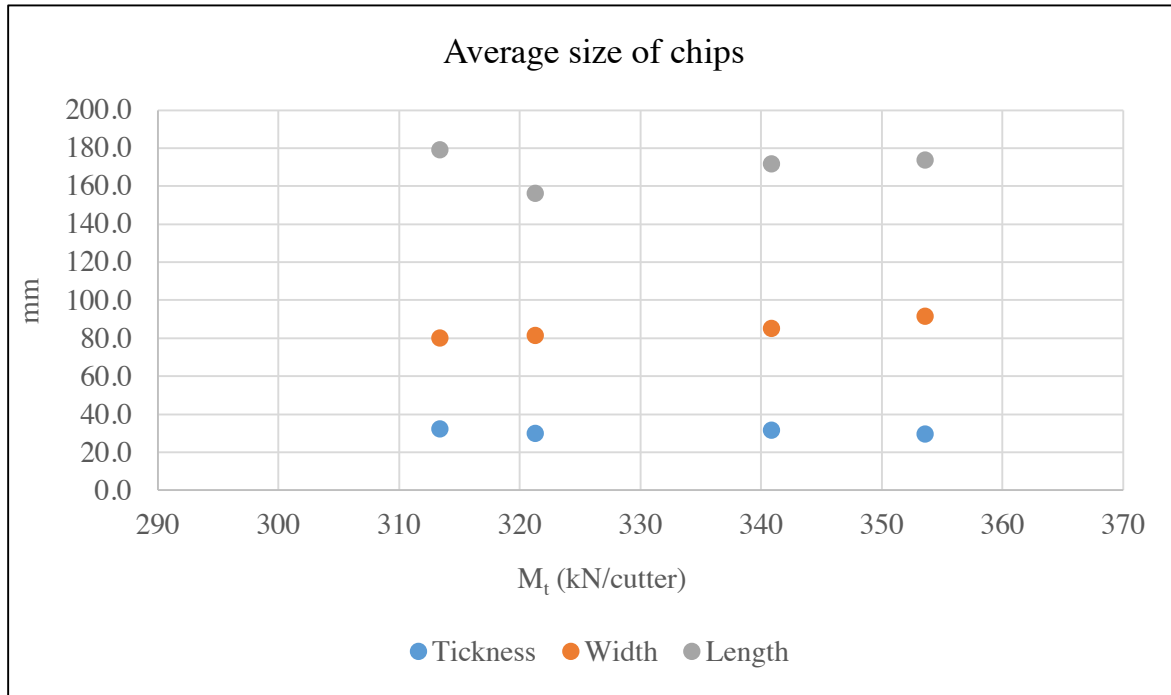


Figure 5.16 Average size of the largest chips from the penetration test at TM 4337.03 – TM 4337.56

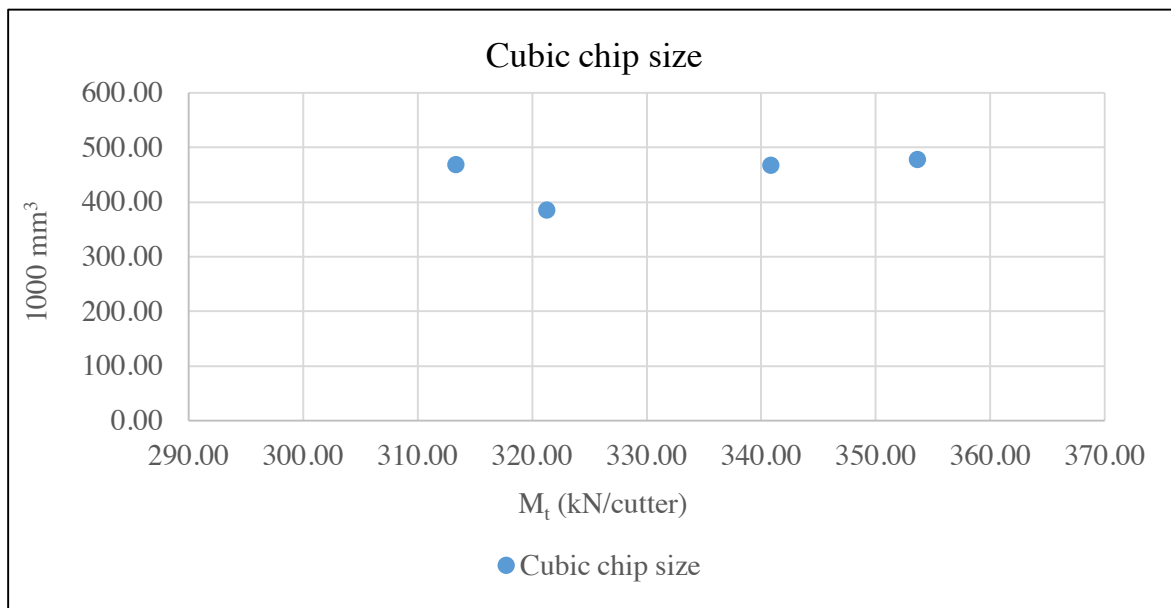


Figure 5.17 Cubic chip size of the penetration test at TM 4337.03 – TM 4337.56

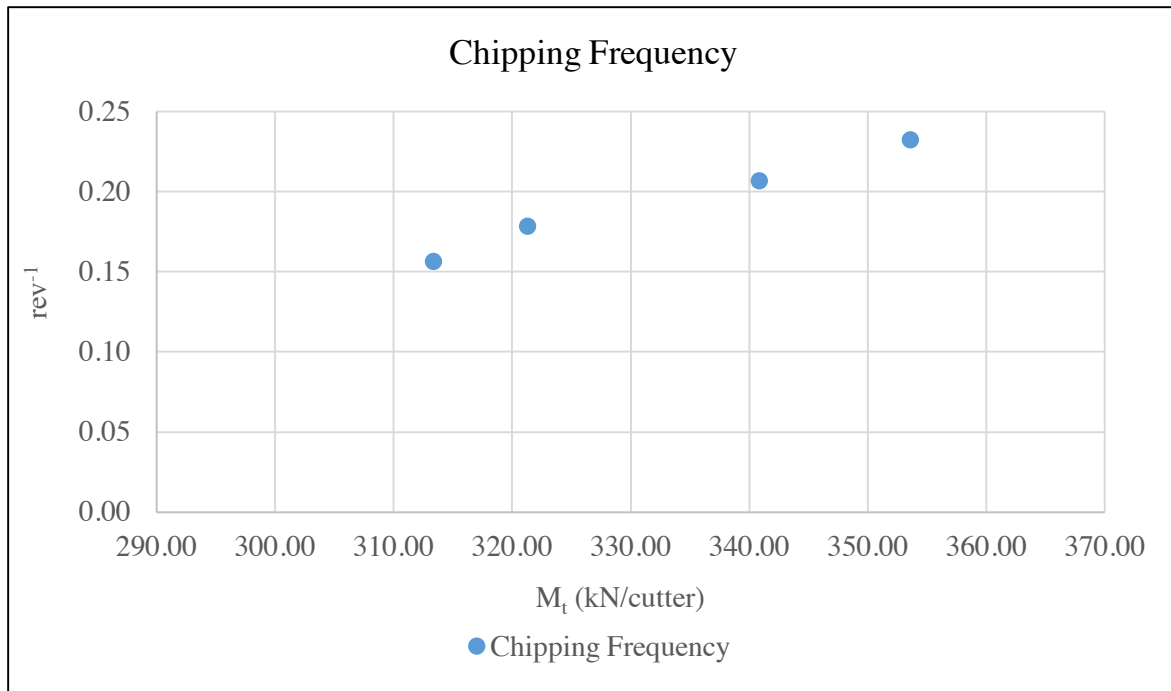


Figure 5.18 Chipping frequency of the penetration test at TM 4337.03 – TM 4337.56

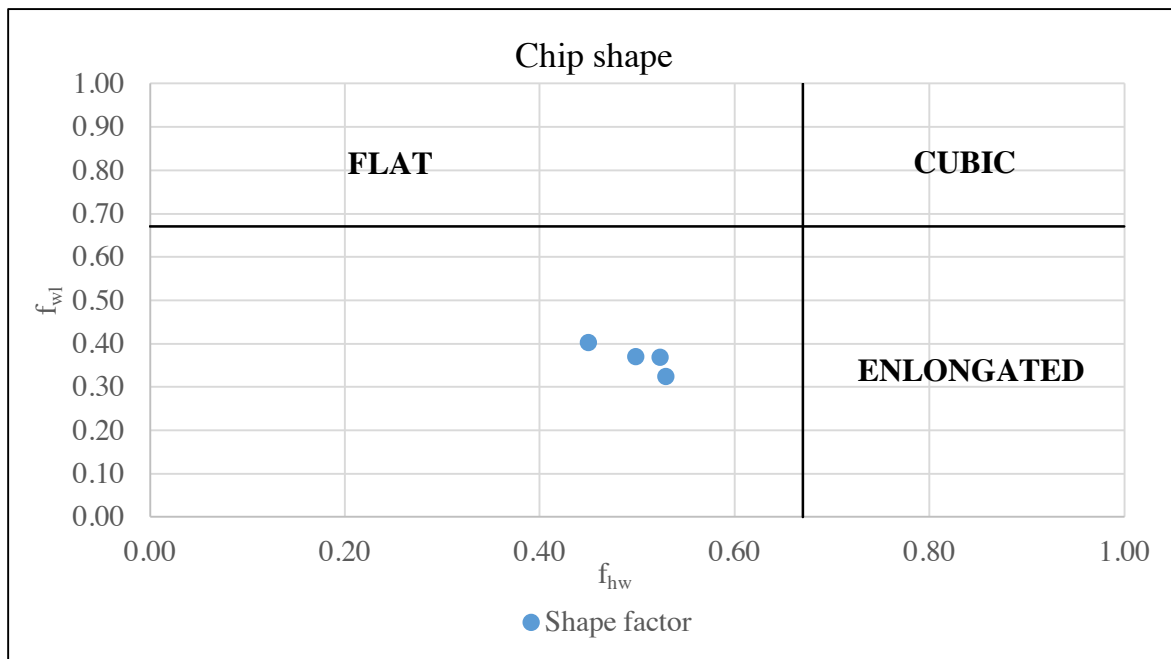


Figure 5.19 Chip shape of the average chip size of the penetration test at TM 4337.03 – TM 4337.56

5.5.2 Chip analysis of the RPM test at TM 4029.31 – TM 4030.03

This chip analysis was conducted in conjunction with the *RPM* test at TM 4029.31 – TM 4030.03. Chips were collected for each thrust level, and the 20 largest for the individual levels were measured. The results are shown in Table 5.14 and displays the average chip size, chipping frequency, cubic chip size and shape factor.

The chipping frequency is highest at the lowest *RPM* level and the trend decreases when the *RPM* level goes up, shown in Figure 5.22.

The cubic chip size indicates that the rock breaking process is most efficient at a *RPM* level of approximately 4.5. At this level the cubic chip size is at its largest, and the penetration is correspondingly at a high level.

The chip shape trend moves from flat and elongated at low *RPM* to more elongated and more cubic at higher *RPM*, as displayed in Figure 5.23.

Table 5.14 Summary of chip analysis of the *RPM* test at TM 4029.31 – TM 4030.03

| <i>RPM</i> | Penetration i_0 (mm/rev) | Average Chip Size (mm) | | | Chipping Frequency f_{ch} (rev ⁻¹) | Cubic chip size (mm ³)/1000 | Shape factor | |
|------------|----------------------------|------------------------|----------|----------|--|---|--------------|----------|
| | | h_{ch} | w_{ch} | l_{ch} | | | f_{hw} | f_{wl} |
| 3.49 | 7.32 | 37.0 | 107.8 | 189.8 | 0.198 | 756.49 | 0.34 | 0.57 |
| 4.5 | 6.13 | 47.5 | 141.7 | 217.8 | 0.129 | 1465.10 | 0.34 | 0.65 |
| 5.01 | 5.56 | 42.0 | 127.2 | 226.1 | 0.132 | 1207.17 | 0.33 | 0.56 |
| 5.52 | 5.76 | 47.6 | 130.0 | 224.2 | 0.121 | 1385.89 | 0.37 | 0.58 |

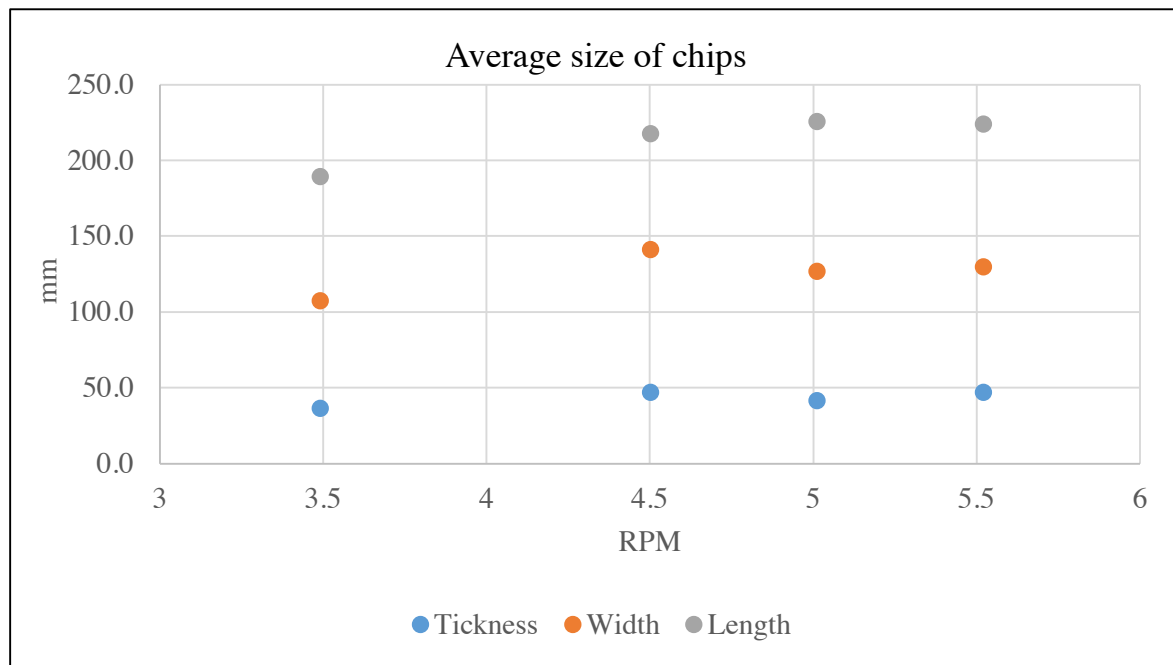


Figure 5.20 Average size of the largest chips from the *RPM* test at TM 4029.31 – TM 4030.03

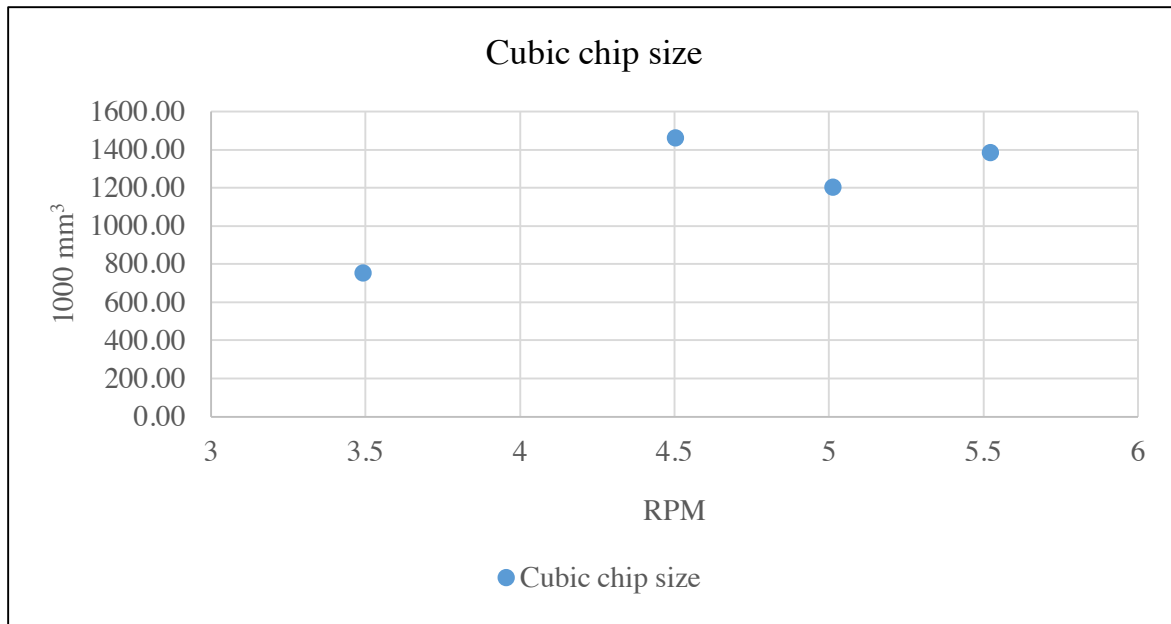


Figure 5.21 Cubic chip size of the RPM test at TM 4029.31 – TM 4030.03

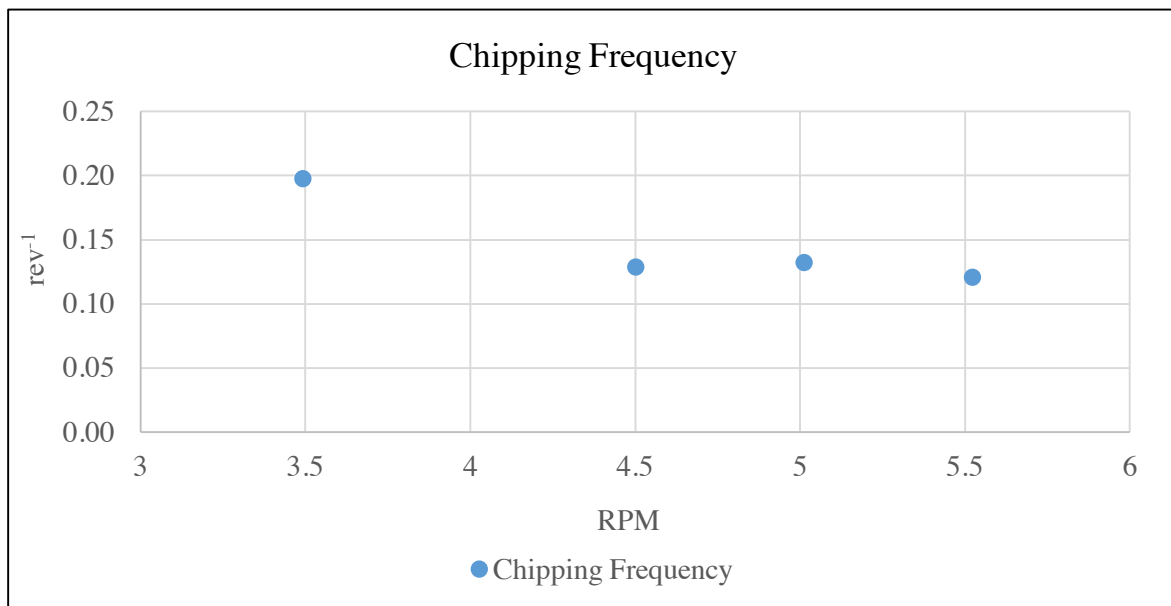


Figure 5.22 Chipping frequency of the RPM test at TM 4029.31 – TM 4030.03

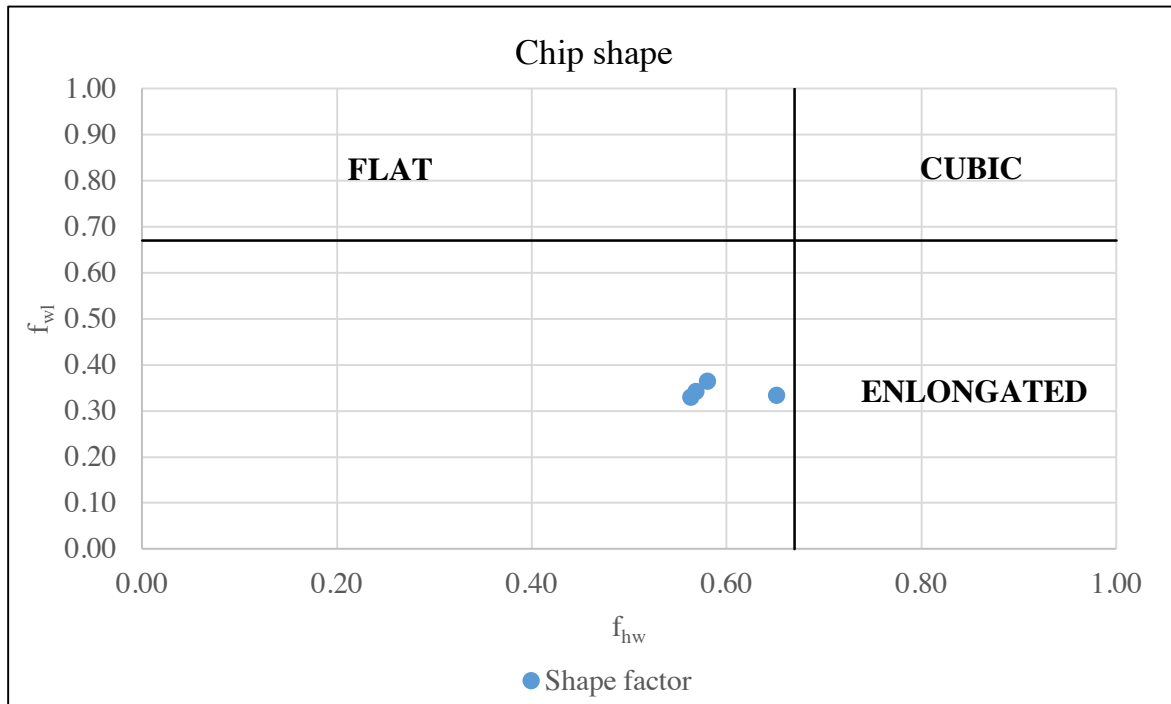


Figure 5.23 Chip shape of the average chip size of the RPM test at TM 4029.31 – TM 4030.03

5.5.3 Chip analysis of the RPM test at TM 4106.53 – TM 4107.72

This chip analysis was conducted in conjunction with the *RPM* test at TM 4106.53 – TM 4107.72. Chips were collected for each thrust level, and the 20 largest for the individual levels were measured. The results are shown in Table 5.15 and displays the average chip size, chipping frequency, cubic chip size and shape factor.

The chipping frequency is highest at the lowest *RPM* level and the trend decreases when the *RPM* level goes up, shown in Figure 5.26.

The cubic chip size indicates that the rock breaking process is most efficient at a *RPM* level of approximately 4.0. At this level the cubic chip size is at its largest, and the penetration is correspondingly at a high level.

The chip shape trend moves from elongated at low *RPM* to flat and elongated at higher *RPM*, as displayed in Figure 5.27.

Table 5.15 Summary of chip analysis of the *RPM* test at TM 4106.53 – TM 4107.72

| <i>RPM</i> | Penetration i_0 (mm/rev) | Average Chip Size (mm) | | | Chipping Frequency f_{ch} (rev ⁻¹) | Cubic chip size (mm ³)/1000 | Shape factor | |
|------------|----------------------------|------------------------|----------|----------|--|---|--------------|----------|
| | | h_{ch} | w_{ch} | l_{ch} | | | f_{hw} | f_{wl} |
| 4.01 | 8.8 | 51.8 | 144.5 | 233.0 | 0.170 | 1741.97 | 0.36 | 0.62 |
| 4.51 | 7.54 | 51.8 | 111.0 | 187.2 | 0.146 | 1075.04 | 0.47 | 0.59 |
| 5.04 | 8.07 | 53.0 | 114.9 | 198.8 | 0.152 | 1210.11 | 0.46 | 0.58 |
| 5.5 | 7.3 | 48.3 | 119.8 | 207.8 | 0.151 | 1200.66 | 0.40 | 0.58 |

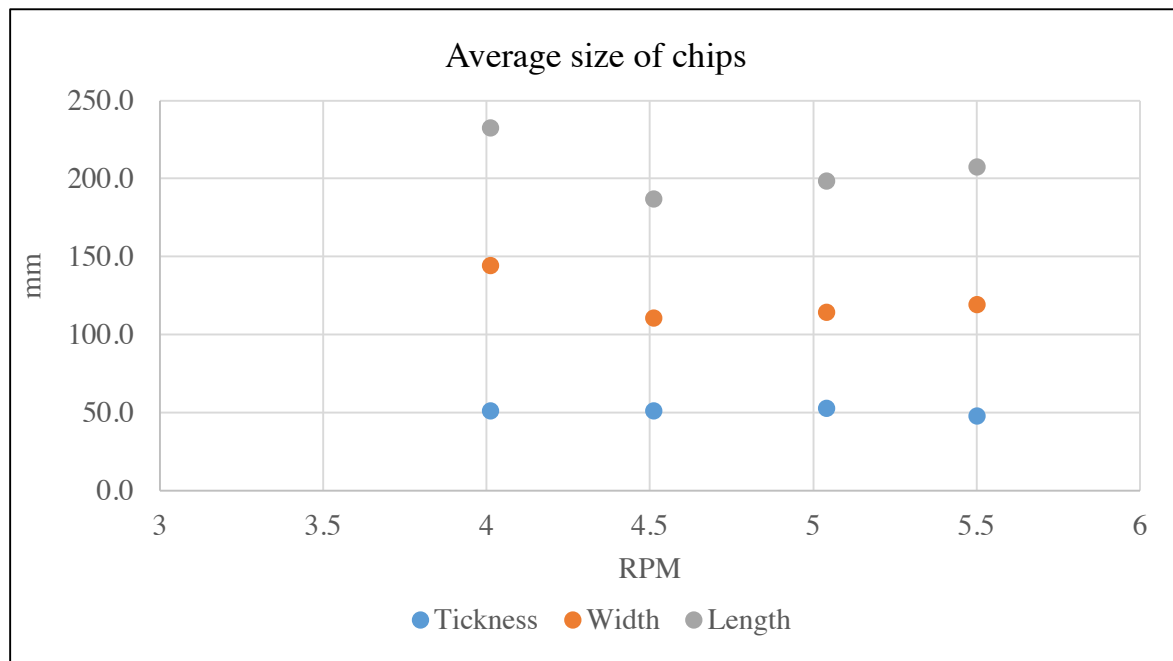


Figure 5.24 Average size of the largest chips from the *RPM* test at TM 4106.53 – TM 4107.72

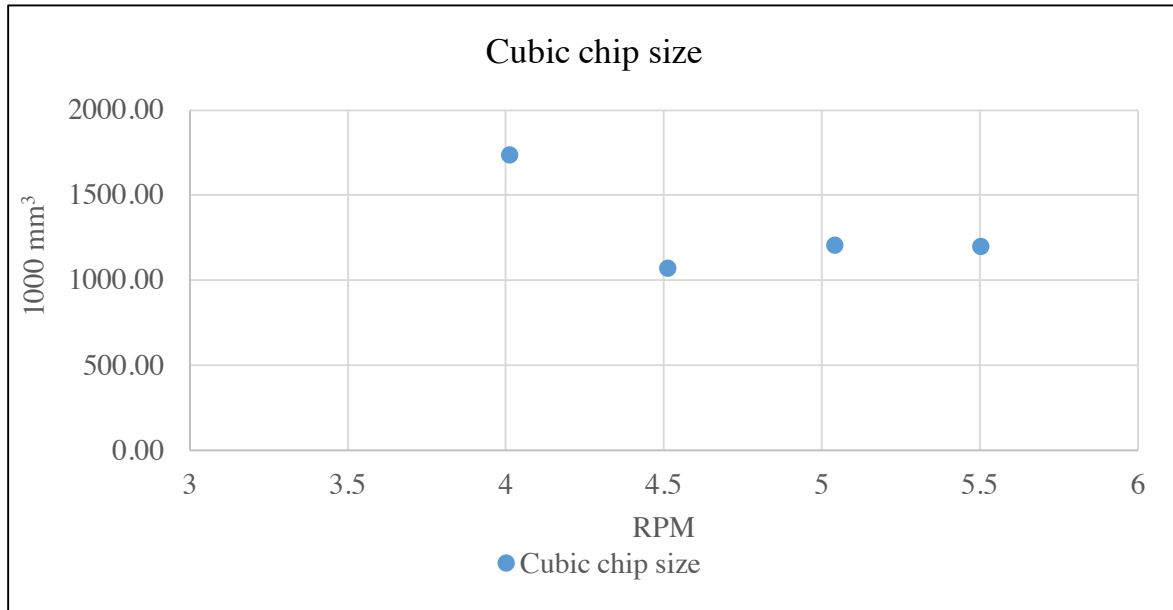


Figure 5.25 Cubic chip size of the RPM test at TM 4106.53 – TM 4107.72

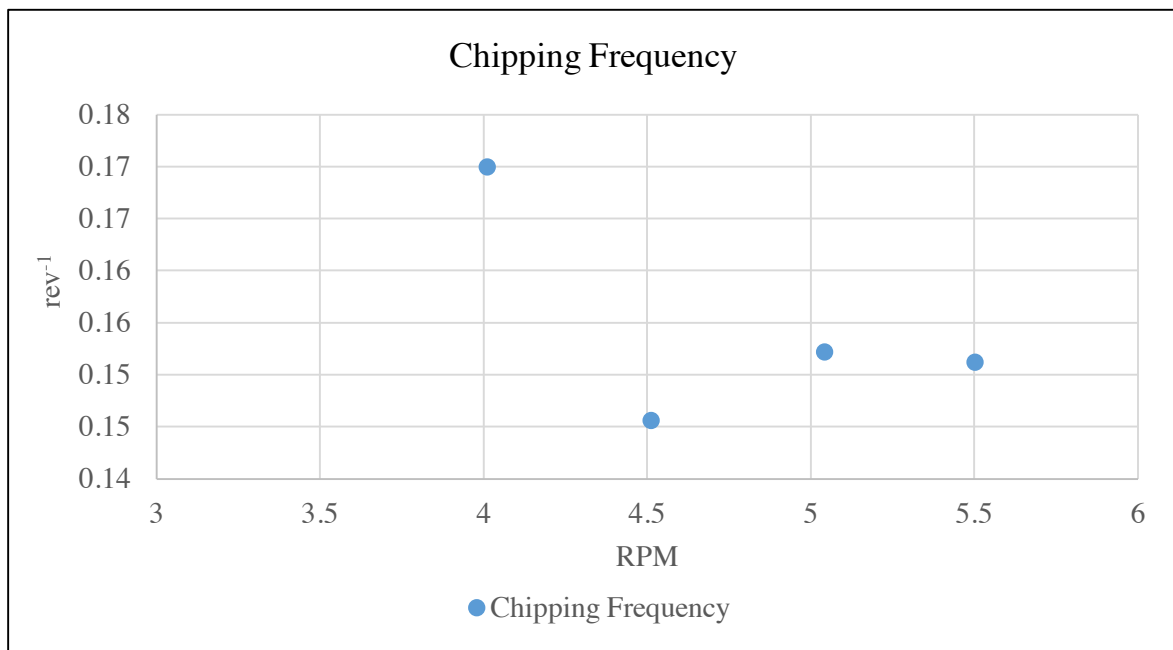


Figure 5.26 Chipping frequency of the RPM test at TM 4106.53 – TM 4107.72

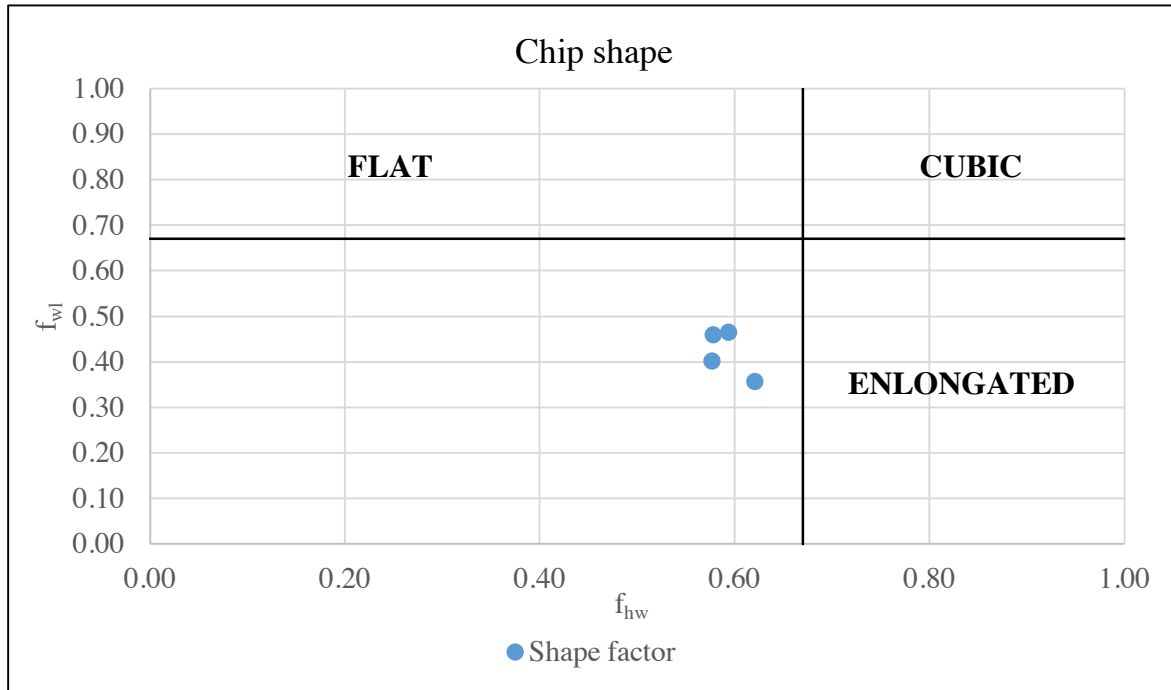


Figure 5.27 Chip shape of the average chip size of the RPM test at TM 4106.53 – TM 4107.72

5.5.4 Chip analysis of the RPM test at TM 4361.59 – TM 4362.47

This chip analysis was conducted in conjunction with the *RPM* test at TM 4361.59 – TM 4362.47. Chips were collected for each thrust level, and the 20 largest for the individual levels were measured. The results are shown in Table 5.16 and displays the average chip size, chipping frequency, cubic chip size and shape factor.

The chipping frequency is highest at the lowest *RPM* level and the trend decreases when the *RPM* level goes up, shown in Figure 5.30.

The cubic chip size indicates that the rock breaking process is most efficient at a *RPM* level of about 5.0. At this level the cubic chip size is at its largest and the penetration is at the highest level in this test. This corresponds well with the calculation of the optimal *RPM* from this *RPM* test, which is found to be 4.74.

The chip shape trend moves from flat and elongated at low *RPM* to more elongated at higher *RPM*, as displayed in Figure 5.31.

Table 5.16 Summary of chip analysis of the *RPM* test at TM 4361.59 – TM 4362.47

| <i>RPM</i> | Penetration i_0 (mm/rev) | Average Chip Size (mm) | | | Chipping Frequency f_{ch} (rev ⁻¹) | Cubic chip size (mm ³)/1000 | Shape factor | |
|------------|----------------------------|------------------------|----------|----------|--|---|--------------|----------|
| | | h_{ch} | w_{ch} | l_{ch} | | | f_{hw} | f_{wl} |
| 3.52 | 6.86 | 26.1 | 67.8 | 154.6 | 0.263 | 273.33 | 0.39 | 0.44 |
| 4.02 | 7.42 | 32.2 | 85.0 | 163.1 | 0.230 | 446.14 | 0.38 | 0.52 |
| 4.51 | 7.65 | 36.2 | 88.2 | 152.3 | 0.211 | 486.27 | 0.41 | 0.58 |
| 5.01 | 7.71 | 36.4 | 85.0 | 177.6 | 0.212 | 549.49 | 0.43 | 0.48 |

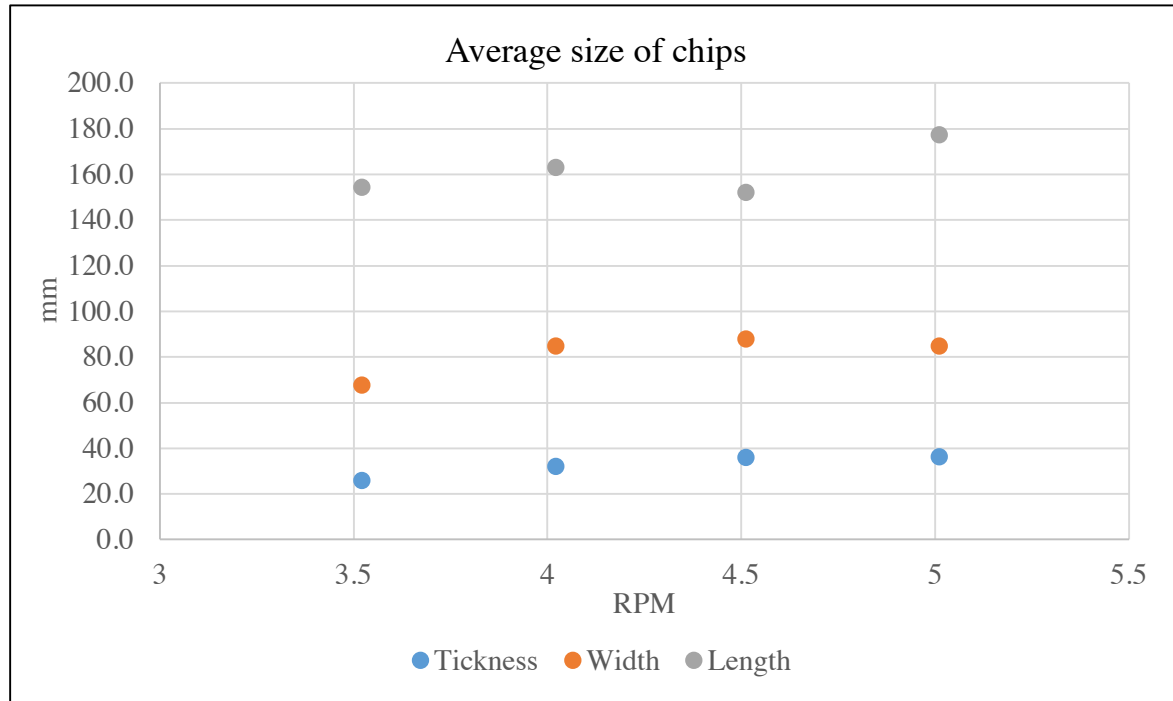


Figure 5.28 Average size of the largest chips from the *RPM* test at TM 4361.59 – TM 4362.47

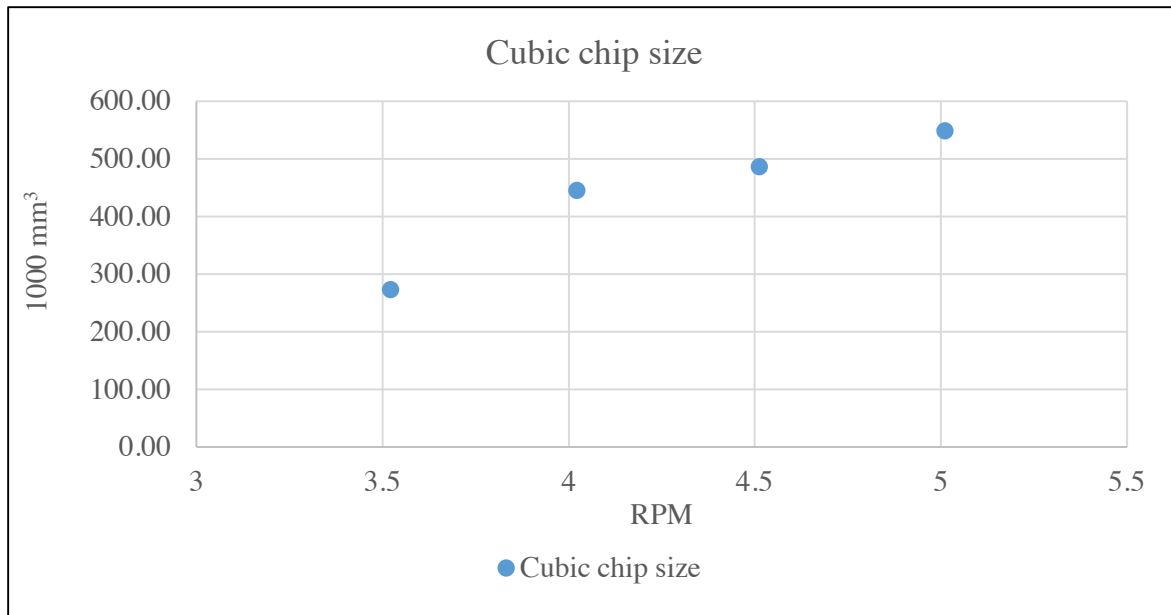


Figure 5.29 Cubic chip size of the RPM test at TM 4361.59 – TM 4362.47

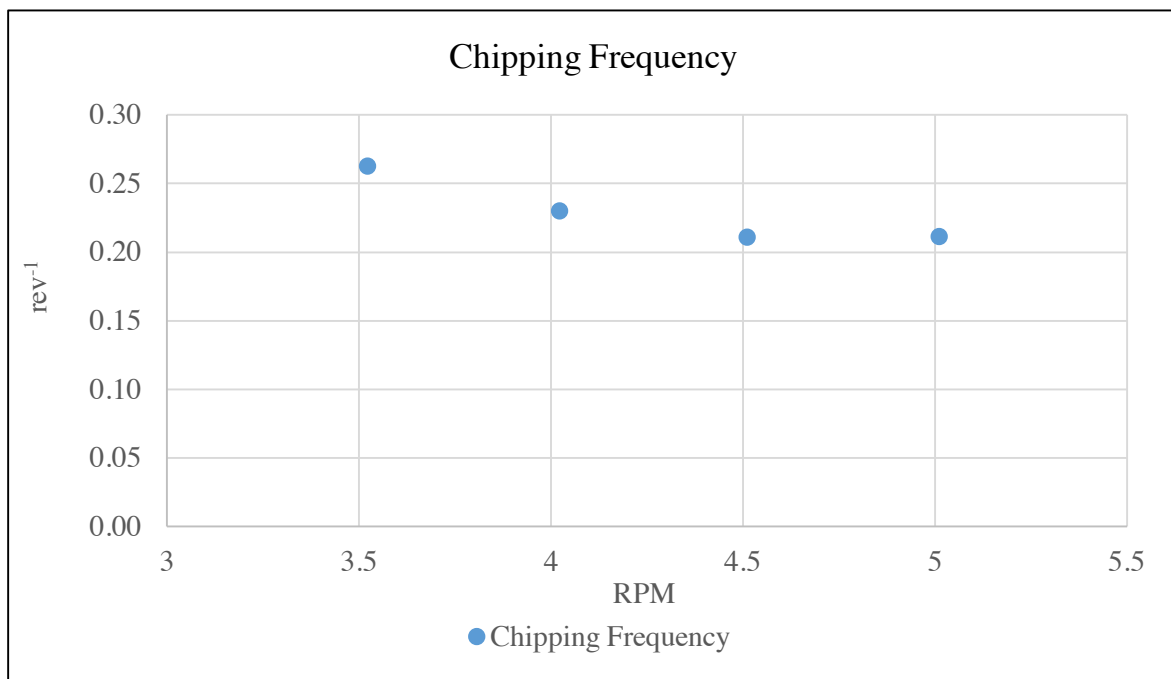


Figure 5.30 Chipping frequency of the RPM test at TM 4361.59 – TM 4362.47

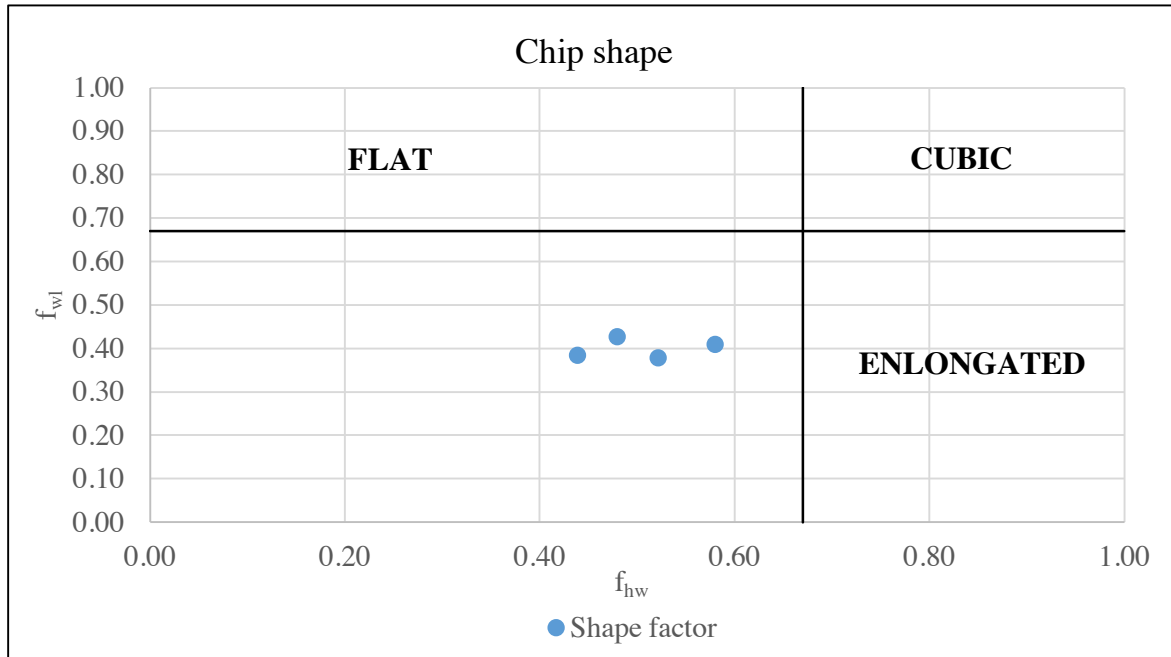


Figure 5.31 Chip shape of the average chip size of the RPM test at TM 4361.59 – TM 4362.47

5.6 Cutter consumption

The cutter consumption log provided from JVSS contain information from the complete tunnel bored. All data from outside of the selected tunnel segment, TM 3775 – TM 4475, has been deleted. The results in this chapter are only representative for this part of the tunnel. As previous values were deleted, the numbers will not be fully representative. Data presented will not take into consideration when a cutter was last changed prior to section TM 3775. Therefore, if a cutter was changed just before this area, the wear of this cutter might appear less than it actually is. Regardless of this, the thesis will only focus on the selected 700 meters. This is due to lack of time and other focus areas.

Below, Figure 5.32 shows the cutter changes and the reason for the change. As this represents recorded changes, it also includes repositioning of cutters as a type of change. According to Macias (2016) abrasive wear, mushrooming and chipping, described as cutter ring wear, should represent more than approximately 70% of the total amount of replacements. Here they represent 64%, which is slightly below what Macias indicates. In addition, he suggests that cutters replaced due to bearing damage, meaning blockage, leakage, damaged hubs, etc., should account for less than 20-30% of the total number of cutter changes. For this section of the New Ulriken Tunnel, changes due to bearing damage represent 33.9% of the total changes made.

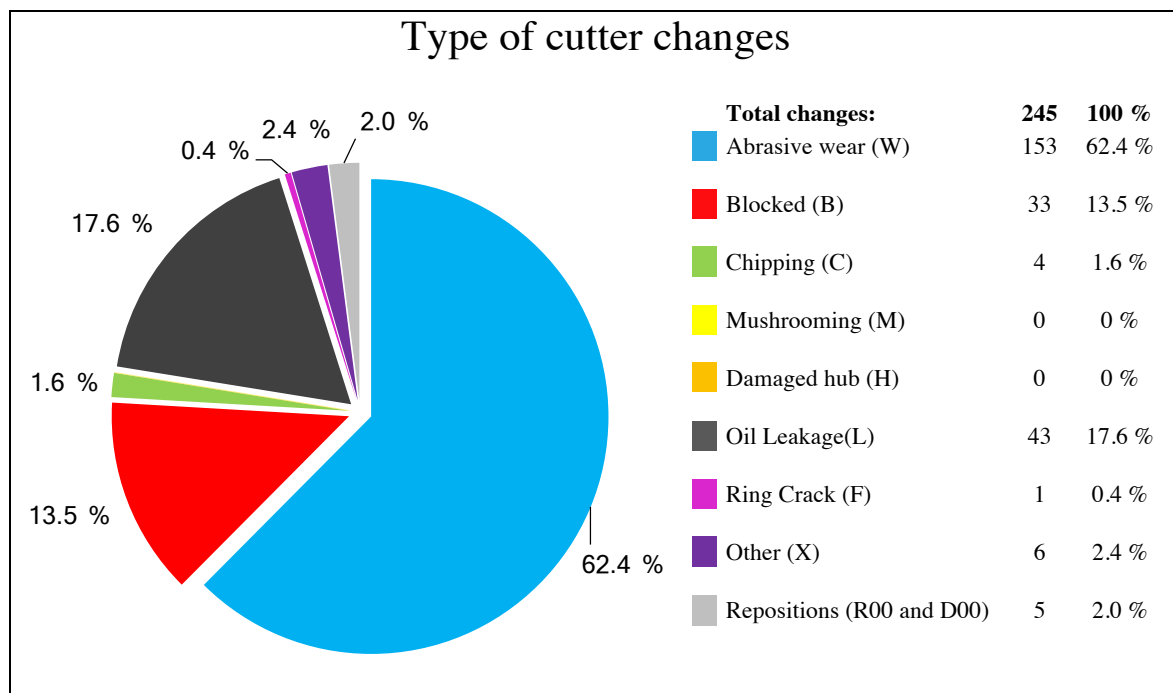


Figure 5.32 Type of cutter changes made for the selected tunnel section TM 3775 – TM 4475

Table 5.17 shows a summary of selected parameters taken from the cutter consumption log. Some of these values will later be compared to calculations from the NTNU-model regarding cutter wear. The values are here shown per cutter, and not per change. This meaning that repositioning of the cutters is not taken into account, as this will not have an impact on the cutter wear values. All data and calculations regarding cutter consumption can be found in Appendix L .

Table 5.17 Results of the cutter consumption from the selected tunnel section

| | |
|---|-----------------------------|
| Meters Bored | 704 m |
| Hours Bored | 370 h |
| Average cutter ring life (meters) | 2.93 m/cutter |
| Average cutter ring life (hours) | 1.54 h/cutter |
| Average cutter ring life (solid cubic meters) | 201 sm ³ /cutter |
| Rolling distance/Cutter | 15.734 km/cutter |

In addition to know the total amount of cutter changes and wear, it is important to understand in what positions the cutters are most prone to wear. Therefore, every time a cutter is changed, its position number is logged. Figure 5.33 shows a graph detailing the number and type of change of each of the 62 cutter positions. A detailed drawing of the cutterhead including position number on each of the cutters can be found in Appendix B .

The cutter positions 51 through 58, and position 61 are most prone to wear. These cutters have a high number of total changes over the 700-meter tunnel segment. Positions 51, 53, 54, 55, 57, 58, and 61 have a high amount of changes for other reasons than abrasive wear, and are most likely exposed to the highest loads. Mainly, these positions have a high total of blocked cutters and oil leakage.

Figure 5.34 show average cutter ring wear and wear limits for the New Ulriken Tunnel. This indicates that the same cutters mentioned above is also exceeding the wear limits sat for the project.

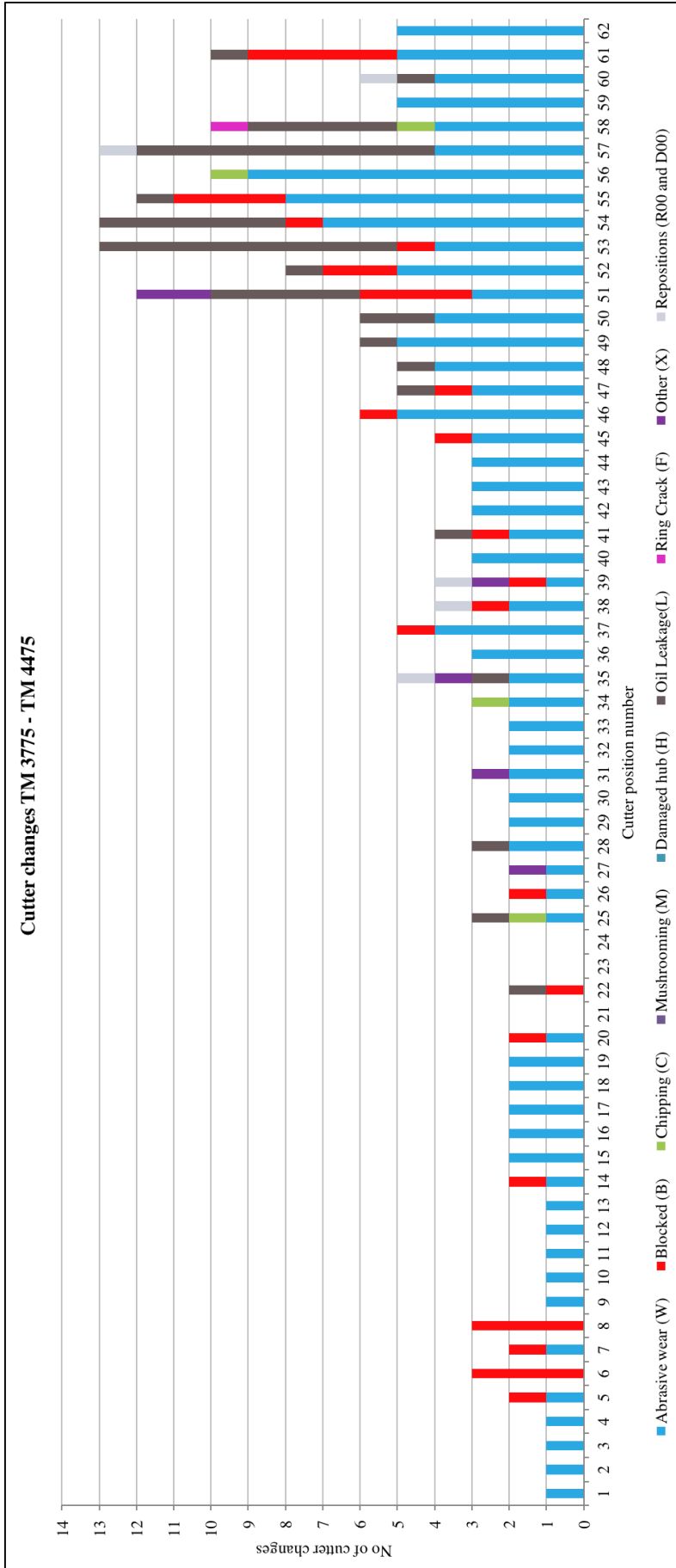


Figure 5.33 The number and type of cutter changes for the 62 cutters over the selected tunnel section

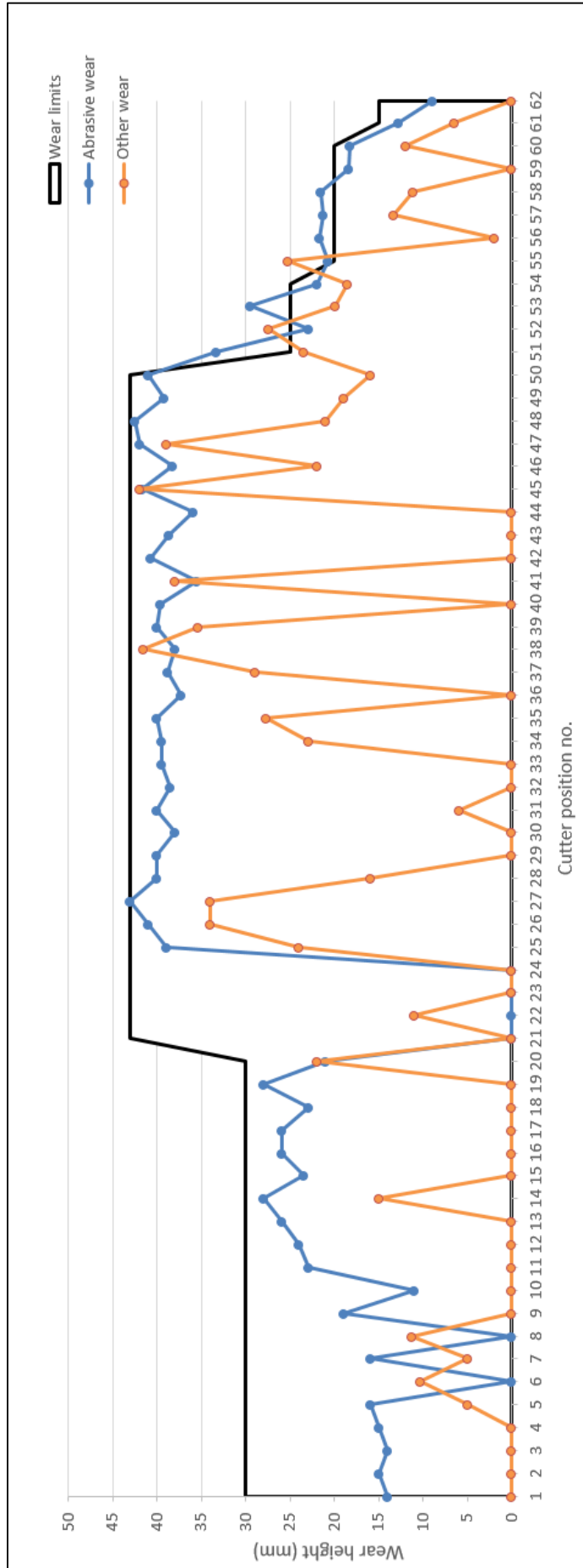


Figure 5.34 Average cutter ring wear and wear limits used in the project. The wear is shown for abrasive wear and other wear related to the bearing set

5.7 Laboratory results

In the subchapters, the obtained test results and calculated indices from the laboratory are presented. A more detailed overview of the results and calculations of the different indices can be seen in Appendix M .

5.7.1 Test results

The results from the laboratory tests presented in chapter 4.3 are given in Table 5.18. Except from density and quartz content, the results are merely performed to calculate the indices shown in Table 5.19.

Table 5.18 Laboratory test results

| Sample number | TM 3843 | TM 4091 | TM 4468 |
|--|---------|---------|---------|
| Density, (g/cm ³) | 2.64 | 2.77 | 2.65 |
| Brittleness Value, S_{20} | 52.7 % | 44.6 % | 49.3 % |
| Sievers' J-value, SJ | 3.90 | 3.78 | 1.72 |
| Abrasion Value Cutter Steel, AVS | 35.5 | 15.0 | 34.0 |
| Quartz content (%) | 19 | 5 | 28 |
| Point Load Strength, $I_{s(50)}$ (MPa) | 7.69 | 8.50 | 10.01 |

5.7.2 Calculated indices

The obtained *DRI*- and *CLI*-values together with the calculated *UCS* and *BTS* values can be seen in Table 5.19. *DRI* is calculated from S_{20} and SJ , while *CLI* is determined from SJ and AVS . The Point Load Strength was used to estimate *UCS* and *BTS*, see chapter 4.3.9 for more detailed information.

For the *DRI*, NTNU/SINTEF have associated formulas for the graph presented in Figure 4.5. As they were not willing to share these, NTNU/SINTEF calculated the *DRI*-values based on our laboratory results using their formulas. This gave more accurate results.

Table 5.19 Calculated indices from laboratory tests

| Sample number | TM 3843 | TM 4091 | TM 4468 |
|-------------------------------------|---------|---------|---------|
| Drilling Rate Index, <i>DRI</i> | 48 | 40 | 40 |
| Cutter Life Index, <i>CLI</i> | 5.9 | 8.1 | 4.4 |
| Uniaxial Compressive Strength (MPa) | 153.8 | 169.9 | 200.2 |
| Brazilian Tensile Strength (MPa) | 6.2 | 6.8 | 8.0 |

5.8 Penetration estimations with the different prediction models

The estimated net penetration rates from the different models are given in the following subchapters. As mentioned in chapter 5.1.2 and 5.2.2, the tunnel segment is divided in different subdivisions. The three subdivisions are split based on; the complete 700-meter segment, after geology and core samples, and from the k_s -values found in this thesis. The results from the models are showed for each of these subdivisions. Estimations are calculated using two thrust settings; gross cutter thrust and net cutter thrust. The net thrust is equal to the gross thrust, minus a constant friction force of 2500 kN. This means that the net cutter thrust is approximately 40 kN/cutter lower than the gross cutter thrust.

5.8.1 NTNU-model

In the NTNU-model, the net penetration rate is found by equation (3.11), after multiple calculations. The first step is to calculate the k_{s-tot} value from the geological mapping, these values are found in chapter 5.1.2.

When the k_s is calculated, the net penetration rate is obtained by going through a number of equations and graphs found in Macias (2016). The next steps include important factors such as *DRI* and *RPM*, as well as a number of correction factors. These are lightly described in the list below, according to Macias (2016):

| | | | |
|-----------|---|---|---|
| DRI | - | Drilling Rate Index | DRI for the different rock samples are found in chapter 5.7.2. |
| k_{DRI} | - | correction factor for DRI of the rock | Found by a graph and as a function of DRI and the k_{s-tot} value. Differ for each subdivision. |
| k_{por} | - | correction factor for porosity of the rock | The rock samples did not have a porosity higher than 2 %, thus $k_{por} = 1$ in the calculations. |
| k_{ekv} | - | equivalent fracturing factor | Found by equation and differ for every subdivision. |
| k_d | - | correction factor for cutter diameter $d_c \neq 483$ mm | Found by a graph as a function of the cutter diameter. $d_c = 483 \Rightarrow k_d = 1.0$. |
| A_c | - | average cutter spacing | Calculated from the number of cutters on the cutterhead. $A_c = 75.24$ mm |
| k_a | - | correction factor for average cutter spacing $a_c \neq 70$ mm | Found by a graph as a function of average cutter spacing, A_c . $k_a = 0.965$ for all subdivisions. |
| M_B | - | applied cutter thrust | The actual cutter thrust used in the tunnel section. Found in chapter 5.2.2. |
| M_{ekv} | - | equivalent thrust | Calculated by equation. |

| | | | |
|-----------|---|--|--|
| M_l | - | critical cutter thrust (necessary thrust to achieve 1 mm/rev) | Found by a graph as a function of the equivalent fracturing factor, k_{ekv} . Differ for each subdivision. |
| b | - | penetration coefficient | Found by a graph as a function of the equivalent fracturing factor, k_{ekv} . Differ for each subdivision. |
| i_0 | - | basic penetration rate | Found by equation. Differ for each subdivision. |
| RPM | - | revolution per minute (<i>rev/min</i>) | The actual RPM used in the tunnel section. Found in chapter 5.2.2. |
| k_{RPM} | - | correction factor for applied cutterhead RPM | Found by a graph. Differ for each subdivision. |

Results for complete 700-meter segment

Result using filtered gross thrust values give a net penetration rate of 2.62 m/h. The filtered net thrust values calculate a net penetration rate of 2.06 m/h. This is shown in Figure 5.35.

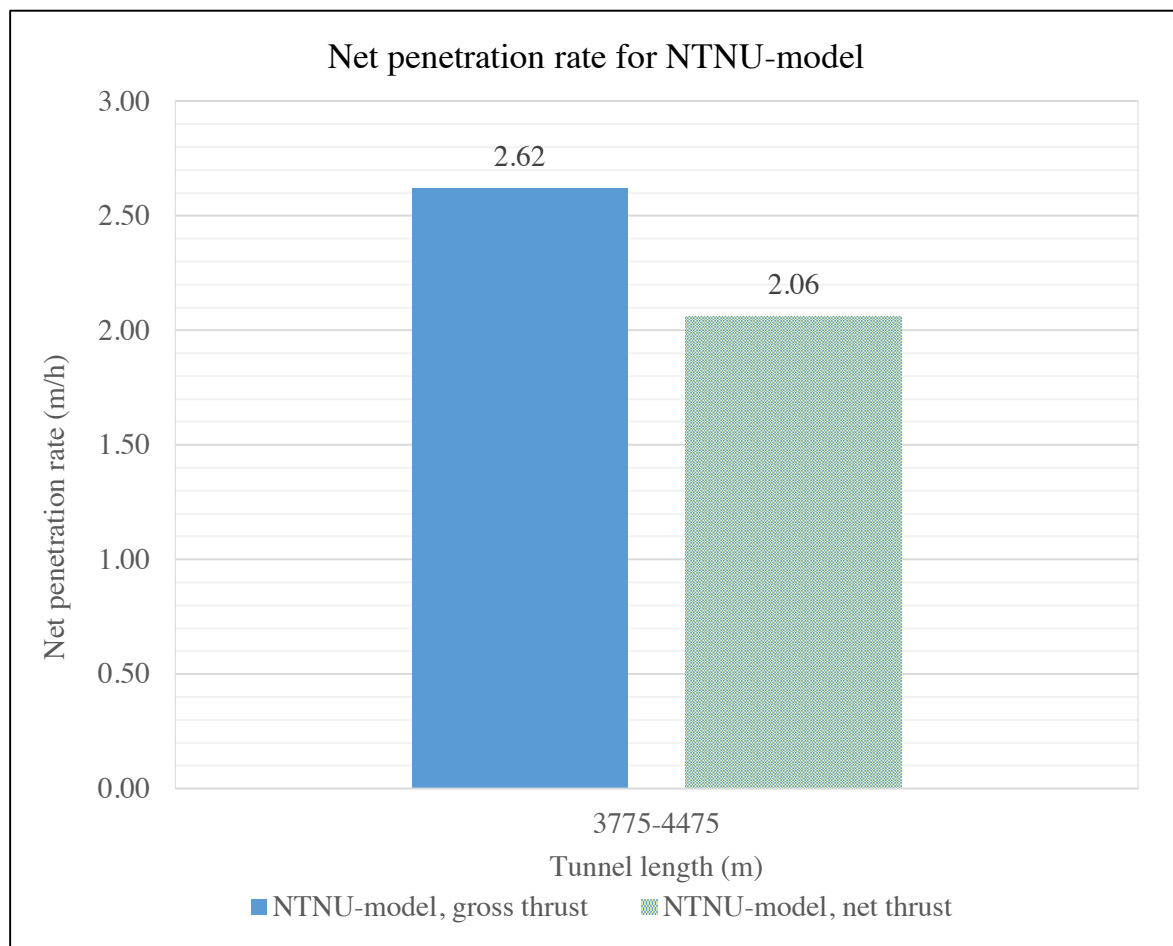


Figure 5.35 Results for NTNU-model calculated with gross and net thrust for the complete 700-meter segment

Results for section divided after geology and core samples

Results from model estimations are shown in Table 5.20 and Figure 5.36. The table includes a weighted average for the tunnel segment.

Table 5.20 Results for NTNU-model calculated with gross and net thrust for section divided after geology and core samples, including a weighted average

| Thrust | Mapped length (m) | Length (m) | NPR (m/h) | Weighted average (m/h) |
|--------|-------------------|------------|-----------|------------------------|
| Gross | 3775-4075 | 300 | 2.50 | 2.66 |
| | 4075-4250 | 175 | 2.66 | |
| | 4250-4475 | 225 | 2.86 | |
| Net | 3775-4075 | 300 | 1.96 | 2.10 |
| | 4075-4250 | 175 | 2.09 | |
| | 4250-4475 | 225 | 2.29 | |

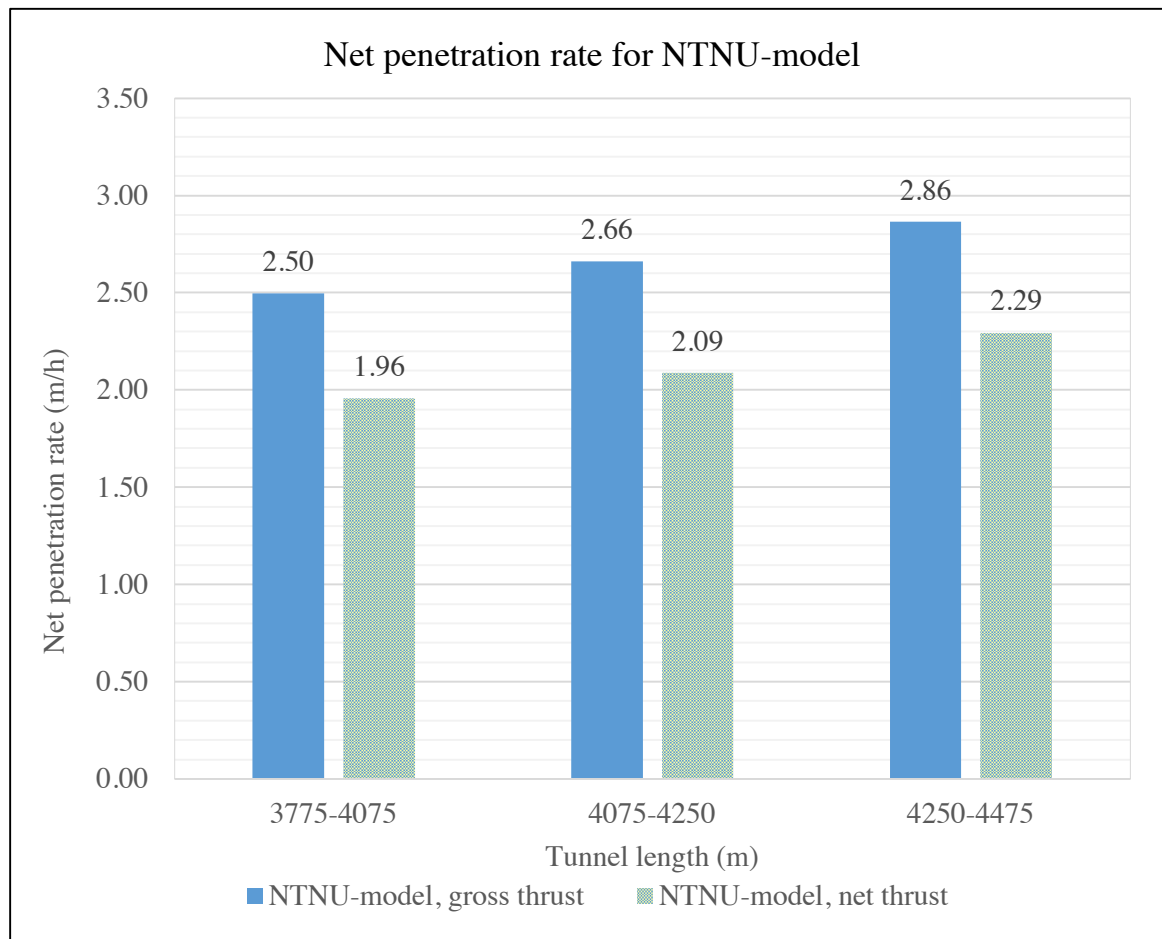


Figure 5.36 Results for NTNU-model calculated with gross and net thrust for section divided after geology and core samples

Results for section divided from k_s -values

Results from model estimations are shown in Table 5.21 and Figure 5.37. The table includes a weighted average for the tunnel segment.

Table 5.21 Results for NTNU-model calculated with gross and net thrust for section divided from k_s -values, including a weighted average

| Thrust | Mapped length(m) | Length (m) | NPR (m/h) | Weighted average (m/h) |
|--------|------------------|------------|-----------|------------------------|
| Gross | 3775-4075 | 300 | 2.50 | 2.66 |
| | 4075-4275 | 200 | 2.64 | |
| | 4275-4475 | 200 | 2.91 | |
| Net | 3775-4075 | 300 | 1.96 | 2.10 |
| | 4075-4275 | 200 | 2.08 | |
| | 4275-4475 | 200 | 2.33 | |

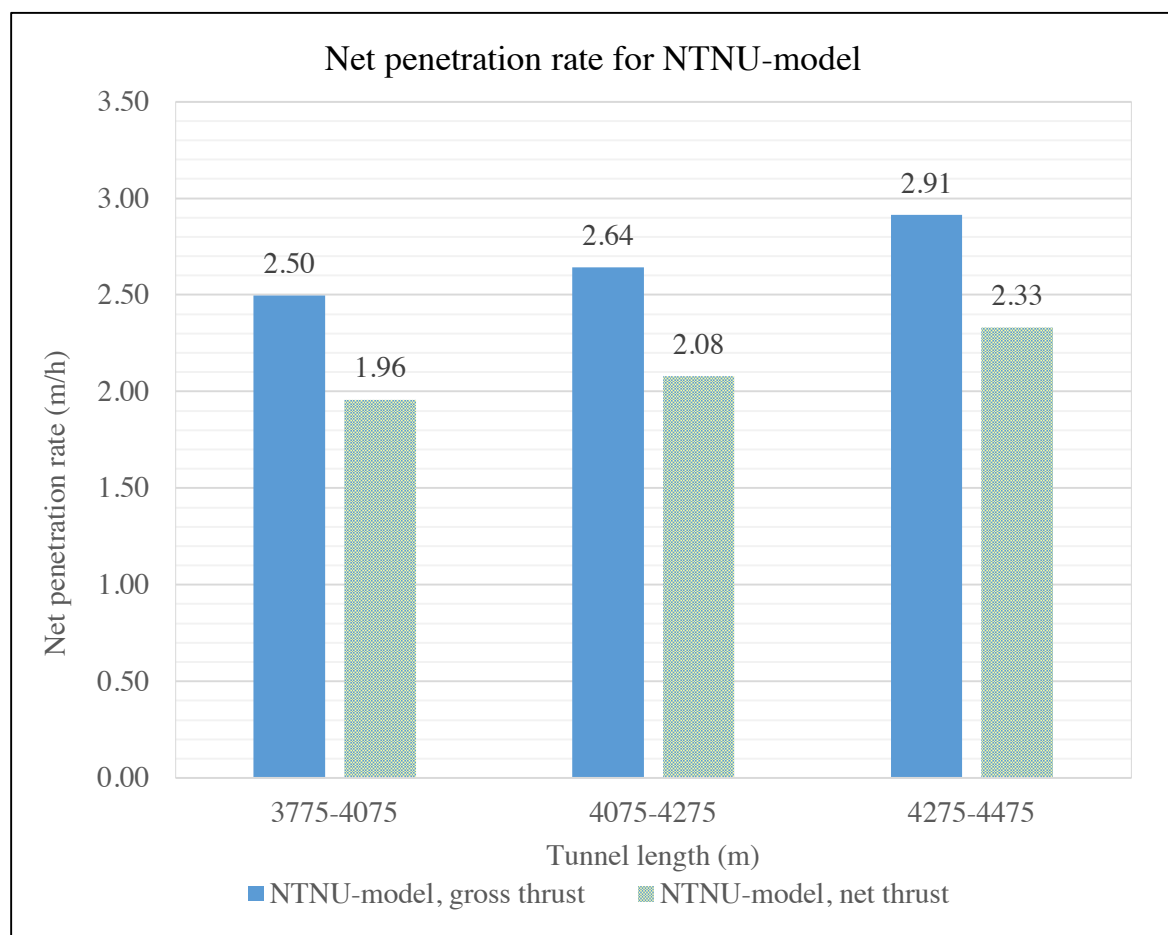


Figure 5.37 Results for NTNU-model calculated with gross and net thrust for section divided from k_s -values

5.8.2 Model presented by Ebrahim Farrokh et al.

The model, presented by Farrokh et al. (2012) in the journal *Tunnelling and Underground Space Technology*. The way this model is set up, just a few parameters are needed to calculate the net penetration rate. The model offers two different equations to calculate the net penetration rate. The results presented are found by using the first equation, which is given as equation (3.14). However, both equations have been calculated and can be viewed in Appendix N . The equation (3.14) was chosen because it has a better coefficient of determination, R^2 , than the second.

The different parameters used in the calculations are discussed below:

- The thrust per cutter, F_n , is the actual cutter thrust used in the tunnel section. Found in chapter 5.2.2
- RQD is found from the Q -values decided by the geologists of Bane NOR and JVSS, found in Table 5.31
- Different rock types are given a code, RTc , that is used in the equation. As most of the rock is classified as gneiss or a type of gneiss, $RTc = 2$ for all the subdivisions
- The RPM is the actual RPM used in the tunnel section. Found in chapter 5.2.2
- The UCS values are found in chapter 5.7.2

Results for complete 700-meter segment

Results for the complete 700-meter segment of the tunnel are 1.56 m/h for filtered gross thrust values, and 1.51 m/h for filtered net thrust values. This is shown in Figure 5.38.

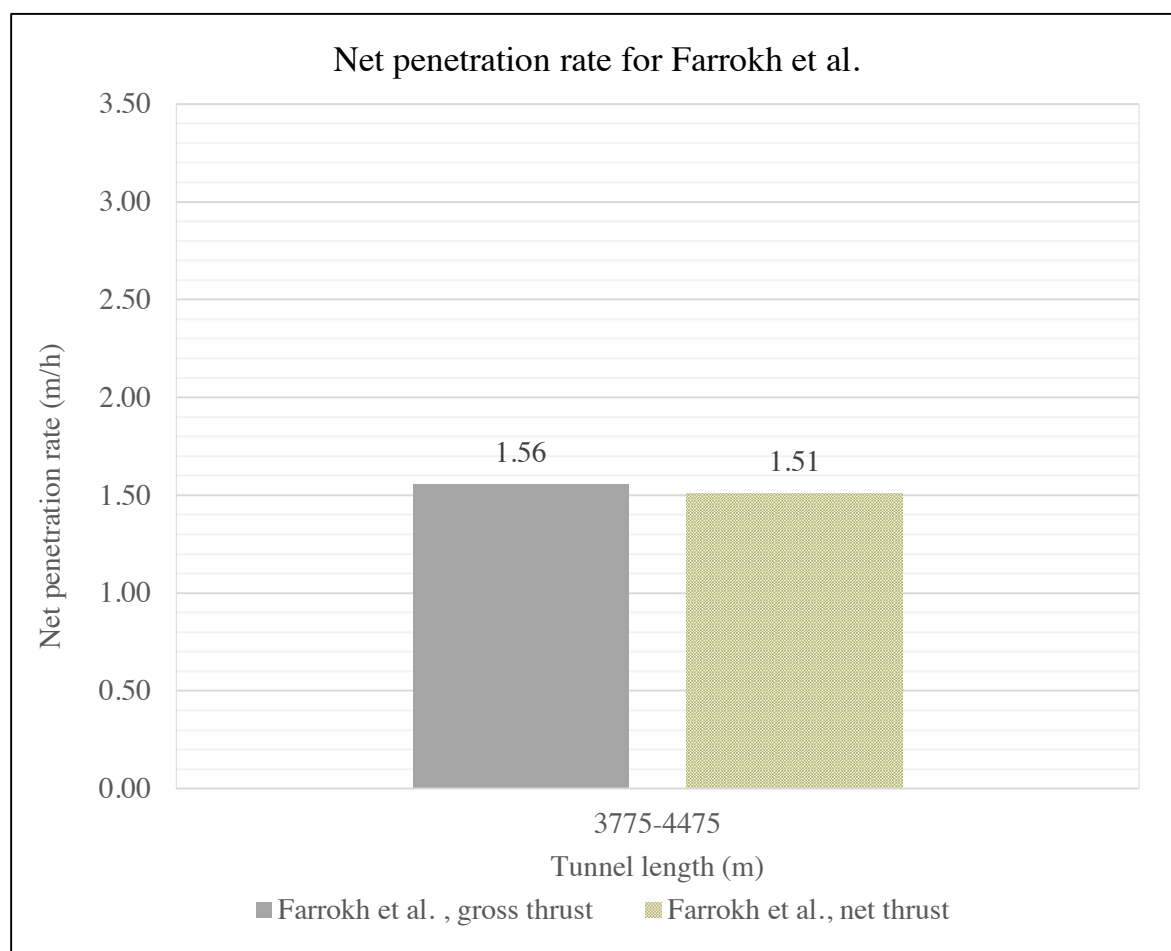


Figure 5.38 Results for Farrokh et al. calculated with gross and net thrust for the complete 700-meter segment

Results for section divided after geology and core samples

Results from model estimations are shown in Table 5.22 and Figure 5.39. The table includes a weighted average for the tunnel segment.

Table 5.22 Results for Farrokh et al. calculated with gross and net thrust for section divided after geology and core samples, including a weighted average

| Thrust | Mapped length (m) | Length (m) | NPR (m/h) | Weighted average (m/h) |
|--------|-------------------|------------|-----------|------------------------|
| Gross | 3775-4075 | 300 | 1.73 | 1.58 |
| | 4075-4250 | 175 | 1.51 | |
| | 4250-4475 | 225 | 1.42 | |
| Net | 3775-4075 | 300 | 1.68 | 1.53 |
| | 4075-4250 | 175 | 1.46 | |
| | 4250-4475 | 225 | 1.38 | |

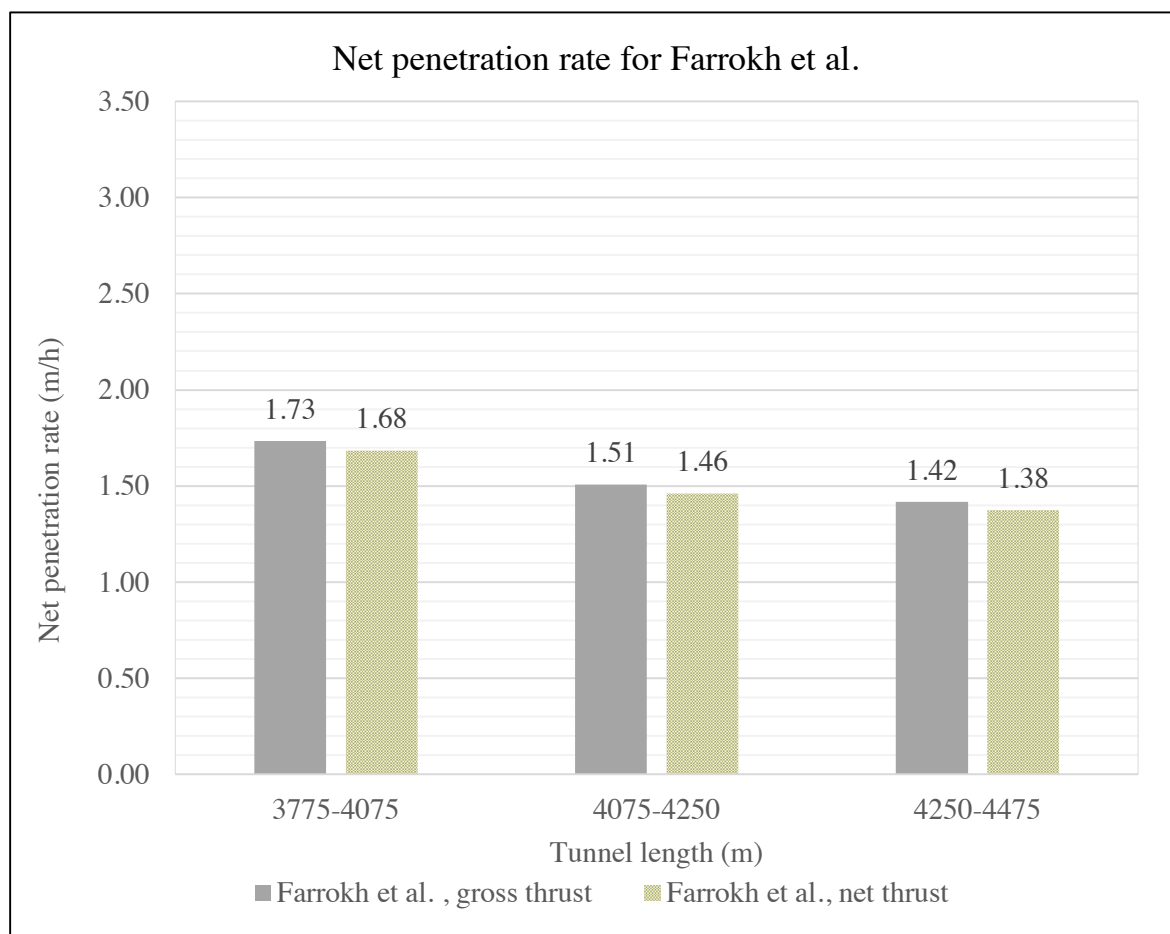


Figure 5.39 Results for Farrokh et al. calculated with gross and net thrust for section divided after geology and core samples

Results for section divided from k_s -values

Results from model estimations are shown in Table 5.23 and Figure 5.40. The table includes a weighted average for the tunnel segment.

Table 5.23 Results for Farrokh et al. calculated with gross and net thrust for section divided from k_s -values, including a weighted average

| Thrust | Mapped length(m) | Length (m) | NPR (m/h) | Weighted average (m/h) |
|--------|------------------|------------|-----------|------------------------|
| Gross | 3775-4075 | 300 | 1.73 | 1.58 |
| | 4075-4275 | 200 | 1.52 | |
| | 4275-4475 | 200 | 1.42 | |
| Net | 3775-4075 | 300 | 1.68 | 1.54 |
| | 4075-4275 | 200 | 1.47 | |
| | 4275-4475 | 200 | 1.38 | |

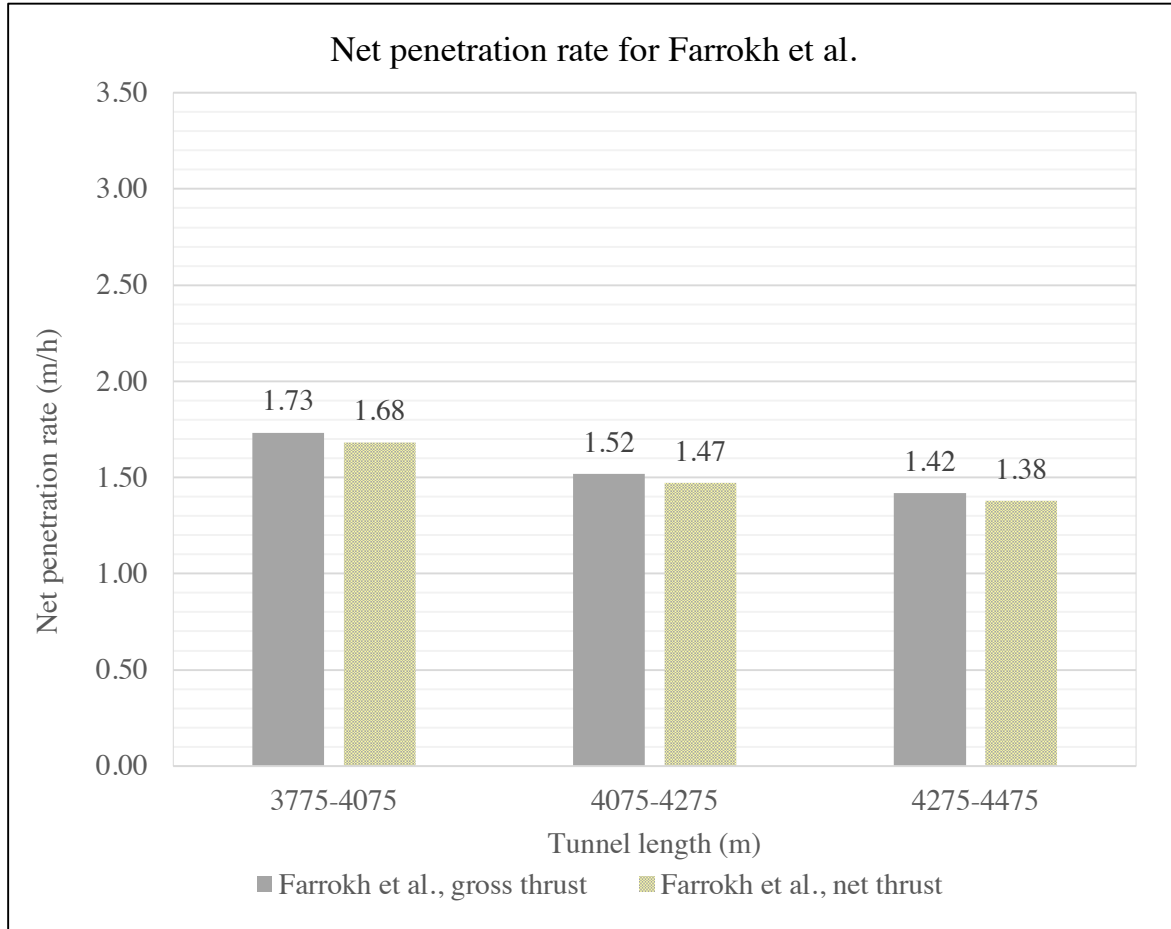


Figure 5.40 Results for Farrokh et al. calculated with gross and net thrust for section divided from k_s -values

5.8.3 Model presented by Hassanpour et al.

The model is presented by Hassanpour et al. (2011) in the journal *Tunnelling and Underground Space Technology*. There are not many parameters needed for the calculating of this model, consisting of only two equations. First, the Field Penetration Index, or *FPI*, is calculated using equation (3.17). Second, the Rate of Penetration, or *ROP*, is found by equation (3.18). All calculations regarding this model can be found in Appendix N. The different parameters used in the model are discussed below:

- To calculate *FPI* two parameters are needed, *UCS* and *RQD*:
 - The *UCS* values are found in chapter 5.7.2
 - *RQD* values are found from the *Q*-values decided by the geologists of Bane NOR and JVSS, found in Table 5.31
- To calculate *ROP*, the parameters F_n , *RPM* and *FPI* are needed:
 - The thrust per cutter, F_n , is the actual cutter thrust used in the tunnel section. See chapter 5.2.2
 - The *RPM* is the actual *RPM* used in the tunnel section. See chapter 5.2.2

Results for complete 700-meter segment

Result using filtered gross thrust values give a net penetration rate of 2.08 m/h. The filtered net thrust values calculate a net penetration rate of 1.85 m/h. This is shown in Figure 5.41.

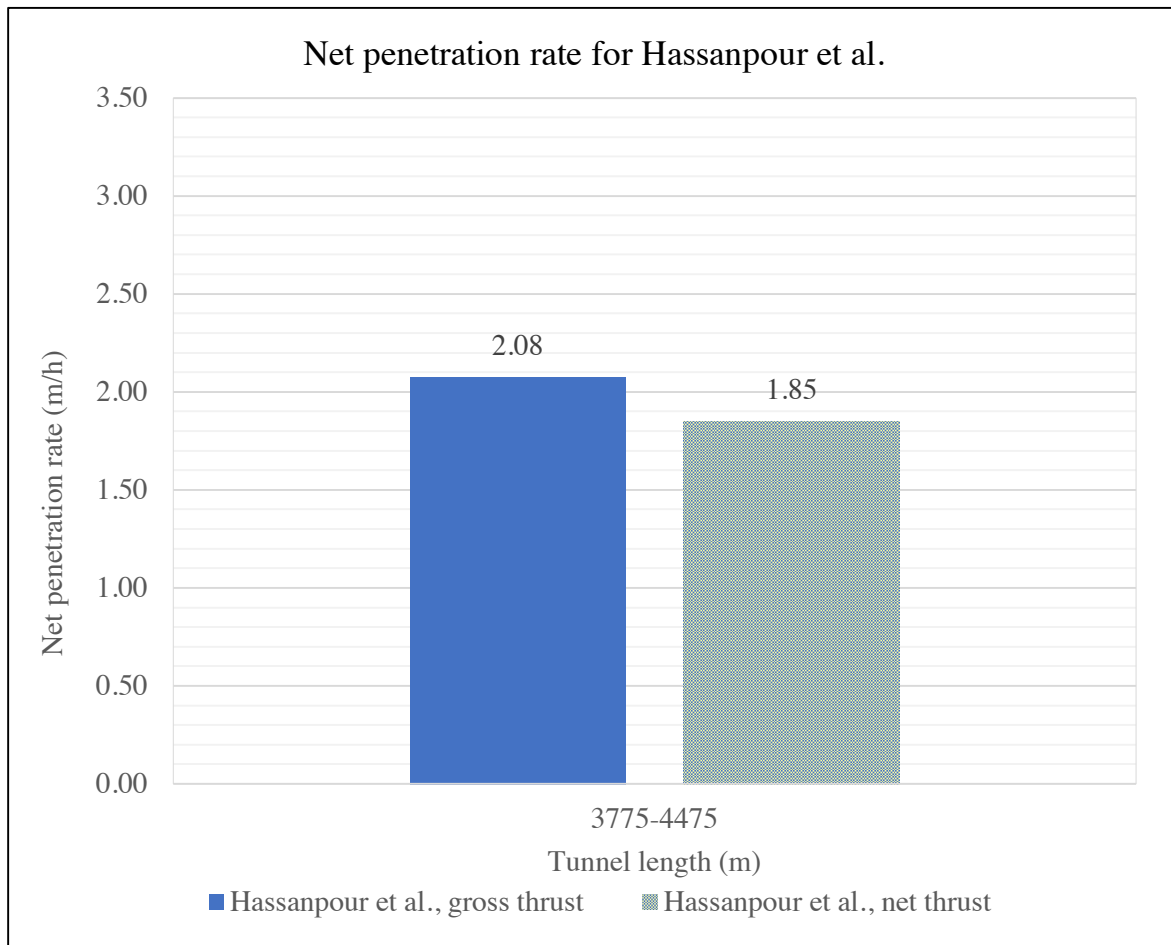


Figure 5.41 Results for Hassanpour et al. calculated with gross and net thrust for the complete 700-meter segment

Results for section divided after geology and core samples

Results from model estimations are shown in Table 5.24 and Figure 5.42. The table includes a weighted average for the tunnel segment.

Table 5.24 Results for Hassanpour et al. calculated with gross and net thrust for section divided after geology and core samples, including a weighted average

| Thrust | Mapped length (m) | Length (m) | NPR (m/h) | Weighted average (m/h) |
|--------|-------------------|------------|-----------|------------------------|
| Gross | 3775-4075 | 300 | 2.50 | 2.13 |
| | 4075-4250 | 175 | 2.06 | |
| | 4250-4475 | 225 | 1.69 | |
| Net | 3775-4075 | 300 | 2.25 | 1.90 |
| | 4075-4250 | 175 | 1.82 | |
| | 4250-4475 | 225 | 1.51 | |

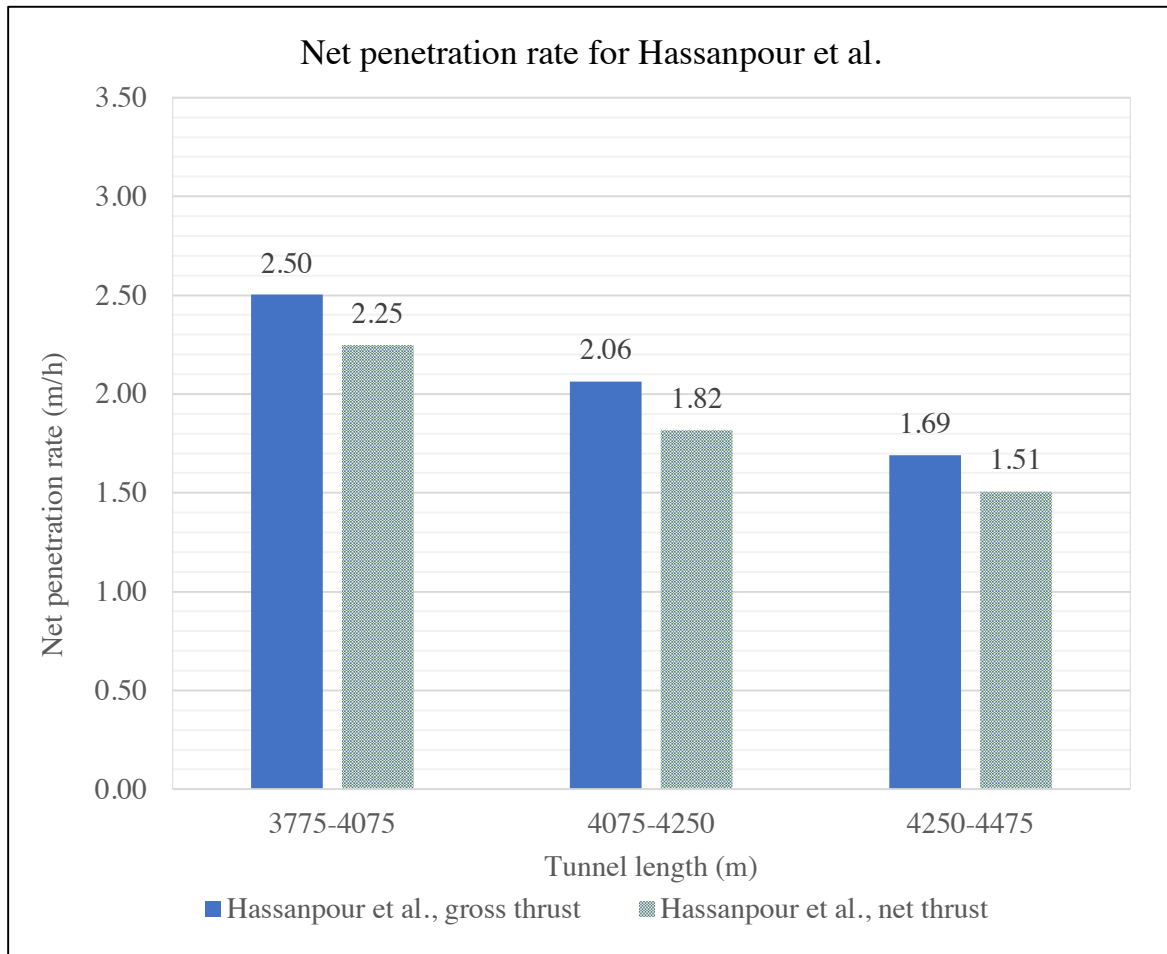


Figure 5.42 Results for Hassanpour et al. calculated with gross and net thrust for section divided after geology and core samples

Results for section divided from k_s -values

Results from model estimations are shown in Table 5.25 and Figure 5.43. The table includes a weighted average for the tunnel segment.

Table 5.25 Results for Hassanpour et al. calculated with gross and net thrust for section divided from k_s -values, including a weighted average

| Thrust | Mapped length(m) | Length (m) | NPR (m/h) | Weighted average (m/h) |
|--------|------------------|------------|-----------|------------------------|
| Gross | 3775-4075 | 300 | 2.50 | 2.15 |
| | 4075-4275 | 200 | 2.07 | |
| | 4275-4475 | 200 | 1.69 | |
| Net | 3775-4075 | 300 | 2.25 | 1.91 |
| | 4075-4275 | 200 | 1.82 | |
| | 4275-4475 | 200 | 1.51 | |

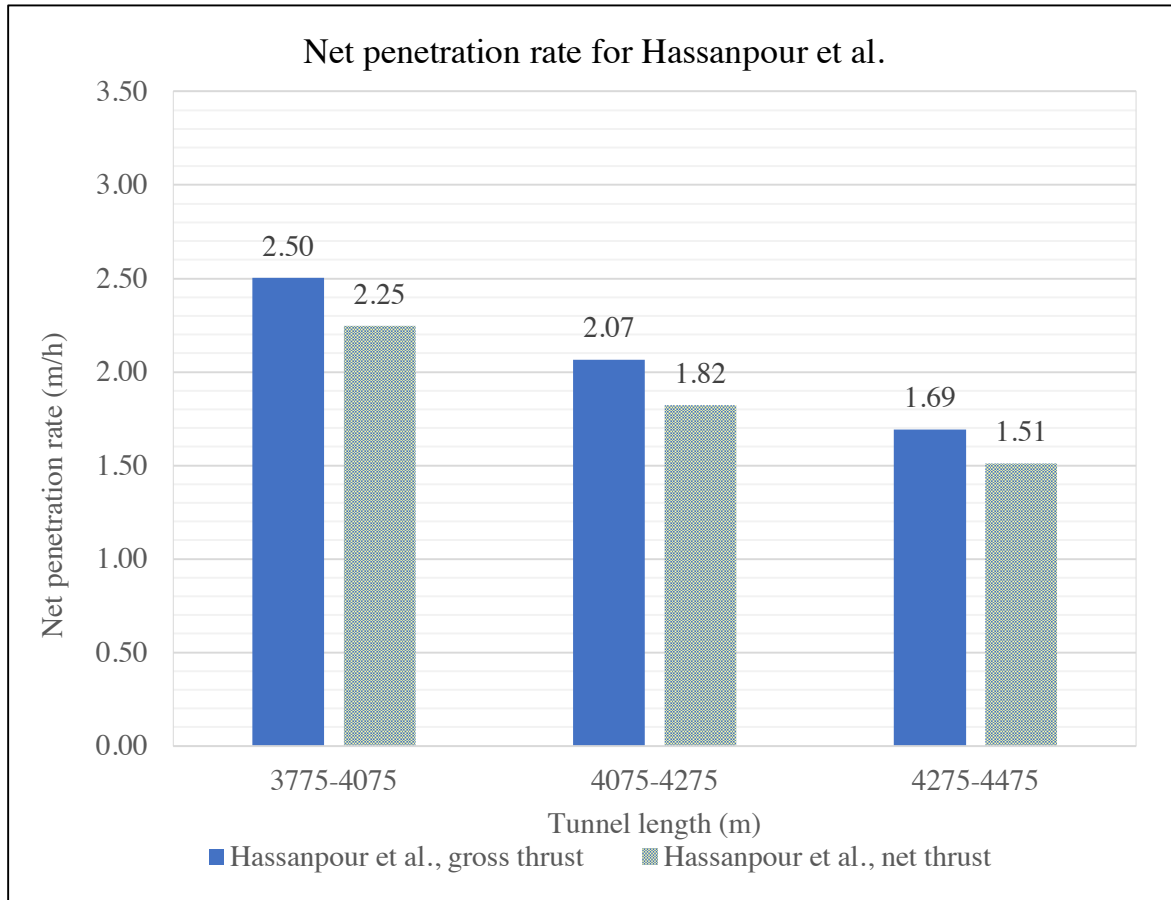


Figure 5.43 Results for Hassanpour et al. calculated with gross and net thrust for section divided from k_s -values

5.8.4 Gehring model

The penetration rate in the Gehring model can be found through equation (3.19). The main parameters in the model are the normal force per cutter (F_n) and the Uniaxial Compressive Strength (σ_u). These values are found in chapter 5.2.2 and 5.7.2. The model also includes several correction factors to take care of issues affecting TBM performance. These factors are discussed below:

- The basic correction factor k_0 in the model is set at 4.0
- The factor for specific failure energy is given by the failure energy of a material. This information was not possible to obtain. Thus, the correction factor k_l was set to 1.0 to not influence the result
- The factor for rock mass fabric was chosen from the major plane of weakness and the spacing of the discontinuity. The orientation and spacing for each subdivision can be found in Table 5.26 and the correction factor is chosen from Table 3.8
- The factor for cutter diameters $\neq 432$ mm is calculated according to equation (3.23), with the cutter diameter used at this project; 483 mm
- The factor for cutter spacing $\neq 80$ mm is found in Figure 3.8. The cutter spacing is given by the number of cutters on the cutterhead

Table 5.26 Average angle and spacing in different sections for the major plane of weakness

| Complete 700-meter segment | | |
|--|-------------------------|-----------------------|
| Subdivisions, TM | Average angle, α | Average spacing, (cm) |
| 3775-4475 | 52.81 | 67.93 |
| Divided after geology and core samples | | |
| Subdivisions, TM | Average angle, α | Average spacing, (cm) |
| 3775-4075 | 55.59 | 84.36 |
| 4075-4250 | 47.63 | 55.64 |
| 4250-4475 | 53.12 | 55.59 |
| Divided from k_s -values | | |
| Subdivisions, TM | Average angle, α | Average spacing, (cm) |
| 3775-4075 | 55.59 | 84.36 |
| 4075-4275 | 48.99 | 52.89 |
| 4275-4475 | 52.45 | 58.34 |

Results for complete 700-meter segment

Result using filtered gross thrust values give a net penetration rate of 2.06 m/h. The filtered net thrust values calculate a net penetration rate of 1.84 m/h. This is shown in Figure 5.44.

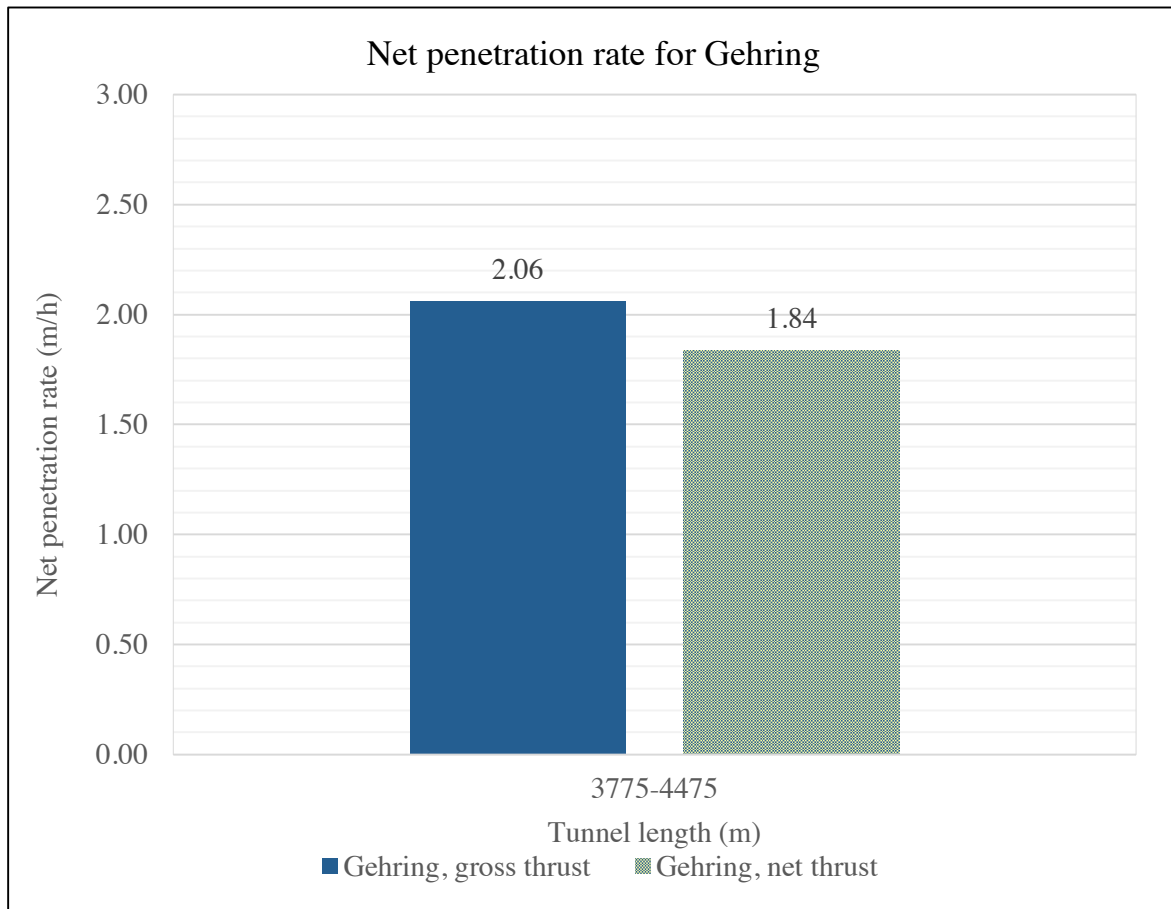


Figure 5.44 Results for Gehring model calculated with gross and net thrust for the complete 700-meter segment

Results for section divided after geology and core samples

Results from model estimations are shown in Table 5.27 and Figure 5.45. The table includes a weighted average for the tunnel segment.

Table 5.27 Results for Gehring model calculated with gross and net thrust for section divided after geology and core samples, including a weighted average

| Thrust | Mapped length (m) | Length (m) | NPR (m/h) | Weighted average (m/h) |
|--------|-------------------|------------|-----------|------------------------|
| Gross | 3775-4075 | 300 | 2.42 | 2.11 |
| | 4075-4250 | 175 | 1.94 | |
| | 4250-4475 | 225 | 1.83 | |
| Net | 3775-4075 | 300 | 2.18 | 1.88 |
| | 4075-4250 | 175 | 1.71 | |
| | 4250-4475 | 225 | 1.63 | |

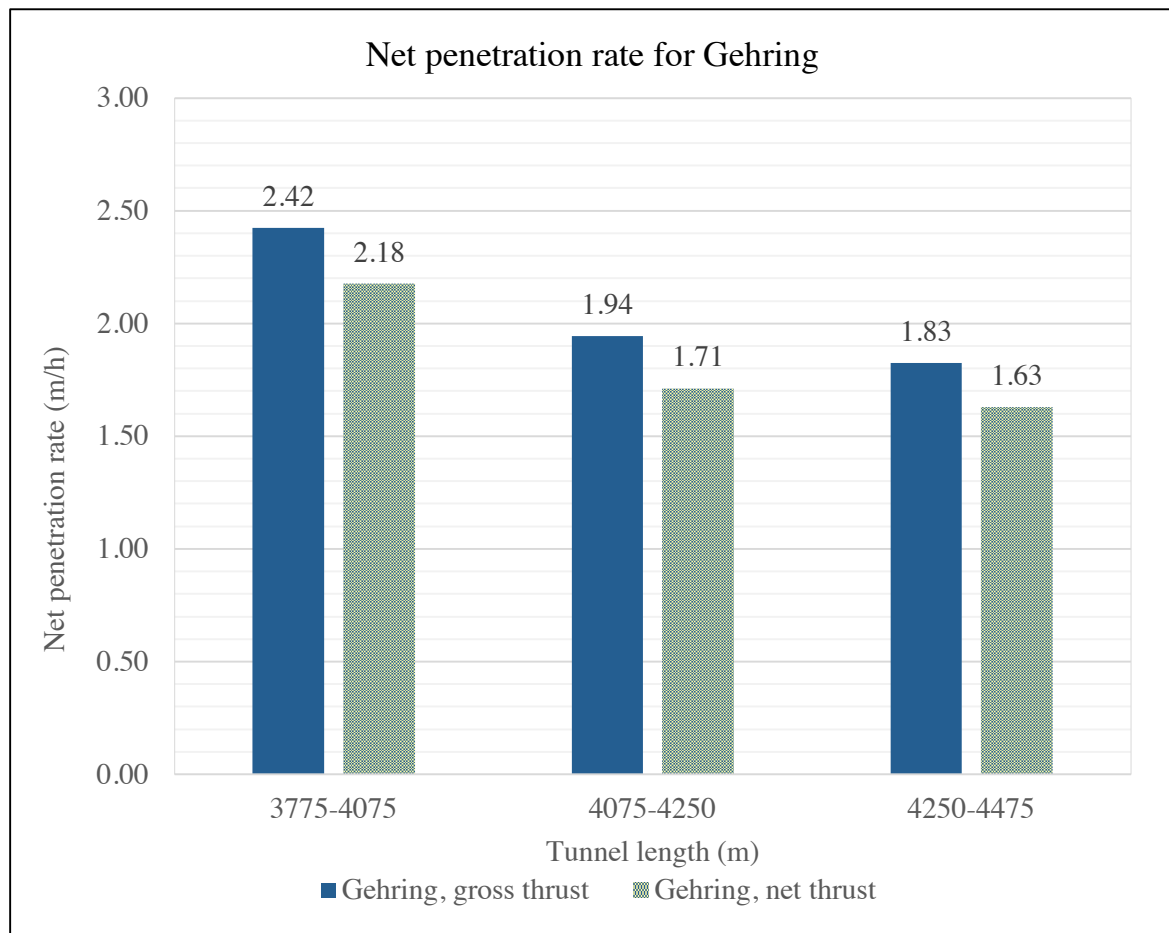


Figure 5.45 Results for Gehring model calculated with gross and net thrust for section divided after geology and core samples

Results for section divided from k_s -values

Results from model estimations are shown in Table 5.28 and Figure 5.46. The table includes a weighted average for the tunnel segment.

Table 5.28 Results for Gehring model calculated with gross and net thrust for section divided from k_s -values, including a weighted average

| Thrust | Mapped length(m) | Length (m) | NPR (m/h) | Weighted average (m/h) |
|--------|------------------|------------|-----------|------------------------|
| Gross | 3775-4075 | 300 | 2.42 | 2.12 |
| | 4075-4275 | 200 | 1.95 | |
| | 4275-4475 | 200 | 1.85 | |
| Net | 3775-4075 | 300 | 2.18 | 1.89 |
| | 4075-4275 | 200 | 1.72 | |
| | 4275-4475 | 200 | 1.65 | |

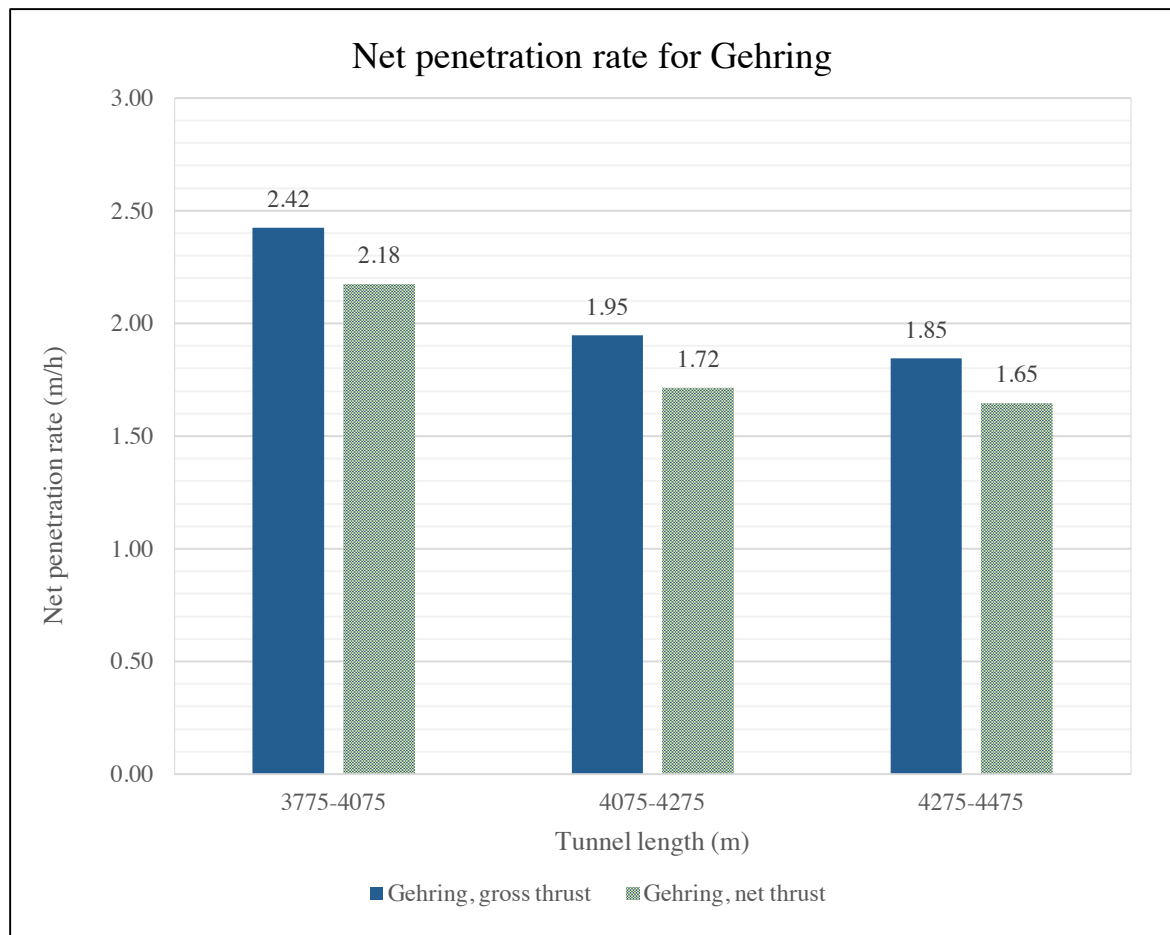


Figure 5.46 Results for Gehring model calculated with gross and net thrust for section divided from k_s -values

5.8.5 Alpine model

The Alpine model is a modification of the Gehring model and calculates the penetration rate from equation (3.26). The main parameters are, like in the Gehring model, the normal force per cutter (F_n) and the Uniaxial Compressive Strength (σ_u). In addition, a y-intercept of *BTS* or *LBC* is added to the main parameters. The y-intercept of *BTS* is used in this thesis. Values for F_n , *UCS* and *BTS* are found in chapter 5.2.2 and 5.7.2. The model also uses several correction factors to take care of issues affecting TBM performance. These factors are discussed below:

- The basic correction factor k_0 is in the model set at 4.0
- The correction factor for discontinuity pattern is here given by the k_{s-tot} from the NTNU-model. These values are found in chapter 5.1.2
- The factor for cutter diameters $\neq 432$ mm is calculated according to (3.23) with the cutter diameter for this project, 483 mm
- The factor for cutter spacing $\neq 80$ mm is picked from Figure 3.8. The cutter spacing is given by the number of cutters on the cutterhead

Results for complete 700-meter segment

Result using filtered gross thrust values give a net penetration rate of 2.21 m/h. The filtered net thrust values calculate a net penetration rate of 1.99 m/h. This is shown in Figure 5.47.

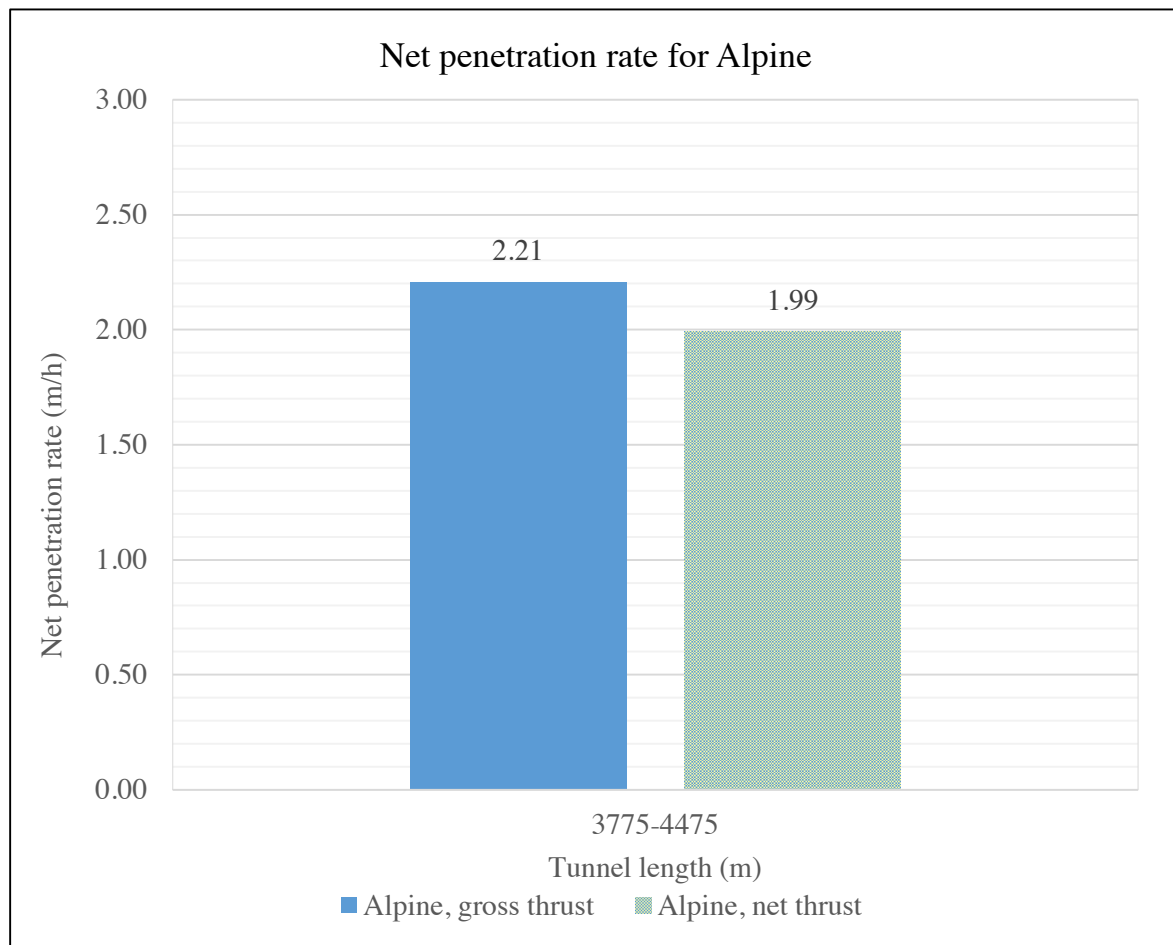


Figure 5.47 Results for Alpine calculated with gross and net thrust for the complete 700-meter segment

Results for section divided after geology and core samples

Results from model estimations are shown in Table 5.29 and Figure 5.48. The table includes a weighted average for the tunnel segment.

Table 5.29 Results for Alpine model calculated with gross and net thrust for section divided after geology and core samples, including a weighted average

| Thrust | Mapped length (m) | Length (m) | NPR (m/h) | Weighted average (m/h) |
|--------|-------------------|------------|-----------|------------------------|
| Gross | 3775-4075 | 300 | 2.20 | 2.26 |
| | 4075-4250 | 175 | 2.37 | |
| | 4250-4475 | 225 | 2.24 | |
| Net | 3775-4075 | 300 | 2.01 | 2.03 |
| | 4075-4250 | 175 | 2.09 | |
| | 4250-4475 | 225 | 2.01 | |

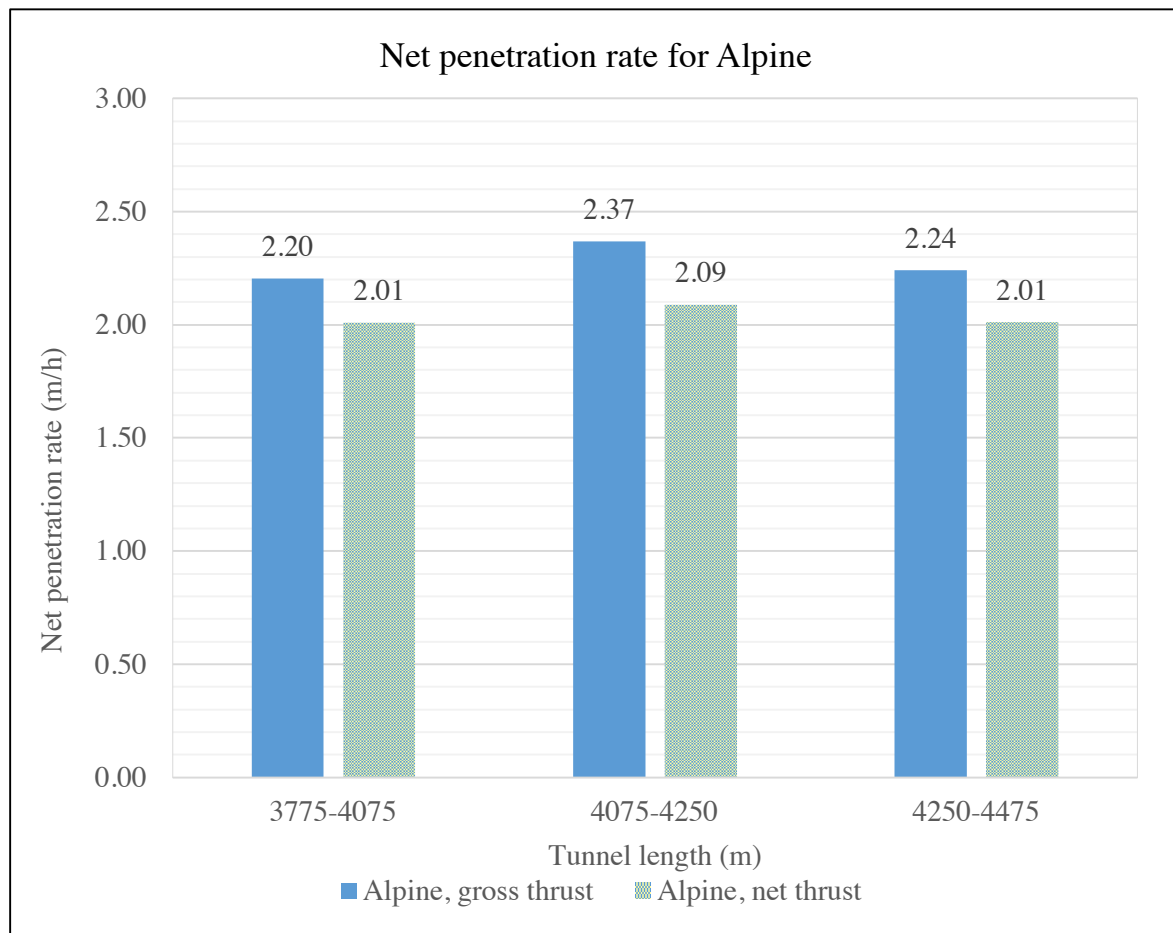


Figure 5.48 Results for Alpine model calculated with gross and net thrust for section divided after geology and core samples

Results for section divided from k_s -values

Results from model estimations are shown in Table 5.30 and Figure 5.49. The table includes a weighted average for the tunnel segment.

Table 5.30 Results for Alpine model calculated with gross and net thrust for section divided from k_s -values, including a weighted average

| Thrust | Mapped length(m) | Length (m) | NPR (m/h) | Weighted average (m/h) |
|--------|------------------|------------|-----------|------------------------|
| Gross | 3775-4075 | 300 | 2.20 | 2.27 |
| | 4075-4275 | 200 | 2.39 | |
| | 4275-4475 | 200 | 2.24 | |
| Net | 3775-4075 | 300 | 2.01 | 2.04 |
| | 4075-4275 | 200 | 2.11 | |
| | 4275-4475 | 200 | 2.01 | |

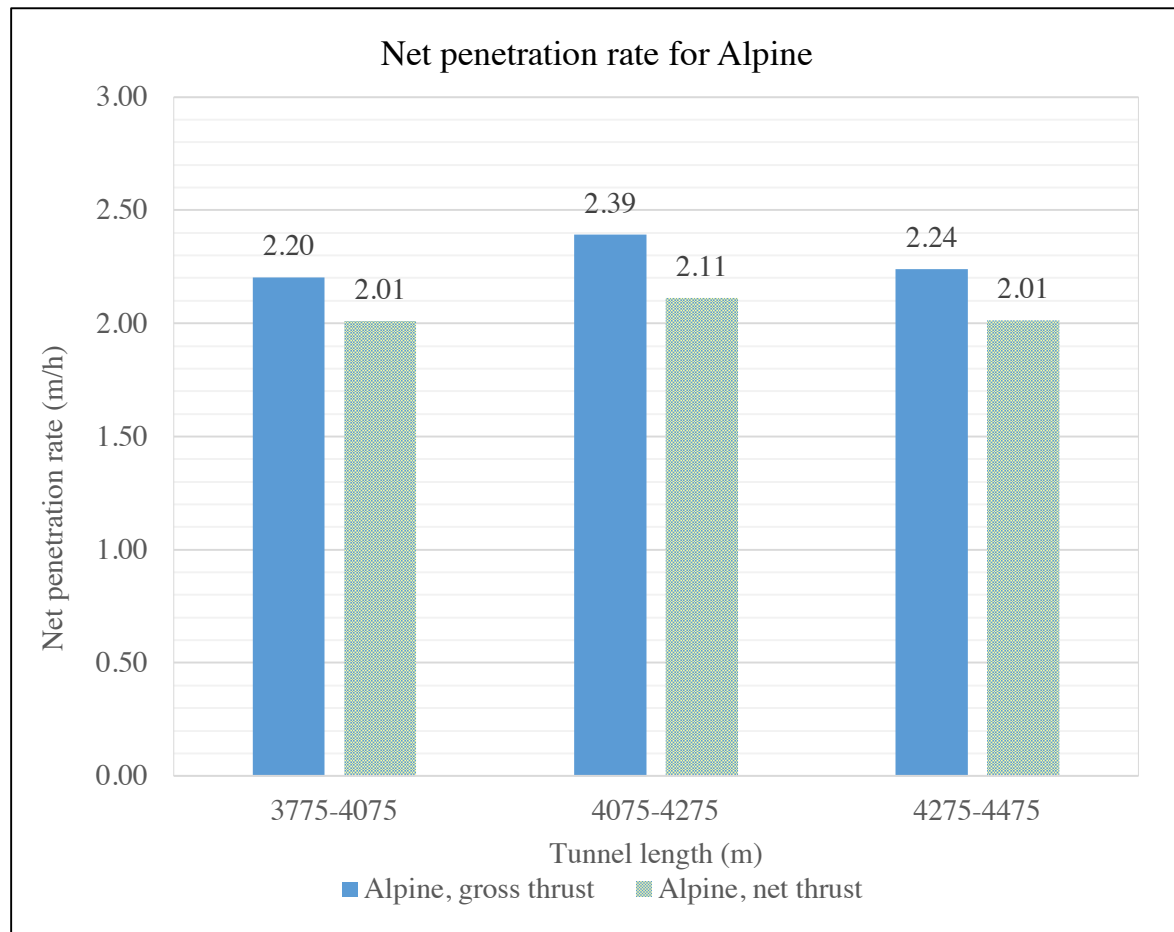


Figure 5.49 Results for Alpine model calculated with gross and net thrust for section divided from k_s -values

5.8.6 Q_{TBM} -model

The penetration rate in the Q_{TBM} -model can be found from equation (3.32). To find the Q_{TBM} value, which is the only factor for net penetration rate, several basic parameters must be known. These are used in numerous calculations to attain the net penetration rate.

The first step is to calculate the Q -value. The different values used in the calculation to find the Q -value are presented in Table 5.31.

Table 5.31 Input parameters to calculate the Q -value

| Complete 700-meter segment | | | | | | |
|--|-------|-------|-------|-------|-------|-------|
| Subdivisions, TM | RQD | J_n | J_r | J_a | J_w | SRF |
| 3775-4475 | 67.79 | 5,8 | 1.19 | 1.95 | 1.00 | 1.02 |
| Divided after geology and core samples | | | | | | |
| Subdivisions, TM | RQD | J_n | J_r | J_a | J_w | SRF |
| 3775-4075 | 68.87 | 4.35 | 1.17 | 1.69 | 1.00 | 1.03 |
| 4075-4250 | 65.07 | 7.37 | 1.28 | 2.04 | 1.00 | 1.01 |
| 4250-4475 | 68.97 | 6.60 | 1.14 | 2.25 | 1.00 | 1.03 |
| Divided from k_s -values | | | | | | |
| Subdivisions, TM | RQD | J_n | J_r | J_a | J_w | SRF |
| 3775-4075 | 68.87 | 4.35 | 1.17 | 1.69 | 1.00 | 1.03 |
| 4075-4275 | 65.06 | 7.28 | 1.28 | 2.08 | 1.00 | 1.01 |
| 4275-4475 | 69.56 | 6.58 | 1.12 | 2.23 | 1.00 | 1.04 |

The next step is to calculate a Q_o -value that is oriented in the tunnel direction. The RQD value is modified to RQD_o . The Q_o -value is the same as the Q -value in this case. The Q -values are decided by the geologists of Bane NOR and JVSS for rock support. This means that the values are oriented in the tunnel direction.

With calculated Q_o -values the rock mass strength named $SIGMA$ can be found. $SIGMA$ is calculated from equation (3.29) or (3.30). The Uniaxial Compressive Strength is used to calculate $SIGMA$. The rock mass properties used in the calculations can be found in Table 5.32.

Table 5.32 Rock mass properties

| Complete 700-meter segment | | |
|--|-------------------------------|------------------|
| Subdivisions, TM | γ (g/cm ³) | σ_c (MPa) |
| 3775-4475 | 2.69 | 174.63 |
| Divided after geology and core samples | | |
| Subdivisions, TM | γ (g/cm ³) | σ_c (MPa) |
| 3775-4075 | 2.64 | 153.80 |
| 4075-4250 | 2.77 | 169.90 |
| 4250-4475 | 2.65 | 200.20 |
| Divided from k_s -values | | |
| Subdivisions, TM | γ (g/cm ³) | σ_c (MPa) |
| 3775-4075 | 2.64 | 153.80 |
| 4075-4275 | 2.77 | 169.90 |
| 4275-4475 | 2.65 | 200.20 |

With those calculations done the Q_{TBM} value can be calculated from equation (3.31). The different parameters listed in Table 5.33 are found from the TBM performance data, laboratory results, and from the calculations.

Table 5.33 Input parameters for calculation of Q_{TBM}

| Complete 700-meter segment | | | | | | | |
|--|-------|----------------|------------------|----------------|------|---------|-----------------------|
| Subdivisions TM | Q_0 | SIGMA (MPa) | F -gross (tnf) | F -net (tnf) | CLI | Q (%) | σ_θ (MPa) |
| 3775-4475 | 7.00 | 30.94 | 32.55 | 28.99 | 6.13 | 17.33 | 88 |
| Divided after geology and core samples | | | | | | | |
| Subdivisions TM | Q_0 | SIGMA (MPa) | F -gross (tnf) | F -net (tnf) | CLI | Q (%) | σ_θ (MPa) |
| 3775-4075 | 10.57 | 33.44 | 33.39 | 29.95 | 5.9 | 19 | 76.9 |
| 4075-4250 | 5.47 | 29.11 | 31.09 | 27.33 | 8.1 | 5 | 84.95 |
| 4250-4475 | 5.14 | 28.83 | 32.56 | 29.00 | 4.4 | 28 | 100.1 |
| Divided from k_s -values | | | | | | | |
| Subdivisions TM | Q_0 | SIGMA (MPa) | F -gross (tnf) | F -net (tnf) | CLI | Q (%) | σ_θ (MPa) |
| 3775-4075 | 10.57 | 33.44 | 33.39 | 29.95 | 5.9 | 19 | 76.9 |
| 4075-4275 | 5.44 | 29.06 | 30.87 | 27.16 | 8.1 | 5 | 84.95 |
| 4275-4475 | 5.11 | 28.76 | 32.96 | 29.37 | 4.4 | 28 | 100.1 |

Results for complete 700-meter segment

Result using filtered gross thrust values give a net penetration rate of 3.76 m/h. The filtered net thrust values calculate a net penetration rate of 2.99 m/h. This is shown in Figure 5.50.

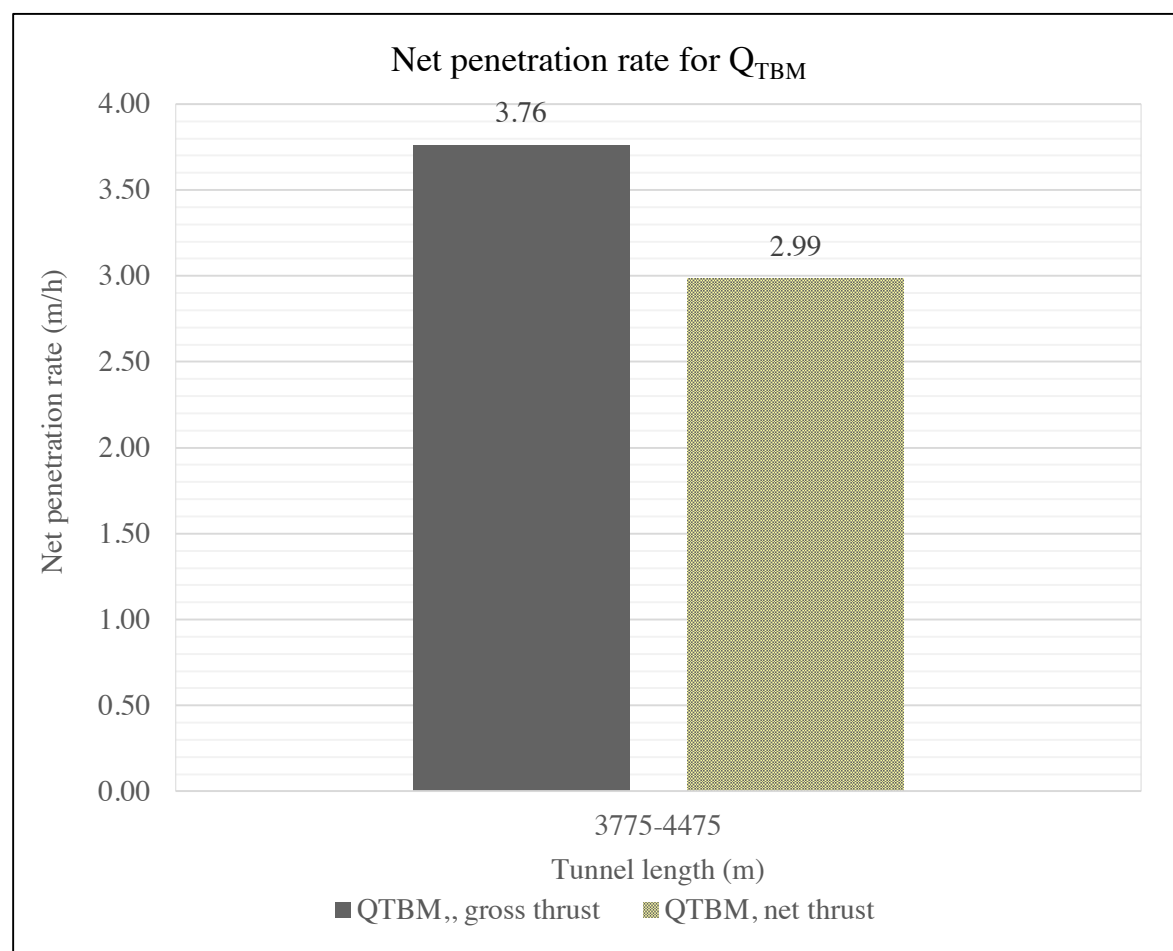


Figure 5.50 Results for Q_{TBM} calculated with gross and net thrust for the complete 700-meter segment

Results for section divided after geology and core samples

Results from model estimations are shown in Table 5.34 and Figure 5.51. The table includes a weighted average for the tunnel segment.

Table 5.34 Results for Q_{TBM} model calculated with gross and net thrust for section divided after geology and core samples, including a weighted average

| Thrust | Mapped length (m) | Length (m) | NPR (m/h) | Weighted average (m/h) |
|--------|-------------------|------------|-----------|------------------------|
| Gross | 3775-4075 | 300 | 3.59 | 3.87 |
| | 4075-4250 | 175 | 4.99 | |
| | 4250-4475 | 225 | 3.37 | |
| Net | 3775-4075 | 300 | 2.89 | 3.06 |
| | 4075-4250 | 175 | 3.85 | |
| | 4250-4475 | 225 | 2.67 | |

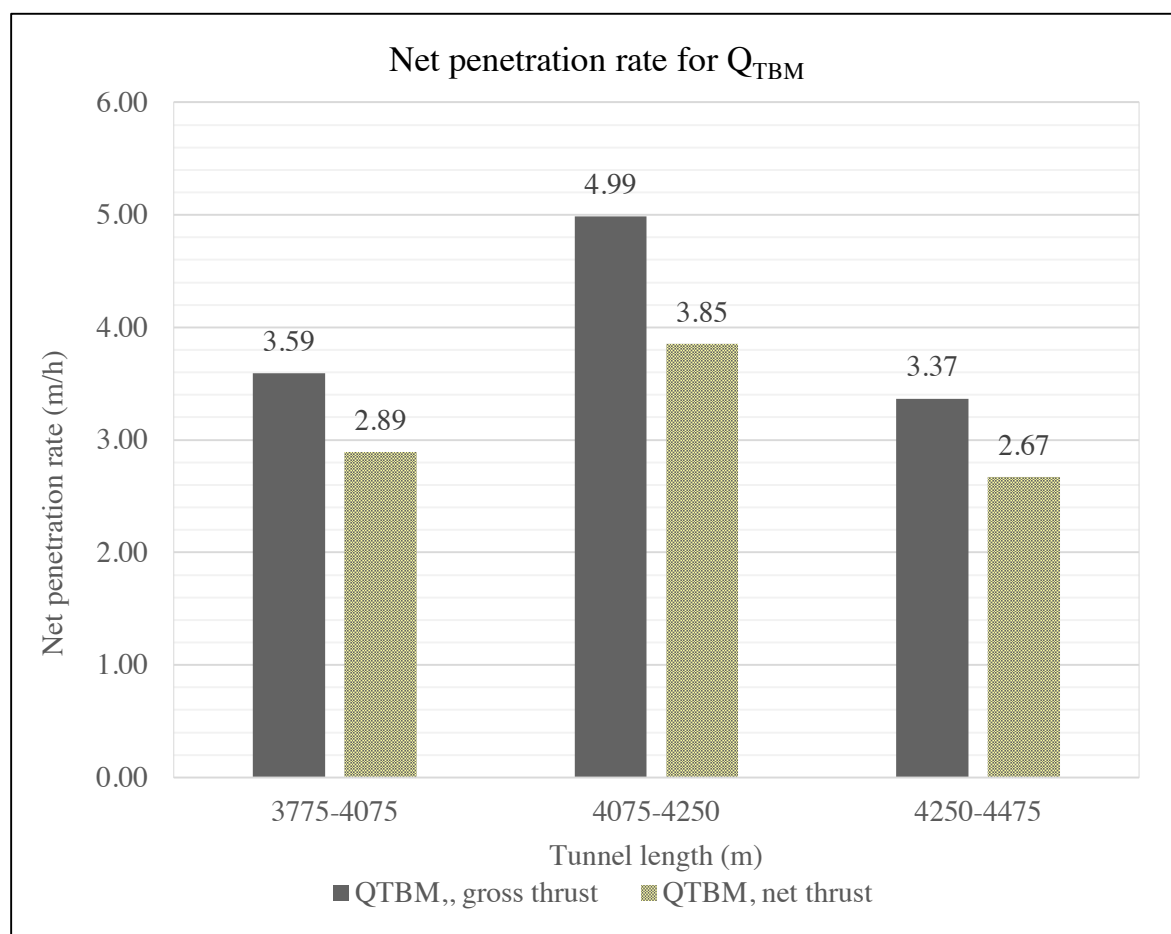


Figure 5.51 Results for Q_{TBM} model calculated with gross and net thrust for section divided after geology and core samples

Results for section divided from k_s -values

Results from model estimations are shown in Table 5.35 and Figure 5.52. The table includes a weighted average for the tunnel segment.

Table 5.35 Results for Q_{TBM} -model calculated with gross and net thrust for section divided from k_s -values, including a weighted average

| Thrust | Mapped length(m) | Length (m) | NPR (m/h) | Weighted average (m/h) |
|--------|------------------|------------|-----------|------------------------|
| Gross | 3775-4075 | 300 | 3.59 | 3.93 |
| | 4075-4275 | 200 | 4.92 | |
| | 4275-4475 | 200 | 3.46 | |
| Net | 3775-4075 | 300 | 2.89 | 3.11 |
| | 4075-4275 | 200 | 3.81 | |
| | 4275-4475 | 200 | 2.74 | |

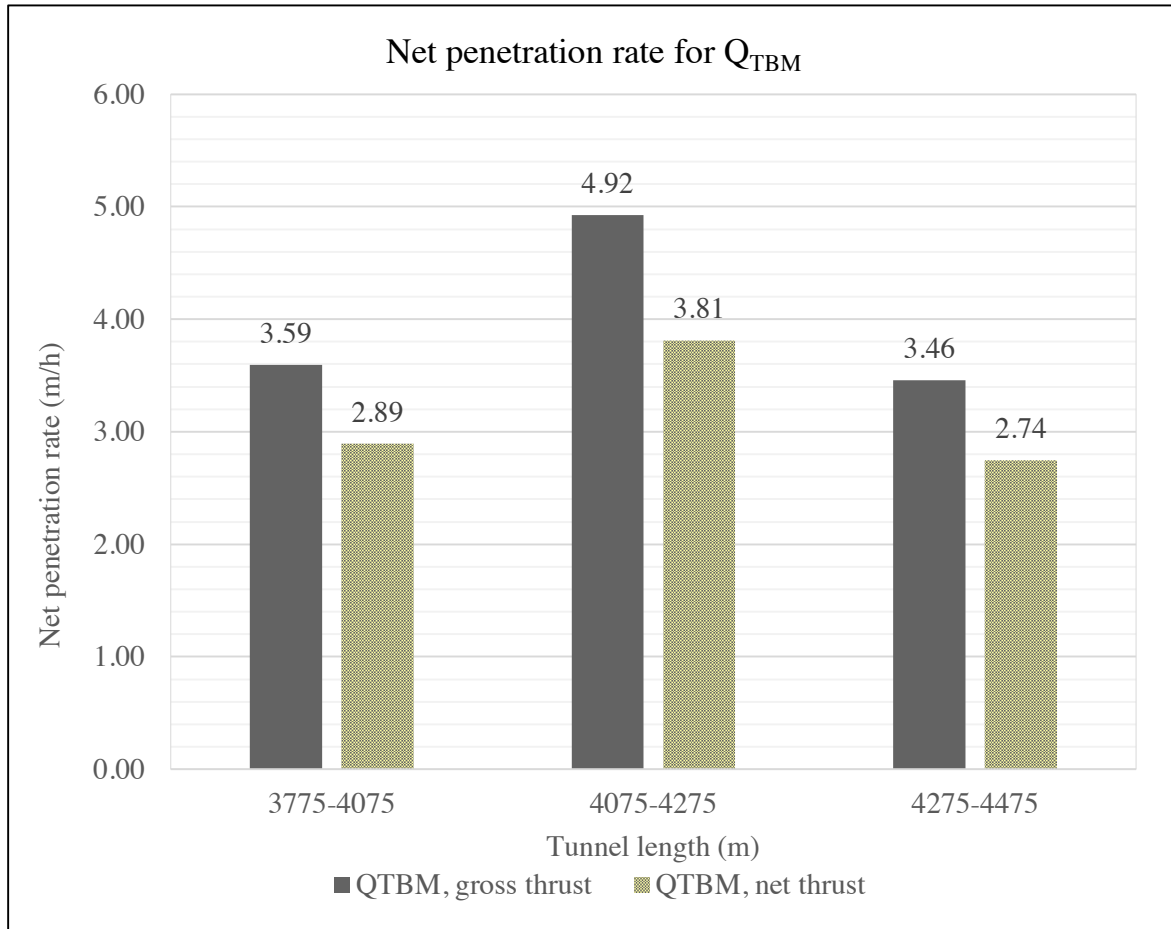


Figure 5.52 Results for Q_{TBM} model calculated with gross and net thrust for section divided from k_s -values

5.8.7 CSM- and MCSM-model

In the Modified Colorado School of Mines (MCSM)-model, the rate of penetration is found by equation (3.43), after going through multiple calculations. The first step is to calculate the rate of penetration from the basic CSM-model. This incorporates several equations to find the maximum rate of penetration. The obtained CSM-model result is further used in the calculations of the MCSM-model. The list below gives a light description of the used parameters, given by Yagiz et al. (2012):

| | | |
|--------|----------------------------|--|
| Φ | - angle of contact | Found by equation based on cutter radius and penetration rate. |
| P^0 | - pressure of contact area | Found by equation incorporating the spacing of cutters, UCS , BTS , and cutter tip width. UCS and BTS values are given in chapter 5.7.2. |
| F_t | - total force per cutter | Found by equation based on pressure of contact area, angle of contact, cutter radius, and cutter tip width. |

| | | | |
|----------|---|---|---|
| F_n | - | normal force per cutter | Found by equation from total force per cutter and angle of contact. |
| F_r | - | rolling force per cutter | Found by equation from total force per cutter and angle of contact. |
| Th^* | - | total thrust requirement | Found by equation based on the number of cutters on the cutterhead and normal force per cutter. An efficiency factor of 0.9 is used for the installed thrust. |
| Tq^* | - | torque | Found by equation from TBM diameter, number of cutters and the rolling force per cutter. |
| RPM | - | rotational speed | The actual RPM used in the tunnel section. Found in chapter 5.2.2. |
| P^* | - | power requirement | Found by equation incorporating torque and rotational speed. An efficiency factor of 0.9 is used for the installed power. |
| BI_p | - | predicted brittleness | Found by equation based on UCS , BTS , and density. Values for each parameter are presented in chapter 5.7. |
| F_s | - | distance between planes of weakness | Found from the mapping done in this thesis. Values are given in chapter 5.1.2. |
| α | - | angle between planes of weakness and the tunnel direction | Found from the mapping done in this thesis. Values are given in chapter 5.1.2. |

What sets the basic CSM-model apart from the other models, is that it uses individual TBM limits for thrust, torque, power, and cutter force to calculate the maximum penetration rate. To find the PR, it is a matter of trial and error. A number of values for the penetration rate have to be attempted as an input, before finding the maximum. The same parameters as for the machine limits are calculated based on the formulas presented in the model; total force per cutter, installed thrust, torque and installed power. When one of the four values reaches the machine limit value, the associated penetration value is the machines maximum penetration ability.

Results from the MCSM-model will be presented in this chapter, as this model incorporates several geological properties compared to the basic model.

Results for complete 700-meter segment

As the MCSM model does not account for the applied thrust, the values for gross and net thrust are the same for this model. The result is 2.25 m/h and is shown in Figure 5.53.

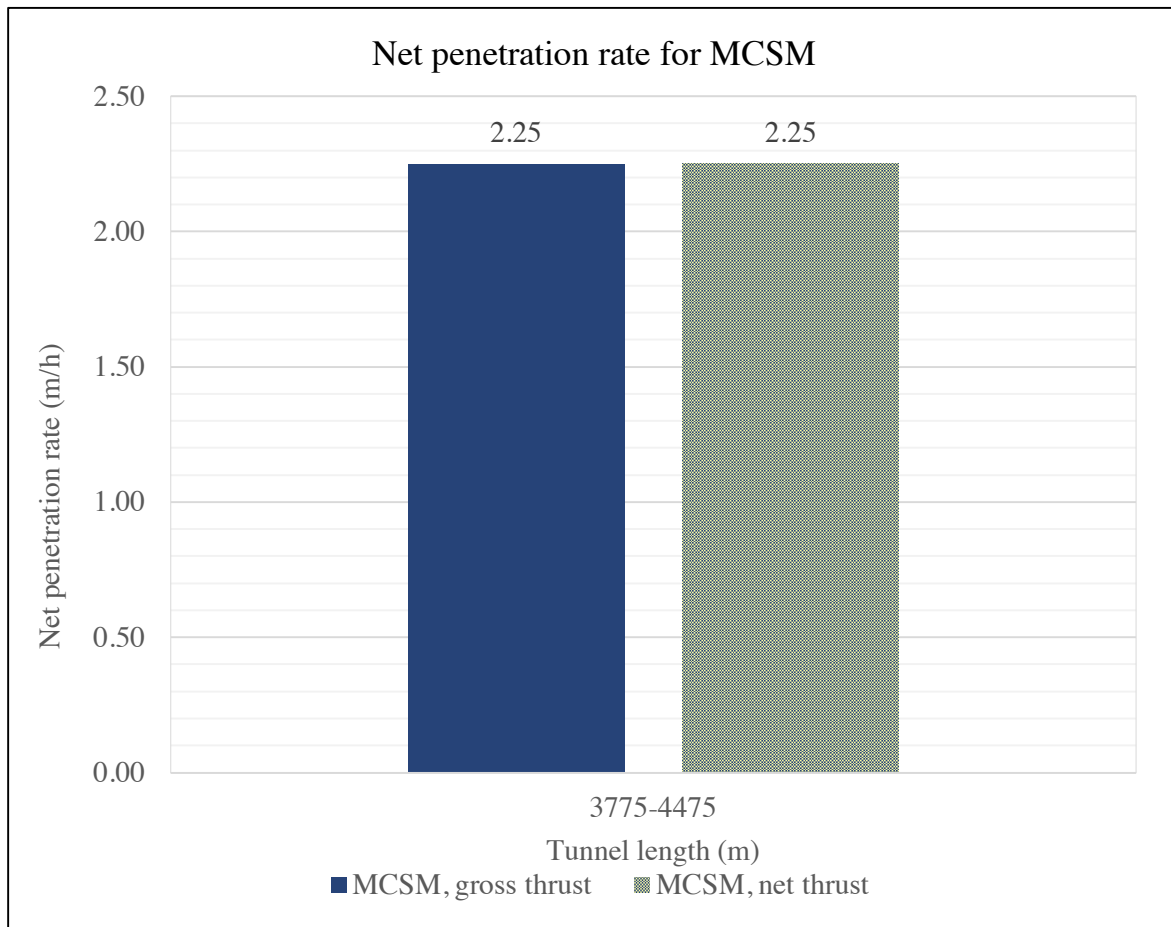


Figure 5.53 Results for MCSM calculated with gross and net thrust for the complete 700-meter segment

Results for section divided after geology and core samples

Results from model estimations are shown in Table 5.36 and Figure 5.54. The table includes a weighted average for the tunnel segment.

Table 5.36 Results for MCSM model calculated with gross and net thrust for section divided after geology and core samples, including a weighted average

| Thrust | Mapped length (m) | Length (m) | NPR (m/h) | Weighted average (m/h) |
|--------|-------------------|------------|-----------|------------------------|
| Gross | 3775-4075 | 300 | 2.15 | 2.26 |
| | 4075-4250 | 175 | 2.34 | |
| | 4250-4475 | 225 | 2.34 | |
| Net | 3775-4075 | 300 | 2.15 | 2.26 |
| | 4075-4250 | 175 | 2.34 | |
| | 4250-4475 | 225 | 2.34 | |

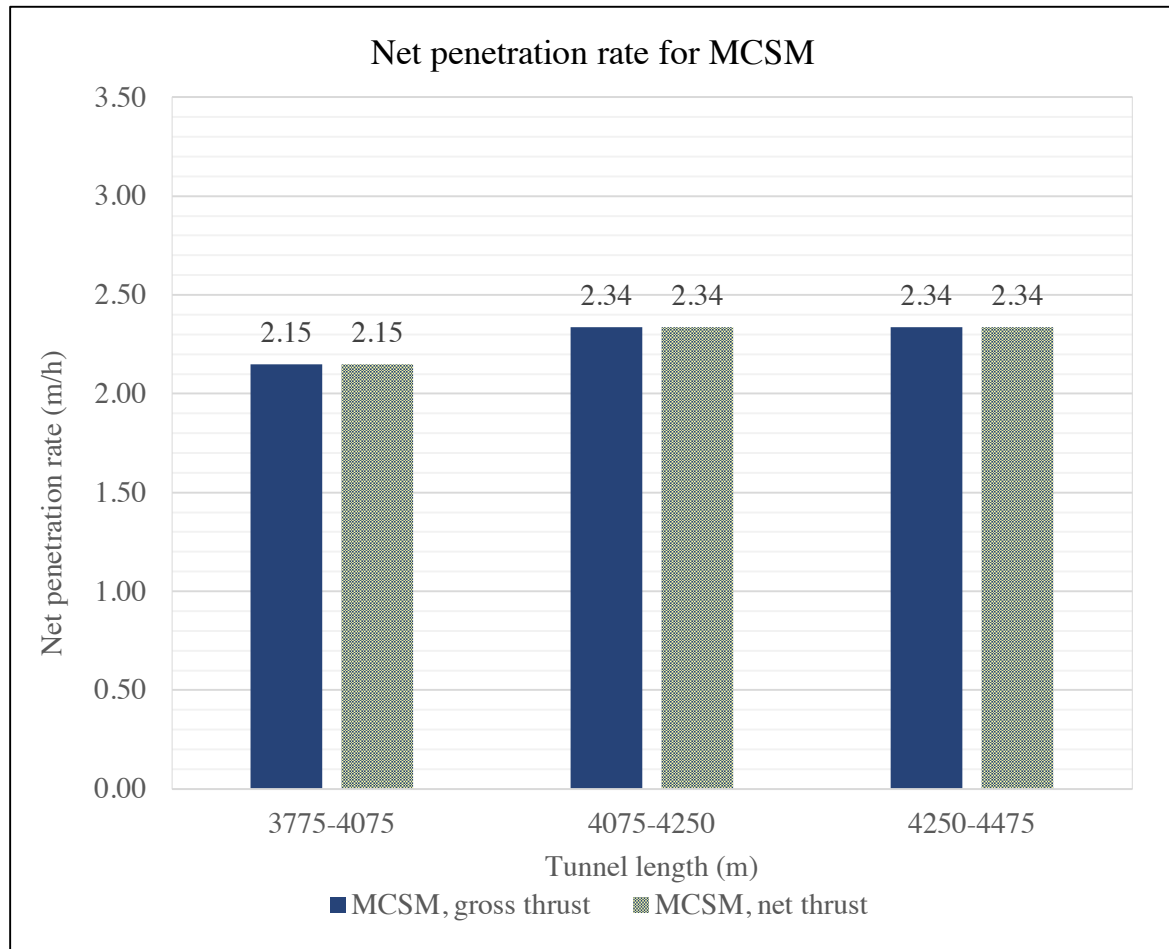


Figure 5.54 Results for MCSM model calculated with gross and net thrust for section divided after geology and core samples

Results for section divided from k_s -values

Results from model estimations are shown in Table 5.37 and Figure 5.55. The table includes a weighted average for the tunnel segment.

Table 5.37 Results for MCSM-model calculated with gross and net thrust for section divided from k_s -values, including a weighted average

| Thrust | Mapped length(m) | Length (m) | NPR (m/h) | Weighted average (m/h) |
|--------|------------------|------------|-----------|------------------------|
| Gross | 3775-4075 | 300 | 2.15 | 2.26 |
| | 4075-4275 | 200 | 2.34 | |
| | 4275-4475 | 200 | 2.33 | |
| Net | 3775-4075 | 300 | 2.15 | 2.26 |
| | 4075-4275 | 200 | 2.34 | |
| | 4275-4475 | 200 | 2.33 | |

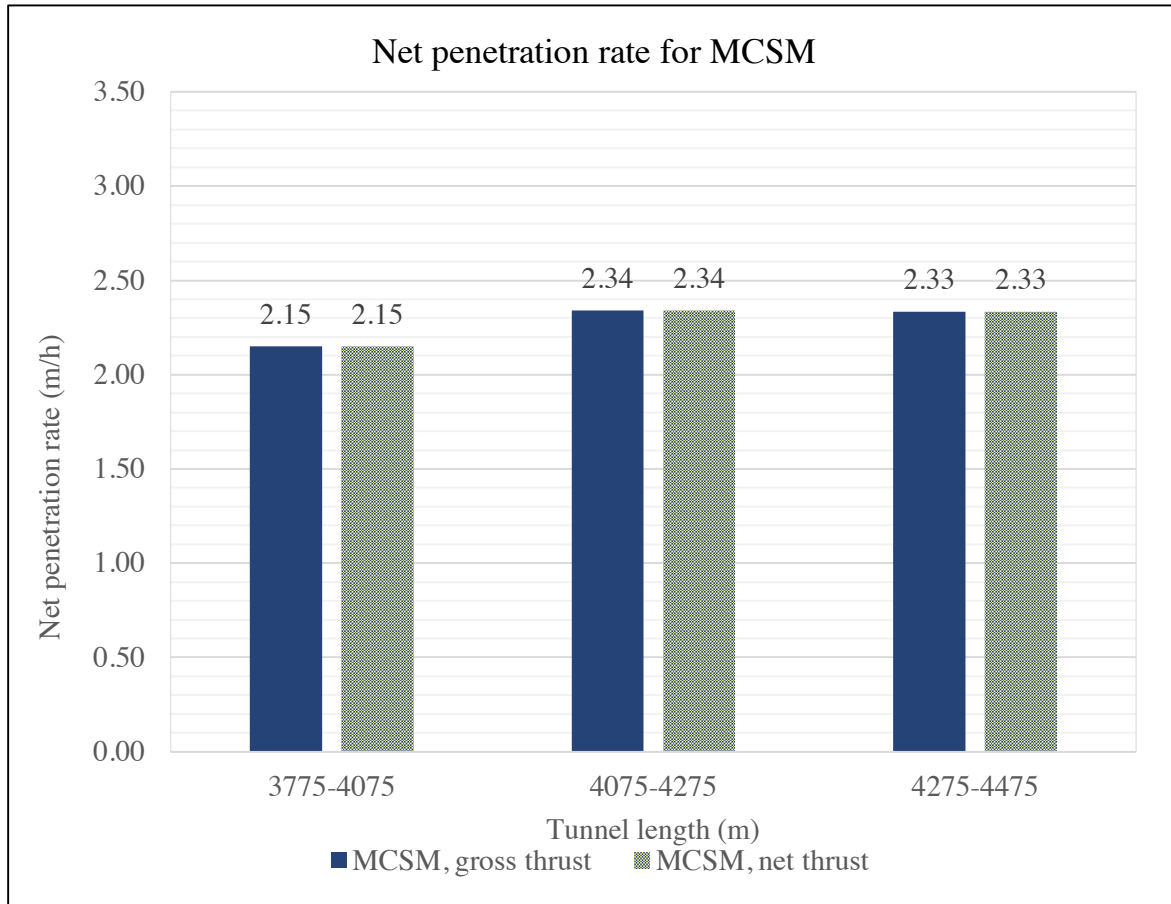


Figure 5.55 Results for MCSM model calculated with gross and net thrust for section divided from k_s -values

5.9 Cutter life estimations

5.9.1 NTNU-model

The average cutter ring life is in the NTNU-model found by equation (3.12). This value is calculated by deciding several parameters, which are briefly discussed below:

| | | |
|-----------|--|---|
| H_0 | - basic average cutter ring life | Found by a graph and the value is dependent on <i>CLI</i> and cutter diameter. The <i>CLI</i> is taken from chapter 5.7.2 |
| k_D | - correction factor for TBM diameter | Found by a graph |
| k_Q | - correction factor abrasive minerals | Found by a graph and the value is dependent on the abrasive minerals content |
| k_{RPM} | - correction factor for cutterhead <i>RPM</i> | Found by equation, dependent on the cutterhead diameter and the cutterhead velocity |
| k_N | - correction factor for the standard number of cutters | Found by equation, dependent on the standard number of cutters found in the model |
| k_T | - correction factor for gross cutter thrust | Found by graph, dependent on the thrust in kN/cutter. Used when <i>CLI</i> is between 4.5-5.9 |

When the average cutter ring life in hours per cutter is found, the average cutter ring life in meters and solid cubic meters can be calculated from equation (3.7) and (3.8).

Results for cutter ring life predictions

The cutter ring life is here calculated with the estimated net penetration rate from the NTNU-model and with the actual NPR for the 700-meter section at the New Ulriken Tunnel. Results for the three subdivisions of the tunnel segment, using both gross and net thrust values, are displayed below.

Table 5.38 Results from cutter ring life predictions using gross thrust values

| Complete 700-meter segment | | | |
|--|-------------|-------------|----------------------------|
| | H_h (h/c) | H_m (m/c) | H_f (sm ³ /c) |
| NPR from NTNU-model | 1.41 | 3.71 | 253.53 |
| Actual NPR | 1.41 | 2.84 | 194.38 |
| Divided after geology and core samples | | | |
| | H_h (h/c) | H_m (m/c) | H_f (sm ³ /c) |
| NPR from NTNU-model | 1.41 | 3.73 | 254.96 |
| Actual NPR | 1.41 | 2.84 | 193.86 |
| Divided from k_s -values | | | |
| | H_h (h/c) | H_m (m/c) | H_f (sm ³ /c) |
| NPR from NTNU-model | 1.48 | 3.90 | 266.87 |
| Actual NPR | 1.48 | 2.99 | 204.29 |

Table 5.39 Results from cutter ring life predictions using net thrust values

| Complete 700-meter segment | | | |
|---|-------------|-------------|----------------------------|
| | H_h (h/c) | H_m (m/c) | H_f (sm ³ /c) |
| NPR from NTNU-model | 1.86 | 3.83 | 261.82 |
| Actual NPR | 1.86 | 3.73 | 254.76 |
| Divided after geology and core samples | | | |
| | H_h (h/c) | H_m (m/c) | H_f (sm ³ /c) |
| NPR from NTNU-model | 1.87 | 3.91 | 267.18 |
| Actual NPR | 1.87 | 3.77 | 257.94 |
| Divided from k_v-values | | | |
| | H_h (h/c) | H_m (m/c) | H_f (sm ³ /c) |
| NPR from NTNU-model | 1.90 | 3.97 | 271.28 |
| Actual NPR | 1.90 | 3.86 | 263.69 |

6 Discussion and comparison

Results presented in chapter 5 will in this chapter be discussed and compared to each other and actual performance data from the New Ulriken Tunnel.

6.1 Comparisons of models towards actual performance data

In this thesis, several prediction models for hard rock TBM has been presented and calculated using data from the New Ulriken Tunnel. The estimations enable a comparison between the results from each model towards actual performance data. The evaluation further shows how the models differ in background, parameters, uncertainty, difficulty and calculation. Tunnel data originates from a segment of 700 meters, at TM 3775 – TM 4475. This segment has been examined closely regarding both machine and geological properties, and forms the basis for the input values in the different models.

The two prediction models presented by Farrokh et al. and Hassanpour et al. are different compared to the NTNU-, Q_{TBM} -, Gehring, Alpine and MCSM-model. The two are easy to calculate, with only one or two equations and few input parameters. This is the main difference, as the other models are more comprehensive which requires multiple machine and geology parameters.

The results and comparisons are presented below following the subdivisions shown in chapter 5.1.2 and 5.2.2. The comparisons are given for the complete 700-meter segment, divisions after geology and core samples, and division from k_s -values. Some models are either unclear or differ as to whether they use gross or net values for the thrust. Thus, all three sets of results are presented with calculations for average filtered gross and net thrust values. This is to secure a better comparison between the models. The filtration was set to 50 kN/cutter, and values below this have been deleted.

6.1.1 Complete 700-meter segment

For the complete segment, the achieved net penetration rate was 2.01 m/h. All the geological and machine input parameters have been averaged over the complete 700 meters.

Gross thrust

Estimations with gross thrust for the 700-meter tunnel segment, shows that all models predict too high net penetration, with the exception of Farrokh et al. The Q_{TBM} and NTNU-model predict the highest values, with 87% and 30% higher than the achieved NPR, respectively. Hassanpour et al., Gehring, Alpine and MCSM correlates better, predicting slightly above achieved NPR. Farrokh et al. is the only model predicting too low values using gross thrust, with a result 22% below.

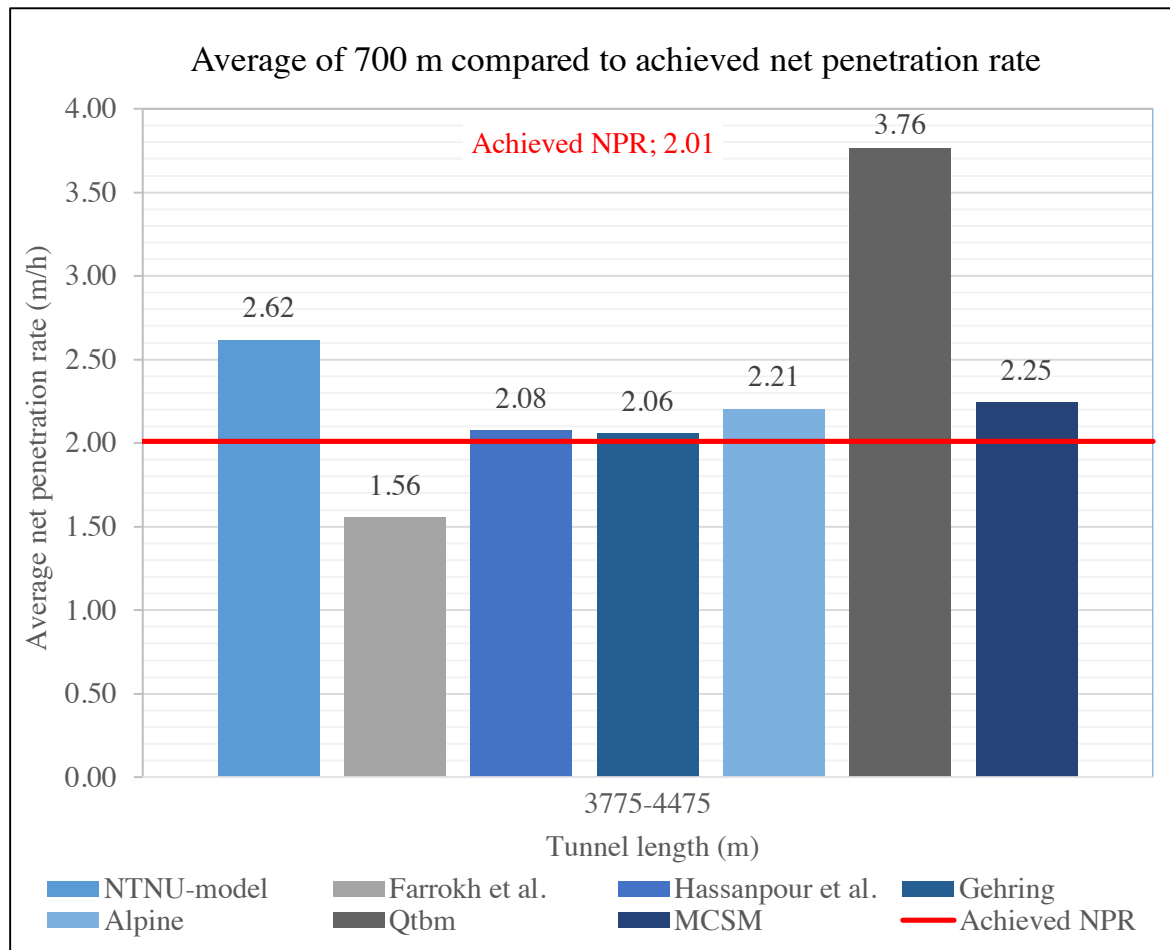


Figure 6.1 All prediction models (calculated using gross thrust) compared to achieved net penetration rate for the complete 700-meter segment

Net thrust

Using net thrust leads to a reduction in NPR results for all models, except MCSM. The MCSM model does not account for thrust in the estimations, thus giving the same result for both gross and net thrust. NTNU and Q_{TBM} is together with MCSM the only model predicting too high values, with a NPR of 2.5%, 68% and 49% higher than achieved. Alpine is very close to the achieved NPR of 2.01 m/h. Hassanpour et al. and Gehring calculates approximately 8% lower values, predicting conservative values. Farrokh et al. is still giving too low values.

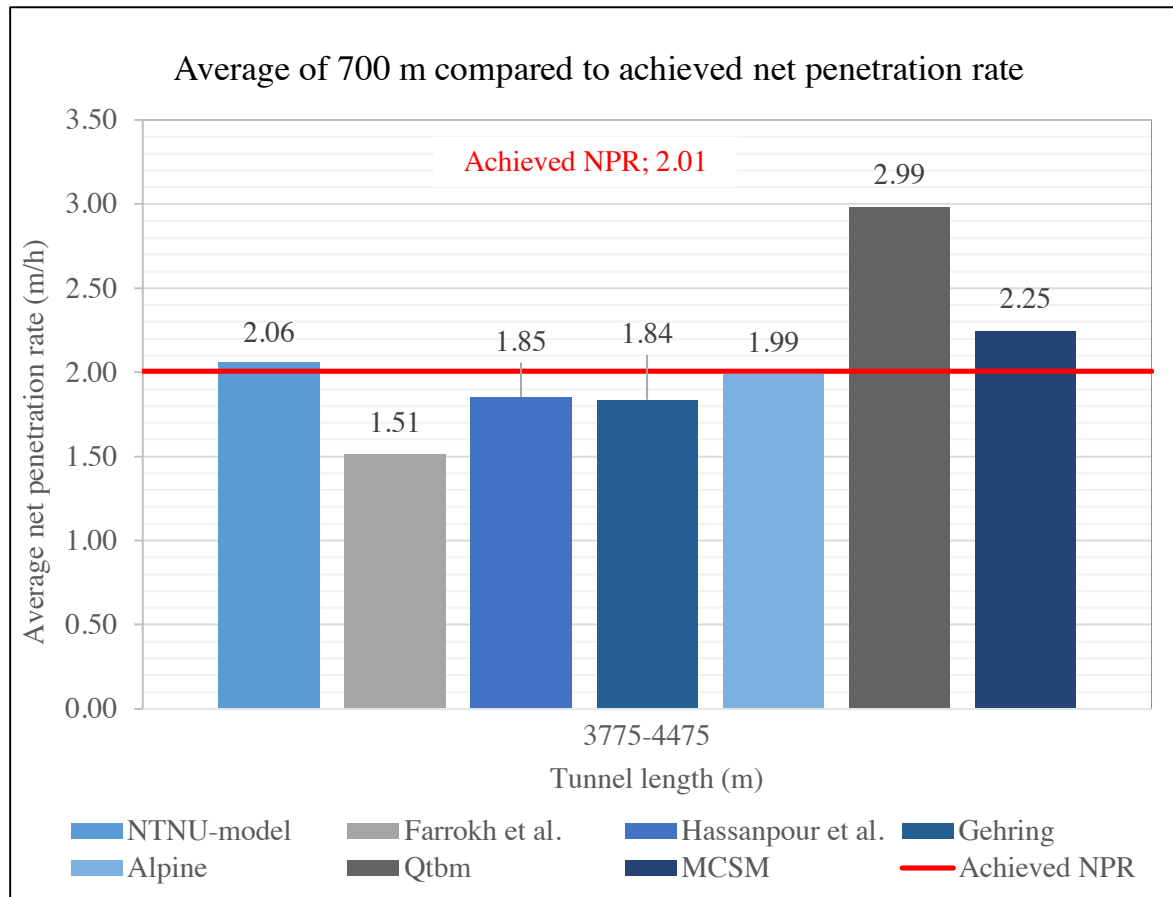


Figure 6.2 All prediction models (calculated using net thrust) compared to achieved net penetration rate for the complete 700-meter segment

6.1.2 Section divided after geology and core samples

For the section divided after geology and core samples, the achieved net penetration rate for each division was 1.87 m/h, 2.10 m/h and 2.12 m/h respectively. The three core samples represent one subdivision each for the geological input parameters. The machine parameters are averaged over the length of each zone.

Gross thrust

For each subdivision Q_{TBM} clearly estimates the highest NPR values, giving rather high predictions. The Alpine, MCSM and NTNU-model is predicting higher values for all three divisions than the achieved NPR. Hassanpour et al. and Gehring predicts too high values for the first subdivision, but drop below the achieved NPR for the other zones. Again, Farrokh et al. estimates low values.

The achieved net penetration rate is increasing throughout the segment. The NTNU-model is the only model following in line with this trend. Other models like Farrokh et al., Hassanpour et al. and Gehring are predicting the opposite, and are all decreasing. Alpine and Q_{TBM} both increases for the subdivision TM 4075 – TM 4250, before falling down again for TM 4250 – TM 4475. The MCSM model also increases from division one to two, but stays at the same net penetration rate for subdivision two and three.

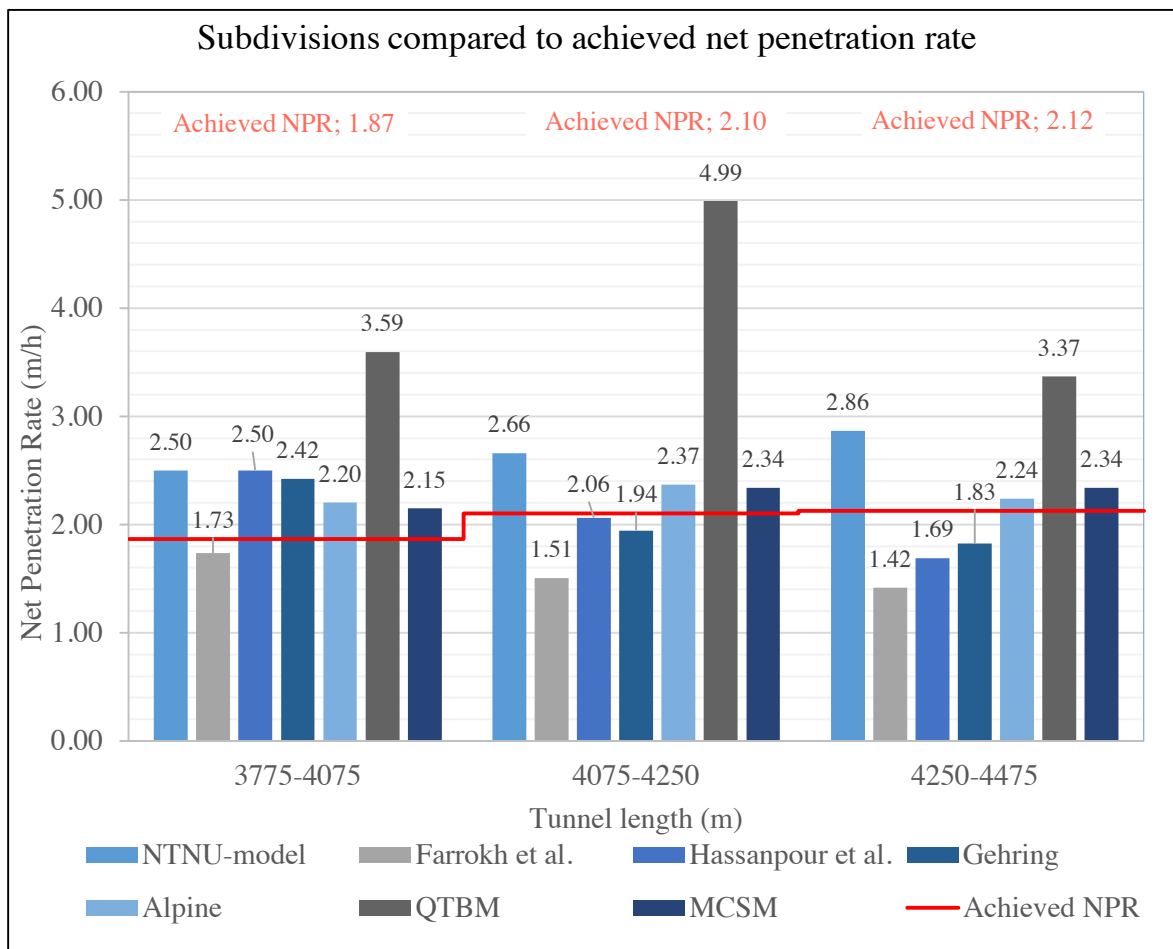


Figure 6.3 All prediction models (calculated using gross thrust) compared to achieved net penetration rate for section divided after geology and core samples

The weighted average of this section using gross thrust values show how the average for the 700-meter segment is estimated based on the three subdivisions. Figure 6.4 show that Hassanpour et al. and Gehring are predicting values closest to the achieved NPR, with a weighted average of 2.13 m/h and 2.11 m/h.

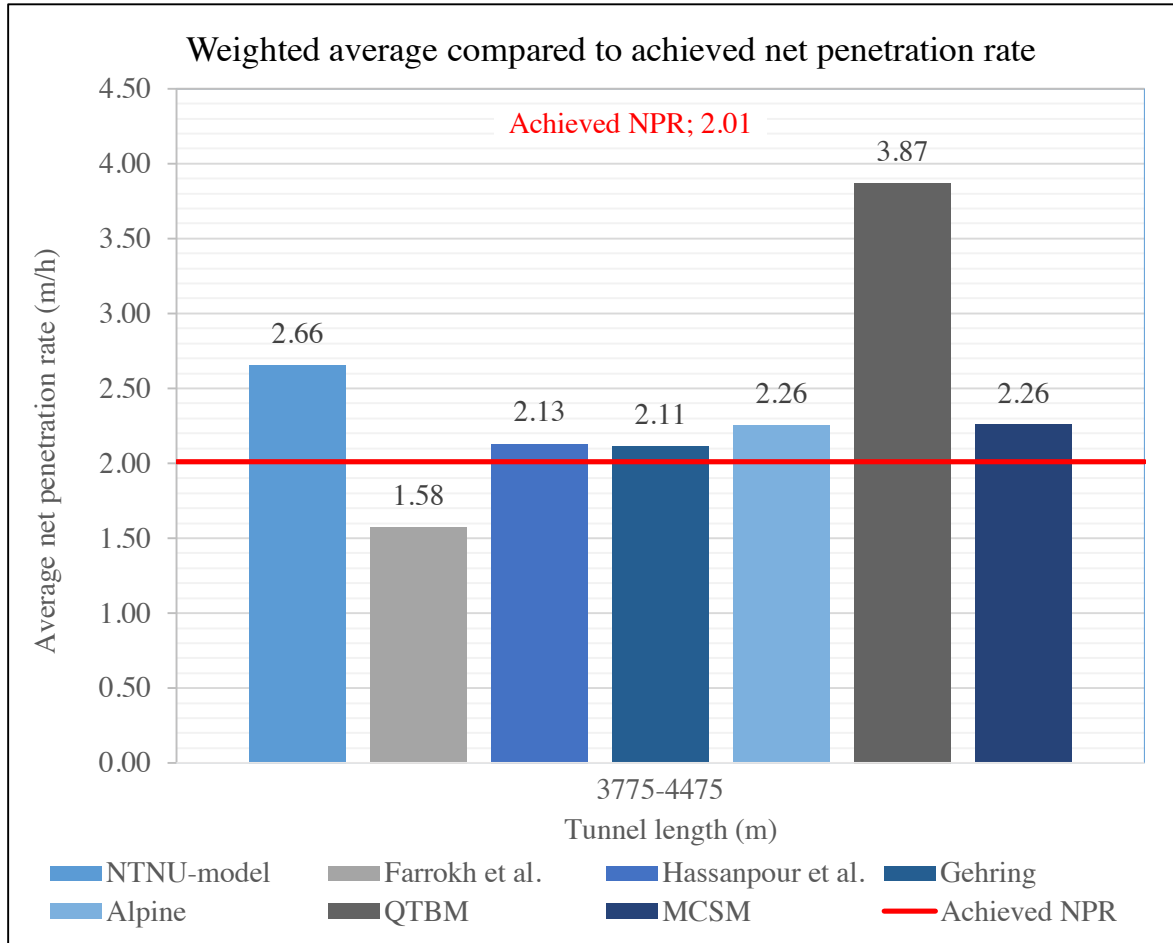


Figure 6.4 Weighted average of all prediction models (calculated using gross thrust) compared to achieved net penetration rate for section divided after geology and core samples

Net thrust

Using net thrust leads to a reduction in NPR results for all models, except MCSM. Q_{TBM} estimates the highest values, predicting above the achieved NPR for all subdivisions. MCSM predicts above the achieved NPR, and the largest deviation is at the first division, predicting 16% more than achieved. NTNU and Alpine varies between calculating slightly above and below achieved net penetration rate. Hassanpour et al. and Gehring predicts too high values for the first subdivision, but decreases below the achieved NPR for the other zones. Again, Farrokh et al. estimates low values.

The achieved net penetration rate is increasing throughout the segment. The NTNU-model is the only model following in line with this trend. Other models like Farrokh et al., Hassanpour et al. and Gehring are predicting the opposite, and are all decreasing. Alpine and Q_{TBM} both increases for the subdivision TM 4075 – TM 4250, before falling down again for TM 4250 – TM 4475. The MCSM model also increases from division one to two, but stays at the same net penetration rate for subdivision two and three.

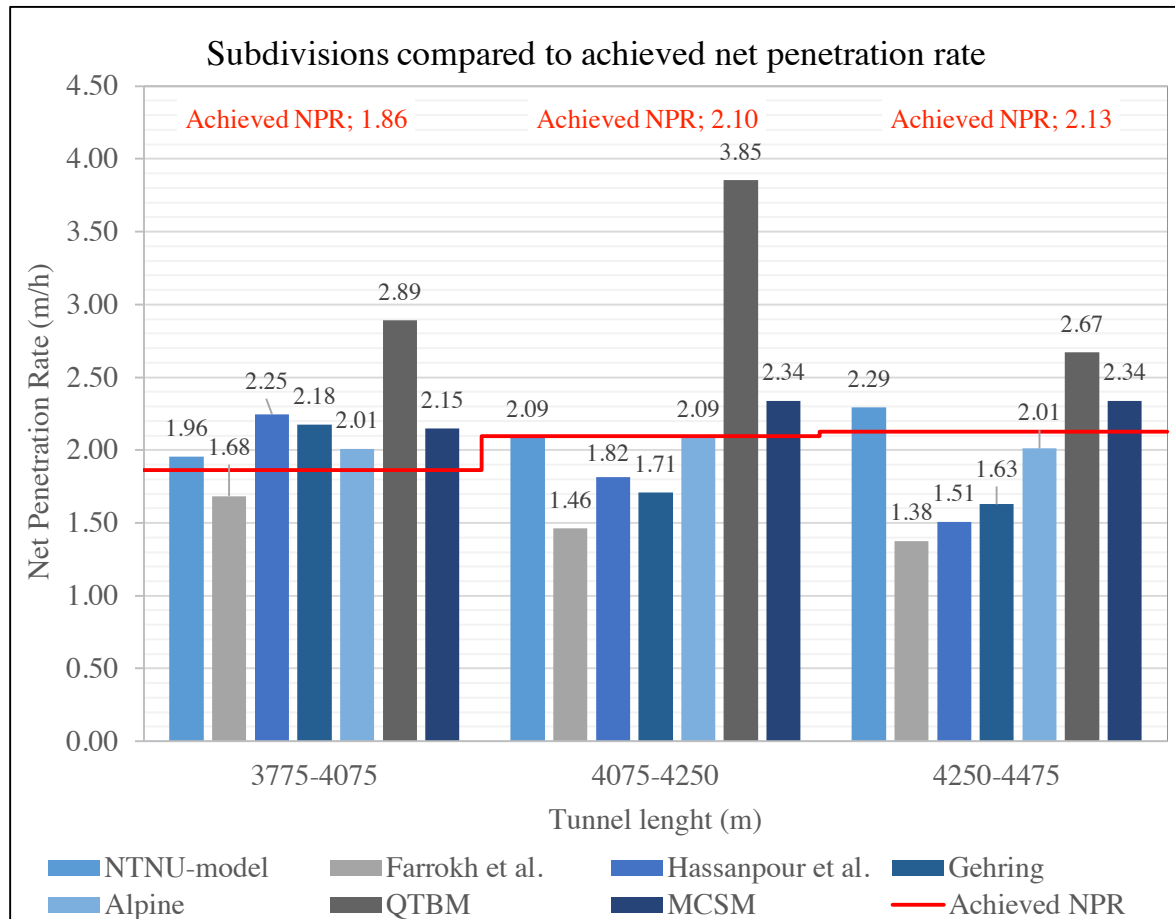


Figure 6.5 All prediction models (calculated using net thrust) compared to achieved net penetration rate for section divided after geology and core samples

The weighted average of this section using net thrust values show how the average for the 700-meter segment is estimated based on the three subdivisions. Figure 6.6 show that NTNU- and Alpine model are predicting values closest to the achieved NPR, with a weighted average of 2.10 m/h and 2.03 m/h. However, if a conservative result is sought for, Hassanpour et al. and Gehring provides more satisfactory results. They predict NPRs that are 5.5% and 6.5% lower than the achieved.

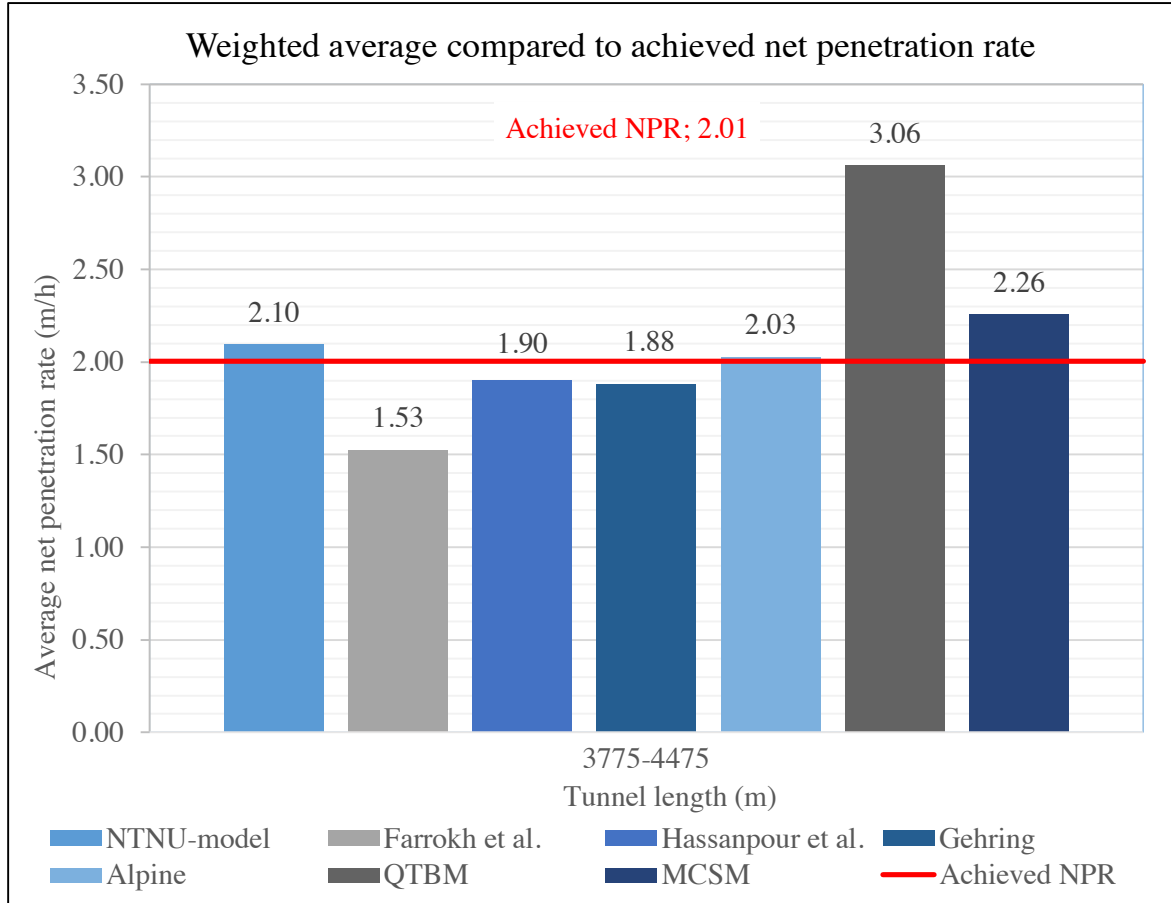


Figure 6.6 Weighted average of all prediction models (calculated using net thrust) compared to achieved net penetration rate for section divided after geology and core samples

6.1.3 Section divided from k_s -values

For the section divided from k_s -values, the achieved net penetration rate for each division was 1.87 m/h, 2.14 m/h and 2.08 m/h respectively. The three core samples represent one subdivision each for the geological input parameters. The machine parameters are averaged over the length of each zone.

Gross thrust

Overall, the Q_{TBM} -model provides the highest net penetration rates for all three subdivisions. Alpine, MCSM and NTNU-model is predicting higher values than the achieved NPR for all three divisions. Hassanpour et al. and Gehring predicts too high values for the first subdivision, but decreases below the achieved NPR for the other zones. Again, Farrokh et al. estimates low values.

Starting at 1.87 m/h for TM 3375 – TM 4075, the achieved net penetration rate for the mid division rises to 2.14 m/h. For the last subdivision, the achieved NPR drops marginally to 2.08 m/h. Alpine and MCSM are the only models following in line with this trend. The NTNU-model rises throughout the section, stopping at a high 2.91 m/h. Other models like Farrokh et al., Hassanpour et al. and Gehring are predicting differently, and are all decreasing. In line with the achieved net penetration, Q_{TBM} has its highest point at TM 4075 – TM 4250. However, the two other subdivisions do not follow the trend.

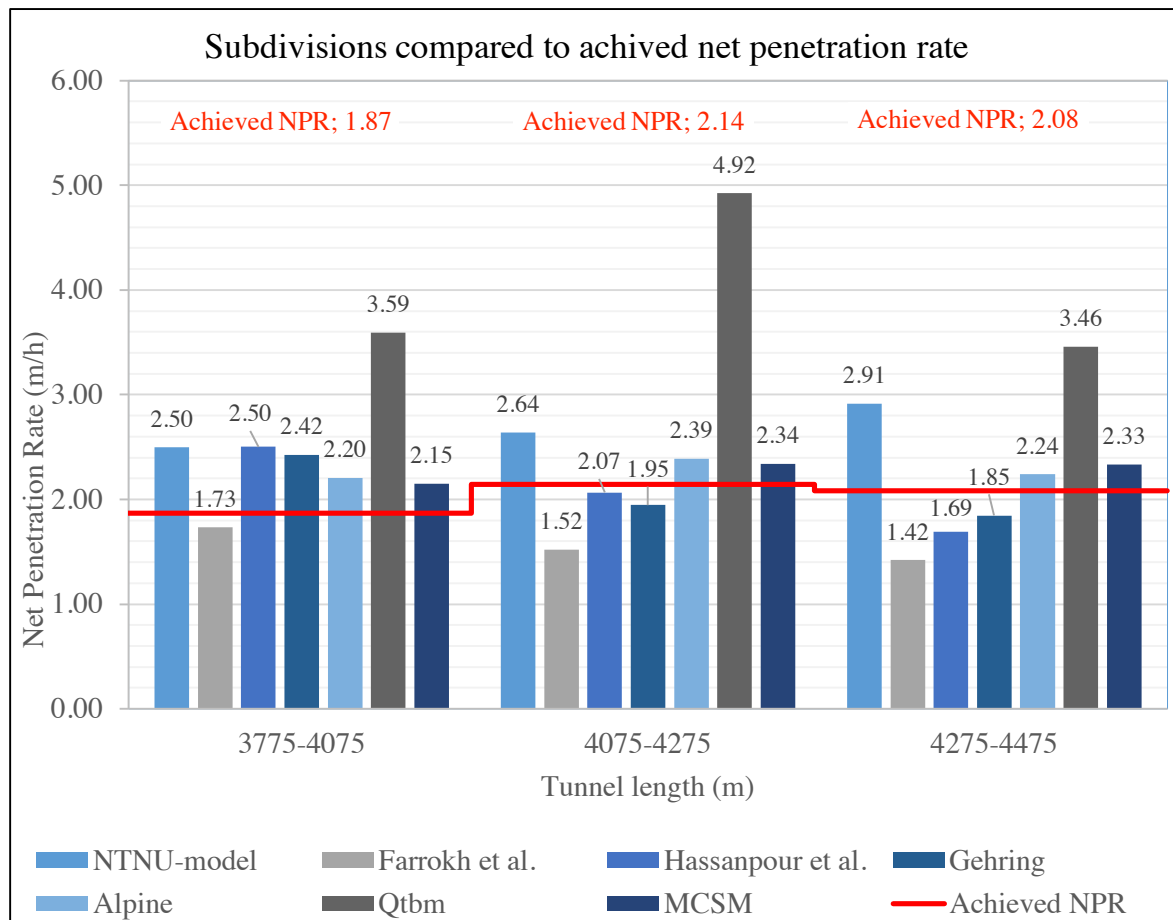


Figure 6.7 All prediction models (calculated using gross thrust) compared to achieved net penetration rate for section divided from k_s -values

The weighted average of this section using gross thrust values show how the average for the 700-meter segment is estimated based on the three subdivisions. Figure 6.8 show that Hassanpour et al. and Gehring are predicting values closest to the achieved NPR, with a weighted average of 2.15 m/h and 2.12 m/h.

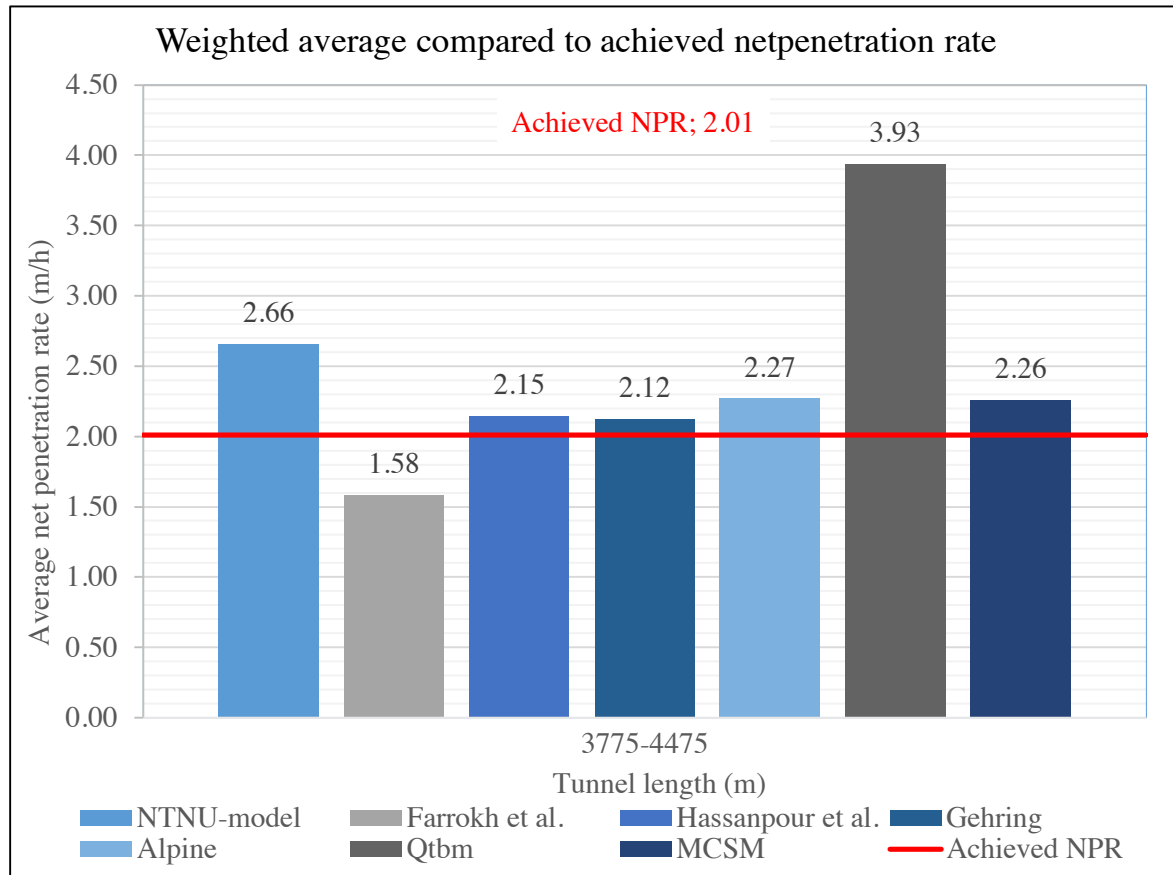


Figure 6.8 Weighted average of all prediction models (calculated using gross thrust) compared to achieved net penetration rate for section divided from k_s -values

Net thrust

Calculations with net thrust leads to a reduction in NPR results for all models, except MCSM. In general, the Q_{TBM} -model provides the highest net penetration rates for this section. MCSM predicts above the achieved NPR, and the largest deviation is at the first division, predicting 16% more than achieved. NTNU- and Alpine model varies between calculating slightly above and below achieved net penetration rate. Hassanpour et al. and Gehring predicts too high values for the first subdivision, but decreases below the achieved NPR for the other zones. Again, Farrokh et al. estimates low values.

Starting at 1.86 m/h for TM 3375 – TM 4075, the achieved net penetration rate for the mid division rises to 2.14 m/h. For the last subdivision, the achieved NPR drops marginally to 2.09 m/h. Only the MCSM-model is able to predict in line with this trend. The NTNU-model rises throughout the section, stopping at 2.33 m/h. Other models like Farrokh et al., Hassanpour et al. and Gehring are predicting differently, and are all decreasing. In line with the achieved net penetration, Q_{TBM} and Alpine have their highest points at TM 4075 – TM 4250. However, for the two other subdivisions the estimated values do not correlate with the trend of the achieved net penetration rate.

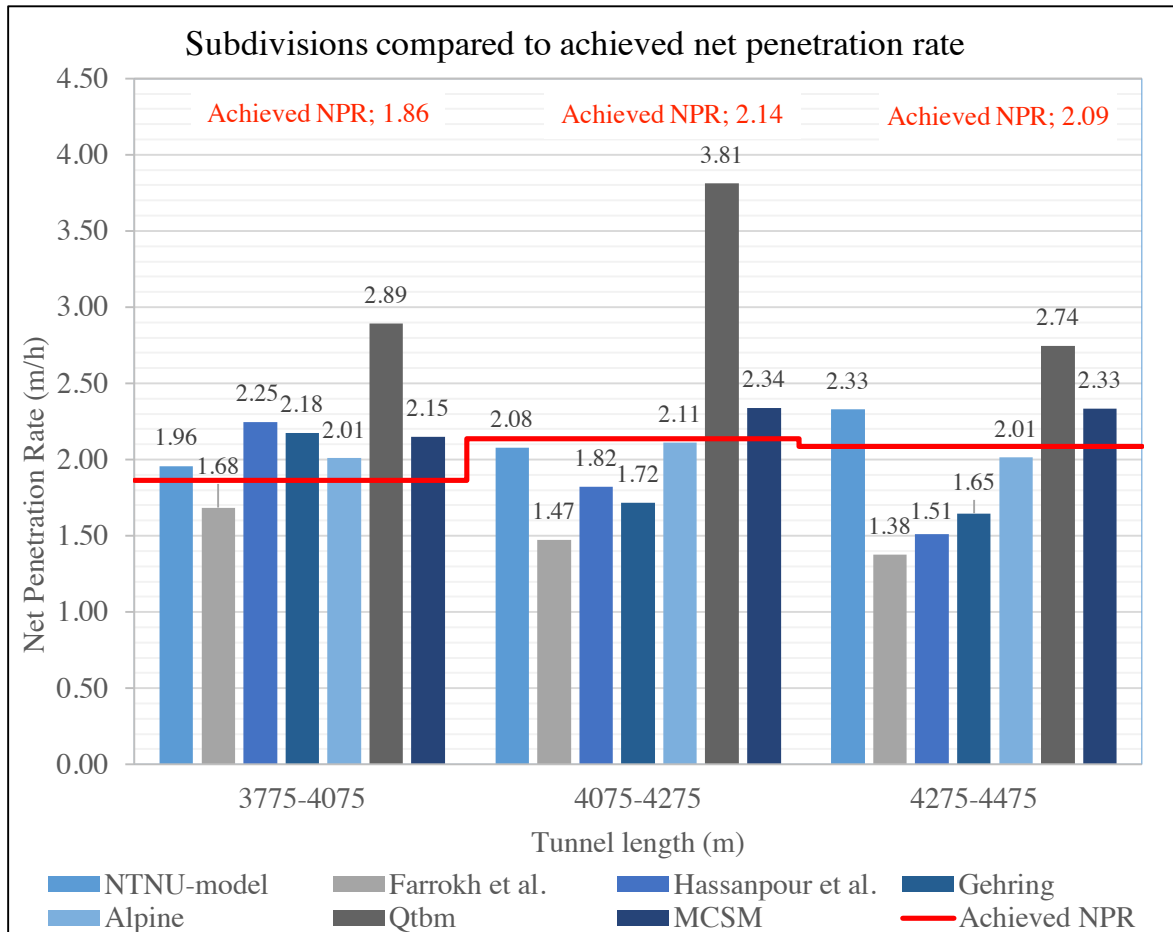


Figure 6.9 All prediction models (calculated using net thrust) compared to achieved net penetration rate for section divided from k_s -values

The weighted average of this section using net thrust values show how the average for the 700-meter segment is estimated based on the three subdivisions. Figure 6.10 show that NTNU and Alpine are predicting values closest to the achieved NPR, with a weighted average of 2.10 m/h and 2.04 m/h. However, if a conservative result is sought after, Hassanpour et al. and Gehring provides more satisfactory results. They predict 5% and 6% lower NPRs compared to the achieved.

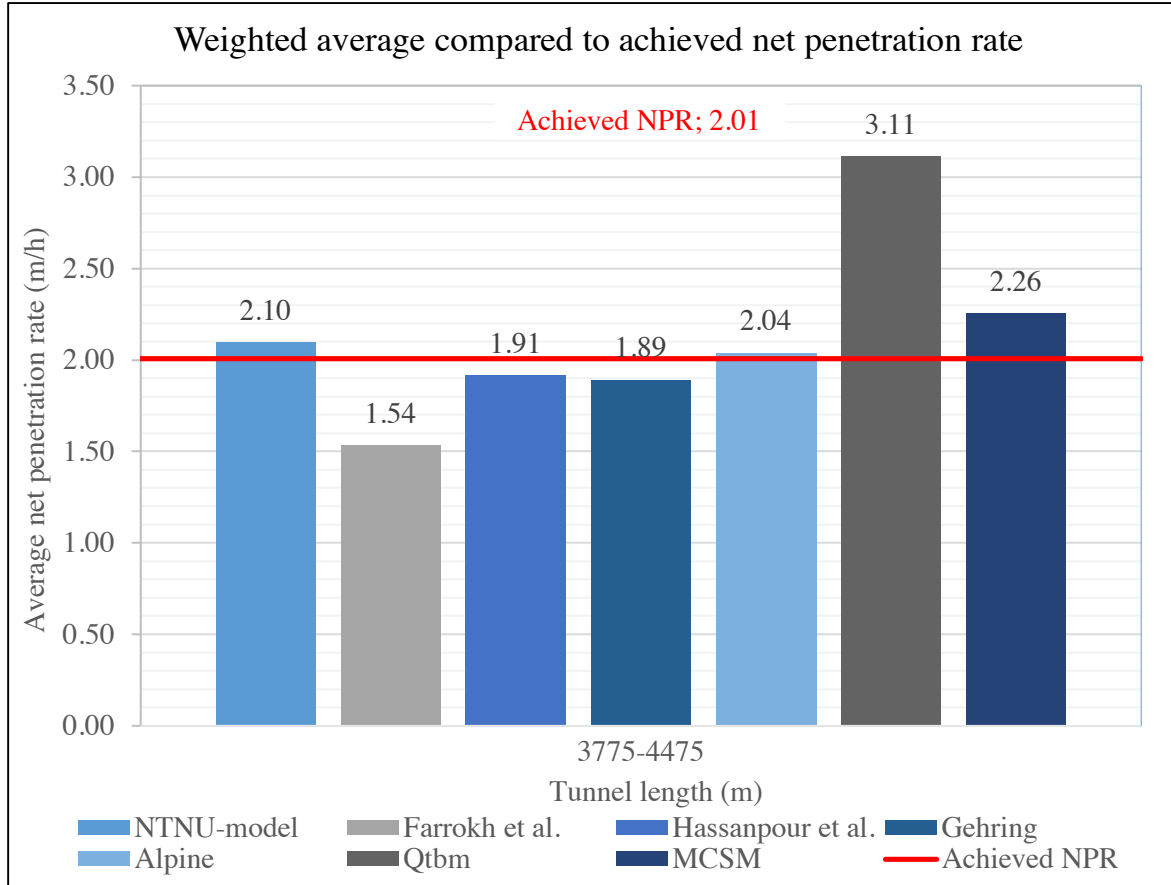


Figure 6.10 Weighted average of all prediction models (calculated using net thrust) compared to achieved net penetration rate for section divided from k_s -values

6.1.4 Cutter ring life comparison

The comparison of the predicted cutter ring life using gross thrust values show good correlation with the actual data in hours/cutter. The values for meters/cutter and solid cubic meters per cutter deviate when using the NPR estimated from the NTNU-model. This is due to the predicted net penetration rate being higher than the achieved. When using the actual NPR, all values show promising results.

Table 6.1 Comparison of predicted cutter ring life with gross thrust values towards actual cutter ring life at the New Ulriken Tunnel

| Complete 700-meter segment | | | |
|--|-------------|----------------------------|----------------------------|
| | H_h (h/c) | H_m (m/c) | H_f (sm ³ /c) |
| NPR from NTNU-model | 1.41 | 3.71 | 253.53 |
| Actual NPR | 1.41 | 2.84 | 194.38 |
| Divided after geology and core samples | | | |
| | H_h (h/c) | H_m (m/c) | H_f (sm ³ /c) |
| NPR from NTNU-model | 1.41 | 3.73 | 254.96 |
| Actual NPR | 1.41 | 2.84 | 193.86 |
| Divided from k_s-values | | | |
| | H_h (h/c) | H_m (m/c) | H_f (sm ³ /c) |
| NPR from NTNU-model | 1.48 | 3.90 | 266.87 |
| Actual NPR | 1.48 | 2.99 | 204.29 |
| Actual cutter ring life at the New Ulriken Tunnel | | | |
| H_h (h/c) | H_m (m/c) | H_f (sm ³ /c) | |
| 1.54 | 2.93 | 201.00 | |

In Table 6.2, the comparison of the predicted cutter ring life using net thrust values show that all the estimated values are higher than the actual data. The results using estimated and actual NPR are similar when net thrust is the input parameter. The reason for high values are directly linked to the cutter thrust correction factor in the NTNU-model. This correction factor will reduce the cutter ring life for high thrust levels, and increase it when lower thrust levels are used.

Table 6.2 Comparison of predicted cutter ring life with net thrust values towards actual cutter ring life at the New Ulriken Tunnel

| Complete 700-meter segment | | | |
|--|-------------|----------------------------|----------------------------|
| | H_h (h/c) | H_m (m/c) | H_f (sm ³ /c) |
| NPR from NTNU-model | 1.86 | 3.83 | 261.82 |
| Actual NPR | 1.86 | 3.73 | 254.76 |
| Divided after geology and core samples | | | |
| | H_h (h/c) | H_m (m/c) | H_f (sm ³ /c) |
| NPR from NTNU-model | 1.87 | 3.91 | 267.18 |
| Actual NPR | 1.87 | 3.77 | 257.94 |
| Divided from k_s-values | | | |
| | H_h (h/c) | H_m (m/c) | H_f (sm ³ /c) |
| NPR from NTNU-model | 1.90 | 3.97 | 271.28 |
| Actual NPR | 1.90 | 3.86 | 263.69 |
| Actual cutter ring life at the New Ulriken Tunnel | | | |
| H_h (h/c) | H_m (m/c) | H_f (sm ³ /c) | |
| 1.54 | 2.93 | 201.00 | |

Evaluation and sources of error

The NTNU-model is a complex model that needs multiple input parameters to calculate the cutter ring life. As mentioned earlier, the model is a well-known TBM prediction model. Still the model has its weaknesses, especially in an international environment. The reason for this is that the parameters are acquired from laboratory experiments only used in Norway. (Hassanpour et al., 2011)

Calculating the cutter ring life is done in multiple steps and with the use of various graphs in order to attain the different values. Some of these graphs are not very easy to read accurately. Results on the cutter ring life could vary from one person to another, simply because of different readings and interpretations of these graphs. It would be much easier to gain more accurate results if the equations of the different graphs were available.

Another source of error is the correction factor for abrasive minerals. This factor incorporates several hard and abrasive minerals, like quartz, garnet, epidote, and others. Only the quartz content is known from the laboratory testing. This leads to less impact of the correction factor, giving higher cutter ring life values which may not correspond with the actual situation.

6.2 Study and discussion of model behavior

Each of the prediction models are discussed in regard to influence of parameters and trends in results. The subchapters below will discuss the models divided by the use of gross and net thrust as an input parameter.

To evaluate every model, a back calculation of the main parameters influencing the net penetration has been performed. This has only been done for the complete 700-meter section, for gross and net thrust values. Each parameter was changed, using trial and error, to find the value needed to get a net penetration rate matching the achieved. The difference between the back calculated value and the original value is given as a percentage. This to show if the parameter needs to be increased or decreased to reach the achieved net penetration value for the New Ulriken Tunnel. Only one parameter was changed at a time, to display the sensitivity of that specific parameter. The back calculations can be viewed in Appendix Q .

6.2.1 NTNU-model

The NTNU-model is developed to be a conservative model, and the goal is to present estimations about 10% below what a project actually can achieve. The gross average thrust is used in the model, including friction or drag of the cutterhead as well as cutterhead support systems.

For the NTNU-model, the parameters that have the largest influence on the NPR calculations in this thesis, are the thrust and fracturing factor. The *DRI* is also important. The thrust is the most sensitive and impressionable parameter. Neither the fracturing factor nor the *DRI* are nearly as sensitive, thus a much larger change would be needed to achieve any difference in net penetration rate. Further, both the k_s and *DRI* are geology parameters, and not adjustable in reality. This is merely shown to get an indication of what would have been needed to obtain the achieved NPR.

Gross thrust

The NTNU-model calculates high values for net penetration when using gross thrust in the estimations. For all three calculated sections, the model predicts too high values for NPR. As this is a conservative model, it is not common that calculations give numbers approximately 30% higher than achieved net penetration rate. These high predictions are consistent for all averages calculated with the NTNU-model using gross thrust in this thesis.

Back calculations show how much the different parameters have to be changed to reduce the net penetration rate by 30%, from an estimated 2.62 m/h to the achieved 2.01 m/h. Calculations provide the following changes in the parameters:

- Gross thrust must be reduced by 13.6%, down to 281 kN/cutter
- Rock mass fracturing factor k_s has to be decreased by 41%, down to 0.69
- *DRI* has to be lowered by 70.5%, down to 25.02

A *DRI* of 25 is categorized as extremely low, and is unlikely to encounter in hard rock conditions. Changes in gross thrust and rock mass fracturing factor are more acceptable values, and are not inconceivable under given rock mass conditions.

Net thrust

Using net cutter thrust values as an input in the NTNU-model calculates similar results as the actual performance at Ulriken, just above the achieved NPR. The NTNU-model is a conservative model, and it is surprising that even with net cutter thrust values, it calculates too high net penetration rates. The optimal result would lay around 10% less, and this emphasize the influence of thrust in the model.

Back calculations show how much the different parameters have to be changed to reduce the net penetration rate by 2.5%, from an estimated 2.06 m/h to the achieved 2.01 m/h. Calculations provide the following changes in the parameters:

- Gross thrust needs to be reduced by 1.2%, down to 281 kN/cutter
- Rock mass fracturing factor k_s has to be lowered by 3.2%, down to 0.94
- *DRI* must be decreased by 4.5%, down to 40.85

All parameters are close to actual conditions, and only smaller changes are needed to obtain the achieved net penetration rate of 2.01 m/h.

Evaluation and sources of error

The NTNU-model is a complex model that needs multiple input parameters to calculate the net penetration rate. As mentioned earlier, the model is a well-known TBM prediction model. Still the model has its weaknesses, especially in an international environment. The reason for this is that the parameters are acquired from laboratory experiments only used in Norway. (Hassanpour et al., 2011)

Calculating the net penetration rate is done in multiple steps and with the use of various graphs in order to attain the different values. Some of these graphs are not very easy to read accurately. Results of the net penetration rate could vary from one person to another, simply because of different readings and interpretations of these graphs. It would be much easier to gain more accurate results if the equations of the different graphs were available.

6.2.2 Farrokh et al.

The Farrokh et al. model calculations in this thesis show low values for net penetration rate. In addition, calculations with both gross and net thrust values show small variations in NPR results. Some models are unclear as to whether they use gross or net values for the thrust. However, Farrokh et al. states that when calculating cutter thrust, this model uses gross values as an input. The model has been consistent in its results, showing too low net penetration rate values in all calculations.

For Farrokh et al., the parameter that has the largest influence on the NPR calculations in this thesis, is the *RPM*. This is also reflected in the results for both the gross and net thrust calculations. Changes in thrust filtration gave small to none changes in average *RPM*

values. This explains why there is little difference in net penetration rates calculated with this model.

The cutter thrust and *UCS* are not nearly as sensitive as the *RPM*, thus a much larger change would be needed to achieve any difference in net penetration rate. In addition, the *UCS* is a geology parameter, and not adjustable in reality. This is merely shown to get an indication of what would have been needed to obtain the achieved NPR. In that case, all the other input parameters in the model are held constant.

Gross thrust

Back calculations show how much the different parameters have to be changed to increase the net penetration rate by 22%, from an estimated 1.56 m/h to the achieved 2.01 m/h.

Calculations provide the following changes in the parameters:

- Gross thrust has to be increased by 47.2%, to 605 kN/cutter
- Cutterhead velocity, *RPM*, must be increased by 22.6%, to 6.25
- *UCS* has to be reduced by 51.9%, down to 115.00 MPa

Looking at the values for especially gross thrust, the needed cutter thrust to obtain the achieved net penetration rate is 605 kN/cutter. This equals to an impossible gross total thrust of 37510 kN, above the machine limit of 22500 kN. The cutterhead velocity is also high, and a *RPM* of 6.25 is unlikely for this machine. As for the geology, a *UCS* value of 115 is possible for these type of hard rock conditions.

Net thrust

Using net thrust values Farrokh et al. estimates 1.51 m/h, which is 25% lower than the achieved net penetration at 2.01 m/h. Back calculations show that the parameters have to be changed hereafter:

- Net thrust has to be increased by 53%, to 605 kN/cutter
- Cutterhead velocity, *RPM*, must be enlarged by 24.8%, to 6.44
- *UCS* has to be reduced by 61.2%, down to 108.3 MPa

As for the gross thrust, net cutter thrust values needed to obtain the achieved net penetration rate is 605 kN/cutter. This equals to an impossible net total thrust of 37510 kN, way above the machine limit of 22500 kN. In addition, a cutterhead velocity of 6.44 *RPM* is unlikely for this machine.

Evaluation and sources of error

A lower number of parameters reduces the risk of errors. The question is then how accurate the equations are in the first place. The equations are based on a database containing more than 200 projects. However, equation 1 and 2 presented by Farrokh et al. (2012) only gives a regression of 63% and 58%, respectively. This supports the skepticism pinned to this prediction model.

The model does not incorporate the rock mass fracturing. This is stated in several of the other models to have an impact on the net penetration, resulting in an uncertain factor in this particular model. The *RQD* numerical code is also a source of error, as it could give an incomplete description of the *RQD* of the rock mass.

Another source of error is the *UCS* values. Due to lack of sample material for laboratory testing, only the point load strength test was used to determine the strength properties. Further, conversion formulas were used to obtain values for *UCS*. These conversion formulas give some uncertainties in the values, which can lead to less precise model estimations.

6.2.3 Hassanpour et al.

All section averages show that the Hassanpour et al. model calculations present values slightly above the achieved net penetration rate using gross cutter thrust. Net cutter thrust gives values for the section averages 6-8% below the achieved NPR. Some models are unclear as to whether they use gross or net values for the thrust. Hassanpour et al. has not stated what values for cutter thrust that are used as an input in this model.

For Hassanpour et al., the parameter with the largest influence on the NPR calculations, is the *UCS*. However, the *UCS* is a geology parameter and is not adjustable in reality. This is merely shown to get an indication of what would have been needed to obtain the achieved NPR. In this model, all parameters are sensitive and need small changes to make an impact on the model result.

Gross thrust

The Hassanpour et al. model calculates a bit too high values for net penetration when using gross thrust in the estimations. Back calculations show how much the different parameters have to be changed to decrease the net penetration rate by 3.5%, from an estimated 2.08 m/h to the achieved 2.01 m/h. Calculations provide the following changes in the parameters:

- Gross thrust has to be lowered by 3.3%, to 309 kN/cutter
- Cutterhead velocity, *RPM*, must be reduced by 3.3%, to 4.68
- *UCS* has to be enlarged by 2.4%, up to 179 MPa
- *RQD* needs to be increased by 3.2%, to 70

All back calculated values show that small possible adjustments for the machine parameters will give the achieved net penetration. The geological parameters are also within reasonable proportionality limits.

Net thrust

When using net cutter thrust values, the Hassanpour et al. model estimates approximately 10% lower values than actual performance data.

Back calculating the different parameters show how much they have to be changed to increase the net penetration rate from an estimated 1.85 m/h to the achieved 2.01 m/h. Calculations provide the following changes in the parameters:

- Net thrust has to be increased by 8.0%, to 309 kN/cutter
- Cutterhead velocity, *RPM*, needs to be enlarged by 7.8%, to 5.25
- *UCS* has to be reduced by 6.3%, down to 164.35 MPa
- *RQD* must be lowered by 8.8%, to 62.30

A 6-9% individual change for the parameters are needed. This shows that all are rather sensitive, affecting the model more or less equally.

Evaluation and sources of error

The main weakness with this model is that it is only based on data from four different TBM projects. Compared to some of the other models, which have a substantial database from numerous projects with a diverse geology and TBM parameters, this model's database is weak. That will definitely have an effect on its credibility. Furthermore, it can be noted that three of the four projects in the database are double shielded TBMs, and only one is an open-type TBM. Calculating this model for open- TBMs, may give some uncertainty for friction of the shield.

Hassanpour et al. (2011) states that the model should be applied with caution in highly fractured rock masses, as it does not account for rock mass fractures. This is stated in several of the other models to have an impact on the net penetration, giving an uncertain factor for this model.

Another source of error is the *UCS* values. Due to a lack of sample material for laboratory testing, only the point load strength test was used to determine the strength properties. Further, conversion formulas were used to obtain values for *UCS*. These conversion formulas give some uncertainties in the values, which can lead to less precise model estimations.

6.2.4 Gehring model

The Gehring model calculations present values slightly above the achieved net penetration rate using gross cutter thrust. Net cutter thrust gives values for the section averages 7.5-10.5% below the achieved NPR. The Gehring model states that net thrust values should be used in the calculations. This means that the results show conservative numbers.

The parameters that have the largest influence on the NPR calculations, are the thrust and *UCS*. With small changes, the achieved net penetration rate can be found. Even though *UCS* is a geology parameter and not adjustable in reality, this is shown to get an indication of how to obtain the achieved NPR. In this model, all parameters are sensitive and need small changes to make an impact on the model result.

Gross thrust

The Gehring model calculates close to the achieved net penetration rate, with only slightly higher values when using gross thrust in the estimations. Back calculations show how much the different parameters have to be changed to decrease the net penetration rate by 2.5%, from an estimated 2.06 m/h to the achieved 2.01 m/h. Calculations provide the following changes in the parameters:

- Gross thrust needs to be lowered by 2.3%, to 312 kN/cutter
- Cutterhead velocity, *RPM*, must be reduced by 2.7%, to 4.71
- *UCS* has to be enlarged by 2.4%, up to 179 MPa

All back calculated values show that small possible adjustments for the machine parameters will give the achieved net penetration. The *UCS*, which is a geological parameter, are also within reasonable proportionality limits.

Net thrust

Using net cutter thrust values, the Gehring model estimates 8.5% lower values than actual performance data.

Back calculating the different parameters show how much they have to be changed to increase the net penetration rate from an estimated 1.84 m/h to the achieved 2.01 m/h. Calculations provide the following changes in the parameters:

- Net thrust has to be increased by 8.9%, to 312 kN/cutter
- Cutterhead velocity, *RPM*, needs to be enlarged by 8.7%, to 5.30
- *UCS* must be reduced by 9.5%, down to 159.5 MPa

Approximately 9% individual change for the parameters are needed. All properties are rather sensitive, affecting the model more or less equally.

Evaluation and sources of error

There are only a few parameters that need to be known to calculate the penetration rate using the Gehring model. The machines standard setup with 432 mm cutters and a cutter spacing of 80 mm can easily be corrected for by some equations.

The main weakness of this model is that it is based on a small data set of tunnel projects with a certain machine setup. The model was published in 1995 with data from the 1990s. Since then, the TBM technology has evolved and the machine setup has changed compared to the prerequisites in the Gehring model.

Another weakness with the model is the correction factor for rock mass fabric. Only the orientation and spacing of the major plane of weakness is considered to affect the penetration. This may not completely reflect the actual characteristics of the rock mass. Also, only spacing <50 cm gives a correction for the rock mass fabric. This is not sufficient compared to the NTNU-model. The updated NTNU-model in chapter 3.1.5 counts for spacing up to 480 cm. The Gehring model will therefore not account for all the factors affecting TBM performance with respect to rock mass fabric.

The lack of information of the specific failure energy is also an uncertainty. The correction factor is here set to 1.0 and does not influence the penetration rate at all. Thus, the failure energy will not be corrected as a parameter that affects the penetration.

Another source of error is the *UCS* values. Due to a lack of sample material for laboratory testing, only the point load strength test was used to determine the strength properties. Further, conversion formulas were used to obtain values for *UCS*. These conversion formulas give some uncertainties in the values, which can lead to less precise model estimations.

6.2.5 *Alpine model*

The Alpine model calculations present values higher than the achieved net penetration rate using gross cutter thrust. Net cutter thrust estimates approximately the same as the achieved NPR. The Alpine model states that net thrust values are used in the calculations.

The parameters with the largest influence on the NPR calculations for the Alpine model, are the thrust and *RPM*. With some changes, the achieved net penetration rate can be found.

Gross thrust

Back calculations show how much the different parameters have to be changed to decrease the net penetration rate by 10%, from an estimated 2.21 m/h to the achieved 2.01 m/h.

Calculations provide the following changes in the parameters:

- Gross thrust needs to be lowered by 10.9%, to 288 kN/cutter
- Cutterhead velocity, *RPM*, has to be reduced by 9.9%, to 4.40
- Rock mass fracturing factor, k_s , must be decreased by 16.9%, down to 0.83
- *UCS* has to be enlarged by 14.8%, up to 205 MPa
- *BTS* needs to be increased by 32%, up to 10.3 MPa

The machine parameters have the biggest influence on the results, and the values need small reductions to get the estimations down to 2.01 m/h. The geological parameters require a higher adjustment to meet the achieved net penetration.

Net thrust

Using net cutter thrust values the Alpine model calculates approximately the same value as the achieved net penetration rate.

With an estimated NPR of 1.99 m/h, back calculations show how much the individual parameters have to be changed to increase results to the achieved 2.01 m/h. Calculations provide the following changes in the parameters:

- Net thrust must be increased by 1.3%, to 288 kN/cutter
- Cutterhead velocity, *RPM*, has to be enlarged by 1.0%, to 4.89
- Rock mass fracturing factor, k_s , needs to be increased by 2.0%, to 0.99
- *UCS* has to be reduced by 1.7%, to 171.7 MPa
- *BTS* must be decreased by 5.6%, down to 6.63 MPa

Slight changes are needed back calculating this model, as it already predicts rather accurate values.

Evaluation and sources of error

The Alpine model is quite alright to calculate when all parameters are known. The model is based on a machine setup with 432 mm cutter and a cutter spacing of 80 mm. This can be corrected for by some simple equations.

The main weakness with this model is that the incorporation of the y-intercept is only based on one tunnel project. The y-intercept is found from a regression analysis of the stress under a disc cutter at subcritical penetration. This shows that the Brazilian Tensile Strength and *LCPC* breakability coefficient have best correlation. The y-intercept of *BTS*, which is used in this thesis, has a very low regression coefficient. Using this value leads to an uncertainty in the results.

Another source of error, is the *UCS* and *BTS* values. Due to a lack of sample material for laboratory testing, only the point load strength test was used to determine the strength properties. Further, conversion formulas were used to obtain values for *UCS* and *BTS*. These conversion formulas give some uncertainties in the values, which can lead to less precise model estimations.

The correction factor for discontinuity pattern is also an uncertain factor, since this factor is not sufficiently developed in the model. The author of the model suggested that the correction factor from Gehring or the k_{s-tot} from the NTNU-model could be used. It is therefore difficult to know how good these factors correlate in this model.

6.2.6 Q_{TBM} -model

The Q_{TBM} -model results are way too high compared to the actual performance data, giving estimations 87% - 95.5% above. Net cutter thrust is also high, exceeding the achieved NPR with 49% - 55%. The Q_{TBM} -model has not stated if gross or net thrust values are used in the calculations.

Thrust is by far the parameter that has the largest influence on the NPR calculations for the Q_{TBM} -model. High adjustments of the input parameters are needed to achieve the net penetration rate of 2.01 m/h. This is related to the high model estimations. Variation in the *UCS* values was also tested, but this parameter is barely affecting any results, and unreasonable values are needed.

Gross thrust

Back calculations show how much the different parameters have to be changed to decrease the net penetration rate by 87%, from an estimated 3.76 m/h to the achieved 2.01 m/h.

Calculations provide the following changes in the parameters:

- Gross thrust has to be lowered by 36.8%, to 233.48 kN/cutter
- Cutter Life Index, *CLI*, needs to be reduced by 2214.5%, to 0.27
- *Q*-value has to be enlarged by 90.5%, up to 74

The *CLI* value needed is way too low to reflect any real geological situations. The *Q*-value changes are high, and show how big of an influence the cutter thrust has in this model.

Net thrust

Using net thrust calculation this model gives a predicted net penetration rate of 2.99 m/h, a high 49% above the achieved 2.01 m/h. Back calculations provide the following changes in the parameters:

- Net thrust has to be lowered by 21.8%, to 233.48 kN/cutter
- Cutter Life Index, *CLI*, must be reduced by 621.6%, to 0.85
- *Q*-value has to be enlarged by 77.4%, to 31

The needed change for the *CLI* value is very high and unlikely to happen in reality. An increase of the *Q*-value is possible in hard rock conditions since the *Q*-system is based on a logarithmic scale. Still, the best way to lower the net penetration rates for the Q_{TBM} -model is to lower the thrust.

Evaluation and sources of error

The Q_{TBM} -model is a comprehensive model that consider 20 basic parameters to cover different geological situations. The concept behind the model is a step in the right direction to better predict TBM performance. However, the model is complicated and it is an expensive process to obtain all parameters needed. In addition, calculations often give too high values for penetration rate compared to the actual achieved rate. Both Farrokh et al. (2012) and Hassanpour et al. (2016) addresses this issue, and it is also the case in this thesis.

There are several sources of error in the calculations. The input parameters for the *Q*-value are based on an average from the mapping done by Bane NOR and JVSS. The averaging of the values over longer sections, might not completely give a right description of the conditions. Further, the value for biaxial stress on tunnel face where only chosen from a stress table given in the geological profile. This will not reflect the actual situation, as measurements in the field are needed.

The *UCS* values are also an uncertain factor. Due to a lack of sample material for laboratory testing, only the point load strength test was used to determine the strength properties. Further, conversion formulas were used to obtain values for *UCS*. These conversion formulas give some uncertainties in the values, which can lead to less precise model estimations.

6.2.7 MCSM-model

The CSM- and MCSM-models are comprehensive models and requires multiple equations and parameters. The various steps in the model are interdependent, making back calculations a difficult task. Changing one parameter will change the outcome of multiple calculations. Thus, this has not been done for the model.

As stated earlier about the CSM-model, the calculations are based on reaching the machine limits to define the maximum net penetration rate. This means that the actual thrust is not included in the model, but a theoretical estimate is used to compare towards the limit.

In the basic CSM-model the intact rock mass properties *UCS* and *BTS* are the most sensitive parameters affecting the penetration rate. For the modified version, the intact rock brittleness value is of great significance to the result.

Evaluation and sources of error

As mentioned in chapter 3.6; to determine the brittleness index a punch penetration test is needed. The laboratory equipment to perform this test however, is expensive and uncommon in Europe. As a solution, Yagiz (2009) made an empirical equation to estimate rock brittleness. This equation is calculated using Uniaxial Compressive Strength, Brazilian Tensile Strength and rock density. Thus, this was used to calculate the brittleness index for the MCSM-model. The predicted *BI* is an uncertain factor as it does not completely reflect the brittleness of a rock mass. This can affect the model predictions.

The basic CSM-model is a complicated model to calculate. The trial and error procedure to find the maximum penetration rate makes it more exposed to possible mistakes in the calculations.

Due to a lack of sample material for laboratory testing, only the point load strength test was used to determine strength properties of the rock material. Further, conversion formulas were used to obtain values for Uniaxial Compression Strength and Brazilian Tensile Strength instead. These conversion formulas give some uncertainties in the values, which can lead to less precise model estimations.

6.3 Final result of prediction models compared to achieved NPR

The models have been presented in chapter 6.1 using both gross and net cutter thrust input values. Some models use gross cutter thrust while others use net cutter thrust. Here, they are presented as a final result, using its associated cutter thrust value. All models except Hassanpour et al. and the Q_{TBM} -model have stated whether they use gross or net values for cutter thrust. In the presentation of the final results in this thesis, gross thrust values are used for these two models. Below, a graph for the weighted average of the three subdivisions of the 700-meter tunnel segment is presented.

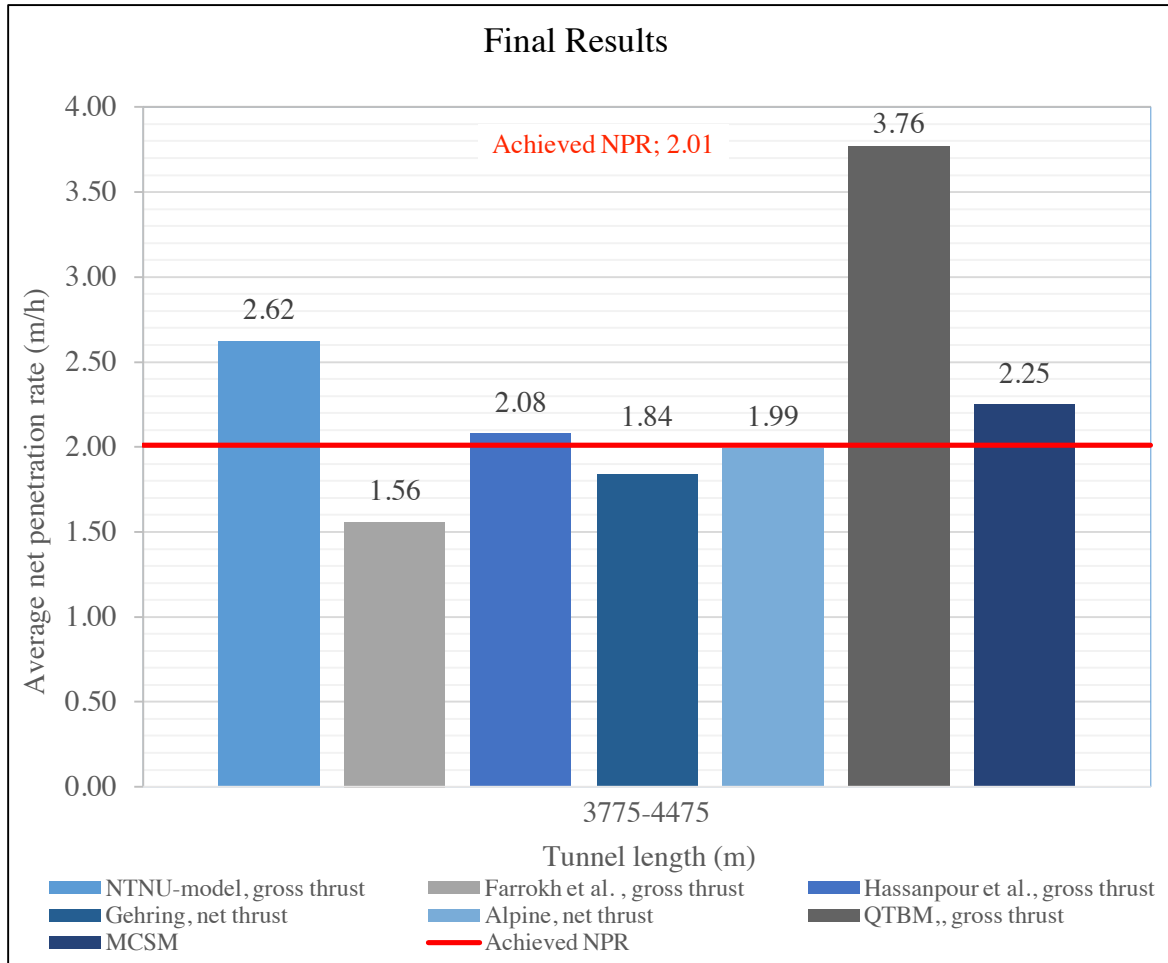


Figure 6.11 Final results compared to the achieved net penetration rate over the 700-meter section

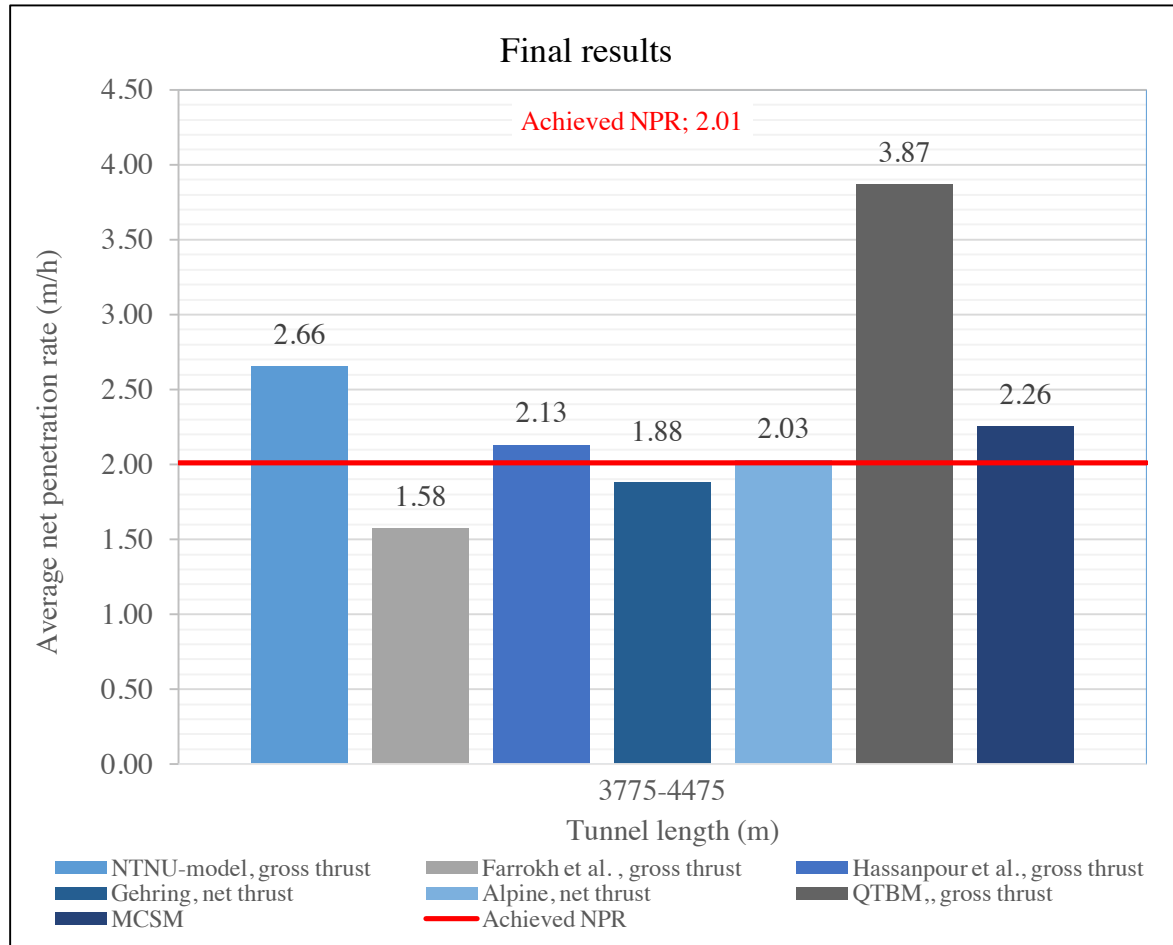


Figure 6.12 Final results compared to the achieved net penetration rate over the section divided after geology and core samples

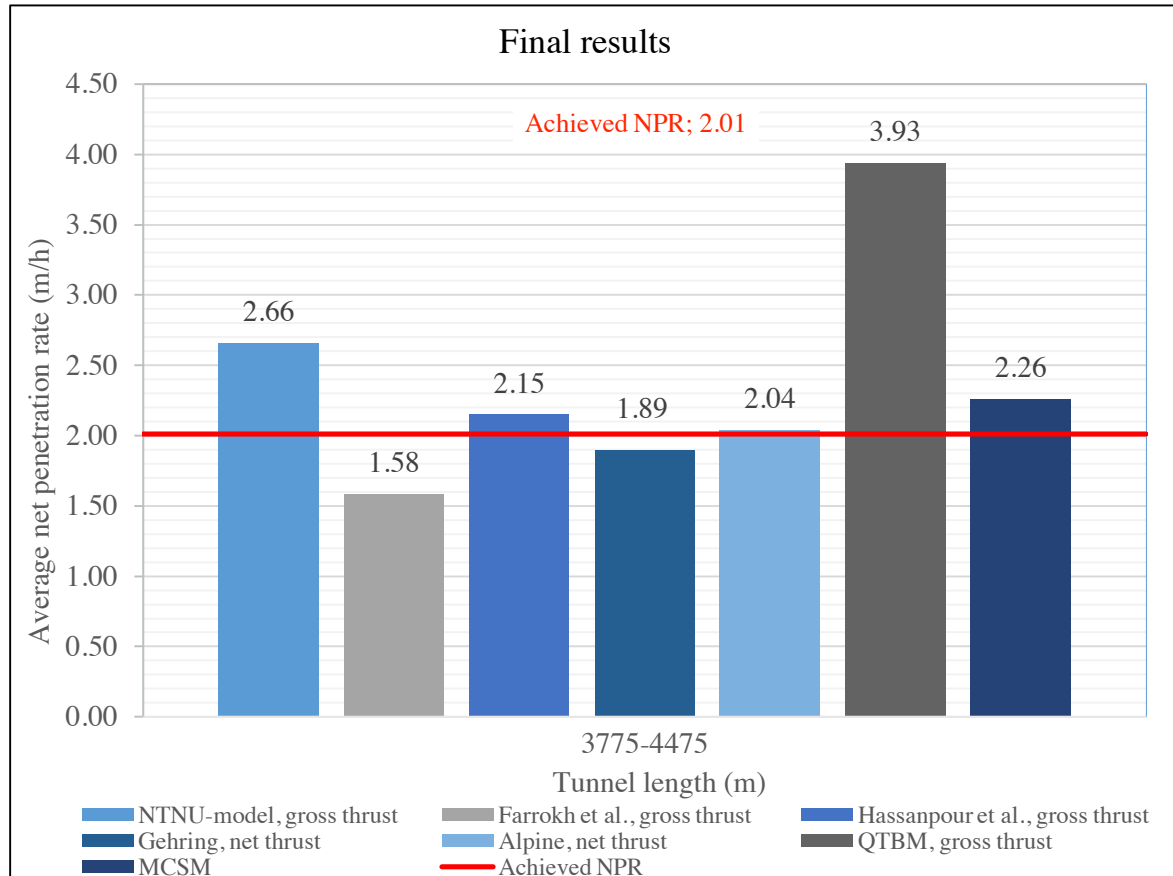


Figure 6.13 Final results compared to the achieved net penetration rate over the section divided from k_s -values

6.4 Possible sources of error

Possible sources of error and evaluation of every model separately were presented in the previous chapter. In this chapter, additional and more general information about possible errors are discussed.

All models are based on empirical data and contain weaknesses regarding accurate performance prediction. Some of the models are based on extensive databases of tunnel project data, while others are based on only a few projects. However, even with a large database a model may not completely reflect the situation and present parameters at the New Ulriken Tunnel. Deviations may occur on the basis of:

- Databases can contain a limited number of rock types and rock mass properties; this may not reflect the situation at New Ulriken Tunnel causing uncertainty
- Some databases are based on old machine specifications. As the development of the TBMs has improved, machine limits are higher. As an example, older models may not be able to calculate accurate predictions for high thrust values
- The machine at New Ulriken Tunnel is a rather large open-type TBM. Many of the databases contain TBMs with smaller diameters and often a mix of shielded and open-type machines. This may cause deviations in the results

Many of the models includes rock mass fracturing as an important factor for the net penetration rate. The degree of the rock mass fracturing at the New Ulriken Tunnel has been decided upon by the authors of this thesis. The authors are fairly new to geological mapping in TBM tunnels, causing ambivalence to this part of the work. To secure the mapping results, a comparison was made to JVSS/Bane NORs mapping over the same tunnel segment.

Cutter thrust (kN/cutter) is a main parameter in almost all models, having a great influence on the results. The numbers for cutter thrust in this project are, in conjunction with achieved net penetration rate and geological parameters, rather high. This is reflected in the estimations of the net penetration rate using gross thrust values, as almost all models calculate too high values. The highest average value registered for gross cutter thrust for a 25-meter section is 340 kN/cutter. According to Macias (2016), the maximum recommended cutterhead thrust for similar TBMs is 312 kN/cutter. The same value is stated by the cutter manufacturer as the maximum cutter load capacity. Applying such a high thrust may cause damage to the cutters. Looking at the cutter consumption logged at the project, cutter changes due to bearing damage accounts for 33.9%. This is somewhat higher than the recommended value from the NTNU-model.

In Macias (2016), the highest recommended wear limits for cutters are set to 35 mm for the cutters exposed to the highest loads. In the project at Ulriken, the top limit is set to 43 mm, making the contact surface between the cutter and the rock face considerably larger. This might be a reason for the high level of applied thrust compared to the achieved net penetration rate. Worn-down-cutters will have less indentation in the rock. Thus, a higher thrust is needed to keep the net penetration rate at a similar level as a cutter that has been changed more recently. The project management at the New Ulriken Tunnel have experimented with a mix of 19 inch and 20 inch cutters with different cutter tip widths. However, the calculations are only performed using 19 inch cutters as an input in the

models. This may cause uncertainty in the predictions for both net penetration rate and cutter ring life.

All performance data is gathered from IRIS.tunnel, which logs data continuously. The raw data was downloaded from the software in 25 meter sections and treated in Excel. Errors might occur in both the logging and the treating of the raw data. It is unclear how precise the software is, and how much this can deviate from real numbers. In addition, for net thrust values a constant friction estimate, done by the manufacturer of the TBM, is set to 2500 kN. This will not reflect reality as friction measurements would be needed instead of a constant reduction to acquire true values.

7 Conclusive remarks

This chapter summarizes the thesis and provides conclusive remarks for the main and secondary objectives.

The main objective of this thesis was to study and compare a number of existing prediction models for TBM. The thesis has been written in correlation with the project New Ulriken Tunnel in Norway. A detailed field study was conducted over a period of eight weeks to acquire all the necessary model parameters. A tunnel section of 700 meters, from TM 3775 – TM 4475 was investigated. The field study included geological back-mapping of the tunnel, gathering actual TBM performance data, collecting core samples and logging of cutter consumption. After the field study, the in-situ samples were tested in the laboratory at SINTEF.

Most of the models require simple calculations once all the needed parameters are known. Therefore, the calculations of net penetration rate present a low degree of possible errors, since geological and machine data was made available.

The models showing most promising results compared to the achieved net penetration rate proves to be the model by Hassanpour et al. and the Alpine model. In the final results, these two models predict values very close to the achieved net penetration rate at the New Ulriken Tunnel. If a conservative result is more sought after, the Gehring model calculates the best values; approximately 7% below the achieved TBM performance.

The study of the different models shows that cutter thrust is the machine parameter most affecting the net penetration rate. All the models except MCSM are using this parameter and small adjustments will in most models provide rather large differences in calculated results. For the geological parameters, the rock mass fracturing factor and *UCS* are most sensitive for variations regarding net penetration rate. The *UCS* describes the intact rock strength properties, while the rock mass fracturing factor describes the degree of fracturing in the rock mass. A model should include all three of these important parameters to better reflect real life situations in its predictions.

Cutter estimations with the NTNU-model correlates well with actual cutter ring life when using achieved net penetration rates and gross cutter thrust in the calculations. However, while using calculated NPR predictions for both gross and net cutter thrust, this is not the case.

The results from this thesis show that TBM prediction models are important both in the early stages as well as during the construction of a project. The models calculated show some uncertainties, and it is recommended to use several models in the predictions. This will give the possibility to compare and secure the reliability of the obtained results.

8 Further work

This chapter presents the authors' thoughts about possible topics for further work and research, both for the field of study and the New Ulriken Tunnel.

This thesis has studied seven prediction models for TBM in hard rock, all estimating net penetration rate. Several models for TBM predictions exist; it is possible to evaluate other models than the ones used in this study. This is to get a more comprehensive model database to compare with achieved net penetration rates. Evaluation of sections longer than 700 meters are also beneficial and can be a topic for further study.

Many of the prediction models are empirical based on field data from a range of different TBM projects. Using new acquired empirical data to update the models is a possible field of study. This is to improve the models and secure that the models are applicable to a wider range of project situations.

Only one model has been used for cutter ring life predictions in this thesis. The NTNU-model was calculated yet a number of models exists to assess cutter life. It is also possible to include these for estimation purposes, enabling comparisons with more than one model prediction. Using different models will give a better reliability of the results. The cutter life predictions can be used to evaluate the cutter consumption at a project. Further, this may be used to adjust a project's cutter ring life policy.

TBM operations consist of many time-consuming activities. Therefore, a study of machine utilization is of great interest. A complete overview of the activities and correspondent time consumption will provide information that might be used to improve the productivity in a project. When the machine utilization is known, a weekly advance rate is obtainable. Further, cost estimations can be done more realistically for the complete length of the tunnel. These calculations for utilization and cost estimations can be performed both before and during a project. However, in the preliminary stages the utilization has to be assumed.

Mechanical bored tunnels produce large amounts of muck. It is therefore beneficial to find a way to utilize this material. As of today, there are few good solutions for dealing with this TBM «debris». There have been thoughts about using it as aggregates in concrete mixtures, but this and other possible solutions should be considered and studied more closely.

The further work within this field of study mentioned above, is also applicable to the New Ulriken Tunnel. However, as the boring of the tunnel is soon to be completed, these suggestions of further work might be a challenge. Gathering enough data may be complicated, and tests with the machine will no longer be possible.

References

- BANENOR. 2015. *Norgeshistorie i HARD ROCK* [Online]. <http://www.banenor.no/> BaneNor. Available: <http://www.banenor.no/Om-oss/Jernbanemagasinet-arkiv/Bildefortellingen/norgeshistorie-i-hard-rock/> [Accessed 28.10 2016].
- BANENOR 2016a. Arna-Bergen double track. <http://www.banenor.no/>.
- BANENOR. 2016b. *Mer om prosjektet: Hvorfor og hva vi bygger på strekningen Arna-Bergen* [Online]. <http://www.banenor.no/> BaneNor. Available: <http://www.banenor.no/Prosjekter/prosjekter/Arna-Bergen/mer-om-prosjektet/> [Accessed 28.10 2016].
- BARTON, N. 2000. *TBM tunnelling in jointed and faulted rock*, Rotterdam, A.A. Balkema.
- BILGIN, N., COPUR, H. & BALCI, C. 2013. *Hard Rock TBMs. Mechanical Excavation in Mining and Civil Industries*. CRC Press.
- BRULAND, A. 2000a. *Hard rock tunnel boring : Vol. 1 : Background and discussion*, Trondheim, Norwegian University of Science and Technology, Department of Building and Construction Engineering.
- BRULAND, A. 2000b. *Hard rock tunnel boring : Vol. 3 : Advance rate and cutter wear*, Trondheim, Norwegian University of Science and Technology, Department of Building and Construction Engineering.
- BRULAND, A. 2000c. *Hard rock tunnel boring : Vol. 6 : Performance data and back-mapping*, Trondheim, Norwegian University of Science and Technology, Department of Building and Construction Engineering.
- BRULAND, A. 2000d. *Hard rock tunnel boring : Vol. 7 : The boring process*, Trondheim, Norwegian University of Science and Technology, Department of Building and Construction Engineering.
- BRULAND, A. 2000e. *Hard rock tunnel boring : Vol. 8 : Drillability : test methods*, Trondheim, Norwegian University of Science and Technology, Department of Building and Construction Engineering.
- BRAA, J. & HOPLAND, R.-R. 2016. The New Ulriken tunnel: Performance prediction models for TBM in hard rock.
- DAHL, F., BRULAND, A., JAKOBSEN, P. D., NILSEN, B. & GRØV, E. 2012. Classifications of properties influencing the drillability of rocks, based on the NTNU/SINTEF test method. *Tunnelling and Underground Space Technology*, 28, 150-158.
- FARROKH, E., ROSTAMI, J. & LAUGHTON, C. 2012. Study of various models for estimation of penetration rate of hard rock TBMs. *Tunnelling and Underground Space Technology incorporating Trenchless Technology Research*, 30, 110-123.
- GEHRING, K. 1995. Leistungs- und Verschleißprognose im maschinellen Tunnelbau. *Felsbau Magazin*, 13.
- HASSANPOUR, J., GHAEDI VANANI, A. A., ROSTAMI, J. & CHESHOMI, A. 2016. Evaluation of common TBM performance prediction models based on field data from the second lot of Zagros water conveyance tunnel (ZWCT2). *Tunnelling and Underground Space Technology incorporating Trenchless Technology Research*, 52, 147-156.
- HASSANPOUR, J., ROSTAMI, J. & ZHAO, J. 2011. A new hard rock TBM performance prediction model for project planning. *Tunnelling and Underground Space Technology incorporating Trenchless Technology Research*, 26, 595-603.
- HERRENKNECHT 2015. Assembly Cutterhead Drawing.
- HERRENKNECHT. 2016a. *Double Shield TBM, Continuous tunnelling at maximum speed* [Online]. <http://www.herrenknecht.com/> Herrenknecht AG. Available: <https://www.herrenknecht.com/en/products/core-products/tunnelling/double-shield-tbm.html> [Accessed 03.10 2016].
- HERRENKNECHT. 2016b. *Gripper TBM, Experts for tough hard rock* [Online]. <http://www.herrenknecht.com/> Herrenknecht AG. Available:

- <https://www.herrenknecht.com/en/products/core-products/tunnelling/gripper-tbm.html> [Accessed 03.10 2016].
- HERRENKNECHT. 2016c. *Single Shield TBM, Fast tunnelling in changing rock conditions* [Online]. <http://www.herrenknecht.com/> Herrenknecht AG. Available: <https://www.herrenknecht.com/en/products/core-products/tunnelling/single-shield-tbm.html> [Accessed 03.10 2016].
- ISRM 1985. Suggested method for determining point load strength. *International Journal of Rock Mechanics and Mining Sciences & Geomechanics Abstracts*, 22, 51-60.
- ITC-ENGINEERING. 2016. *IRIS.tunnel* [Online]. Available: <http://www.itc-engineering.de/en/products/iris/iristunnel/> [Accessed].
- ITC-ENGINEERING. 2017. *Sensorboard* [Online]. Available: http://iris.itc-23.com/Ulriken-Eisenbahn-Tunnel-S935/form_Sensorboard.html [Accessed].
- JAKOBSEN, P. D., LOG, S., SKJEGGEDAL, T., HANSEN, A. M. & PALM, A. 2015. Kort innføring i bruk av TBM. *Tekniske rapporter*. Norsk Forening for Fjellsprenningsteknikk.
- MACIAS, F. J. 2016. *Hard rock tunnel boring : performance predictions and cutter life assessment*. 2016:350, Norwegian University of Science and Technology, Faculty of Engineering Science and Technology, Department of Civil and Transport Engineering.
- MACIAS, F. J. & BRULAND, A. 2014. D&B versus TBM. *Rock Engineering and Rock Mechanics: Structures in and on Rock Masses*. CRC Press.
- MACIAS, F. J., JAKOBSEN, P. D., SEO, Y. & BRULAND, A. 2014. Influence of rock mass fracturing on the net penetration rates of hard rock TBMs. *Tunnelling and Underground Space Technology incorporating Trenchless Technology Research*, 44, 108-120.
- NILSEN, B., PALMSTRØM, A. & NORSK FORENING FOR, F. 2000. *Engineering geology and rock engineering*, Oslo, Norwegian Group for Rock Mechanics.
- NORCONSULT 2013a. Arna-Bergen, UUT21
Ingeniørgeologisk lengdeprofil. Jernbaneverket.
- NORCONSULT 2013b. Ulriken tunnel: Anvendelse av steinmaterialer.
- OZDEMIR, L. 1977. *Development of theoretical equations for predicting tunnel borability*. PhD, Colorado School of Mines.
- ROSTAMI, J. 1997. *Development of a force estimation model for rock fragmentation with disc cutters through theoretical modeling and physical measurement of crushed zone pressure*. PhD, Colorado School of Mines.
- SINTEF 2010. DTA - Differentialtermisk analyse. SINTEF.
- SINTEF 2011. DRI, BWI, CLI Standard. SINTEF.
- SINTEF 2013. Undersøkelse av bergarter fra Ulriken tunnel for borbarhet og slitasjegenskaper.
- WILFING, L. S. F. 2016. *The Influence of Geotechnical Parameters on Penetration Prediction in TBM Tunneling in Hard Rock*. PhD, Technische Universität München.
- YAGIZ, S. 2002. *Development of rock fracture and brittleness indices to quantify the effects of rock mass features and toughness in the CSM model basic penetration for hard rock tunneling machines*. Ph.D, Colorado school of Mines.
- YAGIZ, S. 2009. Assessment of brittleness using rock strength and density with punch penetration test. *Tunnelling and Underground Space Technology incorporating Trenchless Technology Research*, 24, 66-74.
- YAGIZ, S., ROSTAMI, J. & OZDEMIR, L. 2012. Colorado School of Mines Approaches For Predicting TBM Performance. International Society for Rock Mechanics.

Appendices

| | | |
|------------|---|-----|
| APPENDIX A | TBM_DRAWING | A-1 |
| APPENDIX B | DETAILED_CUTTERHEAD_DRAWING | B-1 |
| APPENDIX C | GEOLOGICAL_PROFILE | C-1 |
| APPENDIX D | MAPPING SHEET | D-1 |
| APPENDIX E | GEOLOGICAL_BACK-MAPPING | E-1 |
| APPENDIX F | RAW_DATA_IRIS | F-1 |
| APPENDIX G | SHEET FOR PENETRATION- AND RPM-TEST | G-1 |
| APPENDIX H | TBM_PERFORMANCE_DATA..... | H-1 |
| APPENDIX I | PENETRATION_TEST | I-1 |
| APPENDIX J | RPM_TESTS | J-1 |
| APPENDIX K | CHIP_SIZE_MEASUREMENTS | K-1 |
| APPENDIX L | CUTTER_JOURNAL_TM3775-TM4475 | L-1 |
| APPENDIX M | LABORATORY_RESULTS..... | M-1 |
| APPENDIX N | MODEL_CALCULATIONS | N-1 |
| APPENDIX O | SIEVE CURVE | O-1 |
| APPENDIX P | AVERAGE_Q-VALUES | P-1 |
| APPENDIX Q | BACK_CALCULATIONS..... | Q-1 |

Appendix A TBM_drawing

(Digital appendix)

Appendix B Detailed_cutterhead_drawing

(Digital appendix)

Appendix C Geological_profile

(Digital appendix)


Appendix E Geological_back-mapping

(Digital appendix)

Appendix F Raw_data_IRIS

(Digital appendix)

Appendix G Sheet for Penetration- and RPM-test

| UUT21 Nye Ulriken Tunnel JV SKANSKA STRABAG |  | | | | | | | | | | | | | | | | | | | | | | | | | | | | | | | | | | | | | | | | | | | | | | | | | | | |
|---|---|----------|--------------|--------|---|--|--|-----|--|--|---|--|--|-----|--|--|---|--|--|-----|--|--|---|--|--|--------|-----|--------|-------|--|--|-------|--|--|-------|--|--|-------|--|--|-------|--|--|-------|--|--|-------|--|--|-------|--|--|
| <h3 style="margin: 0;">TBM - Penetration test</h3> <p style="margin: 5px 0;">Date: _____ Start TM (Chainage) Face: _____ Stop TM (Chainage) Face: _____</p> <p style="margin: 5px 0;">Operator: _____</p> <p style="margin: 5px 0;">Note, run the test for minimum 5 min on each level, use the fixed thrust and rpm as previous stroke</p> <div style="display: flex; justify-content: space-between;"> <div style="width: 45%;"> <p>RPM test Run with fixed thrust and adjust the rpm</p> <table border="1" style="width: 100%; border-collapse: collapse; text-align: center;"> <thead> <tr> <th>RPM test</th> <th>Thrust level</th> <th>mm/min</th> </tr> </thead> <tbody> <tr><td>3</td><td></td><td></td></tr> <tr><td>3,5</td><td></td><td></td></tr> <tr><td>4</td><td></td><td></td></tr> <tr><td>4,5</td><td></td><td></td></tr> <tr><td>5</td><td></td><td></td></tr> <tr><td>5,5</td><td></td><td></td></tr> <tr><td>6</td><td></td><td></td></tr> </tbody> </table> <p style="margin-top: 5px;">Note; The rock conditions determine how high rpm can be used</p> </div> <div style="width: 45%;"> <p>Thrust test Run with fixed rpm and adjust the thrust</p> <table border="1" style="width: 100%; border-collapse: collapse; text-align: center;"> <thead> <tr> <th>Thrust</th> <th>RPM</th> <th>mm/min</th> </tr> </thead> <tbody> <tr><td>17000</td><td></td><td></td></tr> <tr><td>18000</td><td></td><td></td></tr> <tr><td>19000</td><td></td><td></td></tr> <tr><td>20000</td><td></td><td></td></tr> <tr><td>21000</td><td></td><td></td></tr> <tr><td>22000</td><td></td><td></td></tr> <tr><td>23000</td><td></td><td></td></tr> <tr><td>24000</td><td></td><td></td></tr> </tbody> </table> <p style="margin-top: 5px;">Note; The rock conditions determine how high thrust can be used</p> </div> </div> <div style="border: 1px solid black; height: 150px; margin-top: 10px; padding: 5px;"> <p>Comments; (rock type, vibrations, limiting factors or other)</p> </div> | | RPM test | Thrust level | mm/min | 3 | | | 3,5 | | | 4 | | | 4,5 | | | 5 | | | 5,5 | | | 6 | | | Thrust | RPM | mm/min | 17000 | | | 18000 | | | 19000 | | | 20000 | | | 21000 | | | 22000 | | | 23000 | | | 24000 | | |
| RPM test | Thrust level | mm/min | | | | | | | | | | | | | | | | | | | | | | | | | | | | | | | | | | | | | | | | | | | | | | | | | | |
| 3 | | | | | | | | | | | | | | | | | | | | | | | | | | | | | | | | | | | | | | | | | | | | | | | | | | | | |
| 3,5 | | | | | | | | | | | | | | | | | | | | | | | | | | | | | | | | | | | | | | | | | | | | | | | | | | | | |
| 4 | | | | | | | | | | | | | | | | | | | | | | | | | | | | | | | | | | | | | | | | | | | | | | | | | | | | |
| 4,5 | | | | | | | | | | | | | | | | | | | | | | | | | | | | | | | | | | | | | | | | | | | | | | | | | | | | |
| 5 | | | | | | | | | | | | | | | | | | | | | | | | | | | | | | | | | | | | | | | | | | | | | | | | | | | | |
| 5,5 | | | | | | | | | | | | | | | | | | | | | | | | | | | | | | | | | | | | | | | | | | | | | | | | | | | | |
| 6 | | | | | | | | | | | | | | | | | | | | | | | | | | | | | | | | | | | | | | | | | | | | | | | | | | | | |
| Thrust | RPM | mm/min | | | | | | | | | | | | | | | | | | | | | | | | | | | | | | | | | | | | | | | | | | | | | | | | | | |
| 17000 | | | | | | | | | | | | | | | | | | | | | | | | | | | | | | | | | | | | | | | | | | | | | | | | | | | | |
| 18000 | | | | | | | | | | | | | | | | | | | | | | | | | | | | | | | | | | | | | | | | | | | | | | | | | | | | |
| 19000 | | | | | | | | | | | | | | | | | | | | | | | | | | | | | | | | | | | | | | | | | | | | | | | | | | | | |
| 20000 | | | | | | | | | | | | | | | | | | | | | | | | | | | | | | | | | | | | | | | | | | | | | | | | | | | | |
| 21000 | | | | | | | | | | | | | | | | | | | | | | | | | | | | | | | | | | | | | | | | | | | | | | | | | | | | |
| 22000 | | | | | | | | | | | | | | | | | | | | | | | | | | | | | | | | | | | | | | | | | | | | | | | | | | | | |
| 23000 | | | | | | | | | | | | | | | | | | | | | | | | | | | | | | | | | | | | | | | | | | | | | | | | | | | | |
| 24000 | | | | | | | | | | | | | | | | | | | | | | | | | | | | | | | | | | | | | | | | | | | | | | | | | | | | |

Appendix H TBM_Performance_data

(Digital appendix)

Appendix I Penetration_test

(Digital appendix)

Appendix J RPM_tests

(Digital appendix)

Appendix K Chip_size_measurements

(Digital appendix)

Appendix L Cutter_Journal_TM3775-TM4475

(Digital appendix)

Appendix M Laboratory_results

(Digital appendix)

Appendix N Model_calculations

(Digital appendix)

Appendix O Sieve curve

| | | | | | | | | | | | | | | | | | | | | | | | |
|---|----------------|----------------------|----------------------------|--------------------------|----------|----------------|------|------|------|------|------|------------------------------|------|------|---------------|------|------|--|--|--|--|--|--|
| NCC | | Korngradering | | Diverse steinforekomster | | | | | | | | | | | | | | | | | | | |
| Oppdragnr. | 131170002 | Oppdragsnavn | TBM masse nye Ulriken 2017 | | | | | | | | | | | | | | | | | | | | |
| Prosjektnummer | 112012 | Prosjektnavn | TBM v/Gry Stenersen | | | | | | | | | | | | | | | | | | | | |
| Ansvarsområde | 3 | Ansvarlig | Arna | | | | | | | | | | | | | | | | | | | | |
| Prøvedata | | | | | | | | | | | | | | | | | | | | | | | |
| Prøvenr | 2(P) | | | | | | | | | | | | | | | | | | | | | | |
| Uttatt dato | 15.03.2017 | | | | | | | | | | | | | | | | | | | | | | |
| Uttatt kl. | | | | | | | | | | | | | | | | | | | | | | | |
| Uttakssted | På veg Tunnell | | | | | | | | | | | | | | | | | | | | | | |
| Analysetype | Våtsikt | | | | | | | | | | | | | | | | | | | | | | |
| Massetak | | | | | | | | | | | | | | | | | | | | | | | |
| Består av | | | | | | | | | | | | | | | | | | | | | | | |
| Grenseverdigr. | 0-63 | | | | | | | | | | | | | | | | | | | | | | |
| Vegnr/HP | KV1 TM4337,4 | | | | | | | | | | | | | | | | | | | | | | |
| Meter/profil | 467291,4 | | | | | | | | | | | | | | | | | | | | | | |
| Avstand høyre kant | | | | | | | | | | | | | | | | | | | | | | | |
| Dybde | - | | | | | | | | | | | | | | | | | | | | | | |
| Vanninnhold (%) | 1.6 | | | | | | | | | | | | | | | | | | | | | | |
| Vannabsorpsjon (%) | | | | | | | | | | | | | | | | | | | | | | | |
| Humus (Glødetap) | | | | | | | | | | | | | | | | | | | | | | | |
| Fraksjon (mm) | 0.0 - 63.0 | | | | | | | | | | | | | | | | | | | | | | |
| Overstørrelse | 2.7 | | | | | | | | | | | | | | | | | | | | | | |
| Understørrelse | | | | | | | | | | | | | | | | | | | | | | | |
| % <63µm av <delsikt | 12.9 (22,4 mm) | | | | | | | | | | | | | | | | | | | | | | |
| % <20µm av <delsikt | | | | | | | | | | | | | | | | | | | | | | | |
| Finstoffinnhold f | 8.7 | | | | | | | | | | | | | | | | | | | | | | |
| Godkjent siktekurve | Nei | | | | | | | | | | | | | | | | | | | | | | |
| Siktedata - Passert (%) | | | | | | | | | | | | | | | | | | | | | | | |
| | µm | | | | | mm | | | | | | | | | | | | | | | | | |
| Pr.nr. | 63 | 125 | 250 | 500 | 1 | 2 | 4 | 5.6 | 8 | 11.2 | 16 | 22.4 | 31.5 | 45 | 56 | 63 | 80 | | | | | | |
| 2(P) | 8.7 | 11.8 | 14.9 | 18.4 | 22.5 | 28.2 | 34.8 | 39.5 | 45.7 | 52.0 | 59.3 | 67.5 | 80.1 | 91.8 | 96.8 | 97.3 | 98.5 | | | | | | |
| 1 prøve 46 kg levert av Leon Eide | | | | | | | | | | | | | | | | | | | | | | | |
| Sand | | | | | | Grus | | | | | | | | | | | | | | | | | |
| Fin | | | Middels | | | Grov | | | Fin | | | Middels | | | Grov | | | | | | | | |
| | | | | | | | | | | | | | | | | | | | | | | | |
| — 2 (P) — 0-63 min — 0-63 max | | | | | | | | | | | | | | | | | | | | | | | |
| Pr.nr | Vegnr | Meter/profil | HP | Avst.hk. | Dybde(m) | Jordart | | | | | | | | | Cu (* = Cu75) | TG | | | | | | | |
| 2(P) | KV1 | | | | - | | | | | | | | | | 195.9 | | | | | | | | |
| Sted: Arna | | | | | | Dato: 24.03.17 | | | | | | Signatur: <i>Liv Wangnes</i> | | | | | | | | | | | |

Appendix P Average_Q-values

(Digital appendix)

Appendix Q Back_calculations

(Digital appendix)